UNIVERSITY OF LIVERPOOL

Macrophages suppress anti-tumour immunity in metastatic pancreatic cancer

Thesis submitted in accordance with the requirements of the University of Liverpool for the degree of Doctor in Philosophy by

Valeria Quaranta

28/09/2018

Supervisor: Dr. Michael C. Schmid

Declaration

I, Valeria Quaranta, hereby certify that, except where acknowledgment is made, the work contained in this thesis was performed by me at the University of Liverpool.

I also declare that the work described in this thesis is original, and the majority of it has first been published by the American Association for Cancer Research (Quaranta et al., Cancer Research, 2018) and a copy is enclosed.

Acknowledgment

My biggest thank you goes to Michael C. Schmid, my supervisor, who supported and guided me through the scientific adventure of these four years! I am very grateful to you for all your teaching, help and patience! I also feel very lucky for having joined your group and for having the possibility to develop my project! I learned a lot about the research world and I also feel to have changed a lot during these years… beside the fact of being in time… this no…this will never change!

A big thank you is for Ainhoa Mielgo for her strong support and help during these years. For me you are a great example of a successful woman in science!

Thanks to North West Cancer Research for supporting me with a funded PhD scholarship.

A big thanks goes to all the members (and ex-) of Michael and Ainhoa' s teams: my favourite Warrior, Almudena, Sebastian, Lucy, Carlos, Carolyn, Perpetua and Andrea. Thank you for all your help in the lab during these years and for making happy the everyday life in the lab!

Thanks to all the wonderful people that I met here, to all places and experiences I lived, which made shine my days in the UK!

Abstract

Macrophages suppress anti-tumour immunity in metastatic pancreatic cancer.

Pancreatic cancer is a highly aggressive metastatic disease with unmet needs. The presence of an immunosuppressive tumour microenvironment (TME) at the primary tumour site is known to be essential for pancreatic cancer progression and it is proposed to be a critical obstacle for programmed cell death protein 1 (PD-1) immune checkpoint blockade therapy to succeed. However, whether an immunomodulatory TME also exists at the metastatic site, and how this would affect the response to PD-1 blockade remains unknown. Here we show that metastatic pancreatic cancer progression is accompanied by the loss of $CD8^+$ T cells infiltration and function, a mechanism that is critically dependent on the accumulation of immunosuppressive metastasis associated macrophages (MAMs) and the generation of a dense fibrotic stroma, which acts as barrier for T cell infiltration. Mechanistically, we demonstrated that disseminated pancreatic cancer cell-derived Colony stimulating factor 1 (CSF-1) polarizes MAMs toward an M2-like phenotype and induces the expression of granulin in MAMs. Macrophage-secreted granulin is a key factor for hepatic stellate cells (HSCs) activation and fibrosis formation during pancreatic cancer metastasis to the liver. We found that blockade of CSF-1 / CSF-1 receptor axis or genetic depletion of granulin strongly reduces fibrosis and enhances $CD8^+$ T cells infiltration, thus rendering metastatic pancreatic cancer sensible to PD-1 blockade. Interestingly, granulin depletion in combination with anti-PD-1 (αPD-1) therapy rewires the immunosuppressive metastatic TME towards a

pro-inflammatory TME by increasing $CD8^+$ T cells cytotoxic activity and favouring M1-like phenotype in MAMs. We observed that re-education of the metastatic TME induced by granulin depletion in combination with PD-1 inhibition provides a better anti-metastatic effect compared to the combination of αPD-1 therapy with a MAM-depletion approach, though CSF-1 / CSF-1R blockade. Thus, our results identify granulin as potential therapeutic target to restore $CD8^+$ T cell infiltration, thereby sensitising metastatic pancreatic cancer to immune checkpoint inhibition therapy.

Table of contents

List of Figures and Tables

Tables

Abbreviations

ADEX: aberrantly differentiated endocrine exocrine

APC: antigen presenting cell

AT: adoptively transferred

ATRA: all-trans retinoic acid

bFGF: basic fibroblast growth factor

BLI: bioluminescence imaging

BM: bone marrow

BMM: bone marrow derived macrophage

BSA: Bovine Serum Albumin

CAE: carcinoembryonic antigen

CAF: cancer associated fibroblast

CAV1: caveolin 1

CCL: chemokine (C-C motif) ligand

CK: cytokeratin

CM: conditioned media

COX-2: cyclooxygenase-2

CSF-1R: CSF-1 receptor

CT: computer tomography

CTC: circulating tumour cell

CTGF: connective growth factor

CTL: cytotoxic T lymphocyte

CTLA-4: Cytotoxic T-Lymphocyte Antigen 4

CTR: control

CXCL: chemokine (C-X-C motif) ligand

DC: dendritic cell

DDR2: discoidin-containing receptor 2

DMEM: Dulbecco Modified Eagle Medium

DTC: disseminating cancer cells

ECM: extracellular matrix

EGF: epidermal growth factor

EMT: Epithelial to mesenchymal transition process

FAK: focal adhesion kinase

FAPα: fibroblast-activation protein α

FasL: Fas ligand

FBS: Fetal Bovine Serum

FDA: Food and Drug Administration

FOLFIRINOX: combination of folinic acid (leucovorin), 5-fluorouracil, irinotecan and oxaliplatin

FOXP3: forkhead box 3

GM-CSF: granulocyte-macrophage colony-stimulating factor

GRN/Grn: Granulin

GzmB: Granzyme B

H&E: Haematoxylin and eosin

HA: hyaluronic acid

HGF: hepatocyte growth factor

HSC: Hepatic Stellate Cells

i.p.: Intraperitoneal injection

i.v.: Intravenous injection

IDO: indoleamine 2,3-dioxygenase

IF: immunofluorescence

IFNγ: interferon gamma

IGF: insulin-like growth factor

IHC: immunohistochemistry

iNOS: inducible nitric oxide synthase

LOX: Lysyl oxidase

LPA: lysophosphatidic acid

LPS: lipopolysaccharide molecule

LSL: *Lox-STOP-Lox* construct

M-CSF or only CSF-1: macrophage colony stimulating factor-1

MDSC: myeloid-derived suppressor cell

MHC: major histocompatibility complex

MMP: metalloproteinase

MR: magnetic resonance

NET: neutrophil extracellular trap

NGF: nerve growth factor

NK: natural killer

NSCLC: non-small-cell lung cancer

O/N: over night

OCT: Optimal Cutting Temperature

OD: optical density

PanIN: Pancreatic intraepithelial neoplasia

PBS: phosphate buffered saline

PD-1: Programmed cell death-1

PD-L1: programmend cell death 1 ligand 1

PDAC: Pancreatic ductal adenocarcinoma

PDGF: platelet derived growth factor

PDGFR: platelet derived growth factor receptor

PEGPH20: PEG-fused hyaluronidase

PGE2: Prostaglandin E2

PGRN: progranulin

PI3Kγ: gamma isoform of phosphoinoside 3-kinase

Prf: Perforine

qPCR: quantitative PCR

RT: Reverse transcription

Shh: sonic hedgehog pathway

TAM: tumour associated macrophage

TGFβ: transforming growth factor β

T_H: $CD4^+$ helper T cell

TME: tumour microenvironment

TNF: tumour necrosis factor

TNFR: tumour necrosis factor receptor

T_{reg}: regulatory T cells

TSP-1: thrombospondin-1

VEGF-A: vascular endothelial growth factor A

αCD8: anti-CD8

αCSF-1: anti-CSF-1

αCTLA-4: anti-CTLA-4

αPD-1: anti-PD-1

Chapter 1:

Introduction

1 Chapter 1: Introduction

1.1 Cancer, metastasis and tumour microenvironment

1.1.1 The nature of cancer

The process by which normal cells evolve into a neoplastic state is initiated by an incipient cell and it is accompanied by acquisition of specific traits that enable the altered cell to became tumorigenic and then malignant. Cancer development is a phenomenon that requires many years and is driven by somatic mutations and natural selection among cells [1]. In fact, cancer is generally accompanied by alteration of the cancer cell genome which leads to certain growth advantages for certain cell sub-clones, thereby allowing their outgrowth and dominance in the local tissue microenvironment. In the same way, tumour progression is a consequence of the expansion of successful clones [2]. Cancer cells are defined by the presence of two fundamental properties: uncontrolled growth and ability to invade and colonize territories normally reserved to other cell types. Cancer invasion includes the ability of cancer cells to break loose, enter into the bloodstream or lymphatic circulation and form secondary tumours, named metastases, in other parts of the body [2].

1.1.2 Metastatic steps

Metastasis is the main cause of death in people with cancer [3] and it is a process that involves the succession of multiple steps [4] (Figure 1.1).

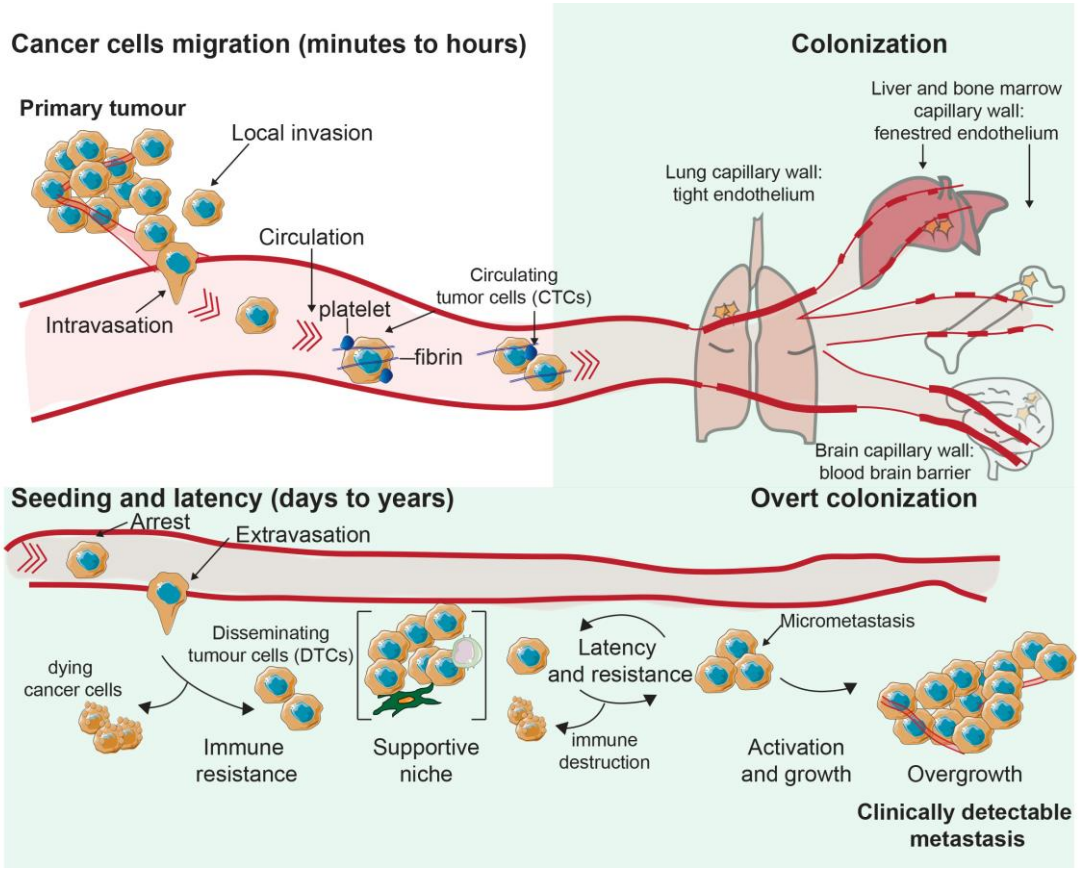

Figure 1.1 The metastatic steps.

The process of invasion and metastasis is a succession of discrete steps that start with cancer cell local invasion and intravasation, it is followed by transit of cancer cells in the near blood and lymphatic circulation and proceeds with subsequent extravasation of cancer cells into the parenchyma of distant tissues. Circulatory patterns (i.e. venous circulation) tend to move the blood and, in consequence, circulating tumour cells (CTCs) preferentially to the lungs and then on, to other organs. In addition to that, the capillary structure of different organs can dictate the extravasation ability of CTCs, thereby influencing their metastatic dissemination. For example, liver and bone marrow endothelium is composed by fenestrated endothelial cells (sinusoids), which might facilitate extravasation; on contrary endothelium of lung or brain capillaries have tight junctions, basement membrane and reinforcement provided by other cell types, thereby generating a barrier for metastatic dissemination instead. The final stage of colonization consists of the formation of small nodules of cancer cells (micrometastasis) that can outgrow and form macroscopic tumours [4]

Cancer cells with invasive abilities disseminate at the primary site and then intravasate into the tumour vasculature as single cells or as a cluster. During this phase, cancer cells undergo cytoskeletal reorganization, lose their cell-to-cell interaction and start to secrete cathepsins and extracellular matrix (ECM) degrading metalloproteinases (MMPs) that allow them to move and migrate through the surrounding stroma. Once in the blood stream, circulating tumour cells (CTCs) are exposed to shear forces, immune system and oxidative stresses. To protect themselves during this process, CTCs associate with platelets and undergo reversible metabolic changes. Once that CTCs arrest on capillaries at distant metastatic sites, they extravasate into the parenchyma of target organs and initiate the colonization process. In this process, CTCs must develop resistance to immunity and host-tissue defences in order to survive [4].

Interestingly, the main rate-limiting step for metastasis formation seems to occur during the colonization of distant organs. Indeed, when disseminating cancer cells (DTCs) reach the new challenging microenvironment of the distant organ they are vulnerable to immune surveillance and host-tissue defence [5].

DTCs settlement into distant organs depends also on the formation of a supportive niche that provides the favourable microenvironment for them to outgrowth [6]. Pre-metastatic niche formation can occur before the arrival of cancer cells through secretion of systemic signals from the primary tumour that induce recruitment of pro-tumourigenic stroma cells at the metastatic site [7]. After initial seeding, cancer cells enter in a latent state as single cells or as a cluster forming micrometastasis. The phase of latency can last months

or decades and this phenomenon explains why months or years after the resection of the primary tumour, patients have a metastatic relapse of the disease [8]. Breaking down latency and/or evasion from anti-tumour immune barriers can be sufficient to initiate the metastatic outgrowth of DTCs [4].

Surgical removal of a malignant tumour is often complemented with radiotherapy and systemic chemotherapy in order to avoid relapse of the tumour. The clinical course of metastatic tumour progression can vary among tumour types and also between patients. For example, locally invasive cancers, such as glioblastoma, form metastasis that only rarely become clinically detectable [9]. Pancreatic cancer, instead is frequently associated with metastasis at the time of diagnosis [10]. If metastasis becomes clinically manifested, systemic therapy such as classic chemotherapy, targeted therapy against oncogenic drivers, immunotherapeutic agents and often a combination of all these is then used. However, despite the advances, therapy usually achieves just a partial reduction of the metastatic tumour [11].

1.1.3 Tumour Microenvironment

Cancer cannot be considered as an aggregate of proliferating cancer cells only. Cancer is a complex tissue formed by multiple distinct cell types that interact with one another. Indeed, cancer cells are able to corrupt and recruit normal cell types, referred as cancer-associate stroma [12].

Stroma cells, including endothelial cells, fibroblasts, pericytes, lymphocytes and myeloid cells are responsible for the formation of the tumour microenvironment (TME) that is the cellular environment in which solid tumour exists. The traditional view for cancer development has portrayed mutated malignant cancer cells as the driving force. However, the TME has

emerged as an equally important determinant in tumour behaviour. The systemic communication between cancer cells and the rich TME sustains the overall tumour growth, homeostasis and progression [13] (Figure 1.2).

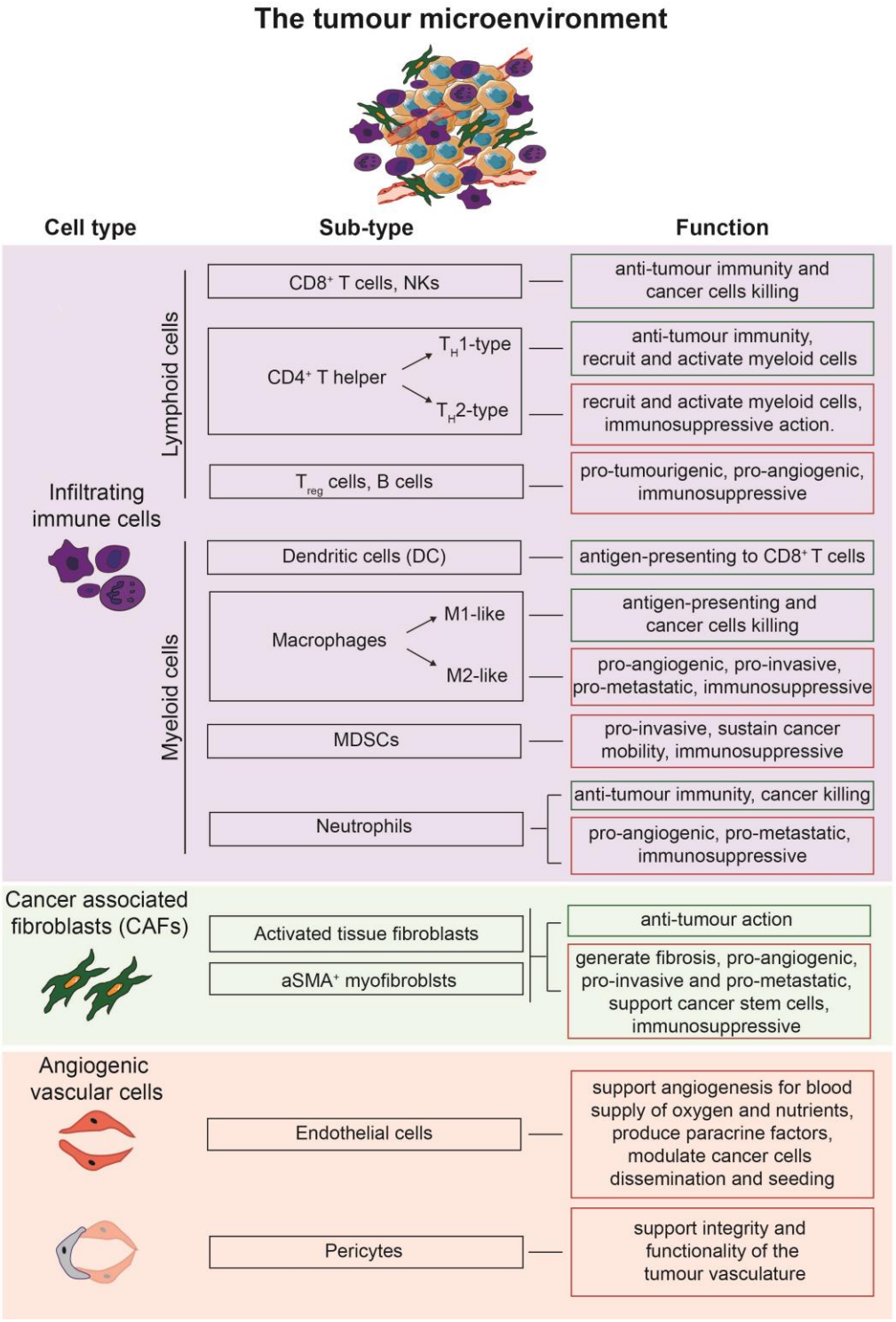

Figure 1.2 The tumour microenvironment.

The figure represents a list of the main cell components of the tumour microenvironment (TME). Tumours do not only consist of cancer cells (orange cells). Normal cell types, which collectively form the tumour stroma, play a key role in either promoting tumourigenesis or in antagonizing it. Tumour stroma includes infiltrating immune cells, cancer associated fibroblatsts (CAFs) and angiogenic vascular cells. Different subtypes for each of these cellular components have been identified and pro- (red) or anti- (green) tumorigenic functions have been associated to the different subtypes. Schematic adapted from [14].

1.1.4 Endothelial cells

Endothelial cells are the stroma cells responsible for the formation of the tumour-associated vasculature in the process of angiogenesis. During the process of angiogenesis, tumour growth is sustained by an 'angiogenic switch' that directs the sprout of new vessels from quiescent existing vasculature [15]. During the angiogenetic process cells deriving from the bone marrow also play a crucial role. Cells like macrophages, neutrophils, mast cells and myeloid progenitors can help the angiogenic switch in previous quiescent tissue. They can infiltrate malignant tumours and assemble at the margin of them, thus facilitating tumour local invasion and protecting the vasculature from drugs targeting endothelial cells [16].

Together with endothelial cells, pericytes are a specialized mesenchymal cells type (related with smooth muscle cells) with finger-like projections that wrap around the endothelial tubing of blood vessels. Tumour associated vasculature integrity and function are highly compromised if pericyte recruitment is impaired, suggesting that pericytes play an important role in promoting angiogenesis and tumour dissemination [17].

1.1.5 Immune inflammatory cells

The long standing knowledge of the role of the immune system in tumorigenesis proposed that immune cells are responsible for recognising and eliminating the majority of nascent tumours [18]. However, today is well accepted that cells of both innate and adaptive immune response can operate in conflicting ways: they can both antagonise and enhance tumour development and progression (Figure 1.2) [19].

The tumour killing action of the immune system is mainly executed by lymphocytes of both innate and adaptive immune response: $CD8^+$ T cells (also known as cytotoxic T lymphocytes (CTLs)), $CD4^+$ helper T (T_H) cells of type-1 (T_H1) and Natural Killer (NK) cells. The implication of these cells in tumour eradication was demonstrated by the fact that tumour arose more frequently and grew more rapidly in immune-deficient mice in comparison with control mice, and that immunodeficiency in the T, NK or both lymphocyte lineages led to increased tumour incidence [20].

Other immune system components are instead pro-tumorigenic. $CD4^+$ T_H cells of type 1, 2, 9, 10, 17 and 22 participate to tumorigenesis in different ways, depending on the type of cytokines they secrete [21]. T_H cells of type-2 (T_H2) cells have tumour promoting capabilities: breast cancer growth has been shown to be accelerated by T_H2 cells via Interleukin (IL)-13 production [22]; T_H2 cells also accelerate the formation of lung metastasis by IL-4 mediated activation of macrophages, which in turn sustain tumour progression via growth factor production [23]. T_H17 cells, depending on the tumour environment they reside, can both exert a pro-tumorigenic role, by sustaining angiogenesis and recruiting myeloid cells, and an anti-

tumourigenic role, by inducing recruitment of $CD8^+$ T cells [24]. Regulatory T cells (T_{reg}) are an immunosuppressive set of T_H cells characterized by the expression of IL-2 receptor α-chain (also known as CD25) and the transcription factor forkhead box 3 (FOXP3). T_{reg} can prevent tumour elimination by inhibiting $CD8^+$ T cells [25]; T_{reg} have been also involved in protecting metastatic mammary tumour cells from immune destruction by secretion of RANKL, which activate its receptor on cancer cells and promotes metastasis [26]. Neutrophils, a class of granulocytic myeloid cells, has been shown to play opposite functions in regulating tumour progression [27]. Indeed, if neutrophil depletion has been shown to induce increase of breast cancer spontaneous metastasis [28]; other reports show that neutrophils can promote metastasis by enhancing entrapment and retention of tumour cells at the metastatic site through production of unique structures called neutrophil extracellular trap (NET), which are composed of extruded DNA and antimicrobial proteins [29]. A type of immature myeloid cells that express CD11b and Gr1 (which comprise Ly6C and Ly6G) molecules is also found in the tumour microenvironment. These cells are referred to as myeloid-derived suppressor cells (MDSCs) and it has been reported that MDSCs suppress immune cytotoxic functions by expressing inducible nitric oxide synthase (iNOS) and arginase 1 at different levels [30]. In a pancreatic tumour mouse model, tumour derived granulocyte-macrophage colony-stimulating factor (GM-CSF) has been shown to recruit MDSCs, leading to the suppression of $CD8^+$ T lymphocytes [31].

B lymphocytes are immunoglobulin (Ig) producer cells. In skin cancer, B cells foster pro-angiogenic and immunosuppressive gene expression programs

and they can activate pro-tumorigenic programs by secreting IL-10 and tumour necrosis factor (TNF) α [32], [33]. A specific subset of B cells, named B_{reg} has been shown to convert $CD4^+$ T cells into T_{reg} cells via transforming growth factor β (TGFβ) secretion [34]. However, the role of B cells in cancer is still under intense examination.

1.1.6 Macrophages

Macrophages constitute the first line of defence of our immune system against invading pathogens. Macrophages are phagocytes and express receptors on their surface that enable them to detect signals that are not normally found in healthy cells [35]. Three different coexisting populations of macrophages can be distinguished in tissues based on their progenitors, development, turnover and mechanism of maintenance. Bone marrow hematopoietic stem cell- derived macrophage precursors are released into the circulation as monocytes and they differentiate in macrophages or dendritic cells upon extravasation into tissues [36]. On the contrary, tissue resident macrophages originate from either the fetal liver or the yolk sac and they develop and persist in adult tissues independently of bone marrow derived hematopoietic stem cells [37]. Tissue resident macrophages include bone osteoclasts, epidermal Langerhans cells, peritoneal macrophages, lung alveolar macrophages, spleen red-pulp macrophages, and liver Kupffer cells. Resident macrophages function as sentinels in order to ensure tissue homeostasis by removing dead cells, toxic materials and pathogens. They can be locally activated, persist in tissue and return quiescent following remission [37]. Infiltrating monocytes derived from bone marrow hematopoietic stem cells are the main source of macrophage replenishment

into inflamed and remodelling tissues, and this process is driven by cytokines and chemokines, such as chemokine (C-C motif) ligand (CCL) -2, CCL5 and macrophage colony stimulating factor-1 (M-CSF-1, or only CSF-1) [38]. There are different markers by which is possible to identify monocyte-macrophages diversity in human and mouse. In human, circulating monocytes, which originate from the bone morrow, can be classified in two subsets: $CD14^+$ $CD16^-$ 'inflammatory' or 'classical' and $CD14^+$ $CD16^+$ 'patrolling' or 'non-classical' monocytes. In the same way, mouse 'inflammatory' monocytes are classified as $CD11b^+$ $Ly6C^{high}$ $CCR2^{high}$ $CX3CR1^{low}$, in contrast 'patrolling' monocytes are $CD11b^+$ $Ly6G^{low}$ $CCR2^{low}$ $CXCR3^{high}$ [39]. A protective role has been associated to 'patrolling' monocytes, for example they seems to monitor the lung microvasculature under steady-state conditions and rarely extravasate into tissue [40]. Macrophages are a population of heterogeneous and plastic cells [41]. Once resident in tissues, macrophages acquire a distinctive phenotype in response to different signals present in the microenvironment (Figure 1.3). Environmental stimuli, like interferon gamma (IFNγ) or microbial products, like lipopolysaccharide molecule (LPS) induce a classical activation of macrophages and skew them toward a M1-like or 'classically activated' macrophage phenotype. M1-like macrophages mediate anti-microbial and tumoricidal response by secreting inflammatory cytokines, such as TNFα, IL-12, reactive oxygen species and nitric oxide (NO), by up-regulating the expression of major histocompatibility complex (MHC II) and by promoting a T_H1-type of response. Alternatively, if the microenvironment becomes populated by different types of cytokines and growth factors, like the T_H type-

2 cytokines IL-4 and IL-13, macrophages are stimulated to acquire an alternative activation state, resulting in an M2-like subtype. M2-like polarized macrophages are characterized by expression of anti-inflammatory cytokines, such as IL-10, lower expression of pro-inflammatory cytokines, up-regulation of scavenger receptors, such as mannose receptors (MRC1/CD206 and CD163) and reduced ability to activate adaptive immune response. As such, M2-like macrophages may facilitate resolution of inflammation and promote tissue repair after acute inflammation phase. The M1-like and M2-like phenotypes are anyhow considered as extreme ends of a continuum of activation states which depend on the signals present in the microenvironment in a given moment [42], [43].

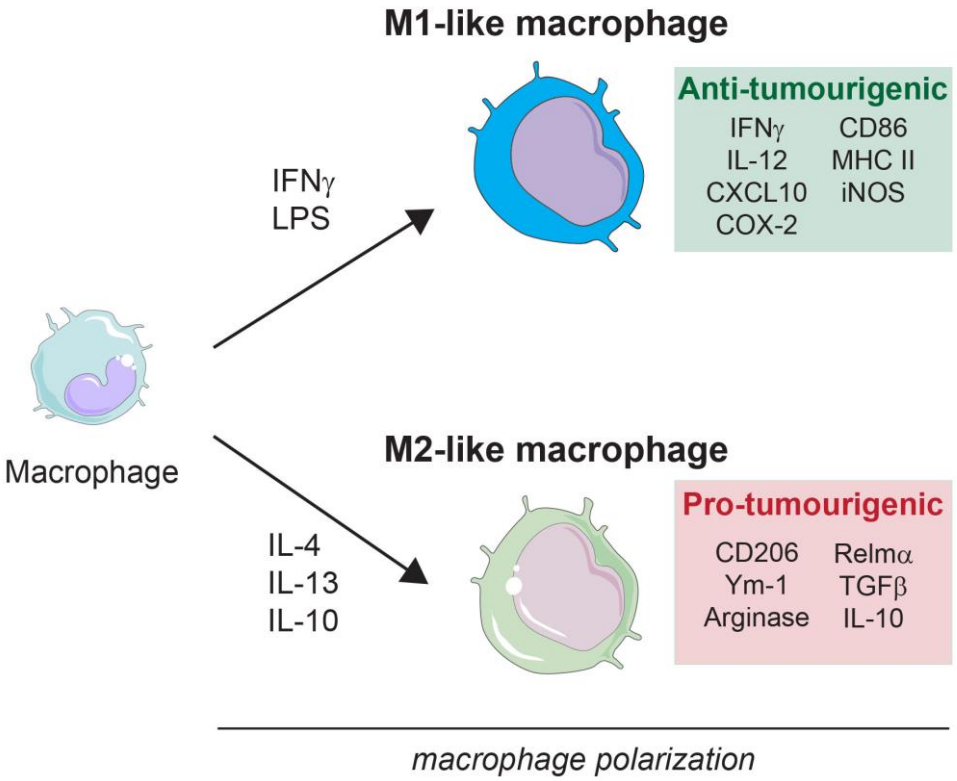

Figure 1.3 Macrophage polarization.

Schematic representation of M1-like and M2-like macrophage phenotypes and common markers used for their identification. Depending on the cytokine milieu in tissue microenvironment, macrophages can acquire a M1-like (or classical) or M2-like (or alternative) activation phenotype. M1-like macrophages are considered anti-tumorigenic, have antigen presenting ability (CD86; MHC II), express pro-inflammatory cytokines (IFNγ; CXCL10; IL-12) and inflammatory factors (Ciclooxigenase-2, COX-2; iNOS). In contrast, M2-like macrophages are pro-tumorigenic, express high level of scavenger receptors (CD206), anti-inflammatory proteins (Chitinase-like protein 3, Ym-1; Resistin-like molecule alpha, Relmα; Arginase) and secrete immunosuppressive factors (IL-10 and TGFβ).

During cancer progression, tumours recruit a variety of immature myeloid cells that include $Ly6C^{+}/CCR2^{+}$ inflammatory monocytes and MDSCs [44]. MDSCs comprise precursors of both the mononuclear monocyte/ dendritic cell (DC) lineage and precursors of the neutrophils, granulocytes lineage.

Inflammatory monocyte and monocyte-related-mononuclear M-MDSC can infiltrate into neoplastic tissues, upon recruitment, and differentiate into tumour associated macrophages (TAMs) [30], [45]. Recruitment of circulating cells is required to maintain TAMs population, instead whether tissue macrophages derived from embryonic precursors contribute to number, location and diversity of TAMs is not fully elucidated [46].

Monocytes are recruited into the tumour site by chemokines secreted by tumour and stroma cells including vascular endothelial growth factor (VEGF), semaphoring 3A (SEMA3A), CCL2 and chemokine (C-X-C motif) ligand (CXCL) -12. In tumours, the signals that orchestrate macrophage function can vary between different tumour types, or even between different parts of the same tumour resulting in diverse TAM phenotypes [47]–[50]. TAMs with a relatively M1-like skewed phenotype are found to be associated with the early phases of tumour development or with regressing tumours. Classically activated M1-like macrophages can kill tumour cells and they mediate tissue-destructive reactions by taking part in the early elimination phase of immunoediting orchestrated by $CD8^+$ cytotoxic T lymphocytes and interferons. Tumour progression and change in the microenvironment dictated by T_H2 cell-derived IL-4 and IL-13 induce a macrophage phenotypic switch and subversion of their functions toward an M2-like activation state [51]. Generally, TAM polarization toward an M2 phenotype seems to be a common feature for many cancers although their relative abundance depends on the tumour type. [52]–[54].

TAMs are involved in all the step of cancer progression by supporting tumour cell invasion, angiogenesis, intravasation, motility, extravasation and

metastasis formation. Indeed, epidemiological evidences indicate that the presence of TAMs is often correlated with a poor disease prognosis in different forms of cancer, such as colon, breast and lung [55].

1.1.7 Fibroblasts

Fibroblasts are the principal component of the connective tissue [56]. In particular, fibroblasts are embedded in the fibrillar ECM of the connective tissue and they are also involved in its synthesis. The ECM is a network of fibrous proteins such as collagens and fibronectins, which are nested in a viscoelastic gel of glycosaminoglycans, such as hyaluronic acid (HA), proteoglycans and glycoproteins. The ECM act as a reservoir of cytokines and growth factors, it provide the structural framework for all tissue and it is also involved in regulating the interstitial fluid volume and pressure [57]. Fibroblasts play a crucial role in maintaining ECM homeostasis and in regulating ECM turnover. Fibroblasts synthesize many of the ECM components such as type I, III, V collagens and fibronectins [58] as well as they are an important source of ECM degrading proteases such as MMPs [59]. Fibroblasts have a prominent role in the wound healing process: when tissue damage occurs, fibroblasts invade lesions and enhance the synthesis of ECM contractile fibres including α-smooth muscle actin (αSMA) that function as a scaffold for other cells [57]. In a site of wound healing, fibroblasts are highly proliferative in comparison to fibroblasts present in normal tissues [60]–[62]. Increased activity of fibroblasts results in the deposition of a reactive stroma, referred as desmoplastic reaction. Fibroblasts that mediate this process are said to be ‘activated’ and are referred to as myofibroblasts [63]. Once the wound healing process is

terminated, it is still unclear whether activated fibroblasts revert to a resting phenotype or undergo a particular type of apoptosis called nemosis (programmed necrosis), or are removed by tissue granulation [57], [64].

Fibroblasts in tumours are often referred as CAFs and they are key players in the process of tumorigenesis. CAFs can have multiple origins and they are a heterogeneous population of cells that have the common capacity to alter the tumour microenvironment and change the fate of neoplastic cells [65].

The most predominant source of CAFs consists of resident tissue fibroblasts and mesenchymal stem cells, but several studies have also reported the recruitment of a type of bone-marrow derived precursor cells named fibrocytes to the tumour lesion followed by their differentiation into myofibroblasts and fibroblasts [60], [66]–[68]. Although stellate cells are a different cell type, they share many of the functions of fibroblasts. Stellate cells in a quiescent state are vitamin A storing and lipid droplet containing cells that can be found in the liver, pancreas, kidney, intestine, lung and skin [69]. Upon activation, stellate cells express high levels of αSMA and acquire a myofibroblast like phenotype. Furthermore, in pancreatitis, pancreatic cancer and liver fibrosis, stellate cells are found to be the major responsible for the induction of desmoplastic reaction and thereby are classified as CAFs [70].

An unique consensus has not yet been found for the molecular definition of CAFs since heterogeneous cell populations are involved in generating CAF populations [56]. Several markers have been suggested to define CAFs; so far αSMA has been considered as commonly recognized strong marker to identify CAFs [71]. However, αSMA expression has been detected in other

cell types such as pericytes, smooth muscle cells surrounding the vasculature, visceral smooth muscle cells and cardiomyocytes [72]. Other markers commonly used for CAFs identification in breast, lung, ovarian and pancreatic cancers are fibroblast-activation protein α (FAPα), vimentin, fibroblast specific protein (FSP-1/also known as S100A4), caveolin 1 (CAV1), platelet derived growth factor receptor (PDGFR) -α or β, desmin and discoidin-containing receptor 2 (DDR2) [73], [74]. However, it is important to note that none of these markers are completely specific for CAFs, thus rendering their study more complicated.

Due to the intrinsic role of fibroblasts in maintaining epithelial homeostasis and proliferative quiescence [75], it has been shown that normal tissue-associated fibroblasts (NAFs) isolated from different organs can inhibit the growth of neoplastic cells [76]. Therefore, neoplastic cells must acquire the capacity to recruit fibroblasts from the different sources listed before and/or re-programme normal resident fibroblast population to benefit from their tumour supportive role. Several ways exist by which tumours can influence their microenvironment and educate it to promote their growth and progression. Neoplastic cells can drive the production of oncogenic signals by secreting fibroblast-activating factors which promote fibroblast activation in a way that mimic the microenvironment characteristics of the wound healing process [74]. TGFβ is the major regulator of fibrosis and is one of the most studied cancer derived growth factor affecting CAF activation [77].

Tumour cells are also known to express PDGF, which is considered to be an important initiator of desmoplastic reaction in tumours. It binds to its cognate receptors on the surface of fibroblasts, thereby stimulating CAFs proliferation

[78]. In addition, basic fibroblast growth factor (bFGF) [79], secreted cytokines such as IL-6 [80], or lysophosphatidic acid (LPA) [81] are neoplastic cell secreted mitogens involved in stimulating fibroblast activation and proliferation. Beside production of growth factors and cytokines, other mechanisms have been reported to be associated with CAF activation: cancer derived exosomes can transfer proteins and RNAs from one cell to another and mediate the recruitment and activation of fibroblasts within tumours [82]. Hypoxia and reactive oxygen species (ROS) induce activation of CAFs through the accumulation of hypoxia inducible factor (HIF)-1α [83].

If tumour cells reprogram the tumour microenvironment in a beneficial milieu for their development, CAFs in turn orchestrate the main processes underlying cancer progression and invasion through the secretion of different hormones, growth factors and cytokines, such as hepatocyte growth factor (HGF), connective growth factor (CTGF), epidermal growth factor (EGF), insulin-like growth factor (IGF), nerve growth factor (NGF), bFGF as well as cytokines such as CCL7 and CXC12 [56]. The cross-talk between neoplastic cells and CAFs has been shown to influence tumour development in different ways starting from its initiation to the promotion of invasiveness and metastasis.

CAFs are also involved in the recruitment of other cell types to the tumour, promote migration and facilitate invasiveness of cancer cells by regulating ECM remodelling. CAFs induce ECM remodelling by producing Lysyl oxidase (LOX), an enzyme responsible for alteration of collagen crosslinking that confer tumour stiffness and facilitate tumour growth [84].

While the majority of the literature associates CAFs with a tumour-promoting role, some studies suggest that certain fibroblast subsets may also have a tumour restraining activity. It has been shown that CAFs have a restraining role for pancreatic cancer progression, as generation of tumour bearing transgenic mice deficient for αSMA^{+} cells enhanced hypoxia, epithelial to mesenchymal transition (EMT) in tumour cells and lead to increased T_{reg} cells accumulation, thereby reducing animal survival [85]. A report showed evidence that CAFs can be also implicated in promoting anti- tumour host defence by modulating the innate and adaptive immunity through secretion of cytokines such as TNFα, IFNγ and IL-6, which help to recruit and polarize macrophages, T lymphocytes and NKs [86]. Although it was initially postulated that targeting of sonic hedgehog (Shh) pathway leads to stroma collapse and increased vascularity together with enhanced response to gemcitabine treatment in a pancreatic cancer pre-clinic mouse model [87], the same authors, a few years later showed that this was only a short-term effect. Indeed, they observed that genetic or pharmacological inhibition of Shh signalling reduced desmoplasia, but it also induced acceleration in tumour growth, increased metastasis and ultimately induced rapid death of tumour bearing mice [88].

1.1.8 Role of macrophages in fibrosis

Inflammation is a hallmark of cancer and macrophages are one of the main immune cell infiltrates. During the wound healing process, macrophages have been shown to exhibit critical regulatory capacities in all the stages of repair and fibrosis. Indeed, macrophages are important sources of chemokines, MMPs and other inflammatory mediators that drive cellular

response following injury [89]. Similarly, macrophage derived factors have also been linked to cancer [90]. Thus, because macrophages as well as fibroblasts critically modulate cancer progression and metastasis, understanding macrophage contribution to fibrosis may open new opportunities to the discovery of anti-cancer targets able to dampen in parallel both the fibrotic and immune pro-tumorigenic functions of the tumour stroma.

Although it is not generally accepted, many studies involved in understanding the fibrotic regulative role of macrophages indicated that anti-inflammatory, IL-4-induced macrophages are the main macrophage subset involved in modulating tissue repair and fibrosis. Indeed, it has been shown that macrophages are involved in development of (bleomycin) pulmonary fibrosis, as depletion of $Ly6C^{hi}$ population was associated with reduction in fibrosis and decrease expression of several M2-like markers such as Ym-1 and arginase-1 [91]. Macrophage secreted TGFβ also has pro-fibrotic functions as reported in the case of idiopathic pulmonary fibrosis [92]. Liver Kupffer cells also secrete TGFβ upon uptake of pancreatic cancer cell-derived exosomes, thereby triggering the generation of a fibrotic microenvironment responsible for establishing a pre-metastatic niche in pancreatic cancer [7]. In addition, it has been shown that hepatic macrophages can induce survival of activated Hepatic Stellate Cells (HSCs) by stimulation of nuclear factor kappa B (NF-kB) activity, which is then responsible for fibrosis formation in to the liver [93] . Macrophages are also important producers of MMPs, enzyme that degrade all kind of ECM proteins. In the case of pancreatic cancer, delivery of CD40 agonist stimulated the systemic release of IFNγ and CCL2,

thereby promoting intra-tumoural infiltration of anti-fibrotic monocytes/macrophages. The anti-fibrotic role of monocytes / macrophages was mediated by increased MMP13 secretion and led to reduction in desmoplasia and enhanced chemotherapy delivery. The latter study demonstrated that rewiring of macrophage phenotype induced by CD40 and mediated by IFNγ may be a beneficial strategy to target tumour-associated fibrosis [94].

1.1.9 Granulin

The Granulin (*GRN*) gene encodes for progranulin (PGRN) protein, which is also known under the names of acrogranin, granulin/epithelin precursor (GEP), proepithelin (PEI) or PC cell-derived growth factor (PCDGF). Different research groups identified independently the parent protein or its derivatives in specific tissues or cells. Indeed, as the nomenclature suggests, progranulin has been found in association with granulocytes and cells of the innate immune response but also with epithelial cells [95]. PGRN is a highly glycosylated protein that comprises seven full and one half conserved granulin domain connected by a short linker region [96]. PGRN can be proteolytically cleaved to release individual granulin peptides, which possess independent functions, sometimes in contrast to the function of the full-length precursor. Multiple proteases are involved in the cleavage of PGRN such as neutrophil elastase, proteinase 3 and MMP9, MMP12 and MMP14 [97]–[100]. PGRN and granulin peptides can regulate different biological functions even though a unique cell surface receptor has not been identified yet. Up to now, PGRN has been shown to interact with different binding proteins depending on the cell type. PGRN binding with the transmembrane protein sortilin

regulates PGRN levels in the brain by endocytosis [101]. PGRN and granulins interaction with tumour necrosis factor receptor (TNFR) 1 and 2 can induce anti—inflammatory effect [101]. Instead interaction of PRGN with EphA2, a member of receptor tyrosine kinase (RTKs) has been shown to be involved in human urinary bladder cancer cell line through MAPK and Akt signalling pathway [102]. *In vitro* and *in vivo* studies have demonstrated the importance of the role of PGRN in diverse physiological processes such as early embryogenesis [103], wound healing [104], inflammation [99], [105] and angiogenesis [106]. Moreover PGRN is a neurotropic and neuroprotective factor that shields neural tissue from inflammation and degeneration. Indeed loss of function mutations in the *GRN* gene has been associated with neurological and neurodegenerative disease such as in frontotemporal dementia, Alzheimer's disease and Parkinson's disease [107], [108].

PGRN overexpression has been observed in many different types of cancer such as breast, liver, renal and colorectal cancer and high PGRN expression has been correlated with many of the tumour progression steps [101]. Both *in vivo* and in *vitro* studies suggested a mitogenic role for PGRN in stimulating the proliferation of epithelial cells and several cancer cell lines [101]. PGRN has been also found to promote migration and invasion by multiple mechanisms, among which EMT, activation of different MMPs and focal adhesion kinase (FAK) pathway [101]. PGRN function has also been reported to renders hepatocellular carcinoma resistant to NK cell-mediated cytotoxicity thereby suggesting PGRN involvement in mediating tumour-immune evasion [109]. A correlation between high expression of PRGN in tissues, serum or urine from malignant tumour and short overall survival has

been observed in the case of epithelial ovarian cancer [110]–[112], breast cancer [113], bladder [114] and prostate cancer [115], thus suggesting that PGRN can be an useful biomarker for some type of tumours and that its expression can be monitored to predict patient prognosis.

PGRN is often expressed under conditions of tissue remodelling where cells are proliferating and actively migrating; for adult epithelia, it is abundant in regions characterized by high turnover such as epidermal keratinocytes. Fibroblasts and endothelial cells, which are normally quiescent show low level of PGRN, however PGRN expression on these cells increase dramatically during the phase of wound healing as fibroblasts increase their proliferation and migration. Evidences have led to the association between PGRN and tissue repair process. Induced skin wound in mice has been proposed to enhance increased expression of PGRN. PGRN responds to injury both as paracrine mediator from inflammatory cells (macrophages and neutrophils) and also as a locally induced growth factor from dermal fibroblasts and endothelial cells thereby stimulating inflammation, fibroblast accumulation and new blood vessels formation, each of which is essential for tissue repair [104]. In accordance to this, another report identified granulin (GRN) as a protein secreted from a subtype of hematopoietic myeloid cells activated in the bone marrow and recruited in response to breast tumour induction. In this case, GRN has been associated with activation of pro-inflammatory and matrix-remodelling gene expression in fibroblasts, thus inducing tumour stroma desmoplasia and cancer progression [116]. In our group, it has been shown that bone marrow derived macrophages are recruited into the liver in response to pancreatic cancer metastasis

development. Macrophage secretion of PGRN led to the activation of liver resident hepatic stellate cells, which were responsible of fibrotic stroma formation and metastatic growth progression (Figure 1.4) [117]. The precise signalling pathways by which GRN activate tumour fibroblasts are still unknown, and the cognate cell-surface receptor for GRN has been not yet identified.

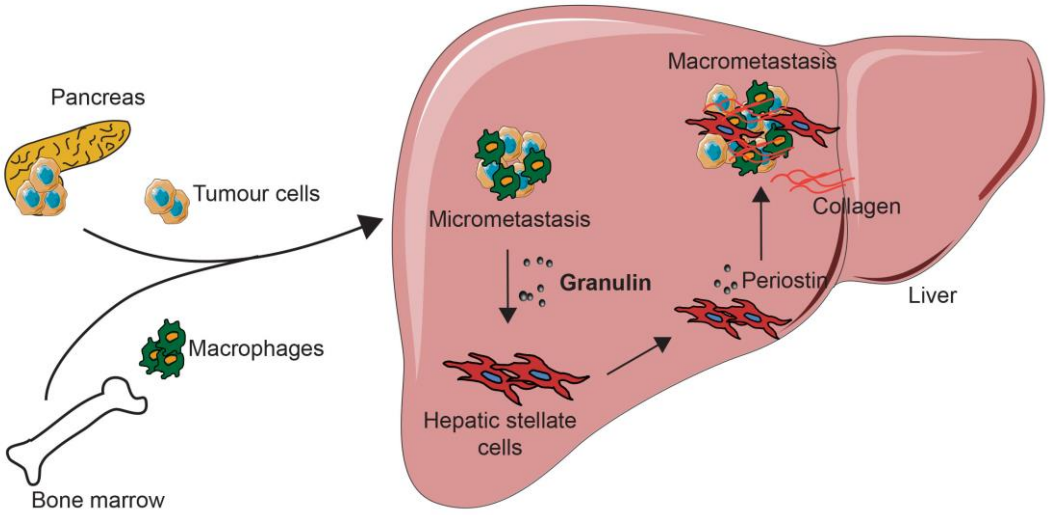

Figure 1.4 Macrophage-secreted granulin supports pancreatic cancer metastasis by inducing liver fibrosis.

Schematic representation of mechanisms by which macrophage-secreted granulin promotes liver metastasis in pancreatic cancer. Bone marrow derived inflammatory monocytes are recruited into the liver and differentiate into metastasis associated macrophages (MAMs). MAM secreted granulin activates liver resident hepatic stellate cells (HSCs), which in turn secrete periostin resulting in a fibrotic microenvironment that sustain metastatic growth [117]. Schematic adapted from [118].

1.2 Immunoncology and Immunotherapy

1.2.1 Immunoediting

Tumour immunoediting is a dynamic process that occurs in cancer and encompasses three sequential phases: elimination, equilibrium and escape (Figure 1.5).

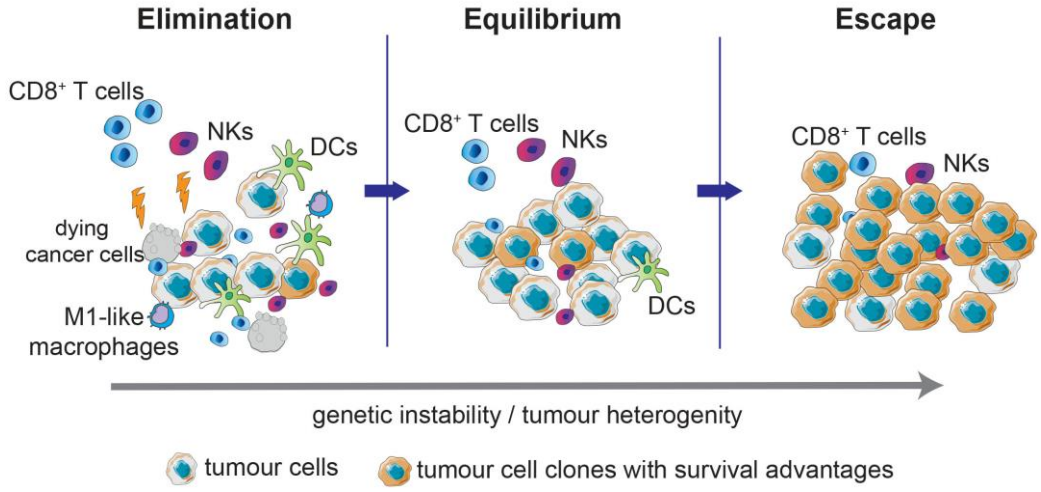

Figure 1.5 Immunoediting.

Schematic representation of the three phases of tumour immunoediting. The elimination phase involves the anti-tumour immune response against tumour development. In this phase, natural killer cells (NKs), $CD8^+$ T cells, dendritic cells (DCs) and M1-like macrophages are involved in tumour cell killing. Many cancer cells die during this phase, but the ones who escape or have a non-immunogenic phenotype, initiate the next phase, which is the one of equilibrium. During equilibrium phase, immune system and tumour cells enter in a dynamic equilibrium in which the anti-tumorigenic pressure exerted by the immune system is enough to contain but not eliminate cancer cells. In this phase, in the cancer cell population new variants arise, thus further increasing overall resistance to immune attacks. In the escape phase, tumour cells resistant to immune killing continue to grow and expand leading to malignancy formation. Schematic adapted from [119].

It relies on the constant interaction between tumour cells, immune cells and tumour microenvironment, and it takes both the tumour protective and the tumour promoting role of the host immune system into account. As previously mentioned, to grow and form metastasis tumours need to circumvent the barriers posed by the host natural immunity. Elimination of the tumour depends on immunosurveillance mechanisms and it is based on the concept that cancer cells represent an “altered self” and express “non-self” antigens, thereby are subjected to activated T and NK cell mediated killing. When the elimination of the developing tumour is successful, it represents the complete elimination process of tumours, without any further progression into the successive phases. In the Equilibrium phase, the host immune system and tumour cells enter into a dynamic equilibrium. The pressure exerted by T lymphocytes and the IFNγ response on the tumour cells is enough to contain but not completely eradicate tumours that at this point contain many genetically unstable and highly mutating cell clones. During this process, many cancer cells are destroyed but many others arise by Darwinian selection of tumour cell clones able to resist immune attacks and/or by generation of non-immunogenic tumour variants. This phase is the longest, it can last many years and it could terminate either with complete extinguishment of the tumour or with escape of the resistant cancer cells from immunologic detection and elimination with subsequent expansion of the tumour in an uncontrolled manner [119].

In 2013, the journal “Science” named cancer immunotherapy its “Breakthrough of the Year” on the basis of the therapeutic benefit obtained by the use of immune check point blockers and T lymphocyte engineered to

express chimeric antigen receptor (CAR) specific for recognizing tumour antigens. Cancer immunotherapy treatment focuses on targeting the host immune system rather than the tumour itself in order to enhance cancer cells recognition and to amplify the endogenous anti-tumour response with the aim of tumour eradication [120].

The revolution of cancer immunotherapy is represented by the durability of the therapy response, most likely due to the ability of T cell mediated adaptive immunity to maintain memory of their target, which then translates into long-term survival for a subset of cancer patients. Indeed, in patients treated with cancer immunotherapy the rate of relapse remain low as opposed to patients treated with targeted oncogene therapies, in which tumour responses last until the cancer develops a way to bypass oncogene blockade.

However, resistance to immune checkpoint blockade therapy is still a major problem, both for cancer types that do not respond at all to the treatment, as well as for the types of cancer that have only an initial response to the therapy [121].

1.2.2 Role of $CD8^+$ T cells

Cytotoxic T cells typically express the molecule CD8 on their surface and exert a cytotoxic cell-mediated function that depends on direct interaction between T cell antigen receptor (TCR) on the surface of $CD8^+$ T lymphocytes and cells bearing the foreign antigen (pathogen infected cells or tumour cells). Tumour antigens can be derived from oncogenic viruses, differentiation antigens or from mutations that occur during the process of carcinogenesis [122]. Antigens are presented as a complex formed by (tumour)-derived peptide bound to the MHC molecule and are exposed on the surface of tumour cells. However, $CD8^+$ T cells recognition of cancer cells can occur only if $CD8^+$ T cells are activated to recognise a specific antigen. Activation of naïve $CD8^+$ T cells does not depend only on TCR binding with tumour antigen, but it needs the presence of additional co-stimulatory signals [123]. Engagement of CD28 on $CD8^+$ T cell surface with B7 molecules (CD80 and CD86) on the surface of antigen presenting cells (APC) leads to activation of naïve $CD8^+$ T cells at the level of tumour draining lymph nodes. B7 molecules are exclusively expressed in a subset of hematopoietic cells, especially DC, which are cells specialized in antigen presentation [124]. Killing of cancer cells mediated by inflammatory processes or by anti-cancer treatments, including chemotherapy for example, enables APCs, such as DCs, to recognize and take up cancer released antigens. APCs process tumour derived peptides and present them as part of the antigen-MHC complex alongside with B7 molecules, to naïve $CD8^+$ T cells, thereby priming their activation. Upon activation, $CD8^+$ T cells acquire effector functions against cancer specific antigen; they are released into the circulation and

infiltrate into the tumour site where they mount an attack against tumour cells that express the specific antigen for which they are activated to. Killing of cancer cells is mediated by $CD8^+$ T cell derived cytotoxic cytokines such as IFNγ, and T cell secreted granules including perforines and granzymes. Cancer cell killing results in the release of new additional cancer cell derived antigens which burst and strengthen the anti-tumour response in subsequent revolutions of anti-cancer immunity cycle [122] (Figure 1.6).

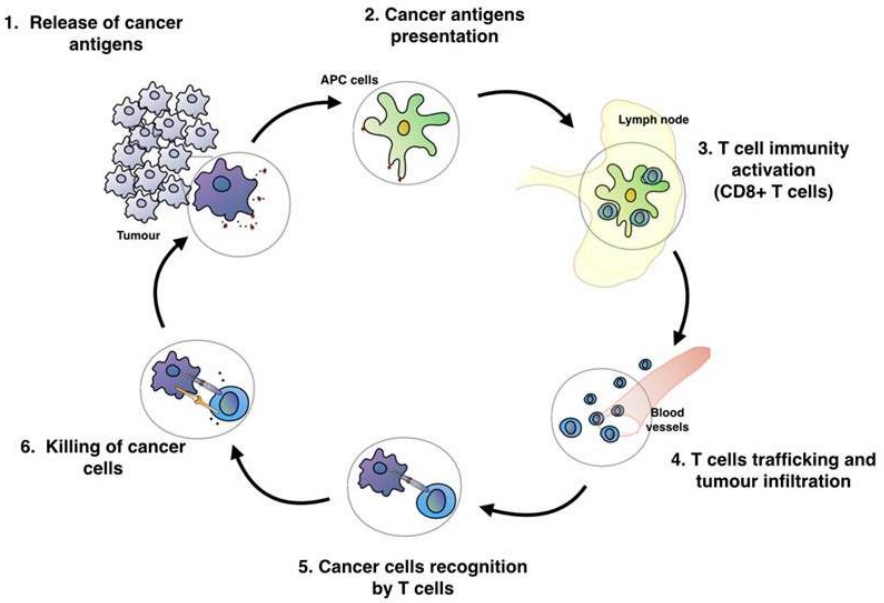

Figure 1.6 Tumour-immunity cycle.

Schematic illustration of the host immune response against tumour formation. Tumour antigens are recognized as “non-self” molecules by antigen presenting cells (APCs), which are responsible of the activation of naïve CD8+ T cells at the level of lymph nodes. Active CD8+ T cells are the effector cells of anti-tumour immune response; they are released into the circulation and reach the tumour site. Upon recognition of tumour cells by T cell receptor (TCR)-MHC molecule interaction, CD8+ T cells promote tumour cells killing by releasing cytolytic factors and inflammatory cytokines. Cancer cell death, in turn, leads to the release of additional antigens that further boost CD8+ T activation and activity. Schematic adapted from [122]

1.2.3 Immune Checkpoints and T cell exhaustion

Regulation of the T cell response is a complex process consisting of both stimulatory and inhibitory cell intrinsic pathways. The process of $CD8^+$ T cell activation not only leads to initiation of T cell proliferation and differentiation, but also involves the induction of inhibitory pathways that can attenuate and terminate T cell responses. The expression of T cell inhibitory pathways is a physiological response to limit $CD8^+$ T activity and prevent the insurgence of autoimmune diseases [125]. In the same way, tumours can exploit T cell inhibitory pathways for their own benefit, thus promoting escape from tumour eradication.

Cytotoxic T-Lymphocyte Antigen 4 (CTLA-4) is expressed upon T cell activation and it has very high homology to CD28, and as CD28, it binds B7 molecules. CTLA-4 accumulates in T cells at the T cell-APC interface until it reaches a level sufficient to block co-stimulation of CD28 by competitively binding to B7 molecules, thereby abrogating T cell activation and response. Based on this knowledge, Allison's group proposed that blockade of CTLA-4 could allow a sufficient T cell stimulation to activate the T cell response and achieve tumour eradication. The group tested in several mouse experiments the use of anti-CTLA-4 (αCTLA-4) antibody in combination with cancer cell killing agents in order to prime antigen release and activation of T cells before CTLA-4 blockade [126]–[129]. The successfully obtained data led to the development and successive approval in 2011 of Ipilimumab, an antibody against human CTLA-4. It considerably improved the overall survival in patients with metastatic melanoma [130], [131], renal cell carcinoma [132],

prostate cancer [133], urothelial carcinoma [134] and mammary carcinoma [129].

In 2000, Programmed cell death-1 (PD-1) emerged as another dominant immune check-point receptor that limits the response of activated T cells [135]. PD-1 has two ligands, PD-L1 (also known as B7H1 or CD274), which is broadly expressed by many cell types mainly upon exposure to pro-inflammatory cytokines, and PD-L2 (also known as CD273 or B7-DC) which instead has more restricted expression on antigen presenting cells [125]. The function of PD-1 is different from the one of CTLA-4. CTLA-4 interferes with co-stimulation of T cells, it is involved in the regulation of the amplitude of T cells activation at the early stages and it acts at the level of lymphatic organs. In contrast, the major role of PD-1 is in peripheral tissues where it limits the activity of T cells during inflammation [125].

$CD8^+$ T cells repetitively recognize cognate antigens as the tumour develops and form metastases. Triggering of TCR results in the production of inflammatory cytokines, including IFNγ, which is the main stimulator of PD-L1 expression in targeted cells. Chronic PD-L1 engagement by PD-1 results in continuous PD-1 signalling in T cells and induction of epigenetic programs that lead to T cell exhaustion [125], [136]. T cell exhaustion is a state of T cell dysfunction in a chronic inflamed environment (Figure 1.7).

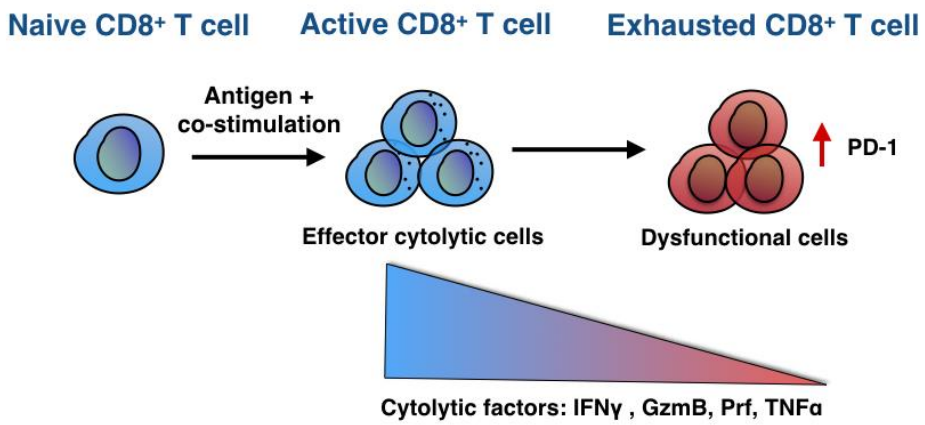

Figure 1.7 CD8+ T cell exhaustion.

Naïve $CD8^+$ T cells differentiate and activate into effector $CD8^+$ T cells upon antigen recognition and co-stimulation mediated by antigen presenting cells (APC). Once at the tumour site, active $CD8^+$ T cells recognise the tumour by T cell receptor (TCR)-tumour antigen interaction and direct their effector anti-tumour activity through secretion of cytokines and lytic molecules such as IFNγ, TNFα, Granzyme B (GzmB) and perforin (Prf). However, within the tumour microenvironment, $CD8^+$ T cells can acquire a dysfunctional or exhausted phenotype characterized by a progressive loss in effector cytolytic factors and increased expression of inhibitory receptors, including PD-1 [138].

During an effective immune response, naïve $CD8^+$ T cells rapidly differentiate into effector T cells with unique metabolic, functional and migratory properties that promote cellular proliferation and infiltration into peripheral tissues. Following antigen recognition, T effectors rapidly express cytokines and lytic molecules that mediate specific killing of pathogenic or transformed cells. The majority of T effector cells undergo apoptosis following antigen clearance, a minor fraction instead differentiate into long lasting T memory cells that will rapidly respond if the same antigen is again encountered [137]. During chronic infections and in the setting of many progressing tumours, the

functional capacity of T effectors cells is compromised. The principal characteristic of exhausted T cells is the progressive loss of effector functions, which generally occurs in a hierarchical manner and includes loss of IL-2, TNFα, IFNγ, Granzyme B (GzmB) and Perforine (Prf) production. Moreover, exhausted T cells express high level of inhibitory receptors in addition to PD-1, such as LAG-3, CD244, TIM-3, CTLA-4; and it has been observed that the pattern of inhibitory receptors that are co-expressed by the same $CD8^+$ T cell can substantially affect the severity of dysfunction. The phenotype acquired by dysfunctional T cells affects their survival, proliferation and cytotoxic function and although exhaustion is not a terminal state, it can lead to T cell apoptosis [138].

PD-1 is therefore a negative regulator of a pre-existing immune response and its blockade has become relevant in cancer therapy because of its potential to reverse T cell exhaustion with subsequent stimulation of anti-tumour immunity. Furthermore, the induction of the PD-1 pathway during chronic stimulation and its specific action on anti-tumour T cell immunity renders the therapeutic activity of its blockade restricted toward cancer cells, with limited toxicity for patients in comparison to αCTLA-4 inhibitory antibody therapy [139] [140].

Antibodies targeting the PD-1 /PD-L1 axis have shown clinical durable response in multiple tumour types. The first anti-PD-1 (αPD-1) inhibitory antibodies (Pembrolizumab and Nivolumab) received the Food and Drug Administration (FDA) approval in 2014 and since then, a total of eleven anti-PD-1 / PD-L1 inhibitory antibodies are under development and/or have been approved for treatment of melanoma, metastatic non-small cell lung cancer,

head and neck cancer, renal cell carcinoma, Hodgkin's lymphoma and gastroesophageal, bladder and urothelial cancers [140]. Also, CTLA-4 and PD-1 regulate distinct inhibitory pathways and have non-overlapping mechanisms of action, thus suggesting that the use of combinatorial treatment could improve the efficacy of single treatment [141]. Clinical trials have reported increased survival advantages after the combinatorial treatment in more than 80 % of advanced melanoma patients with almost 50 % in tumour reduction [140], [142].

However, despite the enormous clinical benefits given by the use of immune checkpoint therapy, only a small fraction of patients and only certain tumour types respond positively to this kind of therapy. Therefore, there are ongoing attempts to identify predictive biomarkers that could be used to select patients for treatment.

Because PD-1 ligand can be expressed on tumour cells but also on epithelial, endothelial, fibroblasts and immune infiltrate cells, there have been efforts to use expression of PD-L1 as a criterion for selecting suitable patients for treatments with antibodies targeting the PD-1 / PD-L1 pathway. However, it is now become clear that PD-L1 expression in tumour tissue could not be used a predictive biomarker since it was noticed that PD-L1 negative tumours, although at a lower response rate than PD-L1 positive tumour, were responsive to αPD-1 treatment [120], [143], [144]. Moreover, it was also reported that PD-L1 expression was discordant between primary and metastatic tumours in patients with metastatic melanoma and that patients with PD-L1 positive tumours together with high infiltration of $CD8^+$ T cells had an overall increased survival in comparison to tumours that had

only one of these features [145]. These data suggest that the presence of an active T cell response within the tumour is the key factor for prediction of anti-PD-1 / PD-L1 therapeutic benefits. Indeed, the therapeutic potential of PD-1 / PD-L1 therapy is determined by a pre-existing anti-tumour T cell response. In such a response, recognition of tumour antigens by TCR on $CD8^+$ T cells triggers the expression of PD-1 on the T cell surface and release of IFNγ, which in turn induces expression of PD-L1 by cancer cells [146]. This process, named adaptive immune resistance is the mechanisms by which PD-L1 expressing tumour cells are able to evade immunosurveillance mechanisms and it can be reversed by blockade of PD-1 - PD-L1 interaction [147].

1.2.4 Obstacles to anti-tumour immunity

The plethora of mechanisms by which tumours evade immunity is currently the subject of intense investigation and comprises tumour cell-intrinsic and extrinsic mechanisms. Understanding anti-tumour immunity resistance is crucial because it can also determine the response of cancer treatment to immune checkpoint blockade.

The induction of $CD8^+$ T cells mediated anti-tumour response depends on the ability of the immune system to recognize cancer cells from normal cells. The most common mechanism for this differential recognition is related to cancer mutational load [148]. High number of mutations, with subsequent increase of antigen release is correlated with enhanced αPD-1 treatment response due to increased infiltration of $CD8^+$ T cells [149]. Indeed, multiple components within the tumour microenvironment allow distinguishing immunogenic (hot) tumour that are characterized by high infiltration of T cells, high expression of

inflammatory cytokines and PD-L1, versus non immunogenic (cold) tumour that instead lack these components. Patients whose tumours are immunogenic have a positive response to immune checkpoint blockade therapy with durable clinical benefits. Instead, for patients with non-immunogenic disease, the use of combinational therapy aimed at priming T cells infiltration and function first would need prior treatment with checkpoint inhibitors to obtain clinical benefit. Moreover, not all mutations seem to have the necessary quality to mount an anti-tumour immune response. Mutations that appear in founder cancer cells and are carried on by most of the progeny cells (clonal mutations) are favourable to trigger an immune response, whereas mutations that appear later in disease progression and may vary among the different cancer cells (subclonal mutations) are refractory to T cell recognition, thus resulting to be insensitive to immune checkpoint blockade [121]. There are some mutations that are able to modulate the TME and interfere with T cell immunity, as in the case of mutations in KRAS, common in pancreatic and ovarian cancer [150], [151]. KRAS mutation induces GM-CSF expression, which it has been shown to be responsible for the recruitment of myeloid cells and neutrophils, which have immunosuppressive activity into pancreatic tumour for example [152]. Similarly, KRAS mutation is also responsible for inducing increase in Hedgehog ligands Ahh and Ihh expression [87] or IL-6 secretion, both involved in CAFs activation, fibrotic stroma formation and T cell exclusion [153].

Other than cell intrinsic pathways, the $CD8^+$ T cell response depends also from extrinsic, environmental factors. Activation and recruitment of T cells into the tumour is crucial for an effective anti-tumour response to occur.

However, once in the TME, the success of anti-tumour defence is determined by the ability of $CD8^+$ T cells to overcome additional barriers that they may encounter by tumour cells, fibrotic stroma, T_{reg} cells, MDSCs, inhibitory cytokines and any other components of the tumour microenvironment that act to mitigate the anti-tumour response (Figure 1.8).

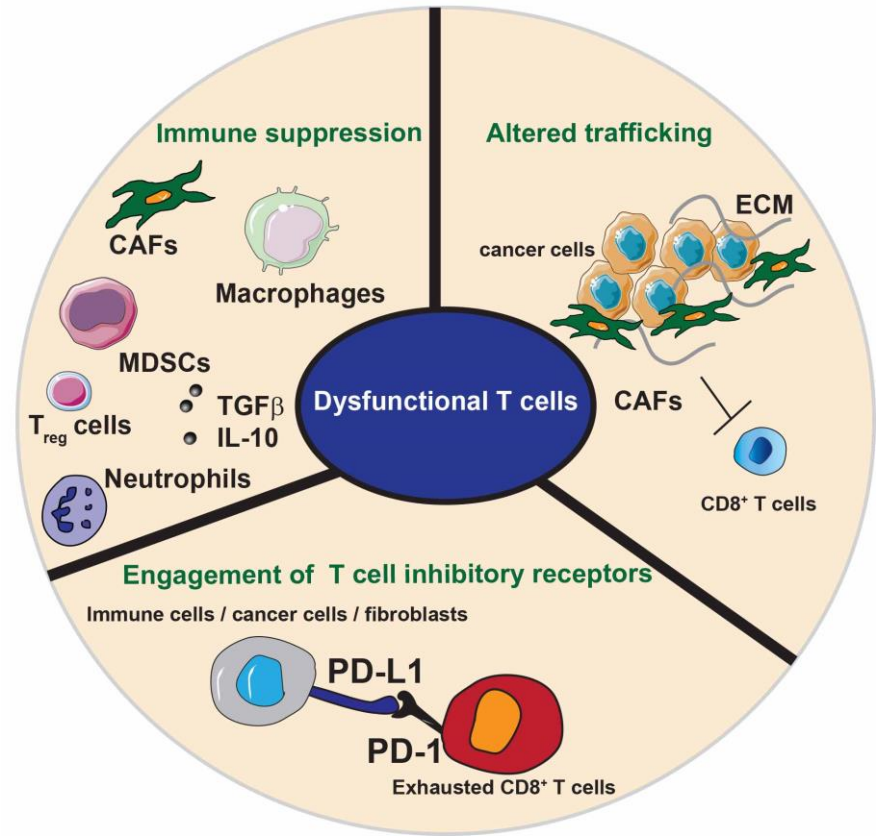

Figure 1.8 Tumour microenvironment induced CD8+ T cell dysfunction.

Schematic illustration of the contribution of tumour microenvironment (TME) to T cell dysfunction. T cell dysfunction (or exhaustion) can be caused by the presence of an immunosuppressive TME generated by cancer-associated fibroblasts (CAFs), macrophages (specifically the one with a M2-like phenotype), myeloid derived suppressor cells (MDSCs), T regulatory (Treg) cells and neutrophils. IL-10 and TGFβ are the main secreted factors that have been associated with immunosuppressive functions. Another cause of T cell dysfunction is determined by altered CD8+ T cell trafficking within the tumour site: the presence of dense

fibrotic stroma and ECM stiffness can generate a barrier that imped T cell entry within the tumour site. T cell dysfunction is also caused by engagement of T cell inhibitory receptors such as PD-1. Binding of PD-1 with its ligand, PD-L1, expressed by different cell types, induces CD8+ T cell exhaustion, which is accompanied by loss of T cells killing activity. Schematic adapted from [150].

The dominant effect of the TME in inducing T cell suppression has been identified upon examination of the relationship between $CD8^+$ T cells and cancer cells in tissues of tumours that do not respond to anti PD-1 / PD-L1 therapy, including colorectal, ovarian, and pancreatic cancer. Exclusion of $CD8^+$T cells from the tumour nest in colorectal cancer has been associated with poor prognosis [154], and exclusion of T cells from the vicinity of cancer cells has been also observed in the case of ovarian [155] and pancreatic cancer [156]. Overcoming the restrictions posed by the immunosuppressive TME is necessary to overcome tumour resistance to single agent Immune checkpoint antagonists.

The heterogeneous cell populations within the TME contribute to T cell suppression through both direct contact and by secretion of soluble factors. Stromal cells can limit T cell trafficking within the TME, promote $CD4^+$ T_{reg} development and inhibit T effector cells proliferation [157]. Endothelial cells can directly prevent T cell trafficking and promote T cell apoptosis by Fas ligand (FasL) expression, for example [158]. Myeloid cells, including TAM, granulocytes and inflammatory monocytes can mediate $CD8^+$ T cell suppression by PD-L1 expression or by production and/or induction of anti-inflammatory cytokines such as IL-10 and TGFβ, which are considered to be mediators of T cell exhaustion [138], [157]. Regulatory B cells interfere with anti-tumour T cell immunity by promoting T_{reg} development, by secreting

suppressive cytokines such as IL-10 and by stimulating suppressive myeloid cells [159]. Other immunesuppressive T cell subtypes, including γδ T cells can produce IL-10 and TGFβ and express inhibitory ligands such as PD-L1 [160], [161].

In the light of these observations, the intensive study of cellular and molecular mechanisms mediating the resistance to an anti-tumour immune response had revealed an opportunity to design combinatorial treatment aimed at targeting the immunosuppressive role of the TME together with Immune checkpoint antagonists, at least in the setting of low pre-existing level of T cells infiltration into the tumour. Furthermore, it is worth mentioning that other modes of cancer therapy, such as radiotherapy, chemotherapy or oncogene-targeted therapy have been shown to change the immunosuppressive TME and successfully increase the response of immune checkpoint blockade therapies [121].

1.2.5 Immunoregulatory role of macrophages

Macrophages, and in particular TAMs, critically affect anti-tumour immunity and response to immunotherapy (Figure 1.9).

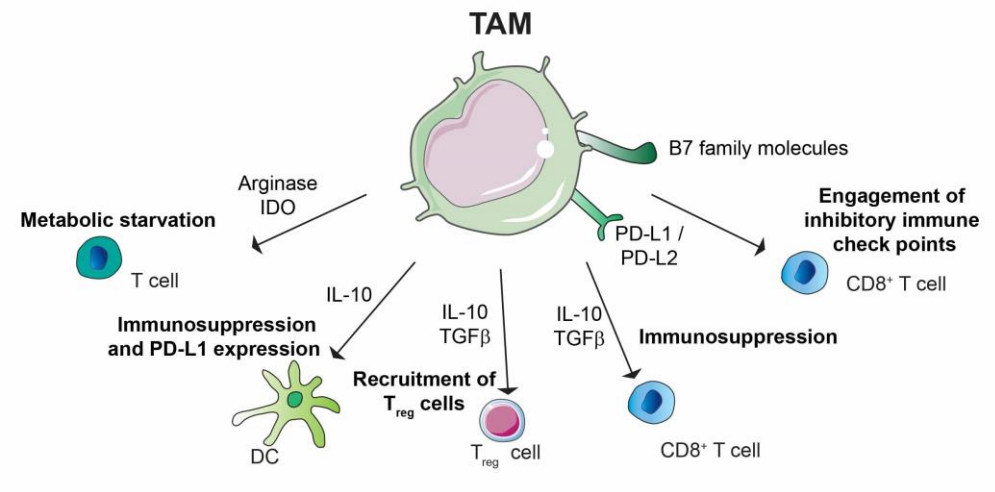

Figure 1.9 Immunosuppressive role of TAM.

Tumour associated macrophages (TAMs) promote immunosuppressive activities by different mechanisms. TAMs can express PD-L1 and PD-L2, which bind the T cell inhibitory receptor PD-1, thereby inducing T cell exhaustion. TAMs expression of B7 family molecules, such as B7-H4 can have similar function. TAMs secrete immunosuppressive cytokines such as IL-10 and TGFβ, which can have direct suppressive function on CD8+ T cells, or can induce recruitment of CD4+ T regulatory (Treg) cells with immunosuppressive functions. TAM secreted IL-10 can impair T cells effector functions indirectly either by inhibit dendritic cells (DCs) anti-tumorigenic role or by inducing DCs expression of PD-L1. Moreover, amino acid metabolism in TAMs results in production of arginase and immunosuppressive metabolites via the indoleamine 2,3-dioxygenase (IDO) pathway, which are responsible of metabolic starvation in T cells. Schematic adapted from [51].

Macrophages can express PD-1 ligands PD-L1 and PD-L2, as wells as CTLA-4 ligands CD80 and CD86 and the protein B7-H4 (which interacts with unidentified inhibitory receptor on T cells). PD-L1 and PD-L2 are up-regulated in macrophages in response to different stimuli including cytokines

and hypoxia [162], [163]. High level of PD-L1 expression in TAMs has been found in different types of cancer such as hepatocellular carcinoma [164], glioblastoma [165], pancreatic cancer [166]. Interestingly, in pre-clinical model of pancreatic cancer it has been found that macrophages are the main source of PD-L1 within the TME [167]. In addition, TAMs suppress T cell activation and proliferation by producing suppressive mediators, including IL-10 and TGFβ. TAMs secreted TGFβ directly exerts suppressive functions on $CD8^+$ T cells by transcriptional repression of genes encoding functional cytokines such as perforin, granzyme and cytotoxines [168], [169]; TAM derived TGFβ [170] and IL-10 [171] can act indirectly by stimulating the differentiation of T_{reg} cells. IL-10 can mediate stimulation of PD-L1 expression on DCs [172] or it can suppress DCs anti-tumour function by inhibiting their secretion of IL-12 [173]. In addition, amino acid metabolism induced in M2-like macrophages or TAM is responsible for arginase activity and/or production of immunosuppressive metabolites via indoleamine 2,3-dioxygenase (IDO) pathway, resulting in metabolic starvation of T cells [174], as such, prostaglandine production by TAM has an immunosuppressive effect [175].

Considering the high immunomodulatory effects of macrophages, their targeting has become one of the most promising approaches to enhance anti-cancer immunity.

1.2.6 Targeting the immunosuppressive role of macrophages

The signalling processes involved in macrophage recruitment and/or activation are important targets for anti-cancer therapies. CSF-1 is a monocyte attractant as well as the major growth and differentiation factor for

monocyte-macrophage lineage, it leads to TAM polarization toward an immunosuppressive, tumour promoting M2-like phenotype and it is abundantly expressed by several tumour types [176]. Therefore, CSF-1 / CSF-1 receptor (CSF-1R) axis has been extensively investigated and it is considered as an obvious target to interfere with TAM functions. High level of CSF-1 or CSF-1R expression in the tumour or peritumoral tissue have been associated with poor patient survival in different malignancies such as lymphoma, breast cancer and hepatocellular carcinoma [177]–[181]. CSF-1R is a receptor tyrosine kinase and a number of small molecules and antibody antagonists have been developed and tested in pre-clinical models. For example, mice treatment with the humanized mAb Emactuzumab, which bind CSF-1R, prevents receptor dimerization thereby abrogating CSF-1 receptor binding and activation of downstream signalling. In this study, CSF-1R inhibition reduced TAMs and circulating monocytes numbers and increased $CD8^+$: $CD4^+$ T cell ratio compared with mice treated with control antibody [182]. The use of combinational therapies has been developed to potentiate the effect of CSF-1 / CSF-1R inhibitors. For example, radiotherapy has been demonstrated to increase CSF-1 expression and myeloid cell infiltration in preclinical mouse xenograft models of human glioblastomas and combinational treatment of radiotherapy with CSF-1R small molecule inhibitors has shown to potentiate radiotherapy efficacy [183]. Another small molecule inhibitor, BLZ945, has shown to decrease glioma progression and improved survival in preclinical models. Interestingly, CSF-1R blockade, in this model, did not induced decrease in TAMs number, but instead generated phenotypic changes in macrophage population from a M2-like pro-tumoral to

anti-tumoral M1-like cell types [184]. In a mouse model of ovarian cancer, CSF-1R inhibitor, GW2580, decreased the numbers of tumoral infiltrating M2-like macrophages when administered at late stage of the disease [185]. The same inhibitor has been shown to enhance the activity of gemcitabine in a transgenic mouse model of gemcitabine-resistant pancreatic ductal adenocarcinoma (PDAC) [186]. Along this line, in a transgenic mouse model of mammary adenocarcinoma, paclitaxel-based chemotherapy led to increased production of CSF-1 and IL-34 (another cytokine involved in CSF-1R mediated signalling). Inhibition of CSF-1R enhanced chemotherapy effectiveness, reduced primary tumour development, metastasis formation and increased $CD8^+$ T cell numbers [187]. This was one of the first studies that demonstrated the inverse correlation between $CD68^+$ macrophages and $CD8^+$ T cells in tumour. Pharmacological blockade of CSF-1 / CSF-1R targeted specifically breast cancer $CD11b^+$ $Ly6G^{neg}$ $Ly6C^{low}$ $F4/80^+$ TAM and induced an increase in anti-tumour immunity mediated by enhanced $CD8^+$ lymphocyte infiltration, thereby highlighting the immune suppressive capacity of TAMs [187]. Accordingly with the immunosuppressive role of TAMs, the same authors identify macrophages as a primary source of IL-10 and that inhibition of IL-10 receptor induced reduction of breast cancer tumour if combined with chemotherapy, with an equivalent effect caused by blockade of CSF-1R. Also in this case, tumour reduction was associated with increased $CD8^+$T cell mediated anti-tumour activity. Mechanistically it was observed that the immune suppressive activity of IL-10 was not directly interfering with $CD8^+$ T cells function, but it was mediated by suppression of IL-12 production by intra-tumoral DCs, which in turn limited $CD8^+$ T cell

cytotoxic activity [173]. Similar results have been obtained in the case of pancreatic cancer. Blockade of CSF-1R or CCR2 resulted in altered infiltration of MDSCs both by reducing mature $CD11b^{+}Ly6G^{neg}Ly6C^{low}MHCII^{high}F480^{+}$ macrophages, in the case of CSF-1R blockade and by affecting $CD11b^{+}Ly6G^{neg}Ly6C^{high}MHCII^{+}F480^{+}$ monocytes, in the case of CCR2 blockade. CSF-1R or CCR2 inhibition in combination with chemotherapy resulted in restored $CD8^{+}$ T cells anti-tumoral activity [188]. The enhanced anti-tumoral effect of $CD8^{+}$ T cells as consequence of pharmacological inhibition of CSF-1 / CSF-1R axis has been also exploited for combinational therapy with immune checkpoint blockade, especially for tumours resistant to single-agents immunotherapy. In PDAC, $CD11b^{+}Ly6G^{neg}Ly6C^{low}F480^{+}CD206^{high}$ M2-like polarized macrophages have been observed to be more sensitive to CSF-1 / CSF-1R blockade, thereby revealing the effect of CSF-1 / CSF-1R inhibition in rewiring TAM polarization toward a pro-inflammatory, antigen stimulating phenotype. In this model, CSF-1 / CSF-1R targeting resulted in increased expression of immune checkpoint molecule on tumour cells, including PD-L1 and CTLA-4, thus resulting in only modest increase of $CD8^{+}$ T cell anti-tumour ability. Combination of αPD1 or αCTLA-4 checkpoint immunotherapy with CSF-1 / CSF-1R blockade improved anti-tumour immunity and led to the regression of even established primary pancreatic tumours [189]. However, targeting CSF-1 / CSF1-R axis could lead also to compensatory effects, which translate to enhanced tumour progression. For instance, in a series of mouse tumour models, it has been shown that CSF1-R is also expressed on CAFs. Interestingly, in this study the inhibition of CSF-1R increased the production

of chemokines in CAFs including CXCL1, thereby provoking the recruitment of immunosuppressive $Ly6G^+$ granulocytes/neutrophils. Inhibition of CXCR2, which is the receptor for most of the up-regulated cytokines in CAFs in response to CSF-1R inhibitor, alongside with CSF-1R resulted in significant delay in cancer progression [190].

Combination of immune checkpoint blockade with myeloid cells targeting agents has been also used in pancreatic cancer; in this case pharmacological selective targeting of the gamma isoform of PI3K (PI3Kγ), highly expressed in myeloid cells, reshaped TME and induced T cell mediated cytotoxic activity [191], [192].

Other approaches have been based on re-directing the function of macrophages with the aim of re-educating macrophages rather than simply targeting them for depletion or destruction. IFNγ is a classical inducer of M1-like polarization and its administration in women with ovarian cancer resulted in increased activation of tumour cytotoxicity and clinical response [193]. Another approach to targeting macrophages has been provided by administration of agonistic anti-CD40 antibody to mice with pancreatic cancer. CD40 agonist treatment resulted in re-education of M2-like macrophages toward an M1-like type with increased antigen presentation capabilities which led to re-establishment of pro-inflammatory microenvironment and a reduction in tumour mass [194]. Translation of the obtained results into clinical trials using a fully humanized antibody CD40 agonist in combination with chemotherapy in patients with advanced stage pancreatic cancer achieved partial response and improved patient survival [195]. Interestingly, a combination of anti-CD40 agonist and inhibition of CSF-

1R induced macrophage pro-inflammatory phenotype prior CSF-1R mediated elimination, which was sufficient to reinvigorate T cell response in transplanted tumours that are either resistant or sensitive to immune checkpoint blockade [196]. Another example is given by a study performed in a preclinical mouse model of pancreatic cancer in which crosstalk between B cells and FcRγ$^+$ TAMs via Bruton tyrosine kinase (BTK)-PI3Kγ signalling promoted M2-like macrophage phenotype. Administration of PI3Kγ inhibitor or BTK inhibitor induced M1-like macrophage phenotypic switch and promoted CD8$^+$ T cell cytotoxicity resulting in a decrease in tumour growth [159]. Clinical strategies using this approach in combination with chemotherapy are in evaluation for patients with pancreatic cancer.

1.2.7 Immunoregulatory role of fibroblasts

Of recent increasing interest is the investigation of the immuno-modulatory functions of CAFs within the TME. As described before, CAFs can adopt a secretory phenotype, which enable the synthesis of ECM proteins, expression of ECM-remodelling enzymes and production of a plethora of cytokines and chemokine. The secretome of CAFs not only contributes to fibrosis-associated tissue remodelling during tumour progression, but it can also differently influence tumour immunity [74] .

Generally, CAFs are considered to have an immunosuppressive function [197], [198]. CAFs can impair CD8$^+$ T cell activation, cytokine production and cytotoxicity through the direct secretion of soluble factors such as IL-10, TGFβ or VEGF as well as through metabolic reprogramming via Prostaglandin E2 (PGE2), IDO and arginase [199], [200]. Additionally, FAP$^+$ CAF-secreted CXCL12 mediates exclusion of CD8$^+$ T cells in pancreatic

cancer [201]. In this regard, two independent studies revealed that targeting FAP^+ CAFs in immunocompetent tumour bearing mice resulted in intra-tumoural recruitment of $CD8^+$ T cells and T cell mediated killing of tumours in both colon [202] and pancreatic cancer [203]. Cultured fibroblasts from normal human colons have been reported to express the negative co-regulator signals PD-L1 and PD-L2 with a potential impact on T cell activity [204]. PD-L1 and PD-L2 expression has also been found in a subset of CAFs derived from patients with lung cancer with *ex-vivo* immunosuppressive capacity on T cell activation [205]. In addition to directly inactivating a $CD8^+$ T cell response, CAFs can also suppress anti-tumour immunity in an indirect way, by affecting T helper (T_H) cell response. Indeed, fibrosis has been associated with T_H2 and T_H17 responses. The T_H2 cytokines IL-4 and IL-13 can induce both fibroblasts proliferation and fibroblast ECM deposition, while T_H17 cells are involved in regulating inflammatory pathways during pulmonary fibrosis [206]. In the case of pancreatic cancer, one of the activated pancreatic stellate cell subtypes, the inflammatory CAF (iCAFs), have been shown to be characterized by a secretory phenotype mainly mediated by IL-6 [65]. IL-6 has been shown to have an immunosuppressive role by acting in a paracrine manner on cancer cells and other stroma cells, for example by driving monocyte precursors toward a MDSC phenotype via STAT3 signalling pathway [207], [208]. In addition, CAF production of CCL17, IL-15 and TGFβ can also regulate T_{reg} cells recruitment and differentiation, in accordance with this, deletion of FAP^+ CAF shifted tumour immunity toward a T_H1 –type with subsequent increase of cytotoxic lymphocytes, decrease in T_{reg} cells and reduction of mammary tumours

[209]. Recently, in the triple negative subtype of breast cancer, four different subsets of CAFs have been identified, with one of them being associated with an immunosuppressive role. CAF-S1 subset of CAFs has been found to be highly associated with IL-17F, IL-1β, IL-10 and IL-6 expression and with high T_{reg} cells infiltration, while the presence of $CD8^+$ T cells was low. The same authors also found that CXCL12 was the main responsible for T_{reg} cells recruitment, whereas the CAF-S1 expression of T cell ligands such as OX40L, PD-L2 and adhesion molecule JAM was responsible of T_{reg} retention at the tumour site. CD73, DPP4 and B7H3 CAF-expressed molecules were able of promoting T_{reg} survival and differentiation in to $CD25^{high}$ $FOXP3^{high}$ cells instead [210].

CAFs can also indirectly mediate T cell immunosuppression by affecting recruitment and modulating the function of TAMs, MDSCs / neutrophils and DCs. Also in this case, IL-6 secreted by CAFs has been shown to be associated with inducing monocyte differentiation program toward the M2-like phenotype of macrophages [211]. Other *in vitro* studies have shown that CAFs isolated from different tumour models secrete a wide range of cytokines such as GM-CSF, CSF-1, CCL2, CCL7, CXCL1, CXCL2 and CXCL8 all involved in MDSC recruitment and M2 macrophage phenotype switch [212]–[214].

In addition to the direct and indirect mechanisms by which the CAF secretome can influence T cell immunity, the dense and collagen rich ECM can also affect T cell infiltration and function [215].

Extensive fibrosis can induce the phenomenon of T cell exclusion (Figure 1.10). For example, high desmoplastic stroma deposition, as in the case of

pancreatic cancer, and ECM stiffness can act as physical barrier for CTLs trafficking. Indeed, different studies in pancreatic cancer and lung cancer pre-clinical models have reported that the ability of T cells to infiltrate and to migrate from the stroma to close proximity to the tumour nest is impaired in the presence of dense stroma compartment [216]–[218]. In this regard, the presence of ECM stiffness, other than limiting T cells infiltration, is likely to be also involved in regulating T cell functionality. However, ECM stiffness not only can influence T cell trafficking, but also it can affects the trafficking and functions of myeloid cells: dense ECM structure, ECM components, such as HA can alter differentiation, polarization and function of macrophages in different tumour models [219], [220].

Tumour associated fibrosis can also induce hypoxia. Indeed, the presence of an extensive fibrosis can lead to poorly innervated tumour with scarce presence of blood vessels necessary for nutrient and oxygen supply. The presence of an hypoxic microenvironment can also be a modulator of tumour immunity: the release of hypoxia induced chemo-attractant within the TME can promote accumulation of TAMs and MDSCs [221]. Hypoxia has been associated with regulating the function of MDSCs through HIF1α mediated expression of PD-L1 [222].

The molecular mechanisms that regulate CAF immune-modulatory processes, as well as the clinical impact of targeting CAFs on anti-tumour immune response are still not well elucidated. It is also unclear whether different origin of CAFs and the presence of different tumour associated CAF subsets can affect differently anti-tumour immunity.

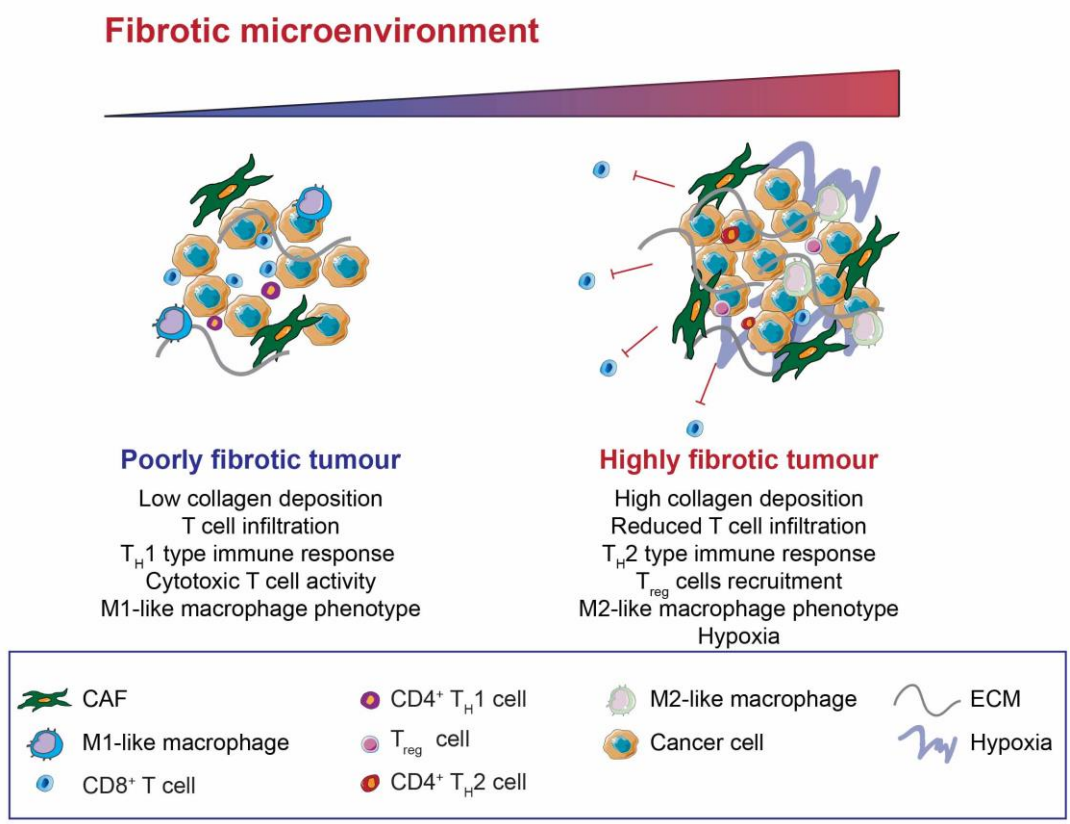

Figure 1.10 Fibrotic impact on CD8+ T cells infiltration.

Schematic representation of a poor (right) and highly (left) fibrotic tumour microenvironment (TME). One of the mechanisms by which cancer associated fibroblasts (CAFs) impact immune cell functions is the formation of a highly fibrotic microenvironment characterized by a dense and collagen-rich ECM, which act as barrier against T cell infiltration. Moreover, ECM components can retain and sequester cytokines and influence macrophage polarization toward an M2-like phenotype with immunosuppressive functions. CAFs secreted factors can inhibit anti-tumour $CD8^+$ T cells functions directly; alternatively, CAFs can also play an immunosuppressive function indirectly either by reprogramming $CD4^+$ T helper (T_H) response toward a pro-tumourigenic T_H2-type of response or by the recruitment of T regulatory (T_{reg}) cells. Tumour associated fibrosis can also generate hypoxia, which, in turn promotes accumulation of immunosuppressive M2-like macrophages. Schematic adapted from [215].

1.2.8 Targeting the immunosuppressive role of fibroblasts.

Abundant collagen deposition is one of the key features of tumour stroma. For this reason, several strategies have been developed to target collagen synthesis, as in the case of Halofuginone, which has been used to target type I collagen in pancreas and liver fibrosis [223]. Alteration of collagen cross-linking by LOX inhibition has been revealed effective in targeting fibrosis and reducing tumour growth in the case of mammary tumour; and in the case of pancreatic cancer, LOX inhibition resulted in increased drug delivery [84], [224], [225]. Similarly, all-trans retinoic acid (ATRA) has been shown to be a potential target to regulate ECM remodelling and inhibit activation of pancreatic stellate cells [226]. Another ECM component is HA, which is abundant in different types of cancer. Accumulation of HA has been shown to increase tumour interstitial pressure and impair drug delivery; thereby it became an attractive drug target. Inhibition of pre-existent HA using PEG-fused hyaluronidase (PEGPH20) has been shown to down-regulate HA level and increase efficacy of chemotherapy in pancreatic cancer. Therefore, this has been translated into successful clinical trials in combination with gemcitabine and nab-paclitaxel [227]. Recent studies have demonstrated that reprogramming pancreatic stellate cells derived CAFs into quiescent fibroblasts using Calcipotriol, a Vitamin D analogue, can reduce fibrosis and inflammation in pancreatic cancer [228]. Similarly, recently approved Pirfenidone for treatment of pulmonary fibrosis is based on targeting fibroblast activation and secretory functions [229].

Another approach that is being in use is the modulation of CAF mediated immune regulation. Examples are the adoptive transfer of FAP-specific T cell,

DNA vaccines against FAP, as well as FAP peptides that lead to FAP^+ CAF targeting, decrease in collagen deposition and increased T cell activity [202], [230], [231].

Targeting of pathways involved in fibrosis formation has also been considered as a valuable approach to enhance immunotherapy efficiency. In the genetic engineered pancreatic cancer mouse model, inhibition of CXCR4, which is the receptor for CAF-secreted CXCL12, by using AMD3100 improved short-term response to immune checkpoint blockade [201]. Other groups have focused on targeting FAK signalling, which has been associated with pathological fibrosis and with regulation of immunesurveillance [232]. Loss of FAK signalling resulted in decreased $FOXP3^+$ T_{reg} recruitment in squamous carcinoma models [233]; in pancreatic cancer mouse model, inhibition of FAK resulted in reduced collagen, reduced immune suppressive cells recruitment (TAMs, MDSCs, T_{reg} cells) and increased $CD8^+$ T cell infiltration, thereby enhancing sensitivity to PD-1 checkpoint antagonist [218]. In pancreatic cancer, CAF mediated immunosuppression has been shown to be reduced by IL-6 targeting and its combination with PD-L1 substantially led to anti-tumour immunity and tumour regression [234].

Despite CAF targeting offering a powerful new tool for anticancer treatment, the function heterogeneity and dynamic polarization of CAFs may require the identification of more specific targets and more detailed understanding of CAF mediated immunomodulation. However, together these data show that CAF-targeted therapies can be useful to improve the therapeutic benefits of checkpoint blockers and sensitize cancer types usually resistant to these single agent therapies.

1.3 Pancreatic Ductal Adenocarcinoma

1.3.1 Tumour pathology

Pancreatic Ductal Adenocarcinoma (PDAC, or simply referred here as pancreatic cancer) is the most common form of pancreatic cancer and it is considered one of the higher causes of cancer death in developed countries [235]. This type of cancer is rarely diagnosed in people younger than 40 years and less than 20 % of patients present with localized, potentially curable surgically resectable tumours. The overall 5-year survival rate is <5 % with the highest survival rate for patients who undergo surgical resection. The causes of pancreatic cancer remain unknown, however risk factors are tobacco smoke, intake of alcohol and coffee, high fat and high cholesterol diet. Some studies have shown that an increased incidence of pancreatic cancer is observed in people with history of diabetes or chronic cirrhosis. Moreover, in around 5 to 10 % of pancreatic cancer patients there is a family history of the disease [236], [237].

Pancreatic cancer results from successive accumulation of gene mutations [238], which dictate the origin of the cancer in the ductal epithelium and its progression from pre-malignant lesions to fully invasive cancer. Pancreatic intraepithelial neoplasia (PanIN) is the best histologically characterized precursor of pancreatic cancer [238].

Genomic analysis of pancreatic cancer reveals that *KRAS*, *TP53*, *SMAD4* and *CDKN2* mutations are the most common oncogenic events, among a milieu of mutated genes at low prevalence. The 90 % of tumours have activating mutations in *KRAS,* whereas inactivating mutations in *TP53*, *CDKN2A* and *SMAD4* occur in 50-80 % of tumour cases [239]. Recently,

genomic analysis of 456 PDAC using whole-genome and deep-exosome sequencing identified 32 recurrently mutated genes that aggregate into 10 common pathways: KRAS, TGFβ, WNT, NOTCH, ROBO/SLIT signalling, G1/S transition, chromatin remodelling, DNA repair and RNA processing. The unbiased expression analysis allowed researchers to identify four subtypes of pancreatic cancer: squamous, pancreatic progenitor, immunogenic and aberrantly differentiated endocrine exocrine (ADEX). The clustering was based on the differential expression of transcription factors and downstream targets important in defining lineage specification and differentiation during pancreas development; moreover, each of the subtypes was found to be associated with specific histological characteristics [240] . The squamous subtype of pancreatic cancer is associated with gene networks involved in inflammation, hypoxia, metabolic reprogramming, TGFβ signalling, up-regulation of TP53, KDM6A and TP63ΔN transcriptional networks. Analysis of transcriptome data of the squamous subtype also identified key factors involved in increased metastatic potential such as PDGFRβ [241] and LOX [224]. Factors involved in determining the cell-fate of pancreatic endoderm define the pancreatic progenitor subtype. An example is PDX1, that is expressed in embryonic progenitor cells and is critical for development of pancreas with ductal, exocrine and endocrine cells [242]. ADEX subtype displays up-regulation of transcriptional networks that are important in later stages of pancreatic development and differentiation. This subtype, for instance, is characterized by up-regulation of genes associated with both exocrine and endocrine differentiation pathways at the same time, rather than one or the other as in the case of normal pancreas development. The

immunogenic subtype is associated with a significant immune cell infiltration. Immune gene-associated pathways that are up-regulated in this subtype include B cell signalling, antigen presentation, $CD4^+$ T cells, $CD8^+$ T cells and Toll-like receptor associated signalling pathways. Interestingly, the expression profile of genes related with B and T cells, including both cytotoxic $CD8^+$ T and T_{reg} cells, were found to be predominant [240].

1.3.2 Tumour microenvironment in pancreatic cancer

A striking pathological feature of this disease is the presence of an extensive stroma compartment termed desmoplastic reaction that in some cases dominates up to the 90 % of the entire tumour mass. The stroma in pancreatic cancer does not constitute only a mechanical barrier that may prevent the efficient delivery of anticancer drugs, but it also represents a dynamic structure that is regulated by cancer cells into a favourable environment critical for tumour formation, progression and metastasis. The dense stroma consists of proliferating myofibroblasts (pancreatic stellate cells), deposition of ECM proteins such as type I collagen, fibronectin, laminin, hyaluronic acid, as well as multiple types of infiltrated inflammatory cells, including macrophages, MDSCs and T cells (the majority of which are $CD4^+$ T_{reg} cells). Pancreatic adenocarcinomas are also characterized by low microvascular density, leaky vasculature and limited perfusion, with consequent generation of a hypoxic microenvironment. The presence of fibrotic stroma also leads to a reduced blood flow and increases interstitial pressure, which results in impaired drug delivery [243]. Recently, a study of 145 early stage pancreatic cancer patients revealed a correlation between moderate to strong αSMA expression and poorer clinical outcome in terms of

overall tumour progression and patient survival [244]. Interaction between pancreatic stellate cells and cancer cells has been demonstrated both by *in vitro* and *in vivo* data, thus supporting the role of pancreatic myofibroblasts in stimulating proliferation, migration of cancer cells and subsequent development of pancreatic cancer [245]. It has also been shown that stellate cells are involved in inhibiting cancer cell apoptosis and development of a cancer stem niche, thereby promoting chemoresistance [246]. Pancreatic stellate cells have also the ability to migrate together with pancreatic cancer cells at the metastatic site and cancer cells secreted PDGF to mediate this process [247]. Interaction of pancreatic stellate cells with other stroma cells has been also reported: VEGF secreted by stellate cells can influence endothelial cell proliferation and angiogenesis [248]. In addition, fibrotic stroma is also responsible for immune evasion by reducing the trafficking of $CD8^+$ T cells [249] and by inducing $CD8^+$ T cell apoptosis via galectin 1 [250] and by stimulating the infiltration of myeloid derived suppressor cells [207].

Another hallmark of pancreatic cancer microenvironment is the restriction of the immune surveillance and generation of an inflammatory microenvironment that supports tumorigenesis [251]. T_{reg} cells and myeloid cells are the main mediator of anti- tumour immunity and they are recruited since the early stages of pancreatic cancer development by GM-CSF secreted by cancer cells [152]. Macrophages are a key driver of pancreatic tumour progression and their recruitment requires interleukin 6- Janus kinase- signal transduction and activation of transcription 3 (STAT3) signalling pathway [252], but also cancer cells secretion of CSF-1 [167].

LSL-KrasG12D/$^{+}$; LSL-Trp53R172H/$^{+}$; Pdx-1-Cre mice (KPC mice) mice [253] have been extensively used to shed light on biological processes involving interaction between neoplastic cells and their microenvironment.

In KPC mice *Kras* coding sequence has been engineered to contain a G to A transition in codon 12 [254], [255]. The G12D mutation introduced in the *KRAS* coding sequence is common in many cases of human PDAC and results in an amino acid change from glycine to aspartic acid in the protein. The mutation compromises Ras GTPase activities and results in constitutive signalling of the Ras pathway. KPC mice recapitulate the pre-invasive stages of the invasive carcinoma, but also develop advanced staged and metastatic PDAC typical of human, conserving the principal clinical, histopathological and genomic features of the cognate human condition. Interestingly, also the metastatic dissemination recall the human one, with liver metastasis present in almost 80 % of cases, followed by lung in 50 % of cases, adrenals and peritoneum with lower frequency [253].

Analysis of the TME in KPC mice allowed an identification of the changes in tumour immunity from inception of pre-invasive lesions to establishment of invasive cancer. Infiltration of immunosuppressive TAMs, MDSCs and T_{reg} cells dominates the early immune response from the lowest grade of pre-invasive neoplasia to invasive pancreatic cancer. Interestingly, in the study performed by Clark et al., it has been found that in KPC mice pre-invasive lesions are scarcely infiltrated by effector T cells (with exception of a subset of advanced cancer) and that $CD8^{+}$ T cells also show little evidence of activation potential. Interestingly this was inversely correlated with the high infiltration of MDSCs with immunosuppressive potential [256]. In a recent

study, RNA sequencing allowed the identification of the presence of elements of all four pancreatic cancer subtypes in KPC mouse tumours. Interestingly, the same authors identified that CSF-1R inhibition in KPC mice induced tumour regression and increased T cell activation but also importantly, it altered tumour architecture both at transcriptional and histological level. Indeed, gene expression programs typical of the squamous pancreatic cancer subtype, including those associated with hypoxia, ECM and TGFβ signalling were down-regulated upon CSF-1R blockade, with subsequent up-regulation of the ADEX and immunogenic subtypes related gene programs [167].

Analysis of KPC autochthonous model using linage tracing has allowed an examination of the evolution of disseminating cancer cells and their associated microenvironment. It has been observed that metastatic development of pancreatic cancer into the liver is accompanied by cancer cell shift from mesenchymal to epithelial phenotype, hypovascularization of the TME, formation of a dense fibrotic reaction [117], [257], and high infiltration of myeloid cells, in particular macrophages [117], thereby recapitulating the primary tumour microenvironment from which they arise.

KPC mice have been used to test different strategies to enhance intratumoral perfusion and drug delivery. Targeting the fibrotic stroma, including use of Hedgehog signalling inhibitors [87], use of pegylated hyaluronidase [227], [258], synthetic D analogues [228] and collagen cross linker enzyme LOX inhibitor [224], are still under investigation and clinical evaluation. Also, early detection strategies for pancreatic cancer have been pioneered in KPC mice, including imaging of the potential imaging biomarkers plectin 1 [259] and

claudin 4 [260], as well as use of blood biomarker panels [261] and use of circulating exosomes containing glypican 1 [262]. Many of these markers have been also validated in human samples and clinical assessments are still on going.

1.3.3 Diagnosis and therapeutic opportunities for pancreatic cancer

Pancreatic cancers are located for the 60 to 70 % of the cases in the head of the pancreas, in the 20 % of the cases instead, it is possible to find tumour in the body and the tail of the organ. The signs and symptoms of the tumour are related to its location, however the most common are usually associated with abdominal pain, weight loss, asthenia and anorexia [263]. Abdominal computer tomography (CT) is usually used to detect the pancreatic mass and to determine the initial steps of treatment. Pancreatic cancer is associated with poor prognosis and it is usually diagnosed at advanced stages, most likely because the symptoms are not specific or sometime they are completely absent. There are no available diagnostic markers that are sensitive and specific enough to detect the disease. The current markers including carcinoembryonic antigen (CAE) and carbohydrate antigen 19-9 (CA19-9), if elevated, are used just to follow patients with known disease [237]. The majority of patients, approximately 90 % of those diagnosed with pancreatic cancer, die from it. Around 70 % of patients die because of the presence of metastasis, usually localised to the liver, lung or abdomen; the other 30 % of patients have limited metastatic disease at the time of death, but they have extended primary tumours [237].

Surgical resection is the only potential curative therapy for pancreatic cancer. Localized tumours, accordingly on their involvement of the local vessels, can

be resected or not, but usually only 15 to 20 % of patients are considered to be suitable candidates for surgical resection. Pancreatic duodenectomy is usually performed as a surgical procedure for pancreatic cancer that develop in the head or neck of the pancreas. Instead for tumours that develop in the tail of the organ, the most used procedure is distal pancreatectomy, which most often includes removal of the spleen [264].

Considering the poor outcome obtained by surgery alone, the use of adjuvant therapy, especially chemotherapy, is necessary to reduce the risk of distant metastases and regional failure after surgery. In 1997, gemcitabine, a nucleoside analogue, was approved by FDA for the therapy of pancreatic cancer based on a randomized clinical trial that revealed clinical benefits in terms of symptoms control and relative modest survival advantages [264]. In 2001, a combination of folinic acid (leucovorin), 5-fluorouracil, irinotecan and oxaliplatin (FOLFIRINOX) demonstrated increased activity in comparison with gemcitabine monotherapy. However, this regimen has significant toxicities such as diarrhoea, nausea, neurophaty, thus FOLFIRINOX treatment is usually restricted to patients with less than 76 years of age and with good performance [265]. In 2012, the combination of gemcitabine and albumin-bound paclitaxel (nab-paclitaxel) was introduced and FDA approved, as it showed improved efficacy in comparison with gemcitabine alone. Also in this case, toxicities are considerable, however the treatment is considered to be safe for older patients with poor performance status [266]. The use of multi-agent combinations administered both pre- and post- surgery has acquired increasing interest, also in the case of patients with locally advanced or metastatic form of the disease. The use of radiotherapy instead,

seems to be controversial. Indeed, for some trials the use of radiation therapy in combination with gemcitabine improved survival of patients [267], other trials aimed at evaluating the response of locally advanced, unresectable disease with gemcitabine followed by chemoradiation or continued chemotherapy, failed to show an increased benefit induced by inclusion of radiation therapy [268]. For patients with metastatic disease, gemcitabine alone or its combination with FOLFIRINOX or nab-paclitaxel is considered standard treatment and in 10 % of treated patients the survival time can increase up to 2 years [265].

Despite advances that have been achieved for the treatment of pancreatic cancer, the disease remains one of the most deadly. New approaches are now in use for treatment of pancreatic cancer and are based on targeting and/or reprogramming the cancer stroma through modulation of interaction between tumour cells, myofibroblasts (pancreatic stellate cells), endothelial cells, and immune infiltrates. Example of fibrotic stroma targeting therapies are represented by clinical trials that inhibit Hedgehog pathway, identified by genetic studies as the core pathway in the development of pancreatic cancer [266]; although the use of Hedgehog inhibitors as neo-adjuvant before chemotherapy did not result in increased drug delivery (ClinicalTrials.gov ID: NCT01064622) [269]. Other therapeutic agents are based on targeting the HA component of the ECM stroma surrounding the primary tumour or on targeting the physical barrier presented by stromal cells. Clinical trials are ongoing for the evaluation of PEGPH20 (a PEGylated form of a recombinant human hyaluronidase) in combination with nab-paclitaxel and gemcitabine (ClinicalTrials.gov ID: NCT01839487) or in combination with FOLFIRINOX

(ClinicalTrials.gov ID: NCT01959139). Another example of stroma targeting approach is represented by the use of CSF-1R blocker to dampen TAMs pro-tumourigenic functions together with gemcitabine [270].

The majority of pancreatic cancer patients are completely refractory to the use of single agent Checkpoint blocker mediated Immunotherapy (αPD-1 or αCTLA-4 inhibitors). The only exception appears to be in <1 % of PDAC patients with high microsatellite instability [271]. One of the main reasons of pancreatic cancer resistance to checkpoint blockade may be associated with the presence of abundant tumour associated stroma with immunosuppressive functions. Indeed, therapeutic strategies that disrupt the immune suppressive network and promote immune mediated tumoricidal activities are under evaluation. Example is AMD3100, a FDA approved inhibitor of CXCR4 that have been used in combination with PD-L1 inhibitor. The aim is to target FAP^+ CAFs in the tumour stroma that exert immunosuppressive activity by secretion of CXCL12 (a ligand for CXCR4) [201]. Moreover, another approach of targeting CAF in pancreatic cancer is constituted by use of fibrosis targeting FAK inhibitor in combination with PD-1, also recently tested in clinical trials (ClinicalTrials.gov ID: NCT02546531 and NCT02758587). Several clinical trials are ongoing to validate the effect of targeting the immune suppressive function of macrophages through targeting CSF-1 / CSF-1R axis in combination with anti-PD-L1 (αPD-L1) or αPD-1 (ClinicalTrials.gov ID: NCT03153410, NCT02777710). A different approach is represented by enhancement of anti-tumour immunity through the activation of CD40 molecule expressed in myeloid cells, in particular macrophages. Anti-CD40 analogue therapy aims to promote accumulation of

tumoricidal macrophages and decrease in stroma stiffness. As mentioned before, CD40 agonist are in trial evaluation in combination with gemcitabine (ClinicalTrials.gov ID: NCT00711191) [195].

1.4 Aim and Objective

Therapeutic options for pancreatic cancer patients remain limited, especially for those patients with advanced metastatic form of the disease. Single agent PD-1 immune-checkpoint blockade is revealing to be an effective treatment strategy for multiple types of cancers, but pancreatic cancer still remains refractory.

The therapeutic efficacy of PD-1 blockade has been reported to be strictly associated with $CD8^+$ T cell infiltration into the tumour. Pancreatic cancer was initially considered poorly immunogenic, but recent evidence suggests that $CD8^+$ T cell mediated anti-tumour immunity is also triggered in this type of disease. Pancreatic cancer metastasis is characterized by the presence of a dense desmoplastic reaction and strong infiltration of immune cells, among which macrophages represent one of the dominant populations. Thus, the aim of this research work is to understand whether the tumour microenvironment in pancreatic cancer metastasis plays an immunosuppressive role and whether its targeting would sensitize pancreatic cancer metastasis to PD-1 blockade.

Experimentally, the main objectives are to:

- Characterize $CD8^+$ T cell infiltration and activity in metastatic lesions of pancreatic cancer, in both patients and pre-clinical mouse models;
- Investigate both *in vivo* and *in vitro* whether some components of the tumour microenvironment, such as macrophages and/or myofibroblasts, could play an immunosuppressive role;
- Identify potential macrophage and/or myofibroblast derived immunosuppressive factors;

- Validate whether *in vivo* targeting of the immunosuppressive microenvironment components and/or identified factors could be beneficial for sensitizing metastatic pancreatic cancer to PD-1 immuno-checkpoint blockade.

Chapter 2:

Materials and Methods

2 Chapter 2: Material and Methods

2.1 Cells

Murine pancreatic cancer cells KPC FC1199, from here on referred as KPC, were generated in the Tuveson lab (Cold Spring Harbor Laboratory, New York, USA) isolated from PDA tumour tissues obtained from $Kras^{G12D/+}$; $p53^{R17H/+}$; Pdx1-Cre mice of a pure C57BL/6 background and authenticated as previously reported [253]. The murine C57BL/6 Panc02 pancreatic ductal carcinoma cell line was obtained from the NCI DCTD Tumor Repository, NIH. $Panc02^{luc/zsGreen}$ or $KPC^{luc/zsGreen}$ cells were generated by using pHIV Luc-zsGreen (gift from B. Welm, University of Utah, USA, Addgene plasmid no.39196) lentiviral particle infection. Infected cells were selected for high zsGreen expression levels using flow cytometry cell sorter (ARIA, BD, and Method 2.11). All cells were maintained at a minimal passage number (<p8) to allow initial expansion prior to use for *in vitro* and *in vivo* experiments. All cells, unless differently stated, were cultured in Dulbecco Modified Eagle Medium (DMEM; Gibco Thermo Fisher Scientific), supplemented with 10 % of Fetal Bovine Serum (FBS; Sigma-Aldrich) and containing Penicillin-Streptomycin (10 ml / L; Sigma-Aldrich) and Amphotericin B solution (2.5 mg / L; Sigma-Aldrich); from here on refereed as complete DMEM. All cells were cultured at 37 °C with 5 % CO_2 and ~18 % O_2. All cells were routinely tested negative for the presence of mycoplasma contamination. None of the cell lines used in this study is listed in the ICLAC and NCBI Biosample database of misidentified cell lines.

2.2 Mice

6-8 weeks old female C57BL/6 mice were purchased from Charles River. Transgenic mice lacking PI3-kinase γ expression (p110γ$^{-/-}$) on the C57BL/6 background were obtained from Dr. Emilio Hirsch, Institute of Molecular Biotechnology Centre, University of Torino, Italy. Grn$^{-/-}$ mice (B6(Cg)-*Grn*$^{tm1.1Aidi}$/J) and tdTomatoRed mice (B6.129(Cg)-Gt(ROSA)26Sor$^{tm4(ACTB-tdTomato,-EGFP)Luo}$/J) both on the C57BL/6 genetic background were purchased from The Jackson Laboratory. Kras$^{G12D/+}$; p53$^{R172H/+}$; Pdx1-Cre mice (KPC mice) were purchased from CRUK, Cambridge Research Institute, Cambridge.

All animal experiments were performed in accordance with current UK legislation under an approved project licence PPL 40/3725 (Dr M Schmid). Mice were housed under specific pathogen-free conditions at the Biomedical Science Unit at the University of Liverpool. In general, for animal studies the group size was calculated by power analysis using a significance level kept at 5 % and the power at 80 % (according to approved corresponding Home Office Project License Application). For tumour studies, female animals of 6-8 weeks were used. Animals were randomly assigned to experimental groups. The investigators were not blinded to allocation during experiments and outcome assessments.

2.3 *In vivo* animal studies

2.3.1 Liver experimental metastasis

Liver experimental metastasis was induced by implantation of cancer cells into mouse spleen. On the day of surgery, cultured KPC $^{luc/zsGreen}$ or Panc02 $^{luc/zsGreen}$ cancer cells were harvested and resuspended in phosphate buffered saline (PBS). Cells were kept on ice until implantation into mice. For each mouse, 1 x 10^6 cancer cells resuspended in 25 µl of PBS were used.

Surgical implantation of cancer cells was performed in the Biomedical Service Unit (BSU) at Liverpool University, under sterile conditions. Mice were anaesthetised using Isoflurane vaporizer before surgical procedure. The surgical area of the mice was shaved to avoid contamination and the area of incision was prepared by using 70 % ethanol and then iodine. In proximity to an area where the spleen is located, an incision was performed though the skin and the peritoneum using aseptic scissors. Spleen was extract and slightly curved, cancer cells were injected using a Hamilton 29 G syringe. After injection, pressure was applied to the spleen in the site of injection with a cotton swap to avoid bleeding. Successively, the spleen was re-placed inside the mouse and peritoneum and skin were closed using a 6.0 stitch. Mice were placed on a heating pad for recovery until they were mobile and with a regular breathing pattern. Animals were returned to the cage and monitored daily for weight loss and presence of adverse condition. Liver metastatic dissemination of cancer cells, in this model, occurs shortly after intrasplenic implantation [7]. For our experiments, we allowed metastatic growth for a maximum of 24 days and mice did not experience any insurgence of severe adverse effects. At the end point, mice were euthanized

by cervical dislocation and livers were harvested by performing an incision through the skin and peritoneum using scissors. Forceps and scissors were then used to cut the liver out of the exposed abdomen.

2.3.2 Mouse treatments

For selected experiments, macrophages were depleted using CSF-1 neutralizing antibody (BioXCell, clone 5A1) or CSF-1R inhibitor (Selleckchem, BLZ945). Anti-CSF-1 (αCSF-1) antibody was administered via intraperitoneal (i.p.) injection every 5 days with the first injection containing 1 mg and subsequent injections containing 0.5 mg for a total of 3 injections in 14 days (early time point treatment, d7) and 2 injections in 10 days (late time point treatment, d14). At the early time point, injections were started 7 days after intrasplenic implantation of cancer cells; for late time point treatment, treatment was started 14 days later intrasplenic implantation. Rat IgG1 (BioXCell, clone HRPN) was used as isotype control.

CSF-1R inhibitor BLZ945 was administered daily at a concentration of 200 mg / kg in 20 % Captisol (Ligand Pharmaceuticals) by oral gavage. 20 % Captisol was used as vehicle control. Treatment was started 7 days after intrasplenic implantation of cancer cells and carried out for 7 days until day 14, the day prior the end point.

For immune checkpoint blockade, PD-1 antagonist (BioXCell, clone RMP-1) or Rat IgG2 (BioXCell, clone 2A3) isotype control were administered every 3 days by i.p. injection at 250 µg / dose for a total of 4 injections in 14 days (early time point treatment, d7) and 3 injections in 10 days (late time point treatment, d14). In the experiments in which CSF-1 and PD-1 inhibitory

antibodies have been used in combination, αPD-1 treatment was started 3 days after the first dose of CSF-1 inhibitor.

For T-cell depletion study, anti-CD8 (αCD8) (BioXCell, clone 2.43, 200 µg / dose) was injected by i.p. 2 days prior intrasplenic implantation of $KPC^{luc/zsGreen}$ cells into mice; at the day of $KPC^{luc/zsGreen}$ implantation, and followed by injections every 4 days for a total of 14 days. As isotype control, Rat IgG2 (BioXCell, clone LTF-2; 200 µg / dose) was used.

To target fibrosis, Calcipotriol (Tocris Bioscience) was administered daily by i.p. injection at a concentration of 60 µg / kg for a total of 10 days starting 14 days after intrasplenic implantation of cancer cells. PD-1 antagonist (BioXCell, clone RMP-1, 250 µg / dose) treatment regimen was started after 3 days of Calcipotriol injections and was performed for 10 days with an injection every 3 days.

Treatment trials were initiated when transplanted tumours reached a mean volume of approximately 40 mm^3 and 180 mm^3, 7 and 14 days after implantation, respectively. Time points for treatment analysis were preselected based on the expected window of efficacy (after 1-2 weeks of treatment).

i.p., i.v. and oral gavage administration of substances in mice were performed accordingly to the Home Office guidelines. Mice were manually restrained for i.p. injection and oral gavage procedures. For i.v. injection, mice were placed for 15 minutes in a warming box at 37 °C. A restraining device was used to perform tail vein injection. *In vivo* antibodies were resuspended in PBS or saline in a maximum volume of 200 µl for both i.p.

and i.v. injections. For oral gavage a maximum volume of 200 µl was administered.

2.4 Metastatic tumour burden quantification

2.4.1 Measurement of metastatic burden by bioluminescence

Liver metastatic tumour burden was assessed, both *in vivo* and *ex-vivo,* by measuring bioluminescence signal (IVIS, Perkin Elmer) generated by KPC$^{luc/zsGreen}$ or Panc02 $^{luc/zsGreen}$ cancer cells. *In vivo* bioluminescence signal was detected in the mice by i.p. injection of Beetle luciferin (Promega; 3 mg / mouse, administered in a volume of 100 µl of PBS). After injection mice were anesthetised using isoflurane vaporizer and placed inside the camera box of the IVIS spectrum imager with the abdomen facing up. Images were taken 10 minutes after luciferin injection. *Ex-vivo* bioluminescence signal was instead detected in resected livers by adding luciferin (3 mg / liver) all over the liver surface. Livers were then introduced into the camera box of the IVIS spectrum on a plate. Images were acquired 5 minutes after luciferin was added. The IVIS spectrum imager expresses the bioluminescence signal as radiance (photons per second) and displays it as intensity map. The luminescence is generated by the photons flux emitted by cells expressing luciferase and it correlates with the size of the tumour. Luminescence generated by metastatic pancreatic cancer cells was measured in the liver using the Living Image © imaging software. Liver tumour was defined by using a region of interest (ROI) tool and the optical emission image was normalized to acquisition time and presented as total flux (photons / second).

2.4.2 Measurement of metastatic burden by Magnetic Resonance Imaging (MRI)

For some experiments, change in tumour volume in response to inhibitory Abs or drug treatment (Method 2.3.2) was assessed by 9.4 Tesla (T) horizontal bore Biospec Magnetic Resonance (MR) Imaging scanning (Bruker Biospin, Inc.).

During the MR scanning procedure, mice were anaesthetized with isoflurane vaporizer and heartbeat monitored. Mouse livers were scanned *in vivo* before and after treatment using a T2-TurboRARE acquisition protocol. MRI images were acquired in coronal plane with 0.5 mm thickness and 0.1 mm spacing between each slice. A set of 23 slices was acquired to monitor the entire liver volume. Metastatic tumour volume was quantified by Image J software. Percentage change in metastatic tumour burden (before and after treatment) was obtained by calculating the sum of tumour area of all slices spanning the liver and multiplying it by 0.6 mm (inter-slice distance). The MRI acquisition used the following parameters: 2500 ms TR; 24 ms TE; 30 x 30 mm FOV; 240 x 240 image size.

2.4.3 Measurement of metastatic burden by haematoxylin and eosin (H&E) staining.

For some experiments, liver metastatic lesions (Method 2.3) size and frequency were quantified based on haematoxylin and eosin (H&E) staining of paraffin-embedded liver sections. H&E staining was performed by Liverpool Tissue Bank, University of Liverpool.

Zeiss microscope and ZEN imaging software was used for images acquisition and for quantification of metastatic area, respectively. The area

measurement tool provided by ZEN imaging software was used to quantify metastatic area for all acquired metastatic tissue images.

2.5 RNA extraction and quantitative reverse transcription PCR (RT-qPCR)

2.5.1 RNA extraction

Total RNA purification was performed by the RNeasy mini kit (Qiagen). Cells were lysed in RLT buffer (Qiagen) + β-Mercaptoethanol (1:100, Sigma-Aldrich). For < 5 x 10^6 cells, 350 µl of RLT buffer + β-Mercaptoethanol were used; alternatively for 5 x 10^6 – 1 x 10^7 cells, 600 µl of lysis buffer were used. After lysis, one volume of 70 % ethanol was added to the homogenized lysates. Samples were then transferred into RNeasy spin columns and centrifuged 15 seconds at 8000 x *g*. Columns were processed according to the manufacturer protocol (Qiagen RNAeasy Cat. No. 74104). At the end, RNA was eluted from the columns by adding 30 µl of RNase-free water. RNA concentration was measured with a Nanodrop (Thermo Fisher Scientific).

2.5.2 Reverse transcription (RT) and quantitative PCR (qPCR)

From total RNA, complementary DNA (cDNA) was obtained using QuantiTect Reverse Transcription kit (Qiagen). Between 500 ng and 1 µg of total RNA was used to perform the reverse transcription (RT) reaction. First, a reaction mix of total 14 µl was obtained by mixing Wipe-out Buffer (Qiagen, provided with the kit) and total RNA. The mixing reaction was incubated for 2 minutes at 42 °C. After incubation, a mix composed of RT buffer 5x, RT primer mix and RT enzyme (all provided by the kit) was added to the reaction suspension to reach a total volume of 20 µl. The prepared reaction mix was

then incubated for 20 minutes at 42 °C and 3 minutes at 95 °C for reverse-transcription to occur.

The obtained cDNA was diluted 1:5 in RNase-free water before its use for quantitative PCR (qPCR) reaction, thus a total of 5 µl cDNA per reaction mix was used. For each qPCR reaction, a total of 20 µl mix containing 3 µl of water, 2 µl PCR primer (QuantiTect Primers Assays, Qiagen) and 10 µl 5x HOT FIREPol EvaGreen qPCR Mix Plus (ROX) (Solis Biodyne) and 5 µl cDNA was used. The reaction was performed on an MX3005P instrument (Stratagene). Three-step amplification was performed (95 °C for 15 seconds, 60 °C for 20 seconds, 72 °C for 30 seconds) for 45 cycles. Relative expression levels were normalized to *Gapdh* expression according to the formula 2^− (Ct *gene of interest* – Ct *Gapdh*). Fold increase in expression levels were calculated by the comparative Ct method 2^- (ddCt).

The list of QuantiTect Primers Assays that were used to assess genes mRNA levels is provided in Table 1. All primers were purchased from Qiagen.

2.6 Immunofluorescence

Murine liver tissues were fixed using a sucrose gradient method to preserve the zsGreen fluorescence. Briefly, livers were fixed in 4 % Formaldehyde + 10 % sucrose in PBS for 4 hours and then transferred to 20 % sucrose in PBS for 8-10 hours. Tissues were transferred into 30 % sucrose for an additional 8-10 hours, embedded in Optimal Cutting Temperature (OCT) medium and stored at -80 °C.

For immunofluorescence staining, 5 µm liver sections were permeabilized by 0.1 % Triton X-100 (Sigma-Aldrich) for 10 minutes. Unspecific binding was

prevented by using PBS + 8 % Normal goat serum for 1 hour at room temperature. Tissue sections were incubated overnight at 4 °C with primary antibodies. The next day, tissue sections were washed in PBS and stained with the secondary antibody goat anti-rabbit conjugated to AlexaFluor594 (Abcam, 1:500) and DAPI (Life Technologies, 1:500) for 1 hour at room temperature. Luciferase / ZsGreen transfected cells were detected using their intrinsic signal. Sections were finally mounted using Dako Fluorescent Mounting Medium.

Immunofluorescence staining was also performed, in some cases, on tissue sections obtained from livers directly embedded in OCT. In this case, tissue sections were fixed in ice-cold acetone for 2 minutes and permeabilized with 0.1 % Triton X-100. Sections were washed and incubated overnight at 4 °C with the primary antibodies. The next day, tissue sections were washed in PBS and stained with the secondary antibody goat anti-rabbit conjugated to AlexaFluor594 (Abcam, 1:500); goat anti-rat conjugated to AlexaFluor488 (Abcam, 1:500) and DAPI (Life Technologies, 1:500) for 1 hour at room temperature. All tissue sections were imaged using an Axio Observer Light Microscope with the Apotome.2 (Zeiss) and quantified using the Zen Software (Zeiss). Quantification of intrametastatic (IM) and peripheral (P) $CD8^+$ T cells was performed using Nis Elements, Advanced Research software (Nikon). Peripheral area of metastatic lesions was defined as the outer 40 % of the total lesion area. For quantification of IF staining, the number of positive stained cells per metastatic lesion area was calculated.

The list of primary antibodies that were used is provided in Table 2.

2.7 Immunohistochemistry (IHC) analysis

Deparaffinization and antigen retrieval was performed using an automated DAKO PT-link. Paraffin-embedded human and mouse liver metastatic sections were immunostained using the DAKO envision+system-HRP. After antigen retrieval, peroxidase block (Dako) was added for 20 minutes, followed by three washes in Tris Buffered Saline with Tween 20 (TBST). Tissue sections were then incubated overnight at 4 °C with primary antibodies. After washes were performed, Secondary-HRP conjugated antibodies (Peroxisade labelled Polymere, Dako) were incubated for 30 minutes at room temperature. Staining was developed using diaminobenzidine (Dako) and counterstained with hematoxylin (Dako). Sections were immersed in Scott's Tap Water (Sigma-Aldrich) and subsequently dehydrated progressively through alcohol steps (from 70 % to 100 %). Sections were fixed in Xylene (Sigma-Aldrich) and slides were mounted using DPX mounting medium (Sigma-Aldrich). All tissue sections were imaged using an Axio Observer Light Microscope and quantified using the Zen Software (Zeiss) or with Image J in the case of quantification of αSMA and PD-L1 staining. For quantification of IHC staining, the number of positive stained cells or positive stained area per metastatic lesion was calculated.

List of primary antibodies that were used is provided in Table 2.

For CD8 staining VECTASTAIN® Elite® ABC-HRP Kit (Peroxidase, Rat IgG) (Vector laboratories) was used. After deparaffinization and antigen retrieval, peroxidase activity was blocked with Peroxidase blocker (Dako). To avoid

unspecific staining, normal blocking serum was used for 20 minutes at room temperature. Primary CD8 antibody (clone 53.7, Biolegend) was incubated for 30 minutes at room temperature. After washing steps were performed, a biotinylated secondary antibody was added for 30 minutes. An Avidin / biotinylated VECTASTAIN ABC reagent was then added for 30 minutes. Staining was developed using diaminobenzidine (Dako) and counterstained with hematoxylin (Dako). Sections were immersed in Scott's Tap Water (Sigma-Aldrich) and subsequently dehydrated progressively through alcohol steps (from 70 % to 100 %). Sections were fixed in Xylene (Sigma-Aldrich) and slides were mounted using DPX mounting medium (Sigma-Aldrich).

2.8 Picrosirius red staining

Paraffin embedded murine liver sections were de-waxed using Xylene (Sigma-Aldrich) and hydrated using a graded ethanol series (100 %, 75 %, 65 %). Tissue sections were then treated with 0.2 % phosphomolybdic acid and subsequently stained with 0.1 % Sirius red F3B (Direct red 80)(Sigma-Aldrich) in saturated picric acid solution for 90 minutes at room temperature. Tissues were then rinsed twice in acidified water (0.5 % glacial acetic acid) (Sigma-Aldrich) before and after the staining with 0.033 % fast green FCF (Sigma-Aldrich). Finally, tissues were dehydrated in three changes of 100 % ethanol, cleared in Xylene (Sigma-Aldrich) and mounted with DPX mounting medium (Sigma-Aldrich). Picrosirius red staining was quantified using Image J software. For quantification, the positive picrosirius red stained area per metastatic lesion was calculated.

2.9 Liver digestion and preparation of single cell suspension.

Resected livers were processed by mechanical disruption using scalpels. When livers were reduced into little pieces, enzymatic digestion was performed by using 1 mg / mL Collagenase P (Roche) in Hanks Balanced Salt Solution (HBSS; Sigma-Aldrich) for 20 minutes at 37 °C. The digestion reaction was stopped by adding HBSS supplemented with 5 % FBS. Cell suspensions were centrifuged for 5 minutes at 270 x *g*, resuspended in HBSS and filtered through a 500 μm polypropylene mesh (Spectrum Laboratories). Cell suspensions were resuspended in 1 ml 0.05 % trypsin (Sigma-Aldrich) and incubated at 37 °C for 5 minutes. Cells were filtered through a 70 μm cell strainer and centrifuged again for 5 minutes at 270 x *g*. Cell pellets were resuspended in 5 ml of Red Blood Cell (RBC) Lysis buffer (1x concentration; BD Pharm Lyse™) for 5 minutes to eliminate red blood cells. Lysis was stopped by adding PBS and another centrifugation step for 5 minutes at 270 x *g* was performed. Cells were finally resuspended in PBS + 0.5 % BSA (Bovine Serum Albumin) for further use.

2.10 Mouse blood collection and preparation

Mice were euthanized using carbon dioxide (CO_2) and cardiac puncture was performed to collect blood. Blood was harvested into EDTA tubes (Microvette, Sarstedt) and successively used for flow cytometry application. Red blood cell lysis was performed using 1 ml of Red Blood Cell (RBC) Lysis buffer (1x concentration; BD Pharm Lyse™) for 5 minutes. Lysis reaction was stopped using PBS. Next, the cell suspension was centrifuged 270 x *g* for 10

minutes at room temperature and further processed for flow cytometry analysis.

2.11 Flow cytometry and cells sorting

Cell suspensions in PBS + 0.5 % BSA were blocked for 10 minutes on ice with FC block (BD Pharmingen, Clone 2.4 G2) prior to antibody staining. For cell-surface marker staining, cells were stained with Sytox-blue dead cells marker (Life Technologies) and incubated with antibodies directly conjugated to a fluorophore (Table 2) for 45 minutes at 4 °C in the dark. Three washing steps in PBS + 0.5 % BSA followed by cells centrifugation for 5 minutes at 270 x *g* were performed prior to sample analysis by flow cytometry.

If intracellular markers staining was also required in addition to cell-surface markers staining, cells were first fixed (eBioscience, IC fixation buffer) for 20 minutes at room temperature in the dark, washed using PBS + 0.5 % BSA and then permeabilized (eBioscience, 1x permeabilization buffer) for 10 minutes. Successively, antibodies against intracellular marker were added and cells were incubated for 45 minutes at 4 °C in the dark. Three washing steps in PBS + 0.5 % BSA followed by cell centrifugation for 5 minutes at 270 x *g* were performed prior to sample analysis by flow cytometry. When intracellular marker staining was performed, Sytox-blue viability marker was not used. List of fluorophore-conjugated antibodies that were used is provided in Table 2.

To assess IFNγ expression levels in metastasis derived $CD8^+$ T cells, magnetically isolated $CD8a^+$ T cells from metastatic livers (Methods 2.9 and 2.13.1) were stimulated with 50 ng / ml phorbol 12-myristate 13- acetate (PMA) (Sigma-Aldrich) and 1 μg / ml of Ionomycin (Sigma-Aldrich) for 5

hours at 37 °C in the presence of Brefeldin A (eBioscience, 1:100) and subsequently stained for IFNγ.

Flow cytometry was performed on a FACS Canto II (BD Bioscience) and FACS cell sorting was carried out using FACS Aria (BD Bioscience). Cells were sorted directly in RLT buffer (Qiagen) + β-Mercaptoethanol (1:100, Sigma-Aldrich) and processed for RNA extraction using RNeasy mini kit (Method 2.5). For each cell sorting experiment, the purity of sorted cells was tested by performing ARIA post-sort analysis. Basically, cells were sorted in 1 ml of DMEM and processed again by the ARIA cell sorter to assess the purity. In average, in the case of ARIA sorted $CD8^+$ T and $F4/80^+$ cells the assessed purity was of around the 94 % and 96 %, respectively.

For data acquisition on both FACS Canto II and FACS Aria, spectra overlap between different fluorophores was removed by compensation of fluorophore spectra using single staining of cell samples for each of the fluorophore being used.

2.12 Splenocyte isolation

Splenocytes were isolated from spleens of 6-8 weeks old female C57BL/6 mice. Spleens were destroyed with a syringe plunger and cells were collected in MAC buffer (PBS without Calcium/ Magnesium plus 2mM Ethylenediaminetetraacetic acid (EDTA) and 0.5 % BSA). Cell suspensions were passed through a 70 µm strainer and centrifuged at 400 x *g* for 10 minutes at room temperature. Cell pellets were resuspended in 5 ml of Red Blood Cell (RBC) Lysis buffer (1x concentration; BD Pharm Lyse™) for 5 minutes to eliminate red blood cells. Lysis was stopped by adding PBS and

an additional centrifugation step at 400 x *g* for 10 minutes at room temperature was performed. Cells were resuspended and cultured in RPMI 1640 (Gibco, Thermo Fisher Scientific) supplemented with 10 % FBS and containing Penicillin-Streptomycin (10 ml / L; Sigma-Aldrich) and Amphotericin B solution (2.5 mg / L; Sigma-Aldrich); from here on refereed as complete RPMI.

2.13 Magnetic beads isolation of cells

Magnetic beads isolation kits (Miltenyi) were used to perform isolation of $CD8^+$ T cells or $F4/80^+$ cells from cell suspensions obtained from mouse livers.

2.13.1 Isolation of $CD8^+$ T cells

$CD8^+$ T cells were isolated by negative selection using a CD8a+ T cells isolation kit (Miltenyi, Cat. No. 130-104-075). First, cells (from Method 2.9 or 2.12) were resuspended in MAC buffer and filtered through a 30 µm filter to avoid cells clumping. Successively, cell suspensions were processed for manual magnetic labelling. From liver, around 2 x 10^7 cells were obtained. Accordingly with the number of cells, 20 µl of Biotin-Antibody Cocktail was added to cells suspension and incubated for 5 minutes at 4 °C. The Biotin-Antibody Cocktail is a cocktail of biotin-conjugated monoclonal antibodies against CD4, CD11b, CD11c, CD19, CD45R (B220), CD49b (DX5), CD105, MHC Class II, Ter-119, and TCRγ/δ, which allow to magnetic label the majority of cells in the cell suspensions with the exception of $CD8^+$ T that in this way remained unstimulated. Successively, 60 µl of MAC buffer were added to the cell suspension, followed by 40 µl of Anti-Biotin MicroBeads.

Cells were incubated with MicroBeads for 10 minutes at 4 °C and magnetic cells separation was performed straight after. For separation, LS MACS Columns (Miltenyi) were used. Columns were placed in the magnetic field of a MACS Separator (Miltenyi) and washed with MAC buffer prior use. Cell suspension was applied onto the columns and the flow-through containing unlabelled cells, representing the enriched $CD8a^+$ T cells, was collected. Isolated $CD8a^+$ T cells were centrifuged and resuspended in the suitable media for further use. For each experiment, the purity of isolated $CD8a^+$ T cells was assessed by flow cytometry using anti- CD8 antibody (Biolegend, clone 53-6.7) (Method 2.11). Approximately 89 % of isolated cells were $CD8^+$.

2.13.2 Isolation of F4/80$^+$ macrophages

For $F4/80^+$ cells isolation, single cell suspensions were first generated from liver tumour (Method 2.9). Next cells were resuspended in MAC buffer and filtered through 30 µm filter to avoid cells clumping. Successively, cell suspensions were processed for manual magnetic labelling. Around 2 x 10^7 cell suspensions were centrifuged at 400 x *g* for 10 minutes and resuspended in 200 µl MAC buffer, and 20 µl of $F4/80^+$ PE conjugated antibody (Miltenyi, Cat. No. 130-102-422) was added for 10 minutes, in the dark, at 4 °C. A washing step was performed and cells were successively centrifuged at 400 x *g* for 10 minutes. Cells were resuspended in 160 µl of MAC buffer and 40 µl of Anti-PE MicroBeads (Miltenyi, Cat. No. 130-048-801) were added for 15 minutes at 4 °C. Cells were washed, centrifuged and resuspended in 500 µl MAC buffer for magnetic separation. For separation, LS MACS Columns (Miltenyi) were used. Columns were placed in the

magnetic field of a MACS Separator (Miltenyi) and washed with MAC buffer prior use. Cell suspension was applied onto the columns and three washing steps were performed to eliminate the unlabelled cell fraction. After last wash, columns were removed from the magnetic separator, placed in suitable tubes and magnetic labelled cells were flushed out. Eluted cells were centrifuged and resuspended in the suitable media for further use. For each experiment, the purity of isolated $F4/80^+$ cells was assessed by flow cytometry using anti- F4/80 antibody (Biolegend, clone BM8) (Method 2.11). Approximately 92 % of isolated cells were $F4/80^+$.

2.14 T cells activation using Dynabeads Mouse T- Activator CD3/CD28

Activation of T cells from splenocyte cell suspension (Method 2.12) or activation of bead-isolated CD8+ T cells (Method 2.14) was performed using Dynabeads Mouse T- Activator CD3/CD28 (Thermo Fisher Scientific). 1 x 10^6 cells were plated in 250 µl of complete RPMI medium in a well of a 96 well plate. 25 µl of pre-washed and resuspended Dynabeads magnetic beads were added to obtain a bead to cell ratio of 1:1. Activated T cells were then incubated at 37 °C, accordingly with the specific experiment requirements.

For flow cytometry applications (Method 2.11), once cells were harvested, beads were removed from the cell suspension. Cells were transferred from the plate into an eppendorf tube and the tube was placed into a magnet for 1-2 minutes to separate the beads from the solution. The supernatant was then transferred into a new tube to proceed into further flow cytometry cell preparation steps.

2.15 Adoptive transfer experiments

For T cell adoptive transfer, experimental metastasis was induced by intrasplenic implantation of $1x10^6$ $KPC^{luc/zsGreen}$ cells into tdTomatoRed+, WT, and $Grn^{-/-}$ mice (Method 2.3.1). After 13 days, tumour bearing tdTomatoRed+ mice were euthanized and spleens were dissected to isolate $CD8^+$ T cells (Miltenyi, $CD8a^+$ T cell isolation Kit, Method 2.13.1). Isolated $CD8^+$ T cells were stimulated with Dynabeads Mouse T- Activator CD3/CD28 (Thermo Fisher Scientific, Method 2.14) and incubated for 24 hours at 37 °C. The next day, 1.5 x 10^6 $tdTomoatoRed^+$ $CD8^+$ T cells were injected into the tail vein of tumours within WT and $Grn^{-/-}$ mice. After 24 hours, mice were sacrificed and livers were collected and embedded in OCT medium. 5 µm liver sections were stained for DAPI (Life Technology, 1:500) and spatial localization of adoptive transferred $dtTomatoRed^+$ CD8+ T cells was assessed by fluorescence microscopy measuring dtTomato Red^+ signal (Quantification as described in Method 2.6).

For MAMs adoptive transfer, experimental metastasis was induced by intrasplenic implantation of 1 x 10^6 $KPC^{luc/zsGreen}$ cancer cells (Method 2.3.1). Mice were treated with CSF-1 and PD-1 inhibitory Abs starting 7 or 14 days after cancer cell implantation (Method 2.3.2). At day 24, metastatic livers from sacrificed mice were dissected to isolate $F4/80^+$ cells (Miltenyi, $F4/80^+$ isolation Kit, Method 2.13.2). 1 x 10^6 $F4/80^+$ isolated cells were then injected into the tail vein of mice bearing experimental metastasis at day 7. After 5 days, injected mice were euthanized and livers were harvested and analysed further.

2.16 Generation of bone marrow derived macrophages (BMMs)

Primary murine macrophages were generated by flushing the bone marrow with a 5 ml syringe and 25 G needle from the femur and tibia of C57BL/6 naïve mice, previously euthanized by cervical dislocation. Bone marrow was collected in ice-cold MAC buffer. Cells were centrifuged at 270 x *g*, 10 minutes at room temperature and resuspended in 5 ml of Red Blood Cell (RBC) Lysis buffer (1x concentration; BD Pharm Lyse™) for 5 minutes at room temperature to eliminate red blood cells. After stopping the lysis reaction with PBS, cells were centrifuged and then resuspended in MAC buffer; cell suspension was successively layered on top of Histopaque 1083 (Sigma- Aldrich) and centrifuged for 25 minutes at 270 x *g* without brakes and without acceleration for isolation of monocyte population by density gradient. After centrifugation, the monocyte- containing layer was transferred in to PBS solution, centrifuged (270 x *g*, 10 minutes at room temperature) and resuspended in complete DMEM medium supplemented with 10 ng / ml murine M-CSF (Peprotech) for differentiation in BMMs. Monocytes were plated and cultured at 37 °C for a total 5 days to obtain full macrophage differentiation. Medium was changed 2 days after cells were plated. After 5 days BMMs were used for further experiments. The purity of BMMs was assessed for each isolation procedure by flow cytometry (Method 2.11) using F4/80 antibody (Biolegend, BM8). Approximately 94 % of isolated BM cells were $F480^{+}$ after 5 days.

2.17 Preparation of conditioned media (CM)

Conditioned medium from Panc02, KPC cancer cells and bone marrow derived macrophages (BMMs) was generated**.** Panc02 and KPC cells were cultured in complete DMEM medium and regularly passaged every two days prior to CM preparation. Murine bone marrow derived cells were cultured and allowed to differentiate into BMMs in complete DMEM medium containing recombinant mouse CSF-1 for five days prior to CM preparation (Method 2.16).

To obtain CM, cell medium was removed from 70 % confluent cells and cells were then washed three times with PBS before addition of serum-free DMEM medium. Cells were incubated for 18-24 hours in serum-free medium and then medium was collected and filtered through 0.45 μm filters before use.

2.18 Granulin expression in BMMs

BMMs were generated as in Method 2.16. BMMs were subsequently stimulated with DMEM containing 2 % serum in the presence or absence of murine recombinant M-CSF-1 (Peprotech) for 24 hours. Alternatively, BMM were stimulated with KPC or Panc02 CM for 24 hours in the presence of absence of αCSF-1 inhibitory antibody (BioXCell; [2.5 μg / ml]). BMMs were finally lysed in RLT buffer (Qiagen) + β-Mercaptoethanol (Sigma-Aldrich) and *Granulin* expression was assessed by quantitative PCR (qPCR, primer: Mm_Grn_1_SG; QT01061634) (Method 2.5).

2.19 ELISA

Assessment of Granulin secretion: BMMs were generated as described in Method 2.16 and subsequently stimulated with DMEM containing 2 % serum in the presence of murine recombinant M-CSF ([20 ng / ml]; Peprotech), IFNγ [20 ng / ml] and LPS ([100 ng / ml];Peprotech and Sigma-Aldrich, respectively), IL-10 ([20 ng / ml] ; Peprotech), IL-13([20 ng / ml]), IL-4 ([20 ng / ml] ; Peprotech) for 24 hours. The supernatant was collected to assess Granulin protein level by ELISA kit (LifeSpan BioScience, LSBio).

Assessment of M-CSF-1 secretion: CM from Panc02, KPC cancer cells and BMMs was obtained to measure the production of murine M-CSF by Quantikine ELISA kit (R&D System).

The performed assays are based on the sandwich ELISA principle. Briefly, each well of the supplied microtiter plate was pre-coated with the target capture antibody (anti-Granulin or M-CSF-1). Standards (provided with the kit) or samples were added to the wells to allow antigen binding to the capture antibody. Washing steps were performed to wash away unbound Standards or samples. A biotin- conjugated detection antibody, which recognizes and binds the captured antigen, was then added. Washing steps were performed to wash the unbound detection antibody. An Avidin-Horseradish Peroxidase (HRP) conjugate was added to bind the biotin. Other washing steps were performed to remove unbound Avidin-HRP conjugates. A TMB substrate was then added to react with the HRP enzyme resulting in colour development. A sulphuric acid stop solution was added to stop the colour development reaction and optical density (OD) of the well was measured at the wavelength of 450 nm ± 2 nm. An OD standard curve was

generated using known antigen concentrations (Standards were used); the OD of the unknown samples was then compared to the standard curve in order to determine its antigen concentration. For each sample, three biological replicates were used. Different dilutions of the samples were tested to obtain the OD.

2.20 *In vitro* T-cell activation assay

Primary splenocytes were obtained from spleens of naïve C57BL/6 mice (Method 2.12). Splenocytes were cultured in complete RPMI. For T cell activation assays, splenocytes were stimulated using Dynabeads Mouse T-Activator CD3/CD28 (Thermo Fisher Scientific, Method 2.14). Usually, 1 x 10^6 activated splenocytes (S) were then co-cultured with BMMs from WT and $Grn^{-/-}$ mice or with macrophages (M) magnetically isolated (Method 2.13.2) from day 6 and day 14 metastasis bearing livers (4:1 ratio, S: M). Cells were plated in 96 well plates and incubated at 37 °C for 24 hours. Subsequently, Brefeldin A (eBioscience, 1:100) was added to the cells for 5 hours. Cells were then harvested and stained with CD8 (Biolegend, clone 53-6.7) and IFNγ (Biolegend, Clone XMG1.2) antibodies and analysed by flow cytometry (Method 2.11). For some experiments, recombinant mouse Progranulin protein (recGrn) (R&D systems; [1 µg / ml]) was used.

2.21 *In vitro* T- cell proliferation Assay

For the T cell proliferation assay, splenocytes derived from naïve C57BL/6 mice (Method 2.12) were resuspended in PBS and incubated with 5 µM Carboxyfluorescein Diacetate Succinimidyl Ester (CFSE) (Biolegend) for 10 minutes at 37 °C in the dark. Successively, the staining was quenched by

adding 5 times the CFSE staining volume using complete RPMI 1640. Cells were centrifuged and resuspended in complete warm RPMI 1640. Labelled splenocytes were then stimulated with Dynabeads Mouse T-Activator CD3/CD28 (Thermo Fisher Scientific, Method 2.14). 1 x 10^6 activated splenocytes (S) were then co-cultured with BMMs from WT and $Grn^{-/-}$ mice or with macrophages (M) magnetically isolated (Method 2.13.2) from day 6 and day 14 metastasis bearing livers (4:1 ratio, S: M). Cells were plated in 96 well plates and incubated at 37 °C for 72 hours. Subsequently, cells were harvested and stained with CD8 antibody (Biolegend, clone 53-6.7). Proliferating $CD8^+$ T cells were tracked by flow cytometry (Method 2.11). For some experiments, recombinant mouse Progranulin protein (R&D systems; [1 µg / ml]) was used.

2.22 Bone marrow transplantation

Bone marrow (BM) transplantation was performed by reconstituting the bone marrow of lethally irradiated (10 Gy) female, 6-week-old C57BL6 mice by tail vein injection of 5 × 10^6 total bone marrow cells isolated from $Grn^{-/-}$ mice or WT mice. After 4 weeks, engraftment of $Grn^{-/-}$ bone marrow was assessed by genomic DNA PCR (5' to 3'; Primer 11080: AGA GGG TGA GCT GCA ATG TT; 11081: AAG GGC ATT AGC CAA GTG TG; 11082: TCT CCC AGG TAG CCC CTA CT) according to The Jackson Laboratory protocol on peripheral blood cells from fully recovered bone-marrow-transplanted mice. WT or $Grn^{-/-}$ transgene were separated by agarose gel electrophoresis. PCR products specific for WT (468 bp) were exclusively detected in mice transplanted with WT BM, while PCR products specific for $Grn^{-/-}$ transgene (211bp) were only detected in mice transplanted with $Grn^{-/-}$ bone marrow

(data not shown). After confirmation of successful bone marrow reconstitution, mice were enrolled in tumour studies (Method 2.3.1). Bone marrow transplantation and subsequent validation of granulin depletion were performed by Sebastian Nielsen, University of Liverpool.

2.23 Nanostring analysis

For nanostring analysis, 30 mg of liver from naïve mice and from mice with liver metastasis generated 6 (Day 6) and 14 (Day 14) days after intrasplenic implantation of cancer cells was used (Method 2.3.1). Three biological replicates for each group (Naïve, Day 6 and Day 14) were used. After resection, livers were stored in RNA later (Qiagen) overnight (O/N) at 4 °C and successively transferred at -80 °C until further analysis was performed. RNA was successively extracted from livers using the RNeasy mini kit (Method 2.5.1). For Nanostring analysis, 100 ng of total extracted RNA, for each liver sample, was used. NanoString assay was performed according to the procedure indicated in the nCounter Gene Expression Assay User Manual and it was performed under the specialized technical supervision of the Centre of Genomic Research at Liverpool University [272]. To validate the expression of specific genes involved in pancreatic cancer metastasis immune response, the *nCounter XT mouse Immunology Code set* was used. Each nCounter Gene Expression Assay was performed using a single nCounter Cartridge containing 12 samples. Nanostring's nCounter technology is based on digital detection and direct molecular barcoding of individual target molecules identified by the use of a unique probe pair for each of the target of interest. The probe pair consists of a color-coded Report probe, which carries the visible signal on its 5' end, and a Capture probe,

which carries a biotin moiety on the 3' end. The first step of the nCounter Gene Expression Assay consists in the hybridization of the probe pair with the specific target. In each reaction, probes are generally used in massive excess to ensure that each target finds a probe pair. Sample preparation for the hybridization reaction was carried out at room temperature. For each sample, 3 µl of Reporter CodeSet, 5 µl of hybridization buffer, up to 5 µl (100ng) of sample RNA, and 2 µl of Capture ProbeSet were used (all reagents were provided by nCounter Master Kit). Reaction tubes were then incubated for 24 hours in the thermal cycler (Bio-Rad Laboratories) at 65 °C to allow hybridization to occur. After hybridization, samples were placed in the Prep Station. The Prep Station is a multi-channel pipetting robot that processes hybridized samples and prepares them for data collection on the Digital Analyzer. The Prep Station performs liquid transfers, magnetic bead separation to wash out excess of probes, and immobilization of molecular labels on the sample cartridge surface. For sample processing in the Prep Station consumable components, including the cartridge, and reagents were all provided by the nCounter Master Kit and loaded onto the Prep Station deck prior to use. The Prep Station was set up to initiate a new run under the 'High Sensitivity' protocol. Instructions appearing on Prep Station screen were followed. At the end of the automated reactions performed by the Prep Station, the cartridge was taken, sealed and inserted into the nCounter Digital Analyzer. The Digital Analyzer is a multi-channel epifluorescence scanner that collects data by taking images of the immobilized fluorescence reporters in the sample cartridge with a CCD camera through a microscope objective lens. The number of images taken corresponds to the number of

reporters counted. Images were processed internally into the Digital Analyzer and a Reporter Code Count (RCC) file containing reporter counts was produced. The RCC file was downloaded via USB flash drive (provided in the nCounter Master Kit) and imported into the nSolverAnalysisSoftware for quality control analysis. Data were also exported as a comma separated value (CSV) format for convenient data analysis using nSolverAnalysisSoftware.

The data were analysed in accordance with nCounter expression data analysis guide using the nSolverAnalysisSoftware. Negative probes were used for background substraction and the data set was normalized to the geometric mean of the samples. The software allowed the identification of genes that were more than two-folds differently expressed at Day 6 in comparison to Day 14 in metastatic livers. A heat map generated by the software was used to represent the differential expression of the selected genes in Naïve, Day 6 and Day 14 liver samples. The identified genes were also subjected to a Gene Ontology Pathway analysis using Reactome Pathway Database, which enabled the association of differently expressed genes with immune-related pathways. Gene Ontology Pathway analysis was performed with the support of Dr. Dean Hammond from the University of Liverpool.

2.24 Assessment of PD-L1 expression *in vitro*

KPC pancreatic cancer cells were plated in complete DMEM culture media and allowed to adhere overnight at 37 °C. The next day, cells were washed and incubated for 48 hours in DMEM supplemented with 2 % FBS and 50 ng

/ ml of murine recombinant IFNγ (Peprotech). Cells were then collected and stained with PD-L1 antibody (Biolegend, 10F.9G2). PD-L1 expression was assessed by flow cytometry (Method 2.11).

2.25 Human tissue samples

Paraffin embedded human tissue sections from control healthy subjects, primary PDAC tumours, and PDAC liver metastasis were obtained from the Liverpool Tissue Bank, University of Liverpool, UK and approved by NRES Committee North West Cheshire REC15/NW/0477. All samples were pathologically confirmed.

2.26 Statistical analysis

Statistical analysis of experiments with two groups was performed using a two-tailed unpaired Student's t-test with 95 % confidence interval. Statistical analysis of experiments with more than two groups was performed using nonparametric analysis of variance (ANOVA) test with comparisons between groups using Bonferroni's multiple comparison test. All statistical analysis were performed using GraphPad Prism software, $p<0.05$ was considered significant. Statistical significance is indicated in the figures as follows: ***, $p<0.001$; **, $p< 0.01$; *, $p< 0.05$; n.s., not significant. Quantification of results is expressed as mean ± SEM unless stated otherwise. Number of patients, healthy subjects and mice used for *in vivo* experiments is reported in the figure legend.

2.27 List of qPCR primers and antibodies

Primers for qPCR	
Gene	Primer and catalogue number
Gapdh	Mm_Gapdh_3_SG; QT01658692
Cxcl10	Mm_Cxcl10_1_SG; QT00093436
Cd86	Mm_Cd86_1_SG; QT01055250
Ifng	Mm_Ifng_1_SG; QT01038821
Il12	Mm_Il12b_1_SG; QT00153643
H2-Aa	Mm_H2-Aa_1_SG; QT01061858
Retnla	Mm_Retnla_1_SG; QT00254359
Tgfb	Mm_Tgfb1_1_SG; QT00145250
Il10	Mm_Il10_1_SG; QT00106169
Arginase	Mm_Arg1_1_SG; QT00134288
Gzmb	Mm_Gzmb_1_SG; QT00114590
Tnf	Mm_Tnf_1_SG; QT00104006
Prf1	Mm_Prf1_1_SG; QT00282002
Mrc1	Mm_Mrc1_SG; QT00103012
Granulin	Mm_Grn_1_SG; QT01061634

Table 1. Primers used for quantitative PCR.

List of QuantiTect Primers Assays (Qiagen) used for qPCR application.

Antibodies for flow cytometry			
Target protein	Clone (F: Fluorophore)	Species and Dilution	Source
CD45	30F-11 (F: PE-Cy7; APC-Cy7)	Rat anti- mouse; 1:100	Biolegend
F4/80	BM8 (F: APC; PerCp-Cy5.5)	Rat anti- mouse; 1:100	Biolegend
CD8	53-6.7 (F: PerCp-Cy5.5)	Rat anti- mouse; 1:100	Biolegend
CD206	C068C2 (F: PerCp-Cy5.5)	Rat anti- mouse; 1:100	Biolegend
PD-1	29F.1A12 (F: PE; APC)	Rat anti- mouse; 1:100	Biolegend
CD69	H1.2F3 (F: PE)	Hamster anti- mouse; 1:100	Biolegend
CD11b	M1/70 (F: PE-Cy7)	Rat anti- mouse; 1:100	Biolegend
Ly6C	HK 1.4 (F: FITC)	Rat anti- mouse; 1:100	Biolegend
Ly6G	1A8 (F: PE)	Rat anti- mouse; 1:100	Biolegend
IFNγ	XMG1.2 (F: PE)	Rat anti- mouse; 1:100	eBioscience
Ki67	16A8 (F: APC)	Rat anti- mouse; 1:100	Biolegend
Granzyme B	NGZB (F: PE)	Rat anti- mouse; 1:100	eBioscience
PD-L1	10F.9G2 (F: PE)	Rat anti- mouse; 1:100	Biolegend
Antibodies for Immunofluorescence			
αSMA	polyclonal	Rabbit anti- mouse and human; 1:100	Abcam, ab5694
Relm-α	polyclonal	Rabbit anti- mouse; 1:100	Abcam, 39626
Cleaved- Caspase 3	polyclonal	Rabbit anti- mouse; 1:100	Cell Signalling, 9661

CSF1R	c-20	Rabbit anti- mouse and human; 1:100	SantaCruz Biotechnology
CD8	53-6.7	Rat anti- mouse; 1:100	Biolegend, 100701
F480	BM8	Rat anti- mouse; 1:100	Biolegend, 123101
Cytokeratin 19	polyclonal	Rabbit anti- mouse and human; 1:100	Abcam, ab53119
Granzyme B	GrB-7	Mouse anti- human; 1:50	Dako, M7235
PD-1	NAT105	Mouse anti- human; 1:100	Abcam, ab52587
CD8	144b	Mouse anti- human; 1:100	Dako, M7103
Antibodies for Immunohistochemistry			
αSMA	polyclonal	Rabbit anti- mouse and human; 1:200	Abcam, ab5694
CD8	144b	Mouse anti- human; 1:100	Dako, M7103
Cytokeratin 19	polyclonal	Rabbit anti- mouse and human; 1:100	Abcam, ab53119
CD3	SP7	Rabbit anti- mouse; 1:100	Abcam, ab16669
Granulin	3337313	Rat anti- mouse; 1:50	R&D Systems, MAB25571
iNOS	polyclonal	Rabbit anti- mouse; 1:100	Abcam, ab15323
MHC II	NIMR-4	Rat anti- mouse; 1:100	Abcam, ab25333
COX-2	polyclonal	Rabbit anti- mouse; 1:100	Cambridge bioscience, aa570-598
Ym-1	polyclonal	Rabbit anti- mouse; 1:200	Stem Cell Technology, 60130
CD206	15-2	Mouse anti- mouse; 1:100	Abcam, ab8918
Ly6G	A18	Rat anti- mouse; 1:100	Biolegend, 127601

B220	RA3-6B2	Rat anti- mouse; 1:50 103201	Biolegend, 103201
PD-L1	E1L3N	Rabbit anti- human; 1:50	Cell Signalling,13684

Table 2. Antibodies list.

List of fluorophore-conjugated antibodies used for flow cytometry analysis and primary antibodies used for Immunofluorescence and Immunohistochemistry applications. F= fluorophores that have been used.

Chapter 3:

Results

3 Chapter 3: Tumour immunity in pancreatic cancer metastasis

$CD8^+$ T cells mediated recognition and killing of tumour cells is the main mechanism of defence that our body has against cancer [122]. The presence of intra-tumoural $CD8^+$ T cells is associated with a good clinical outcome in many tumour types [273], including pancreatic cancer [274]. However, tumours can hide themselves from immune system attacks by exploiting a series of resistance mechanisms [122]. Generation of a immunosuppressive microenvironment that surrounds and protects tumour is one of the main means by which tumours escape anti-tumour immunity [157] . The main aim in this study is to understand whether anti-tumour immunity exists to restrain pancreatic cancer metastasis formation to the liver and whether, instead, the formation of an immunosuppressive microenvironment may overcome the anti-tumour immune defence and lead to establishment of the metastatic lesion.

3.1 $CD8^+$ T cells are infiltrated and activated in small but not in large metastatic pancreatic cancer lesions

Disseminating pancreatic cancer cells mainly generate metastasis into the liver [236], [237]. To investigate $CD8^+$ T cell mediated anti-tumour immunity in pancreatic cancer metastasis, liver biopsies from pancreatic cancer patients with advanced metastasis and healthy livers were first interrogated by IHC and IF techniques. IHC staining revealed that in healthy livers $CD8^+$ T cells were evenly distributed, at a low density (Figure 3.1 a). In human metastatic livers, lesions composed by low number of cytokeratin positive (CK^+) cancer cells and lesions instead composed by high number of CK^+

cancer cells were identified. Thus, within metastatic tissues CK^+ poor and rich lesions (Figure 3.1 a) were discriminated. Interestingly, it was found that an inverse relationship existed between number of CK^+ cancer cells and $CD8^+$ T cells. Indeed, CK^+ poor lesions were highly infiltrated by $CD8^+$ T cells, whereas in CK^+ rich lesions only few $CD8^+$ T cells were found (Figure 3.1 a and b).

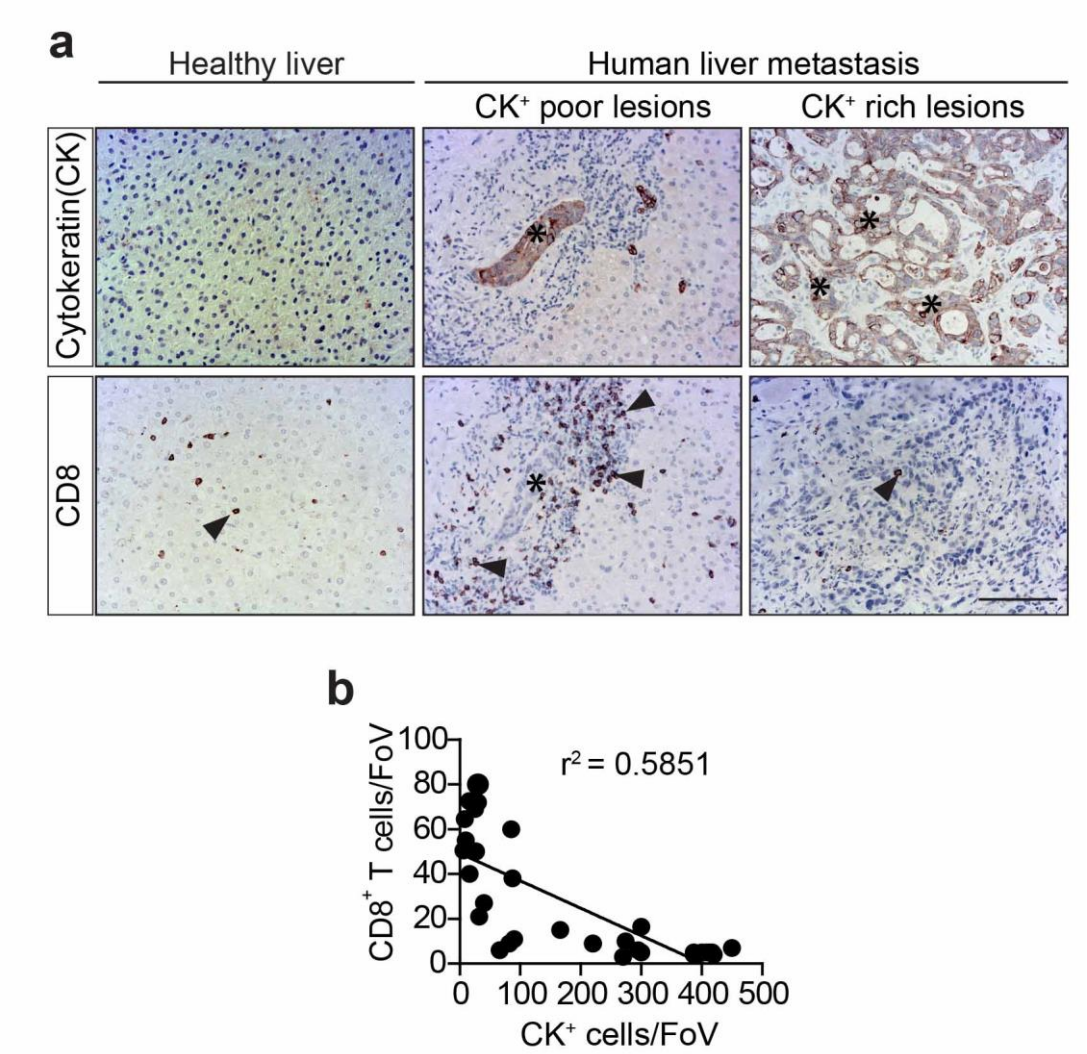

Figure 3.1 Metastasis progression is accompanied by loss of CD8$^+$ T cell infiltration.

a) Representative immunohistochemistry (IHC) images and quantification of cytokeratin positive (CK$^+$) metastatic cancer cells and infiltrating CD8$^+$ T cells in human liver serial sections. Each metastatic pancreatic cancer liver section contained multiple lesions. Individual lesions were captured in one field of view (FoV). Three individual lesions were analysed for each patient. **b)** Dots represent the relationship between CD8$^+$ T cell and CK$^+$ cell number in each lesion. N = 10 pancreatic cancer metastatic livers and n = 5 healthy livers; n = 3 FoV / section were analysed. Scale bar = 100 μm. Black arrows point to CD8$^+$ T cells; asterisks indicate CK$^+$ metastatic lesions.

The ability of $CD8^+$ T cells to kill cancer cells depends on their activation state. Upon activation, $CD8^+$ T cells trigger an effector response against tumours through secretion of cytotoxic factors and inflammatory cytokines (i.e TNFα, IFNγ, GzmB) [275]. However, tumours are able to respond to this attack by the engagement of T cell inhibitory receptors. PD-L1 - PD-1 binding is one of the main mechanisms of tumour-acquired resistance against $CD8^+$ T cell cytotoxicity since it induces loss of $CD8^+$ T cell function. Indeed, PD-1 positive $CD8^+$ T cells tend to lose their ability to secrete cytotoxic factors and are usually associated with an exhausted or dysfunctional phenotype [276].

To evaluate whether $CD8^+$ T cells in human metastatic lesions were active or not, CK^+ poor and rich metastatic lesions were first identified by IF staining (Figure 3.2 a). The expression of the cytolytic marker GzmB and the inhibitory receptor PD-1 in $CD8^+$ T cells was then assessed by IF staining of serial tissue sections in both CK^+ poor and rich metastatic lesions (Figure 3.2 b). $CD8^+$ T cells expressed GzmB at lower level in comparison to PD-1, but $CD8^+$ T cells infiltrating in CK^+ poor metastatic deposits had a higher expression of GzmB (~16 %) compared to large metastatic deposit (~5 %). The majority of $CD8^+$ T cells were PD-1 positive, resulting in ~87 % of $CD8^+$ T cells positive for the expression of the inhibitory receptor in CK^+ rich, large lesion and ~55 % of PD-1 positive $CD8^+$ T cells in small deposits. These results suggested that PD-1 is highly expressed in human metastatic pancreatic cancer; however in small deposits T cells still retain some cytotoxic activity, which is almost completely lost as the metastatic disease progresses (Figure 3.2 c).

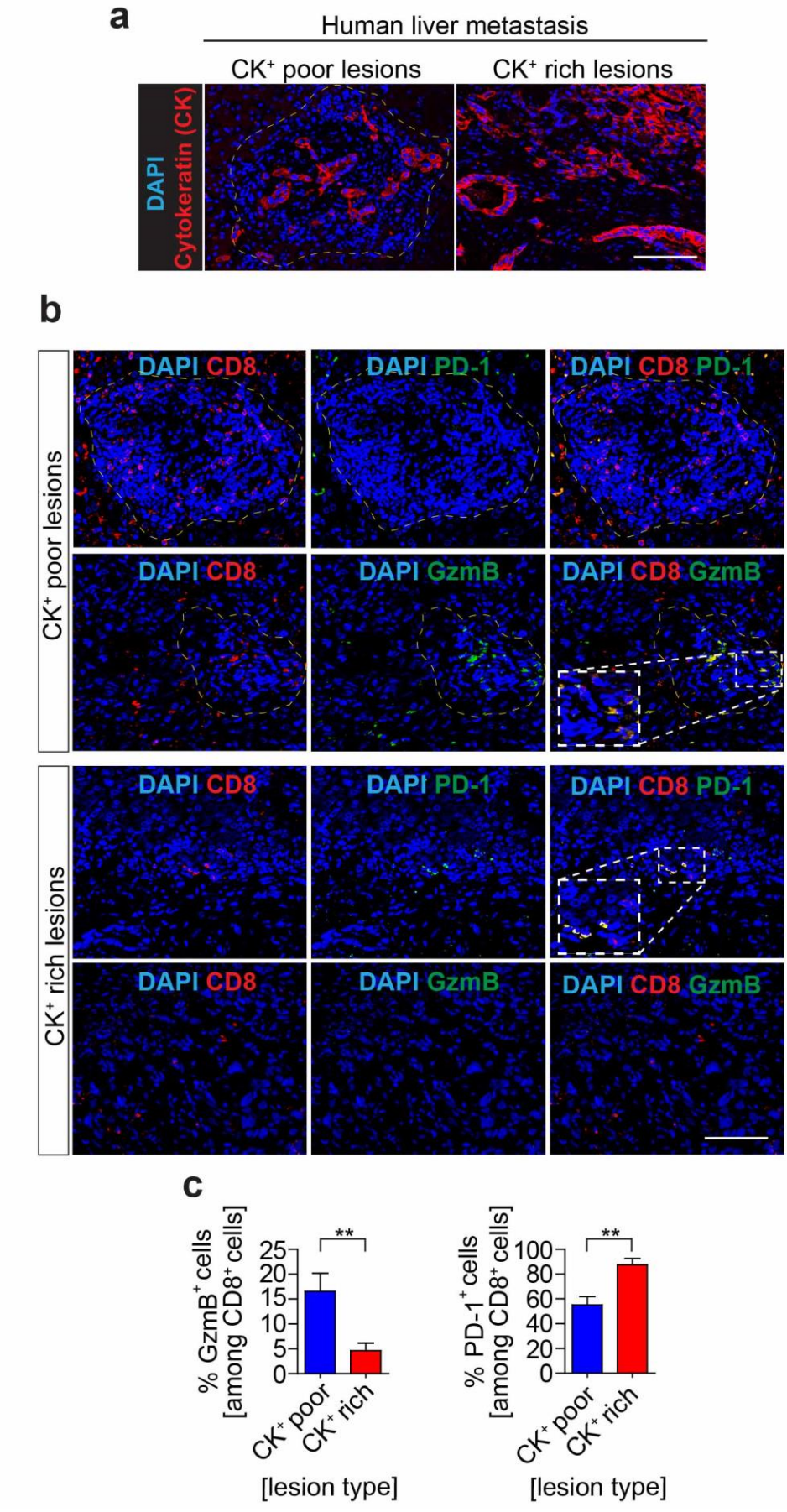
a
Human liver metastasis
CK+ poor lesions
CK+ rich lesions
DAPI
Cytokeratin (CK)
b
CK+ poor lesions
DAPI CD8
DAPI PD-1
DAPI CD8 PD-1
DAPI CD8
DAPI GzmB
DAPI CD8 GzmB
CK+ rich lesions
DAPI CD8
DAPI PD-1
DAPI CD8 PD-1
DAPI CD8
DAPI GzmB
DAPI CD8 GzmB
c
% GzmB+ cells [among CD8+ cells]
25
20
15
10
5
0
**
CK+ poor
CK+ rich
[lesion type]
% PD-1+ cells [among CD8+ cells]
100
80
60
40
20
0
**
CK+ poor
CK+ rich
[lesion type]

Figure 3.2 A CD8+ T cell dysfunctional phenotype is characteristic for large metastatic liver tumour.

a) Immunofluorescence (IF) representative images of metastatic lesions poor and rich in cytokeratin positive (CK^+) cancer cells found in liver biopsies of metastatic pancreatic cancer patients. **b)** Representative IF images of either inhibitory receptor PD-1 or Granzyme B (GzmB) (in green) and CD8 (in red) co-staining in sequential sections of CK^+ poor and rich metastatic liver. Images for single markers staining and markers co-staining are shown. **c)** Quantification of the staining. Nuclei were counterstained with DAPI. N = 10 pancreatic cancer metastatic livers, n = 3 field of view (FoV) / patient. Mean ± SEM. Scale bar = 100 µm. P<0.001; **, P < 0.01; *, P < 0.05; n.s. not significant by unpaired t-test.

Similarly, spontaneous liver metastasis generated in the genetically engineered mouse model of pancreatic cancer (*Kras^{G12D}; Trp53^{R172H}; Pdx1-Cre* mice, KPC) were analysed. Tumour lesions were identified by IHC staining for CK (Figure 3.3 a). It was found that the number of CK^+ cells inversely correlated with that of $CD8^+$ T cells, since higher numbers of effector T cells were found in CK^+ poor but not rich lesions (Figure 3.3 a and b).

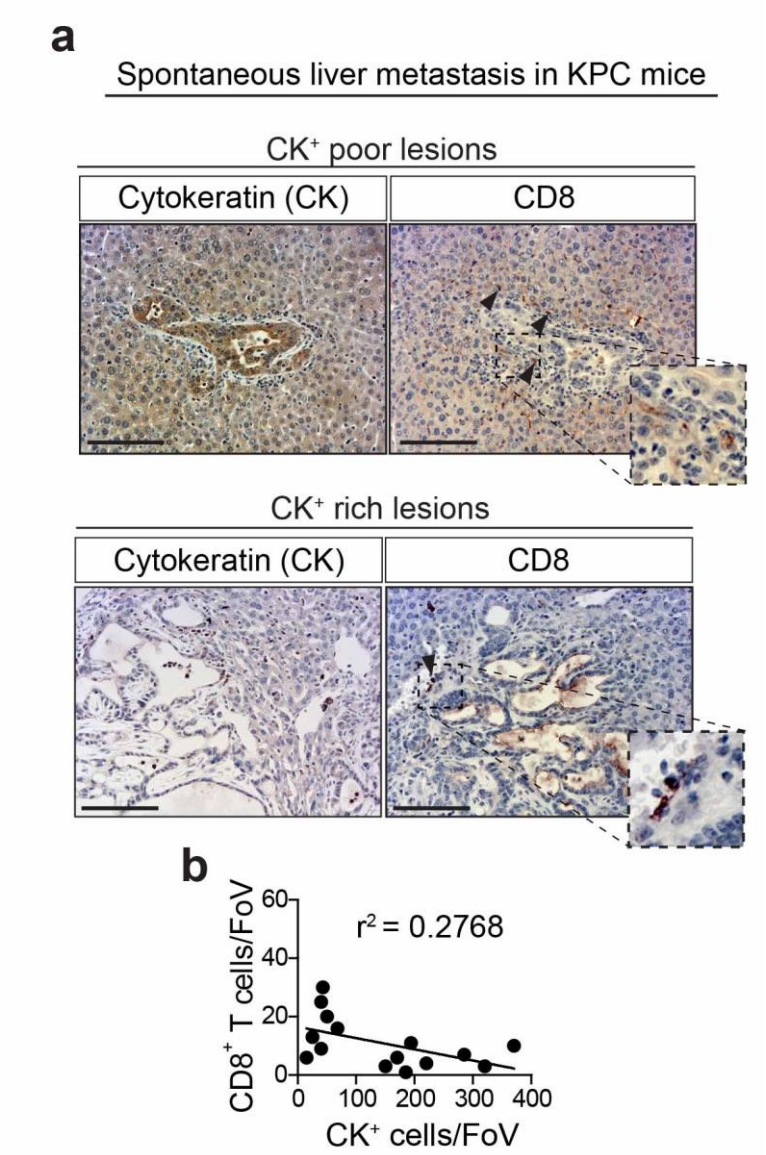

Figure 3.3 CD8+ T cells poorly infiltrate spontaneous large metastatic lesions of KPC mice.

Identification of cytokeratin $(CK)^+$ metastatic cancer cells and $CD8^+$ T cells by immunohistochemistry (IHC) analysis in serial tissue sections derived from KPC spontaneous metastatic lesions showing inverse correlation of $CD8^+$ T cells and CK^+ cancer cells numbers. **a)** Representative micrographs and **b)** quantification of data is shown. Each dot represents the relationship between $CD8^+$ T cells number and CK^+ cells number in each metastatic lesion assessed by staining of serial tissue sections. One metastatic lesion was captured in one field of view (FoV). N = 5 KPC mice, n = 3 FoV / mouse; Scale bar = 100 μm. Black arrows point to $CD8^+$ T cells.

KPC derived metastatic liver tissues were also analysed for PD-1 expression by IHC staining (Figure 3.4). It was found that CK^+ rich lesions were highly infiltrated by $PD\text{-}1^+$ cells in comparison to CK^+ poor lesions, thus suggesting the presence of dysfunctional T cells at the metastatic site in KPC mice and recapitulating the finding obtained from human sample.

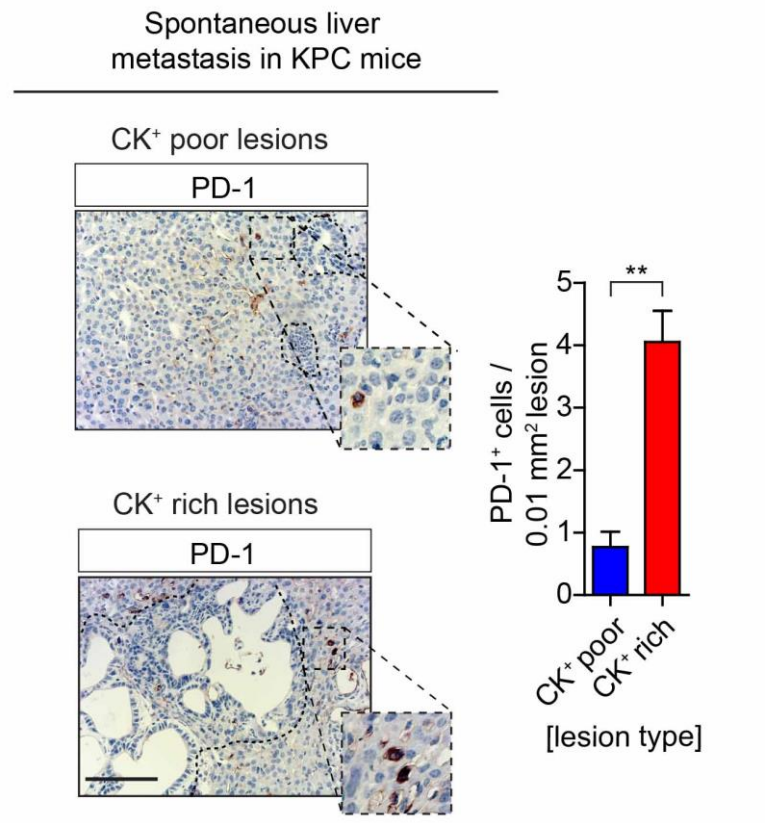

Figure 3.4 PD-1 is expressed in spontaneous metastatic lesions generated in KPC mice.

Representative micrographs and relative quantification of PD-1 expression obtained by immunohistochemistry staining in cytokeratin $(CK)^+$ poor and rich metastatic lesions originated in KPC mice. N = 5 mice, n = 3 field of view / mouse; mean ± SEM. Scale bar = 100 µm. P<0.001; **, P < 0.01; *, P < 0.05; n.s. not significant by unpaired t-test.

3.2 $CD8^+$ T cell effector functions are lost during metastatic progression

So far it has been observed that in both human and KPC mice, small liver metastatic lesions with low numbers of cancer cells were highly infiltrated by cytotoxic $CD8^+$ T cells, whereas large metastatic lesions, rich in cancer cells, presented only few infiltrating $CD8^+$ T, highly positive for PD-1 expression. Therefore, it was hypothesised that in the early phases of metastatic dissemination into the liver, $CD8^+$ T cells fight tumour insurgence, however tumours are successively able to escape from $CD8^+$ T cell attacks as anti-tumour immunity becomes suppressed. To test this hypothesis, pancreatic cancer metastatic progression and the changes in its microenvironment were studied by using a murine experimental liver metastatic model. This model allowed tracking of metastatic growth in the liver over time.

The experimental metastasis model used in our lab was developed by the intrasplenic injection of KPC-derived pancreatic cancer cells expressing the dual reporter genes zsGreen and firefly luciferase ($KPC^{luc/zsGreen}$). In this model, tumour cells seed the liver via the portal circulation (a common way of metastasis occurring in humans), and generate metastasis restricted to the liver. H&E staining of livers resected from mice 6 and 14 days after implantation of cancer cells revealed the presence of small metastatic deposits at day 6, which then progress to form large metastatic deposits with evident ductal structure, typical of pancreatic cancer, after 14 days *(*Figure 3.5*)*.

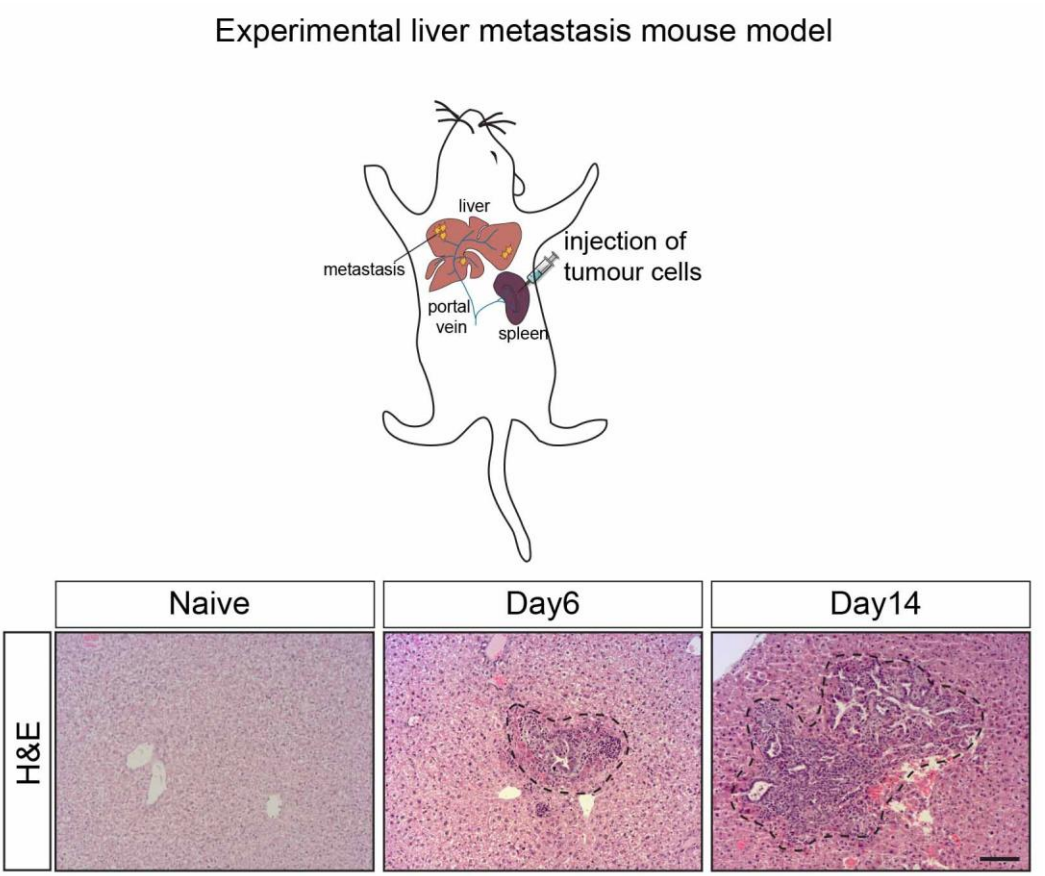

Figure 3.5 Experimental liver metastasis mouse model.

$1x10^6$ $KPC^{luc/zsGreen}$ cancer cells were injected into naïve mice spleen to obtain cancer cells dissemination into the liver via portal vein circulation. In this model, $KPC^{luc/zsGreen}$ cancer cells form small metastatic deposits into the liver after 6 days (Day 6); whereas cancer cells metastatic progression lead to the formation of larger metastatic lesions after 14 days (Day 14). Schematic illustration of the model and representative images of haematoxylin and eosin (H&E) stained tissue sections of naïve liver and livers with experimental metastasis after 6 and 14 days. N = 4 mice, n = 5 field of view / mouse. Scale bar = 100 μm.

The expression of genes involved in immune response in both naïve and metastatic livers was first validated. For this purpose, livers from naïve mice and from mice with metastasis formed 6 and 14 days after implantation of $KPC^{luc/zsGreen}$ cancer cells were resected. Total RNA was extracted from whole tissues and transcript copy numbers for certain immune-related genes were obtained by Nanostring technology. The main interest was to understand whether the immune composition at the metastatic site varied between small and advanced metastatic lesions. Therefore, genes with more than 2-fold change in expression at Day 6 in comparison to Day 14 were analysed. Gene ontology (GO) pathway analysis for the selected genes allowed association of genes with specific immune-related pathways. Interestingly, genes correlated with T_H1 type and inflammatory responses were up-regulated at day 6 in comparison to day 14. Particularly, cytotoxic effector T cell- related genes, like C*d8b1, Prf1, Gzmb, Cd69, Eomes* were higher expressed at the early stages of metastatic progression, thus suggesting that a pro-inflammatory and anti-tumourigenic microenvironment characterized small lesions at day 6. On the contrary, expression of genes such as *Tgfb, Pdgf* and *Vcam,* related with extracellular remodelling pathways and typical of a fibrotic tumour microenvironment, were up-regulated in advanced metastatic lesion at day 14, rather than at day 6 (Figure 3.6).

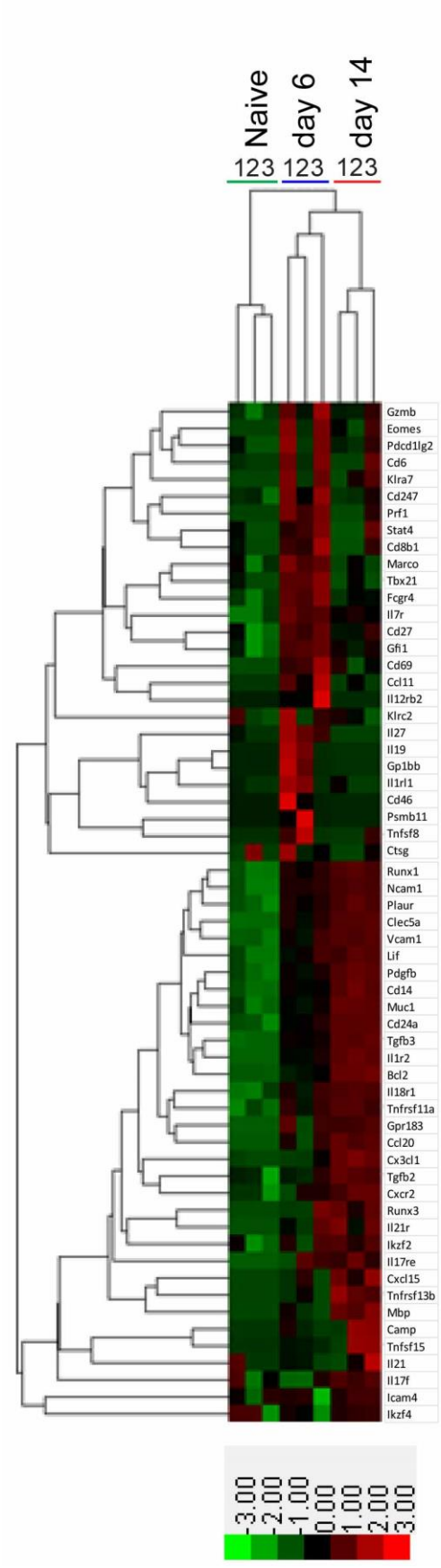

Day 6 versus Day 14

Up-regulated genes

Th-1 cell differentiation

Gene	fold change
Tbx21	10.12
Stat4	3.13
Il12rb2	2.39

Inflammatory response

Gene	fold change
Il1rl1	3.35
Il27	2.96
Cd27	2.57

T cell mediated response

Gene	fold change
Cd8b1	5.69
Prf1	5.47
Cd69	4.08
Gzmb	3.59
Eomes	2.1

Down-regulated genes

Extracellular matrix remodelling

Gene	fold change
Tgfb2	-3.91
Tgfb3	-3.62
Pdgfb	-3.35
Vcam1	-2.14

Figure 3.6 Early metastatic dissemination of cancer cells triggers anti-tumour immunity.

Liver metastasis was induced by intrasplenic implantation of $KPC^{luc/zsGreen}$ cancer cells. Mice were euthanized 6 and 14 days after and livers were harvested. Livers were also resected from naïve mice. Total RNA was extracted from whole naïve and metastatic livers at day 6 and day 14 and subsequently processed using Nanostring technology. Analysis of obtained data, using nSover Analysis Software, identify genes that were up- or down-regulated by more than 2-fold in livers at day 6 compared to day 14. Data were reported in a heat map diagram. Subsequent Gene Ontology (GO) Pathway analysis enabled to associate differently expressed genes with immune-related pathways. Some of the genes up- or down- regulated at day 6 compared to day 14 were found to be associated with T_H1-type, inflammatory, T cytotoxic responses and with extracellular matrix remodelling pathways. N= 3 mice / group were analysed.

To further characterize the anti-tumour immune response against pancreatic cancer metastasis, IF staining of naïve, Day 6 and Day 14 $KPC^{luc/zsGreen}$ cancer cells derived metastatic lesions were analysed for CD8 expression. It was found that metastatic infiltration of $CD8^+$ T cells was dependent on the number of cancer cells forming metastatic deposits in the liver. Small metastatic lesions mainly found at the early stage of metastatic progression (6 days post intrasplenic implantation) and characterized by low numbers of KPC cancer cells ($zsGreen^+$), showed high infiltration of $CD8^+$ T cells in comparison to tumour free livers. In contrast, large metastatic lesions with abundant cancer cell numbers, mainly found at a later stage of metastasis progression (14 days post intrasplenic injection), showed a significant loss of $CD8^+$ T cells (Figure 3.7 a and b).

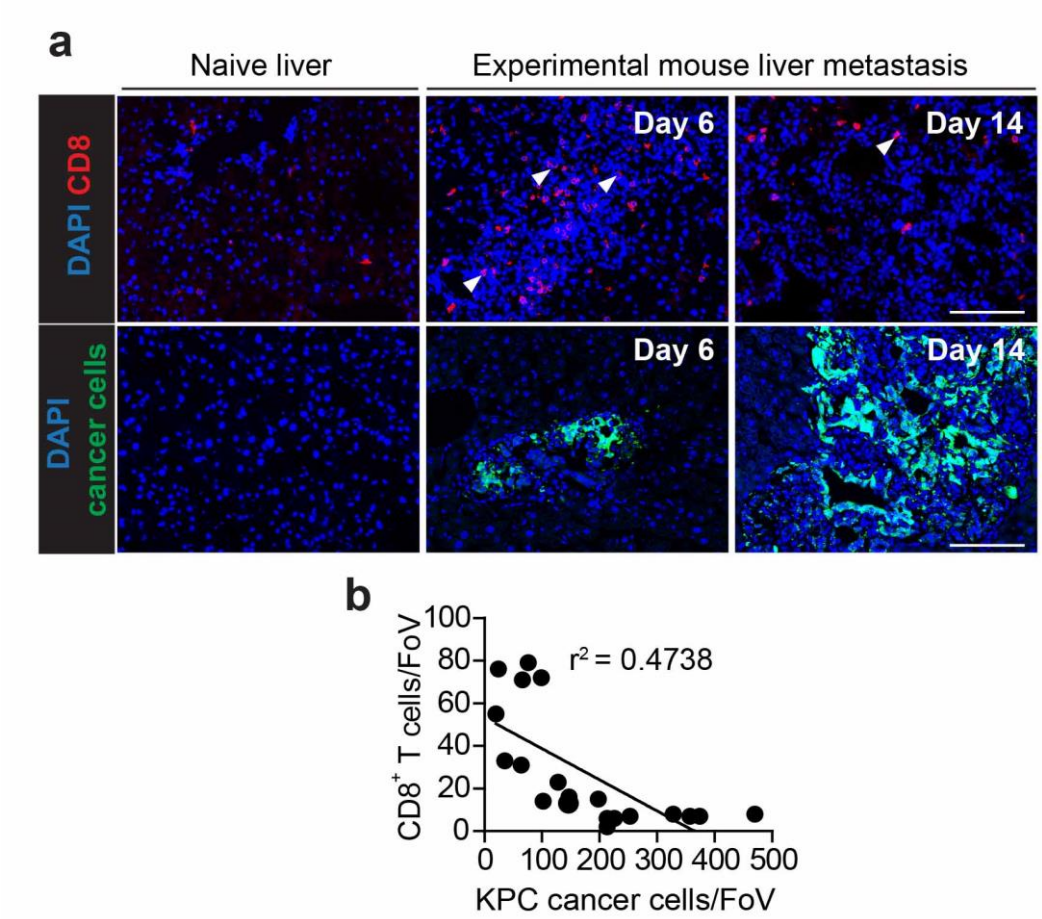

Figure 3.7 CD8$^+$ T cells number decreases in large experimental metastatic lesions.

Liver metastasis was induced by intrasplenic implantation of KPC$^{luc/zsGreen}$ cancer cells. Naïve and metastasis bearing mice 6 and 14 days after cancer cells implantation, were euthanized and livers were harvested. **a)** Immunofluorescence staining representative images of serial section of naïve, Day 6 and Day 14 metastatic livers displaying CD8$^+$ T cells (upper panels) and cancer cells (zsGreen$^+$, lower panels). Individual lesions were captured by one field of view (FoV). **b)** Dots represent the relationship between CD8$^+$ T cells and KPC$^{luc/zsGreen}$ cancer cells numbers in each lesion. Nuclei were counterstained with DAPI. N = 4 mice / time point; n = 5 FoV / mouse. Scale bar = 100 µm. White arrows point to CD8$^+$ T cells (in red).

To further investigate the $CD8^+$ T cell population, multi-colour flow cytometry analysis of disaggregated murine naïve and metastatic livers was performed. Resected livers were mechanically and enzymatically digested with collagenase to obtain a suspension of single cells. Cellular staining using multiple fluorophore-conjugated antibodies allowed discrimination of different cell populations within the liver. Upon acquisition of the samples, data were analysed with Diva FACS software, which allowed the acquired cells to be displayed as dot plots. Hematopoietic cells were recognized among all liver cells for the expression of CD45 marker; subsequent gating of $CD45^+$ cell population for CD8 expression enabled us to identify the $CD8^+$ T cells. A significant increase in $CD45^+$ $CD8^+$ T cells was found in the liver 6 days after cancer cell intrasplenic injection in comparison to naïve livers; reduction in $CD8^+$ T cells number in larger tumours formed after 14 days was instead observed (Figure 3.8 a and b). We next questioned whether the infiltrated $CD8^+$ T cells had an active effector phenotype or if they were instead exhausted. Therefore, we looked at CD69 activation marker and PD-1 expression among $CD8^+$ T cells. Interestingly, $CD8^+$ T cells from small tumours (Day 6) expressed high levels of CD69, while few cells were found to be positive for PD-1; on contrary, $CD8^+$ T cells from large metastatic tumours (Day 14) were highly positive for PD-1, whereas fewer cells expressed the activation marker CD69 (Figure 3.8 a, c, d).

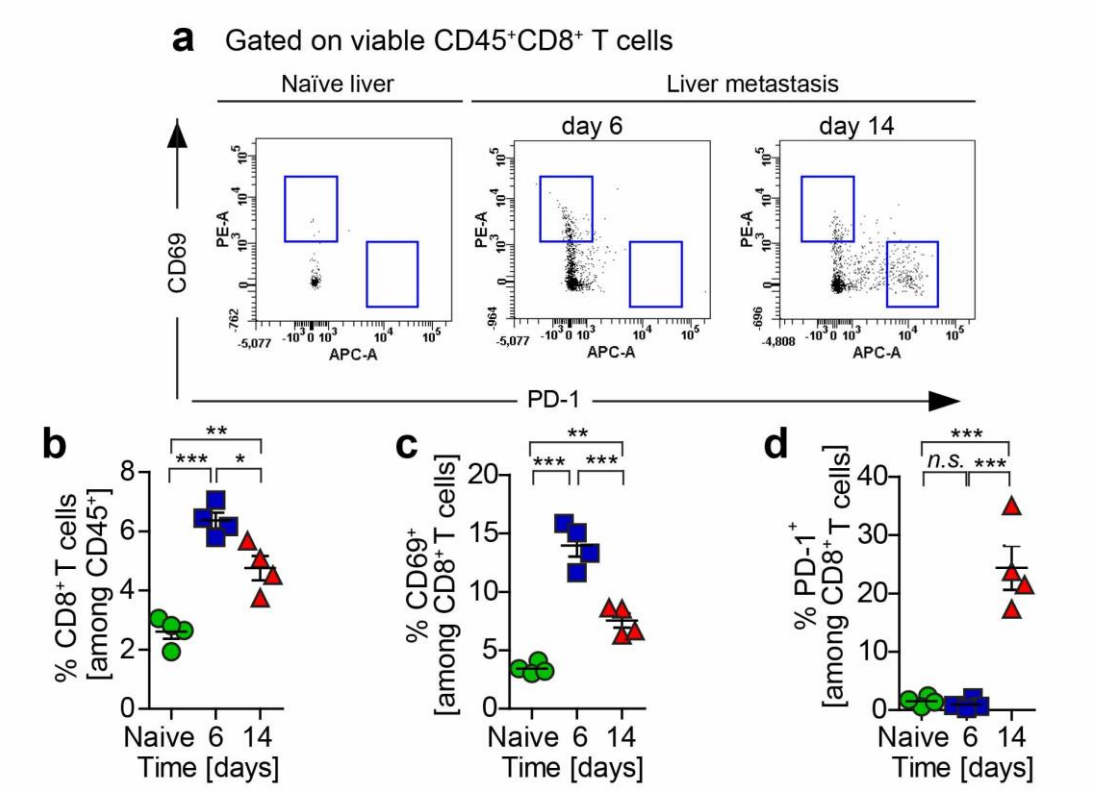

Figure 3.8 CD8$^+$ T cells effector activity is lost during metastasis progression.

Liver metastasis was induced by intrasplenic implantation of KPC$^{luc/zsGreen}$ cancer cells. Naïve and metastasis bearing mice 6 and 14 days after cancer cells injection, were euthanized. Livers were harvested and digested for multi-colour flow cytometer analysis. **a)** Representative dot plot gating strategy used to identify CD45$^+$CD8$^+$ T cells positive or negative for CD69 or PD-1. Percentage of **b)** CD8$^+$ T cells, **c)** CD69$^+$ CD8$^+$ T cells and **d)** PD-1$^+$ CD8$^+$ T cells over time. N = 4 mice / group; individual data points, horizontal line represents mean ± SEM; P<0.001; **, P < 0.01; *, P < 0.05; n.s. not significant by Bonferroni multiple comparison.

To confirm the exhausted phenotype of $CD8^+$ $PD\text{-}1^+$ T cells in large metastatic deposits found 14 days after intrasplenic implantation of cancer cells, quantitative PCR analysis was performed to validate the expression of the cytolytic genes *Tnfa* and *Gzmb* in liver isolated metastasis infiltrating $CD8^+$ T cells positive and negative for PD-1 expression. The reduced cytotoxic capability of $CD8^+$ $PD\text{-}1^+$ T cells was confirmed by loss of *Tnfa* and *Gzmb* expression, which was instead absent in PD-1 negative T cells ($CD8^+$ $PD\text{-}1^{neg}$) (Figure 3.9 a and b).

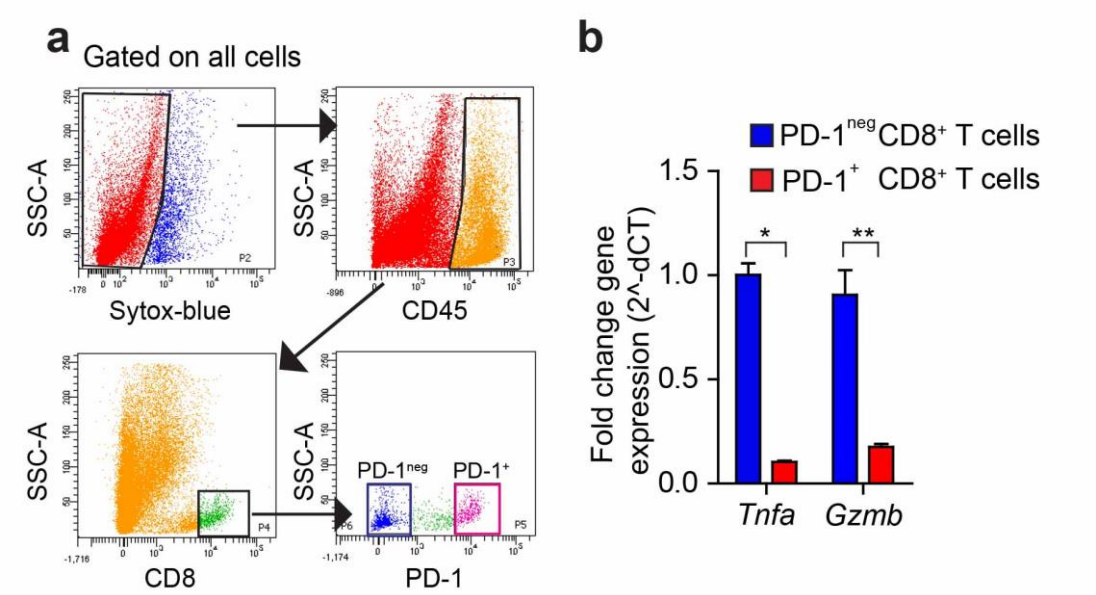

Figure 3.9 *$CD8^+$ $PD\text{-}1^+$ T cells have a dysfunctional phenotype.*

Liver metastasis was induced by intrasplenic implantation of $KPC^{luc/zsGreen}$ cancer cells. After 14 days livers were harvested from metastatic mice and digested for flow cytometry analysis. **a)** Representative flow cytometry dot plot gating strategy used to identify $CD8^+$ PD-1 negative ($PD\text{-}1^{neg}$) or positive ($PD\text{-}1^+$) T cells among all metastatic liver cells in the liver. **b)** $CD8^+$ $PD\text{-}1^{neg}$ and $CD8^+$ $PD\text{-}1^+$ T cells were isolated by flow cytometry ARIA cell sorter and tested for Tnfa and Gzmb expression by qPCR. N = 4 mice / group; mean ± SEM; P<0.001; **, P < 0.01; *, P < 0.05; n.s. not significant by unpaired t-test.

Collectively, these results indicate that $CD8^+$ T cells are able to infiltrate small metastatic tumours, but that during metastatic progression $CD8^+$ T cells infiltration and cytotoxic function are lost.

3.3 Immunosuppressive M2-like MAMs accumulate during pancreatic cancer metastatic progression.

Our group has previously shown that macrophages accumulate in metastatic livers of pancreatic cancer [117]. In addition, several evidences are in support of the immunosuppressive role that macrophages may play in tumour [277]. Thus, it was decided to investigate whether macrophage accumulation at the metastatic site is responsible for the generation of an immunosuppressive microenvironment that acts to dampen $CD8^+$ T cells mediated anti-tumour immunity.

First, liver-infiltrating macrophages were identified by flow cytometry as the $CD45^+CD11b^+Ly6g^{neg}Ly6C^{dim/neg}$ $F4/80^+$ population, which from here on it was considered as the MAM population (Figure 3.10).

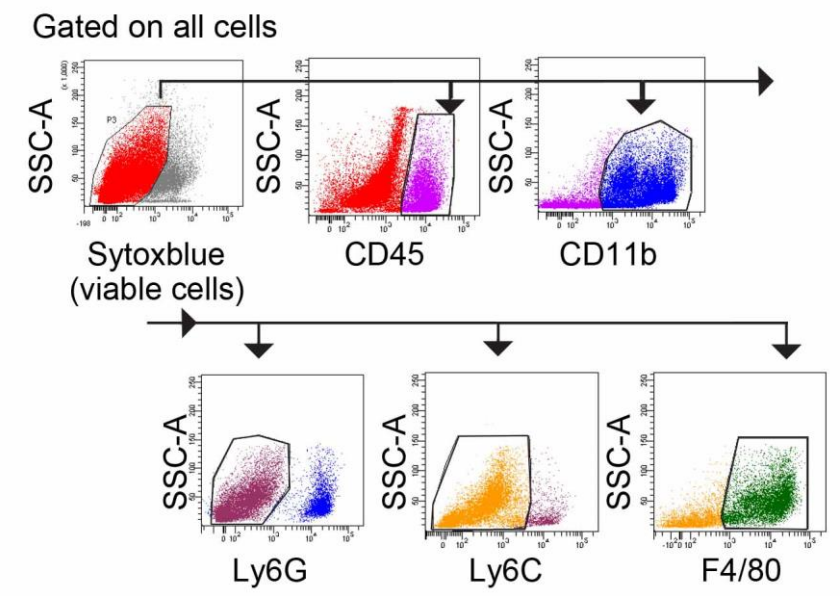

Figure 3.10 Characterization of metastasis associated macrophages (MAMs) population in the liver.

Liver metastasis was induced by intrasplenic implantation of KPC$^{luc/zsGreen}$ cancer cells. Livers from naïve and metastatic mice 6 and 14 days after cancer cells injection were isolated and analysed by multi-colour flow cytometry. Representative flow cytometry gating strategy used to identify Sytox-blue^{neg}CD45^{+}Cd11b^{+}Ly6G^{neg}Ly6C$^{dim/neg}$F4/80^{+} MAM population in metastatic lesions after 6 and 14 days. N = 4 mice / group.

Flow cytometry analysis of MAM population showed increased infiltration of macrophages in metastatic livers in comparison to naïve one, but no differences were detected in infiltration of macrophages between livers containing small lesions at day 6 and large metastatic deposits at day 14 (Figure 3.11 a). However, gene expression analysis of M1-like and M2-like macrophage associated genes revealed that MAMs isolated from small metastatic tumours (Day 6) had significantly up-regulated levels of immune stimulatory genes (*Cxcl10*; *Il12*; *Ifng*) and genes associated with antigen presentation (*H2Aa; Cd86*), resembling a pro-inflammatory M1-like phenotype. In contrast, macrophages isolated from large metastatic tumours

(Day 14) had significantly up-regulated expression of immunosuppressive (*Tgfb*; *Arginase*; *Il10*) and anti-inflammatory, M2-like, markers (*mannose receptor C-type 1, Mrc1; resistin-like-α*, *Retnla*) (Figure 3.11 b). Other macrophage markers were also tested by qPCR, including *Chi3l3* (M2-like macrophage marker)*, Tnfa and Il1b* (genes associated with M1-like inflammatory response). However, several unspecific amplification products were detected as results of the qPCR run; thereby obtained data were not considered and not reported in this thesis.

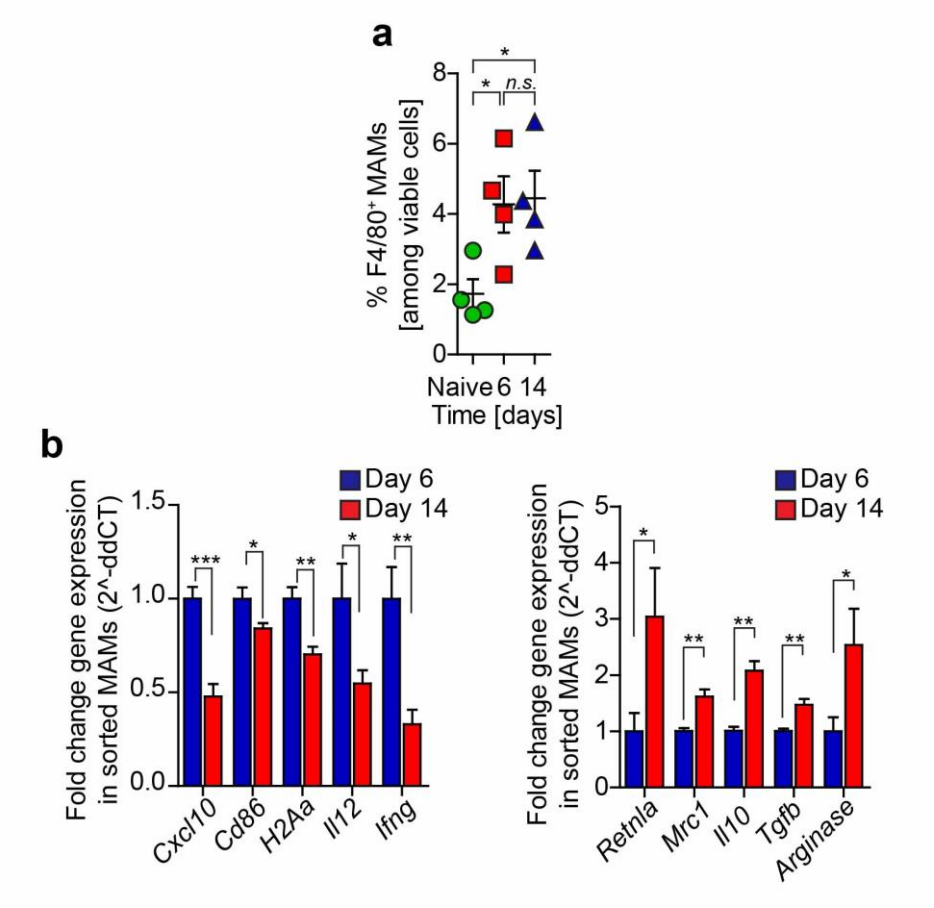

Figure 3.11 Metastatic progression of pancreatic cancer is accompanied by increase in M2-like macrophage accumulation.

Liver metastasis was induced by intrasplenic implantation of $KPC^{luc/zsGreen}$ cancer cells. Livers from naïve and metastatic mice 6 and 14 days after cancer cells injection were isolated and analysed by multi-colour flow cytometry. **a)** Flow cytometry quantification of $F4/80^+$ MAMs in naive and metastatic resected livers. **b)** $F4/80^+$ MAMs were isolated by flow cytometer ARIA cell sorter from day 6 and day 14 metastatic livers. RNA was extracted from isolated MAMs and quantitative PCR analysis for M1-like and M2-like macrophage-associated markers was performed. N = 4 mice / group. For a) individual data point are shown, horizontal line represents mean ± SEM. b) Data are represented as mean ± SEM. P<0.001; **, P < 0.01; *, P < 0.05; n.s. not significant by Bonferroni multiple comparison and unpaired t-test, respectively.

IHC staining was used to validate the presence of M1- or M2- like macrophage populations within metastatic livers. The analysis confirmed that in liver metastasis formed 6 days after intrasplenic injection of pancreatic cancer cells (Day 6), a significantly higher number of cells expressed typical pro-inflammatory macrophage markers, including iNOS, MHC-II and cyclooxygenase-2 (COX-2). In contrast, larger established metastatic tumours formed 14 days after cancer cells injection (Day 14), contained a higher number of cells expressing M2-like alternative activation markers, such as macrophage mannose receptor 1 (CD206) and Ym-1 (Figure 3.12).

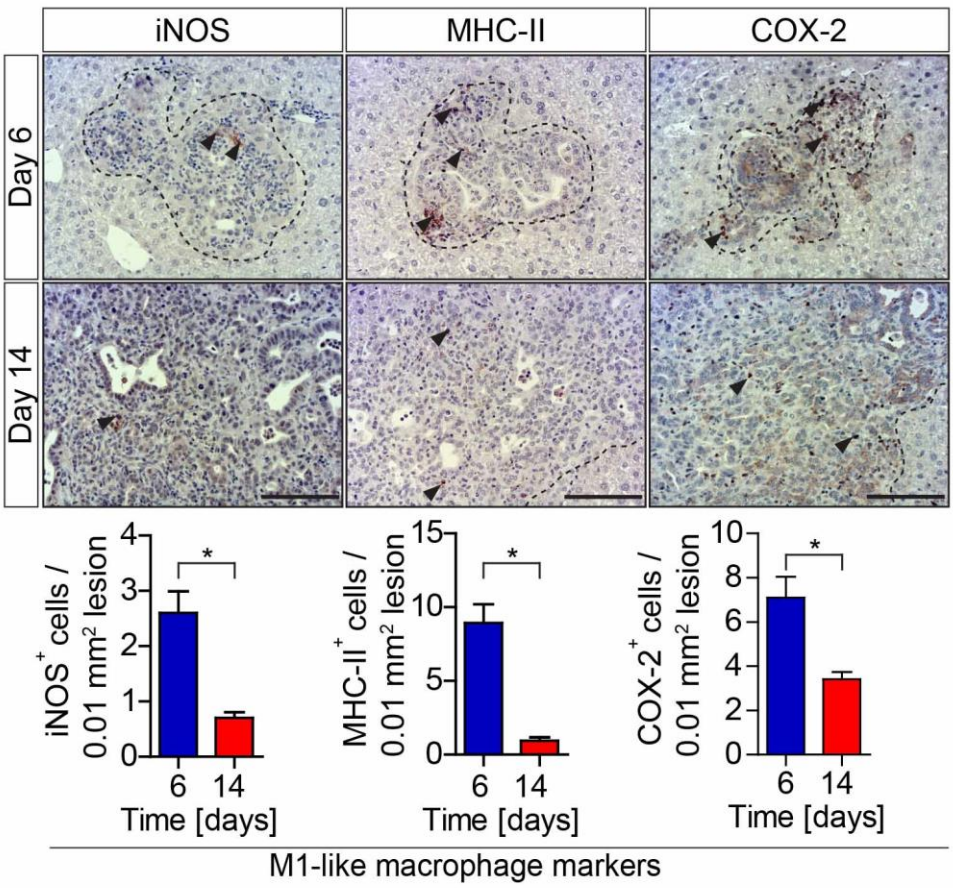
iNOS
MHC-II
COX-2
Day 6
Day 14
iNOS+ cells / 0.01 mm2 lesion
MHC-II+ cells / 0.01 mm2 lesion
COX-2+ cells / 0.01 mm2 lesion
Time [days]
M1-like macrophage markers

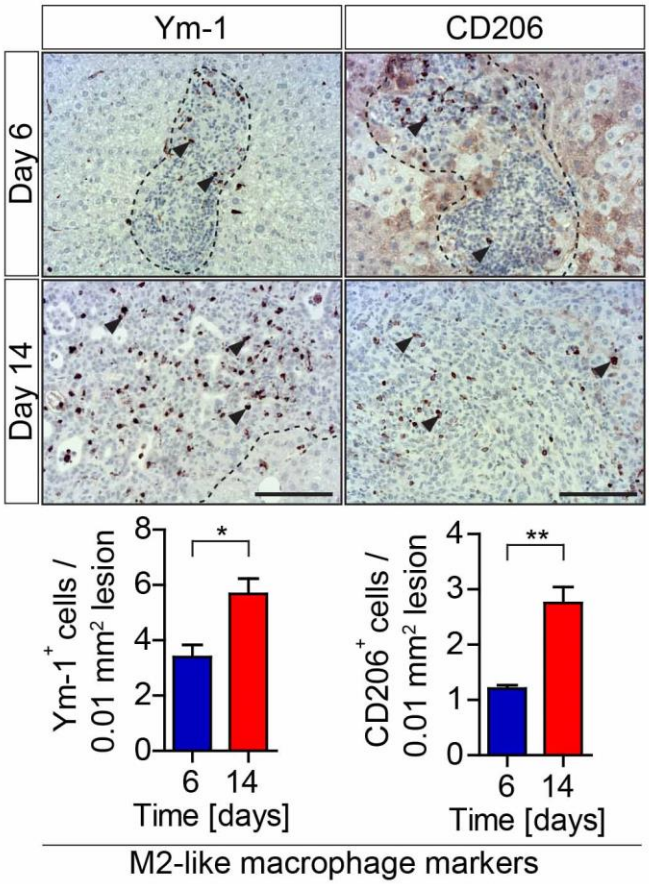
Ym-1
CD206
Day 6
Day 14
Ym-1+ cells / 0.01 mm2 lesion
CD206+ cells / 0.01 mm2 lesion
Time [days]
M2-like macrophage markers

Figure 3.12 Small and large metastatic lesions are infiltrated by M1- and M2- like MAMs, respectively.

Liver metastasis was induced by intrasplenic implantation of $KPC^{luc/zsGreen}$ cancer cells. Livers from metastatic mice were isolated after 6 and 14 days and analysed by immunohystochemistry (IHC). Representative IHC staining micrographs and quantification of M1-like and M2-like macrophage associated markers in Day 6 and Day 14 metastatic liver tissues. N = 4 mice/ group; n = 5 field of view / mouse; mean ± SEM. Scale bar = 100 µm. P<0.001; **, P < 0.01; *, P < 0.05; n.s. not significant by unpaired t-test. In each IHC micrograph black arrows point to positively stained cells.

In addition, IF staining of Day 6 and Day 14 metastatic liver tissues for the M2-like macrophage marker RELMα, further confirmed the accumulation of M2-like $RELM\alpha^+$ MAMs in close proximity to disseminated cancer cells ($zsGreen^+$) in large metastatic lesions but not in small lesions (Figure 3.13).

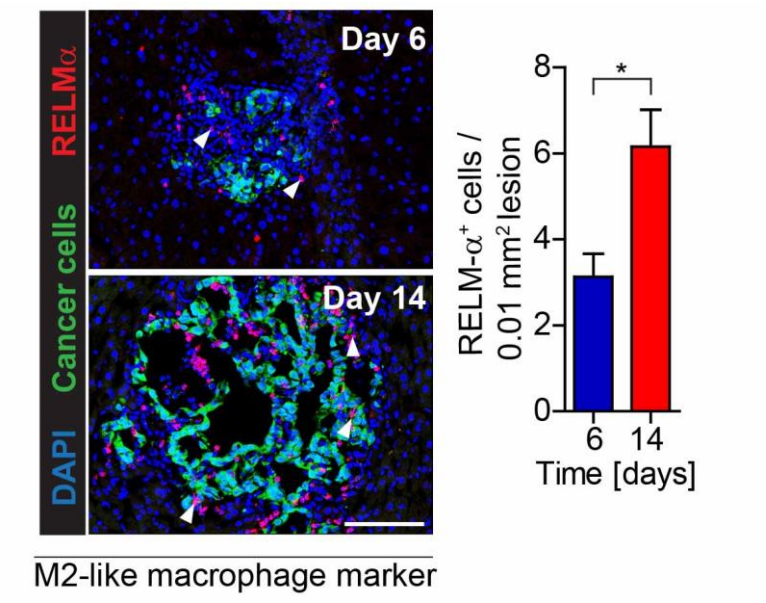

Figure 3.13 Relmα+ M2-like macrophages infiltrate large metastatic lesions.

Liver metastasis was induced by intrasplenic implantation of KPCluc/zsGreen cancer cells. Livers from metastatic mice were isolated after 6 and 14 days and analysed by immunofluorencence (IF). Representative IF images and relative quantification of Relmα$^+$ cells in close proximity with metastatic pancreatic cancer cells (zsGreen+). Nuclei were counterstained with DAPI. N = 4 mice / group, n = 5 field of views / mouse; mean ± SEM. Scale bar = 100 µm. P<0.001; **, P < 0.01; *, P < 0.05; n.s. not significant by unpaired t-test. White arrows point to Relmα$^+$ cells (in red).

It is well known that M2-like macrophages can execute potent inhibitory effects on cytotoxic CD8$^+$ T cell function [51], [278], thus CD8$^+$ T cell function was interrogated in response to the switch of MAM phenotype from a M1-like to M2-like during metastatic progression. First, numbers of apoptotic (Cleaved Caspase 3$^+$ cells, CC3$^+$) disseminating pancreatic cancer cells (zsGreen$^+$) were analysed in metastatic lesions at Day 6 and Day 14. As

expected, it was observed a higher apoptotic rate of cancer cells in small metastatic lesions (Day 6) compared to large metastatic lesions (Day 14) (Figure 3.14).

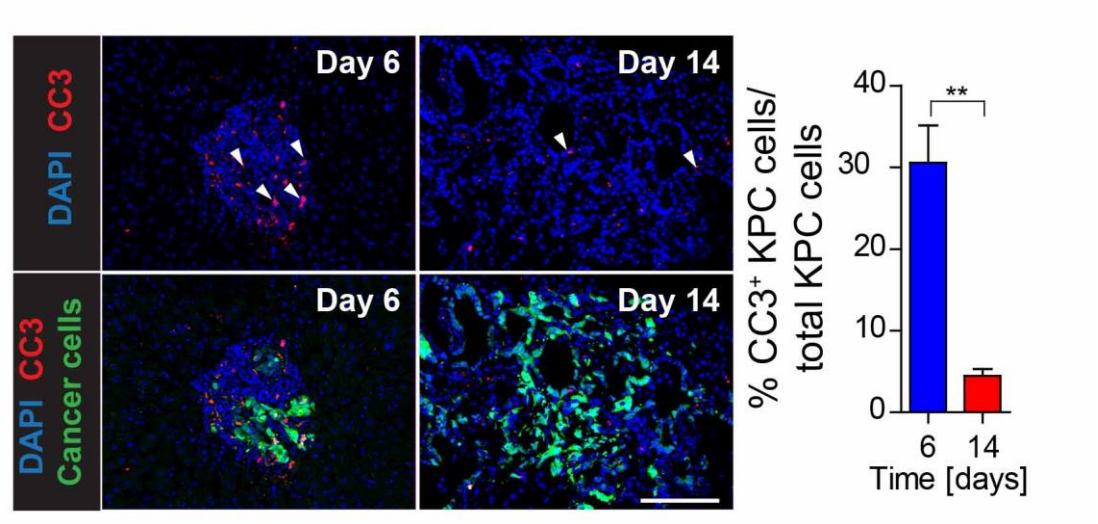

Figure 3.14 Disseminating pancreatic cancer cells are highly apoptotic in small but not in large lesions.

Liver metastasis was induced by intrasplenic implantation of $KPC^{luc/zsGreen}$ cancer cells. Livers from metastatic mice were isolated after 6 and 14 days and analysed by immunofluorescence (IF). Representative IF staining of cleaved caspase 3 (CC3) in metastatic $KPC^{luc/zsGreen}$ ($zsGreen^+$) cells. Graph: Quantification of $CC3^+$ cells among KPC cells in livers during the course of metastasis formation. Nuclei were counterstained with DAPI. N = 4 mice / group, n = 5 field of views / mouse; mean ± SEM. Scale bar = 100 µm. P<0.001; **, P < 0.01; *, P < 0.05; n.s. not significant by unpaired t-test. . White arrows point to $CC3^+$ cells (in red).

Finally, the ability of MAMs to suppress $CD8^+$ T cell proliferation and activation during metastatic progression was assessed. MAMs were isolated by flow cytometry from metastatic livers 6 or 14 days post intrasplenic injection of $KPC^{luc/zsGreen}$ cancer cells. MAMs were then co-cultured with CD3/CD28 dynabeads (DB) pre-activated splenic $CD8^+$ T cells isolated from naive mice. Day 6 and Day 14 MAMs were tested for their capacity to impair T cell proliferation (measured by Carboxyfluorescein Diacetate Succinimidyl Ester, CFSE, dilution signal) and IFNγ secretion. The results obtained indicated that MAM isolated from established metastatic lesions, most likely with an M2-like phenotype, significantly suppressed $CD8^+$ T cell proliferation (Figure 3.15 a) and activation *ex vivo* (Figure 3.15 b), compared to MAMs isolated from small metastatic lesions.

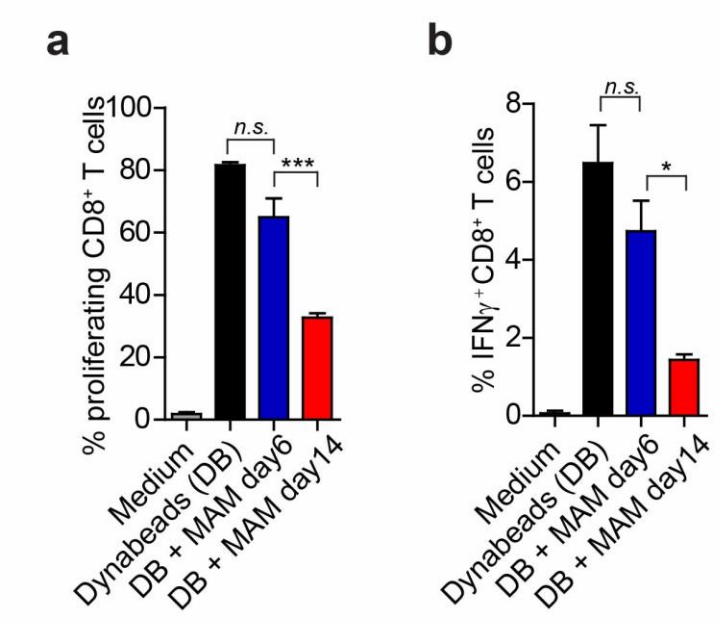

Figure 3.15 MAMs acquire immunosuppressive abilities during metastatic pancreatic cancer growth.

Liver metastasis was induced by intrasplenic implantation of $KPC^{luc/zsGreen}$ cancer cells. Livers from metastatic mice were resected after 6 and 14 days and digested for MAMs identification and isolation. MAMs were isolated using ARIA flow cytometer cell sorter. Isolated MAMs were cultured and assessed for their ability to suppress splenic $CD8^+$ T cell **a)** proliferation (CSFE dilution) and **b)** activation (IFNγ expression level) following CD3/CD28 Dynabeads (DB) stimulation. N = 4 mice / group; mean ± SEM. P<0.001; **, P < 0.01; *, P < 0.05; n.s. not significant by Bonferroni multiple comparison.

Together, these data suggest that metastatic progression in pancreatic cancer is accompanied by the reprogramming of MAMs towards an M2-like immunosuppressive phenotype that can inhibit cytotoxic $CD8^+$ T cell functions.

3.4 Discussion

Tumours that progress and form metastasis need to evade immune defences [4]. Pancreatic cancer is a highly metastatic disease [279] and whether an anti-tumour immune response is triggered to fight pancreatic cancer metastatic formation into the liver, remains undiscovered.

Recognition of tumour antigens is the prerequisite for the activation of a $CD8^+$ T cell mediated anti-tumour response. Studies performed on the KPC mouse model have reported the presence of low mutational burden and poor T cell infiltration not only in the primary tumour, but also at the secondary site, thereby classifying pancreatic cancer as a cold tumour [256], [280]. Although a similar phenotype has been also observed in human pancreatic cancer [281], [282], there are evidences showing that pancreatic cancer can be infiltrated by $CD8^+$ T cells and that anti-tumour immunity is also triggered in this type of cancer [240], [283], [284]. Moreover, in a recent study it has been found that human pancreatic tumours express a range of non-synonymous mutations that are predictive to function as new epitopes. The study also correlated the presence of tumour $CD8^+$ T cell infiltrates together with high neo-antigen numbers and with the longest patients survival, thus emphasizing the critical role of $CD8^+$ T cell in inhibiting pancreatic cancer progression [274], [285].

In this study, $CD8^+$ T cell population in human pancreatic cancer liver metastasis was investigated and it was found that within the same metastatic liver tissue, deposits with high or low number of cancer cells could be discriminated. Metastatic cancer cells in the liver were identified with a CK marker, thus the terms CK^+ rich or CK^+ poor lesions were used to describe

lesions with high and low number of cancer cells, respectively. Interestingly, $CD8^+$ T cells infiltration inversely correlated with CK^+ cells numbers. In accordance, CK^+ poor lesions were strongly infiltrated by $CD8^+$ T cells, whereas in lesions rich of CK^+ cells, T cells infiltration was lost. Importantly, $CD8^+$ T cells in both CK^+ poor and rich human metastatic lesions were highly positive for the PD-1 inhibitory receptor, suggesting that the effector $CD8^+$ T cells response is counteracted by progressive induction of the PD-1 inhibitory pathway. In fact, in CK^+ poor lesions $CD8^+$ T cells still conserved their cytotoxic function as suggested by higher numbers of $GzmB^+$ $CD8^+$ T infiltrating cells, whereas in CK^+ rich lesions very low numbers of $GzmB^+$ $CD8^+$ T cells were found, as the majority of $CD8^+$ T cells population was $PD1^+$ with dysfunctional phenotype. Similarly, CK^+ poor lesions, found in spontaneous metastatic liver of KPC mice, presented high infiltration of $CD8^+$ T cells, which also had low expression of PD-1, whereas large metastatic, CK^+ rich, deposits were correlated with low numbers of effector T cells highly positive for PD-1.

These results suggest that in the early phases of metastatic progression, when still few cells disseminate into the liver, cancer cells are recognized and attacked by active $CD8^+$ T cells. However anti-tumour immunity appears to be lost at later stages and success of metastatic progression is the net result.

The use of a pre-clinical mouse model enabled to better elucidate the change in anti-tumour immunity during metastatic growth. Analysis of immune cell composition of naïve mouse livers and of livers containing small metastatic lesions or large metastatic deposits formed, respectively, 6 or 14 days after intrasplenic implantation of pancreatic cancer cells, confirmed that an anti-

tumour immune response, mainly mediated by cytotoxic $CD8^+$ T cells, do exist at the early stages of metastatic progression. Indeed, a T_H1 type / pro-inflammatory, signature was found in metastatic lesions after 6 days of metastatic dissemination of cancer cells but not at a later time point. $CD8^+$ T cells populated the liver in response to metastasis formation and their anti-tumour activity was reflected by high expression of $CD8^+$ T cell activation marker (CD69), low level of expression of PD-1 inhibitory receptor and high numbers of apoptotic cancer cells. On the contrary, at a later stage of metastatic progression, at day 14, cancer cells were less exposed to apoptotic pressure, survived immune attacks and formed large tumour deposits. In established metastasis, $CD8^+$ T cell infiltration drastically decreased and the cytotoxic activity of the few infiltrating lymphocytes was also lost as suggested by high level of PD-1 expression and low expression of the effector cytokine and cytolytic factors TNFα and GzmB.

A typical feature of pancreatic cancer is the presence of immune infiltrates with pro-tumorigenic role [237] [240].

Also, an immunosuppressive role has been recognized for some of the immune cells present within the TME at the primary site in pancreatic cancer [189], [194], [286]–[288]. For instance, in KPC mice, infiltration of macrophages has been shown to be an early event and is responsible for the suppression of $CD8^+$ T cell activity since the very beginning of the tumorigenic process, thereby preventing an anti-tumour immunity to happen even in the initial phases [256]. Macrophages, depending on the microenvironment cytokine milieu can acquire an M1-like or M2-like phenotype [289]. In the experimental model used in our lab, it was found that

macrophages highly infiltrate livers of pancreatic cancer metastasis, and although we did not find any difference in metastatic macrophages number, we observed that small lesions at day 6 were mainly populated by anti-tumourigenic M1-like MAMs with high expression of pro-inflammatory cytokines such as *Ifng, Il12* and high antigen-presenting capabilities. On the contrary, pro-tumorigenic M2-like MAMs populated large metastatic lesions at day 14. M2-like MAMs expressed high levels of immunosuppressive factors such as *Il10* and *Tgfb* and were also able to negatively regulate $CD8^+$ T cell activation and proliferation.

Taken together, these results suggest that $CD8^+$ T cell mediated anti-tumour immunity is initially built in response to metastatic dissemination of pancreatic cancer cells into the liver. The immune system's ability to fight the tumour is demonstrated by the presence of pro-inflammatory, antigen-presenting MAMs, which in turn can burst and sustain cytotoxic $CD8^+$ T cell activation and function at the early stages of metastasis formation. However, at later stages, MAMs undergo a phenotypic switch toward an M2 alternative state, likely due to accumulation of tumour promoting cytokines and factors recruited by cancer cells within the tumour microenvironment. M2-like MAMs act to suppress anti-tumour immunity and this explains the loss of T cell infiltration and function together with establishment of large metastatic deposit of pancreatic cancer into the liver.

Chapter 4:

Results

4 Chapter 4: Macrophage targeting restores anti-tumour immune response in metastatic livers

Strategies aimed at targeting macrophages are being extensively explored for cancer therapy. These strategies generally are focused on inhibiting macrophage recruitment at the tumour site, thus preventing their tumour-promoting role; other strategies instead are focused at enhancing macrophage anti-tumour activities [51]. Macrophages can modulate the effects of conventional therapies such as chemotherapy and radiotherapy. Furthermore, macrophages contribute to the generation of an immunosuppressive microenvironment through different routes. Recently, great advances in cancer therapy have been accomplished by augmenting anti-tumour effector T cell functions and by depleting immunosuppressive cells, such as macrophages [290]. In the first part of my study, it was identified that MAMs with an immunosuppressive phenotype highly accumulates in metastatic liver of pancreatic cancer and that large established metastatic lesions are poorly infiltrated by cytotoxic T cells (Chapter 3). Based on these findings, it was reasoned that targeting MAMs could increase T cell infiltration and, subsequently favour an effective anti-tumour immune response at the metastatic site.

4.1 Depletion of PI3Kγ affects MAM recruitment and enhances T cell infiltration and function

To understand whether a reduction in MAM recruitment could impair the formation of an immunosuppressive TME, intrasplenic implantation of $KPC^{luc/zsGreen}$ cancer cells into isogenic Phosphoinoside-3-kinase (PI3K)-gamma deficient ($PI3K\gamma^{-/-}$) mice and control WT mice was performed. PI3Kγ is one the isoforms of Class I PI3Ks lipid enzymes and is highly expressed in myeloid cells [291]. Mice lacking the p110γ catalytic subunit of PI3Kγ show reduced myeloid cells recruitment in response to inflammatory mediators and tumour derived signals, including those deriving from pancreatic cancer [292]. Moreover, recent studies have shown that inhibition of PI3Kγ ablates immunosuppressive functions of myeloid cells in pre-clinical melanoma and lung cancer models [293]. Here, the use of the experimental metastasis model enabled to identify that metastatic progression in PI3Kγ deficient mice was markedly reduced in comparison to WT mice. Data were obtained by *in vivo* bioluminescence imaging (BLI) of metastatic liver in $PI3K\gamma^{-/-}$ and WT mice 14 days after intrasplenic injection of cancer cells (Figure 4.1 a). Moreover, H&E staining also revealed that lack of PI3Kγ reduced the number of liver pancreatic cancer metastatic foci (Figure 4.1 b).

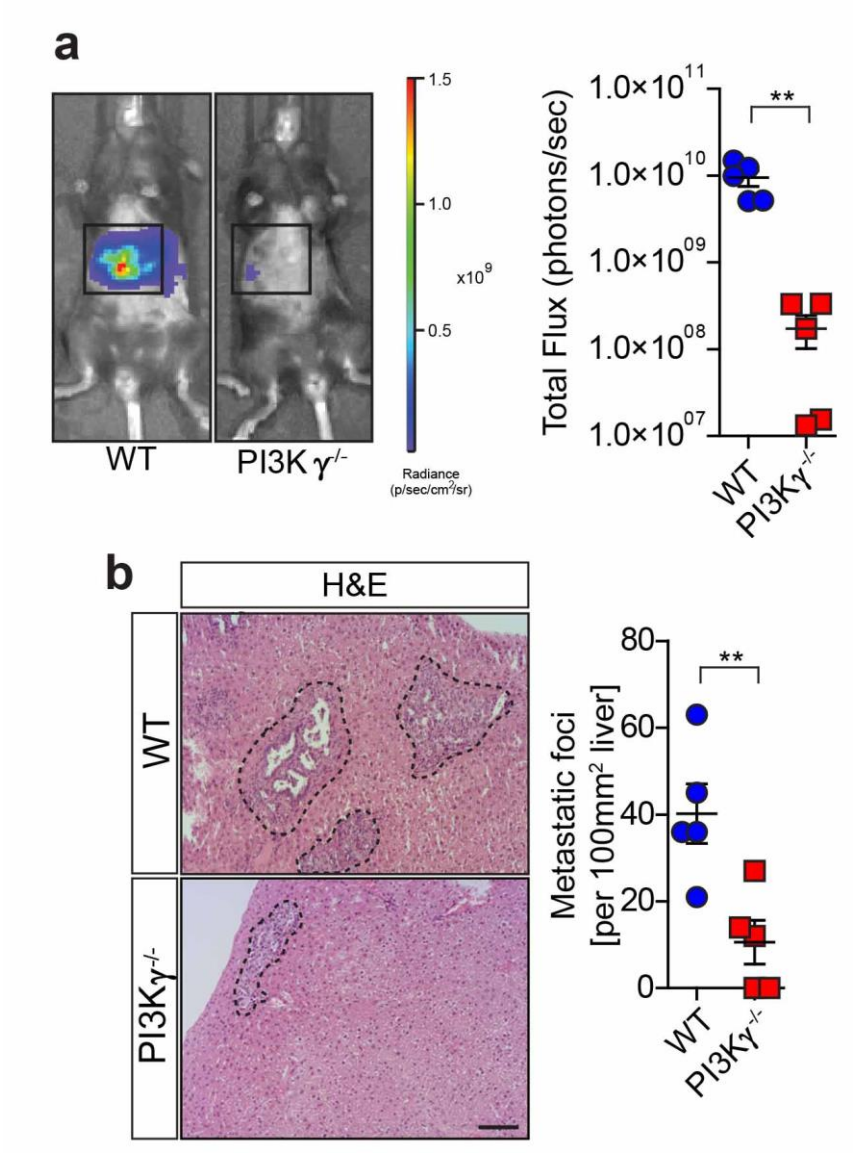

Figure 4.1 Lack of PI3Kγ reduces metastatic progression of pancreatic cancer.

Liver metastasis was induced by intrasplenic implantation of 1x106 KPCluc/zsGreen cancer cells in WT and PI3Kγ -/- mice. Entire livers were harvested and analysed 14 days later. a) In vivo bioluminescence imaging (BLI) was performed to quantify metastatic tumour burden in the liver. Representative images showing radiance in WT and PI3Kγ deficient mice. Graph: quantification of radiance as total flux (photons/sec). Quantification of metastatic lesions frequency in WT and PI3Kγ -/- mice by haematoxylin and eosin (H&E) staining of liver tissue

sections. N = 5 mice / group, n = 5 field of views; individual data points, horizontal lines represent mean ± SEM . P<0.001; **, P < 0.01; *, P < 0.05; n.s. not significant by unpaired t-test. Scale bar = 100 μm.

Flow cytometry analysis of digested metastatic livers coming from WT and PI3Kγ deficient mice revealed that impaired F4/80$^+$ MAM recruitment at the metastatic site in mice lacking PI3Kγ (Figure 4.2 a) was accompanied by a higher infiltrating CD8$^+$ T cells number (Figure 4.2 b).

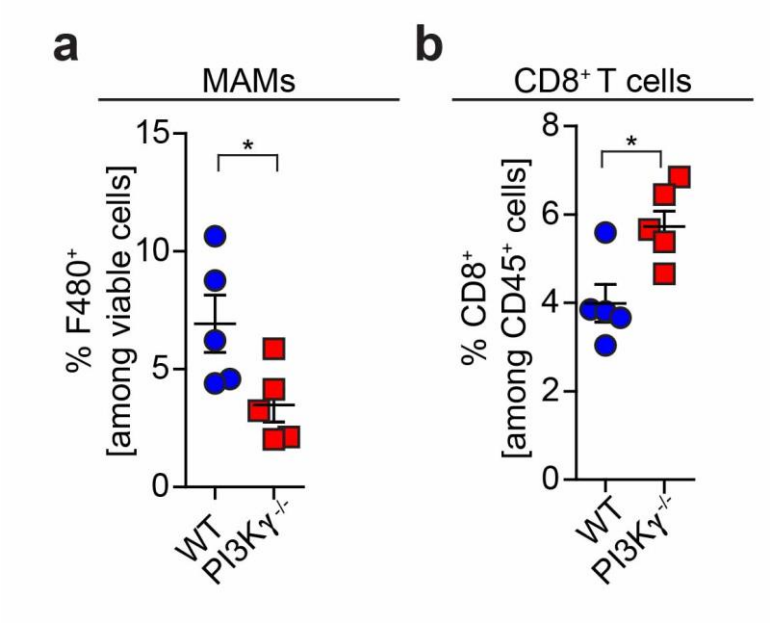

Figure 4.2 PI3Kγ deficient mice have enhanced CD8$^+$ T cell infiltration at the metastatic site.

Liver metastasis was induced by intrasplenic implantation of KPC$^{luc/zsGreen}$ cancer cells in WT and PI3Kγ $^{-/-}$ mice. Entire livers were harvested and analysed 14 days later. Flow cytometry analysis of WT and PI3Kγ$^{-/-}$ disaggregated mouse livers and quantification of **a)** F4/80$^+$ MAM numbers and **b)** metastasis infiltrating CD8$^+$ T cells. N = 5 mice / group; individual data points, horizontal lines represent mean ± SEM. P<0.001; **, P < 0.01; *, P < 0.05; n.s. not significant by unpaired t-test.

Furthermore, in accordance with the high numbers of $CD8^+$ T cells found in the metastatic livers of $PI3K\gamma^{-/-}$ mice, we also detected higher levels of dead cancer cells in metastatic livers of the knock-out mice in comparison to those present in WT mice, as suggested by increased number of apoptotic cleaved caspase 3 positive ($CC3^+$) metastatic cancer cells ($zsGreen^+$) identified by IF staining of $PI3K\gamma^{-/-}$ mice liver tissues (Figure 4.3).

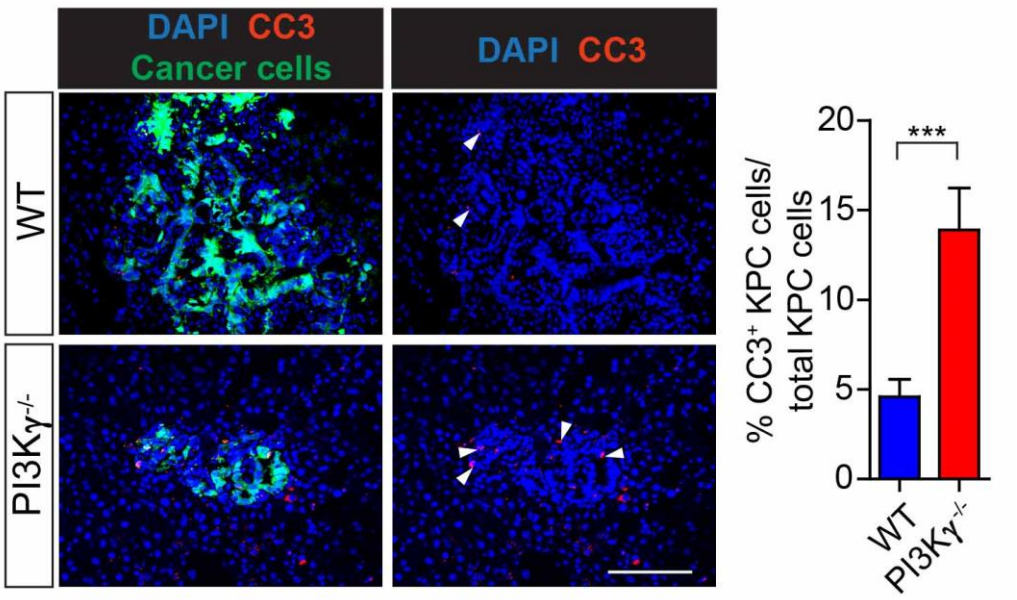

Figure 4.3 Metastatic cancer cells in PI3K□□deficient mice undergo increased apoptosis.

Liver metastasis was induced by intrasplenic implantation of KPCluc/zsGreen cancer cells in WT and PI3Kγ -/- mice. Entire livers were harvested and analysed 14 days later by immunofluorescence (IF) staining. Representative images and quantification of cleaved caspase 3 (CC3, in red) staining in metastatic cancer cells (zsGreen+) in WT and PI3Kγ-/- mice. Nuclei were counterstained with DAPI. N = 5 mice / group, n = 5 field of views / mouse; mean ± SEM. Scale bar = 100 µm. P<0.001; **, P < 0.01; *, P < 0.05; n.s. not significant by unpaired t-test. White arrows point to $CC3^+$ cells (in red).

4.2 CSF-1 / CSF-1R expression within the tumour microenvironment.

Signalling though CSF-1 and its cognate receptor, CSF-1R, promotes macrophage differentiation from myeloid progenitor and drives macrophage polarization toward an M2-like phenotype [294]. Indeed, CSF-1 and CSF-1R are among the most promising targets for inhibition of the tumour promoting functions of macrophages, and they are currently being tested in several early and advanced clinical trials [51], [295]. On this base, it was reasoned that impairment of CSF-1 / CSF1-R signalling axis could be a valuable strategy to target MAMs at the metastatic site and to study their effect on anti-tumour immunity.

CSF-1 and CSF-1R expression in metastatic livers of pancreatic cancer was first characterized. Liver metastasis was induced by intrasplenic implantation of $KPC^{luc/zsGreen}$ cancer cells and, 14 days after, resected livers were processed for flow cytometry analysis. From metastatic lesions $zsGreen^{neg}$ / $CD45^{neg}$ immune depleted stroma cells, $F4/80^{+}$ MAMs and $zsGreen^{+}$ cancer cells were isolated. The three different cell types were then interrogated for quantitative *Csf1* gene expression by PCR. It was found that cancer cells were the main source of CSF-1 within the tumour microenvironment (Figure 4.4 a). Similarly, ELISA quantification of secreted CSF-1 (or also named M-CSF1) in conditioned media (CM) from cultured BMMs, and from KPC and Panc02 pancreatic cancer cells, revealed that CSF-1 is strongly secreted by both cancer cell types but not by BMMs (Figure 4.4 b).

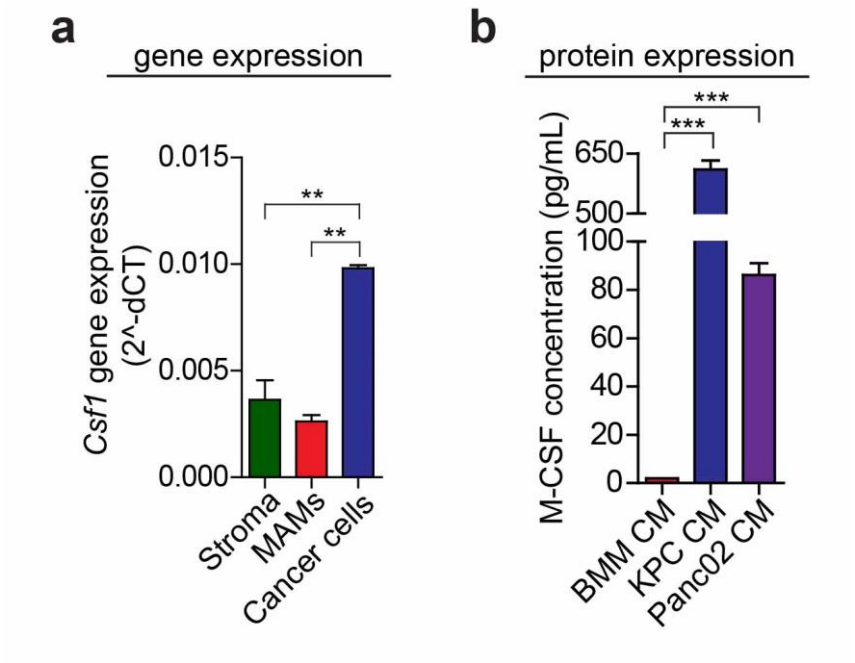

Figure 4.4 Cancer cells are the main source of CSF-1.

a) Quantification of Csf1 mRNA level in immune cell depleted stroma cells ($CD45^{neg}zsGreen^{neg}$), MAMs ($CD45^{+}F480^{+}zsGreen^{neg}$) and disseminated cancer cells ($zsGreen^{+}CD45^{neg}$) isolated by ARIA flow cytometer cell sorting from metastatic tumours. **b)** Quantification of CSF-1 protein level in conditioned medium (CM) generated from bone marrow derived macrophages (BMMs) and KPC and Panc02 pancreatic cancer cells using ELISA. Data are representative of three independent experiments. N = 3 mice / group; mean ± SD. P<0.001; **, P < 0.01; *, P < 0.05; n.s. not significant by Bonferroni multiple comparison.

CSF-1R expression within the TME was successively validated by IF staining of serial tissue sections of murine metastatic livers experimentally derived 14 days after $KPC^{luc/zsGreen}$ cancer cells implantation. It was observed that the CSF1-R^{+} signal co-localized with F4/80^{+} stained cells but not with $zsGreen^{+}$ signal of metastatic cancer cells, thus suggesting that in metastatic lesions, CSF1-R is mainly expressed by macrophages (Figure 4.5).

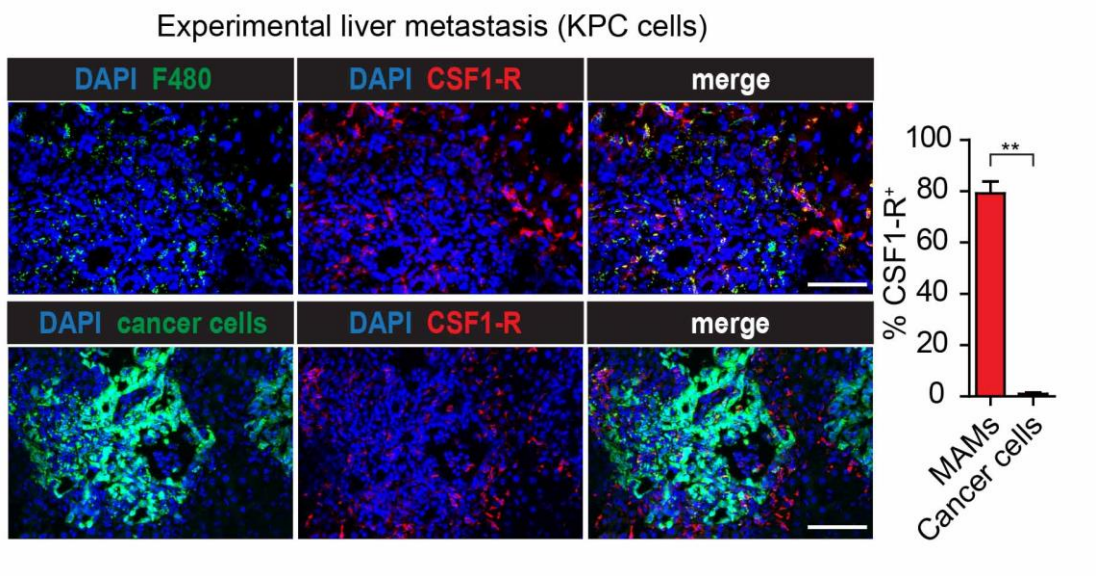

Figure 4.5 CSF-1R is highly expressed by F4/80^{+} MAMs in experimental liver metastasis.

Representative images of immunofluorescence staining (IF) for CSF-1R, F4/80, and zsGreen^{+} metastatic KPC$^{luc/zsGreen}$ cells. CSF-1-R expression was detected only on F4/80^{+} MAMs (upper panel), but not on zsGreen tumour cells (lower panel). Nuclei were counterstained with DAPI. Quantification of percentage of CSF1-R positive cells among MAMs (F4/80^{+} cells) and KPC$^{luc/zsGreen}$ (zsGreen^{+}) cancer cells. N = 4 mice; n = 5 field of views / mouse; mean ± SEM. Scale bar = 100 µm. .P<0.001; **, P < 0.01; *, P < 0.05; n.s. not significant by unpaired t-test.

Similarly, IF co-staining for macrophage marker F4/80 and CSF-1R in liver metastatic tissues derived from the autochthonous KPC mouse model of pancreatic cancer reveals co-localization of CSF-1R signal with F4/80^{+} cells (Figure 4.6).

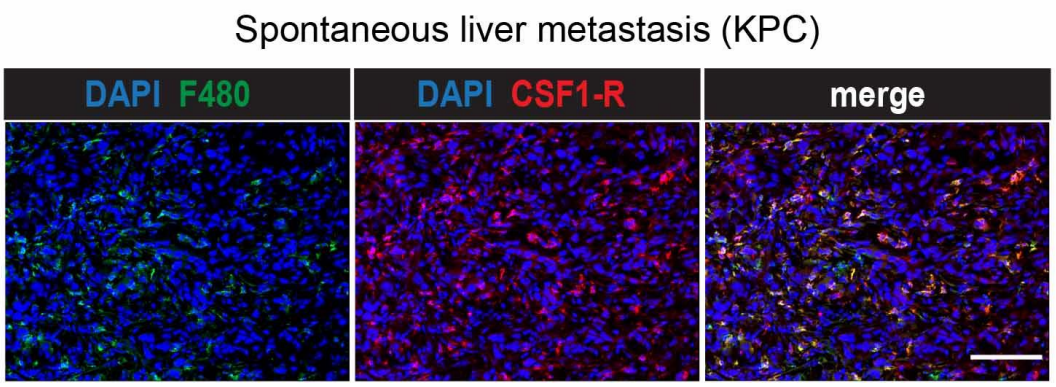

Figure 4.6 CSF-1R is highly expressed by F4/80^{+} MAMs in KPC mice spontaneous liver metastasis.

Representative images of immunofluorescence staining for CSF-1R and F4/80^{+} MAMs in spontaneous liver metastatic lesions derived from KPC mice. N = 4 mice; Scale bar: 100μm.

4.3 Pharmacological blockade of the CSF-1 / CSF-1R axis reprograms MAMs towards an immune-stimulatory phenotype.

Since CSF-1 and its receptor are highly expressed at the metastatic site, it was assessed whether the inhibition of CSF-1 / CSF-1R could affect MAM functions and in consequence, restore T cells infiltration and activation, thereby dampening metastatic pancreatic cancer progression. Intrasplenic implantation of $KPC^{luc/zsGreen}$ cancer cells was performed into WT mice. Starting at day 7, after initial seeding has occurred, BLZ945, a small molecule inhibitor of CSF-1 receptor, which has been previously experimented to target tumour-associated macrophages in cancer was administered [184]. Treatment was carried every day for one week and metastasis volume was assessed by *in vivo* MR imaging prior (Day 6) and after treatment (Day 14) (Figure 4.7 a). Quantification of percentage change in metastatic volume at the end point in comparison to starting treatment point in vehicle treated (CTR) and BLZ945 treated mice revealed that MAM targeting contributed to reduction in metastatic growth of pancreatic cancer (Figure 4.7 b, c and d).

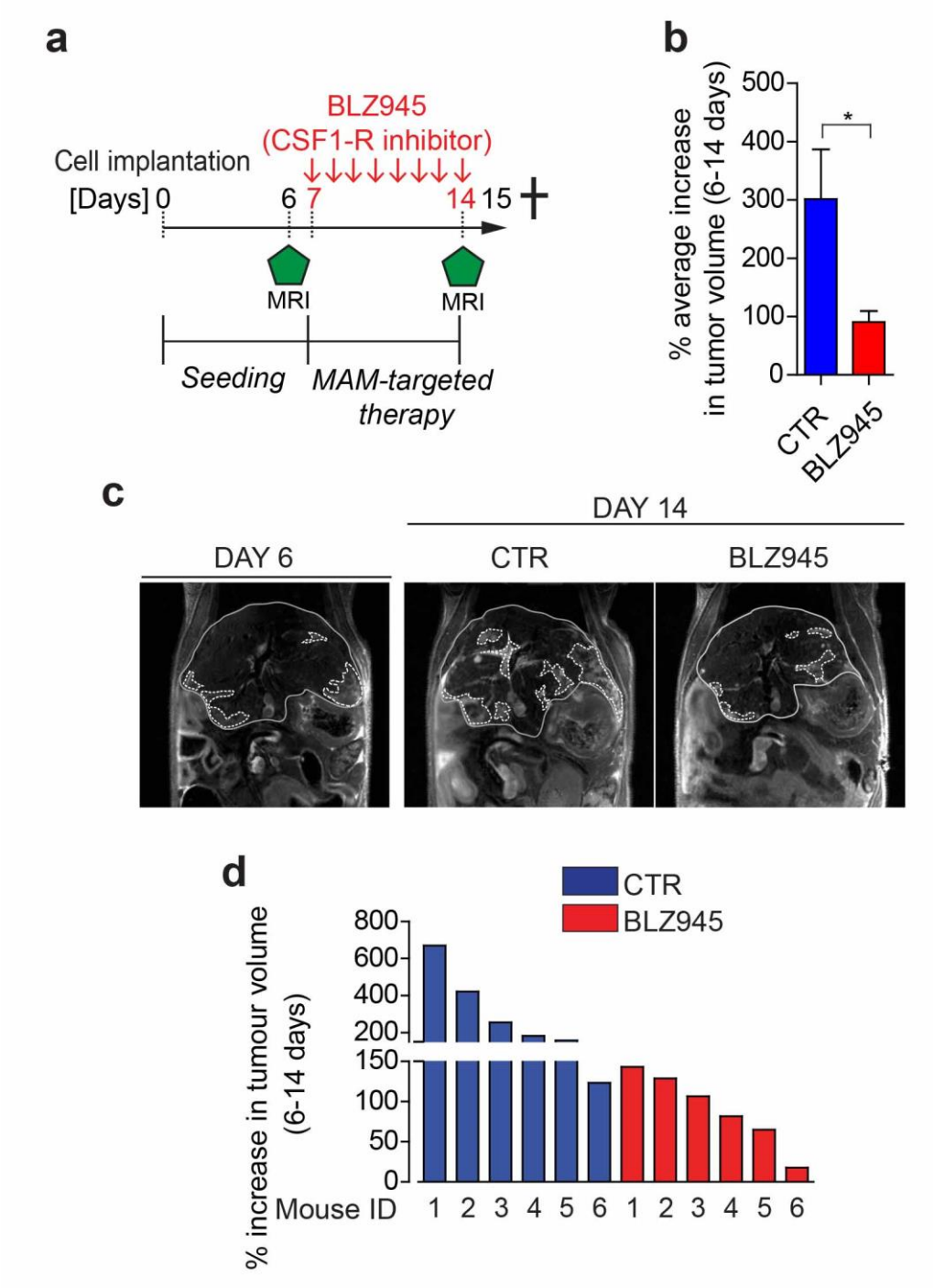
a
BLZ945
(CSF1-R inhibitor)
Cell implantation
[Days] 0
6 7
14 15
MRI
MRI
Seeding
MAM-targeted therapy
b
% average increase in tumor volume (6-14 days)
500
400
300
200
100
0
*
CTR
BLZ945
c
DAY 14
DAY 6
CTR
BLZ945
d
CTR
BLZ945
% increase in tumour volume (6-14 days)
800
600
400
200
150
100
50
0
Mouse ID
1 2 3 4 5 6 1 2 3 4 5 6

Figure 4.7 CSF1-R blockade reduces metastatic progression of pancreatic cancer.

Liver metastasis was induced by intrasplenic implantation of $1x10^6$ $KPC^{luc/zsGreen}$ cancer cells and initial tumour volume was quantified on day 6 by in vivo Magnetic Resonance (MR) imaging. Cohorts were treated with CSF-1R inhibitor (BLZ945) or control vehicle (CTR) for 7 days. At day 14, tumour volume was assessed by MR imaging using T_{2}-weighted sequence and mice were sacrificed on day 15 and analysed. **a)** Schematic illustration of the experiment. **b)** Percentage average increase in metastatic tumour burden (tumour volume) in response to treatment assessed by in vivo MR imaging. **c)** Representative MR images of hepatic metastatic tumours prior treatment (day6) and post-treatment (day14). Livers are delineated with full lines and metastatic tumours with dashed lines. **d)** Percentage increases in metastatic tumour burden (tumour volume) in response to treatment for each mouse (ID 1- 6 / group) assessed by in vivo MR imaging. N = 6 mice / group; mean ± SEM. P<0.001; **, P < 0.01; *, P < 0.05; n.s. not significant by unpaired t-test.

Experimental liver metastasis treated with control vehicle (CTR) or BLZ945 were processed at the end point (day 15) and multi-colour flow cytometer analysis was performed. Data obtained showed reduction in the $F4/80^+$ MAM population upon CSF-1R blockade (Figure 4.8 a). Interestingly, BLZ945 treatment diminished $CD206^+$ M2-like macrophage population among the remaining $F4/80^+$ cells (Figure 4.8 b); and together with this, it was also observed a loss of expression of M2-associated mannose receptor marker, *Mrc,1* and of the immunosuppressive genes *Tgfb* and *Il10* upon BLZ945 treatment, as indicated by quantitative PCR analysis performed on RNA extracted from MAMs isolated from metastatic livers (Figure 4.8 c).

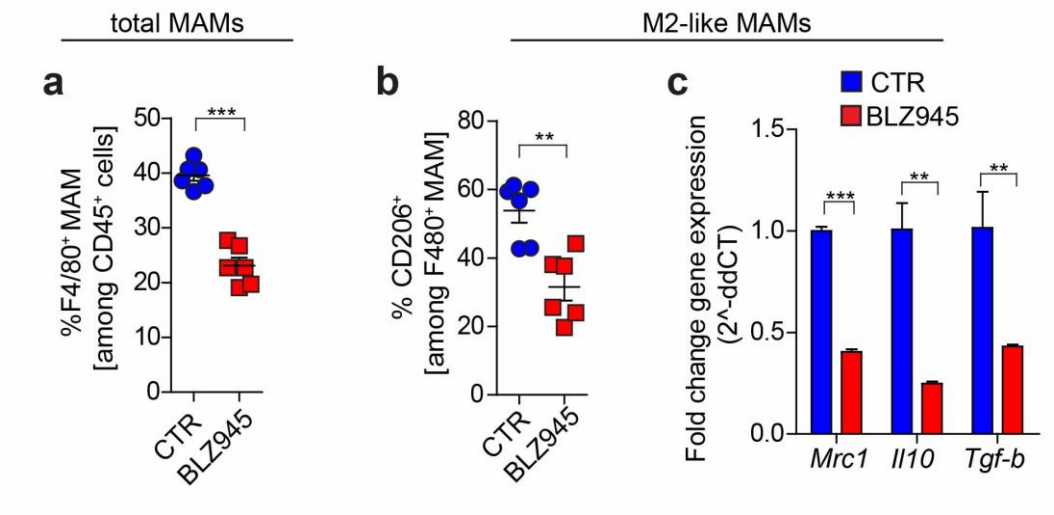

Figure 4.8 CSF-1R inhibition abrogates MAMs immunosuppressive phenotype.

Liver metastasis was induced by intrasplenic implantation of $1x10^6$ $KPC^{luc/zsGreen}$ cancer cells. Cohorts were treated with CSF-1R inhibitor (BLZ945) or control vehicle (CTR). At the end point (day 15) livers were harvested and digested for flow cytometry analysis **a)** Quantification of total $F4/80^+$ MAMs from tumour bearing livers. **b)** Quantification of $F4/80^+CD206^+$ MAMs in each treatment group. Individual data points, horizontal lines represent mean ± SEM. **c)** Quantification of Mrc1, Il10, and Tgfb mRNA levels in MAMs sorted from established metastatic lesions from mice of each treatment group (mean ± SEM). N = 6 mice / group. P<0.001; **, P < 0.01; *, P < 0.05; n.s. not significant by unpaired t-test.

Together with a reduction in total MAMs number and MAM immunosuppressive functions, BLZ945 treatment also augmented an anti-tumour response at the metastatic site. Expansion of $CD8^+$ T cell numbers (Figure 4.9 a) and increased cancer cell apoptosis (Figure 4.9 b) was observed in metastatic livers derived from treated mice compared to CTR mice.

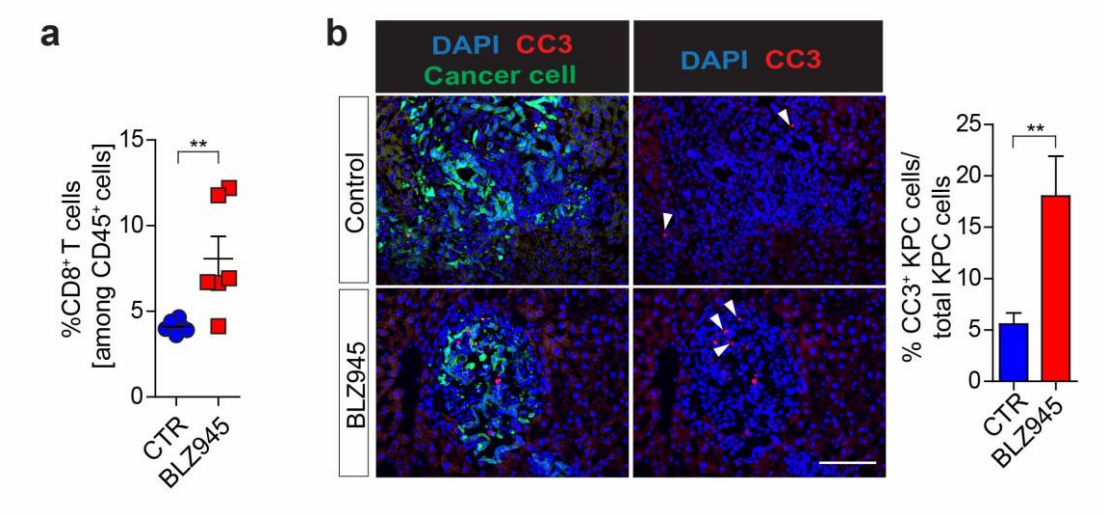

Figure 4.9 MAM targeting enhances anti-tumour immunity.

Liver metastasis was induced by intrasplenic implantation of $1x10^6$ $KPC^{luc/zsGreen}$ cancer cells. Cohorts were treated with CSF-1R inhibitor (BLZ945) or control vehicle (CTR). At the end point (day 15) livers were harvested and analysed. **a)** Metastatic infiltration of $CD8^+$ T cells evaluated by flow cytometry. Individual data point, horizontal lines represent mean ± SEM. **b)** Representative immunofluorescence staining and quantification of cleaved caspase 3 (CC3, red) in metastatic cancer cells ($zsGreen^+$) in liver tissue sections of each treatment cohort. Nuclei were counterstained with DAPI. Mean ± SEM. N = 6 mice/group. n = 4 field of views / mouse. P<0.001; **, P < 0.01; *, P < 0.05; n.s. not significant by unpaired t-test. Scale bar: 100µm. White arrows point to $CC3^+$ cancer cells (in red).

Next it was questioned whether the blockade of CSF-1R ligand could lead to an alteration of MAM population and reinvigoration of anti-tumour immunity similarly to what was observed by blockade of the macrophage receptor CSF1-R. This time a neutralizing antibody targeting CSF-1 was used to treat metastatic mice 7 days after intrasplenic injection of KPC$^{luc/zsGreen}$ cells. Treatment was carried out for 2 weeks and, at the end point (day 20), H&E staining revealed a decrease in metastatic lesion area in response to αCSF-1 inhibitor treatment in comparison to IgG control (CTR) treated mice (Figure 4.10 a and b).

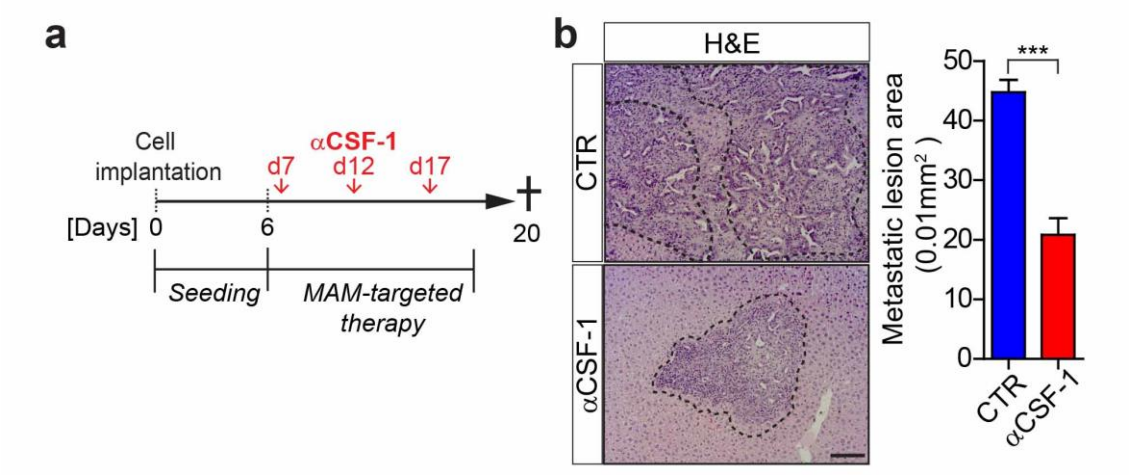

Figure 4.10 Pancreatic cancer metastasis growth is impaired by CSF-1 inhibition.

Liver metastasis was induced by intrasplenic implantation of KPC$^{luc/zsGreen}$ cancer cells. After 7 days, metastasis bearing mice were treated either with IgG control isotype (CTR) or with neutralizing αCSF-1 antibody. Mice were sacrificed at day 20. **a)** Schematic representation of the experiment. **b)** Representative haematoxylin and eosin (H&E) images of metastatic liver tissue sections and quantification of the average of metastatic lesion area in both treatment cohorts. N = 6 mice / group, n = 4 field of view / mouse; mean ± SEM. P<0.001; **, P < 0.01; *, P < 0.05; n.s. not significant by unpaired t-test. Scale bar: 100μm.

In respect to MAMs, flow cytometry analysis of dissociated livers derived from the two treatment cohorts showed that αCSF-1 inhibitor reduced not only overall MAMs number (Figure 4.11 a), but markedly decreased the presence of M2-like F4/80^{+}CD206^{+} MAMs (Figure 4.11 b).

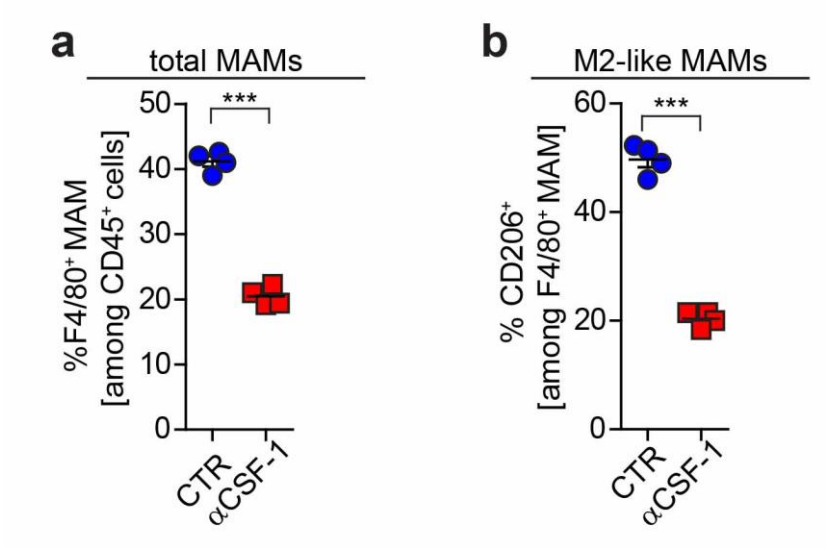

Figure 4.11 CSF-1 inhibition reduces MAM infiltration.

Liver metastasis was induced by intrasplenic implantation of KPC$^{luc/zsGreen}$ cancer cells. After 7 days, metastasis bearing mice were treated either with IgG control isotype (CTR) or with neutralizing αCSF-1 antibody. Mice were sacrificed at day 20 and livers digested for flow cytometry analysis. **a)** Quantification of total MAMs (F4/80^{+}) and **b)** F4/80^{+} CD206^{+} M2-like MAMs in tumour bearing livers. N = 4 mice / group; Individual data point, horizontal lines represent mean ± SEM; P<0.001; **, P < 0.01; *, P < 0.05; n.s. not significant by unpaired t-test.

To further characterize MAM population upon CSF-1 inhibition, MAMs were sorted by flow cytometry and interrogated for the expression of M1-like and M2-like macrophage associated markers. Quantitative PCR further confirmed that inhibition of CSF-1 induced a reprogramming of MAMs towards an immune-stimulatory M1-like phenotype. MAMs isolated from αCSF-1 treated mice showed increased expression of pro-inflammatory

cytokines and markers (*Cxcl10, Ifng, Il12, Cd86, H2Aa*), whereas the levels of M2-like immunosuppressive factors (*Tgfb, Il10, Arginase, Mrc, Relmα*) were reduced (Figure 4.12).

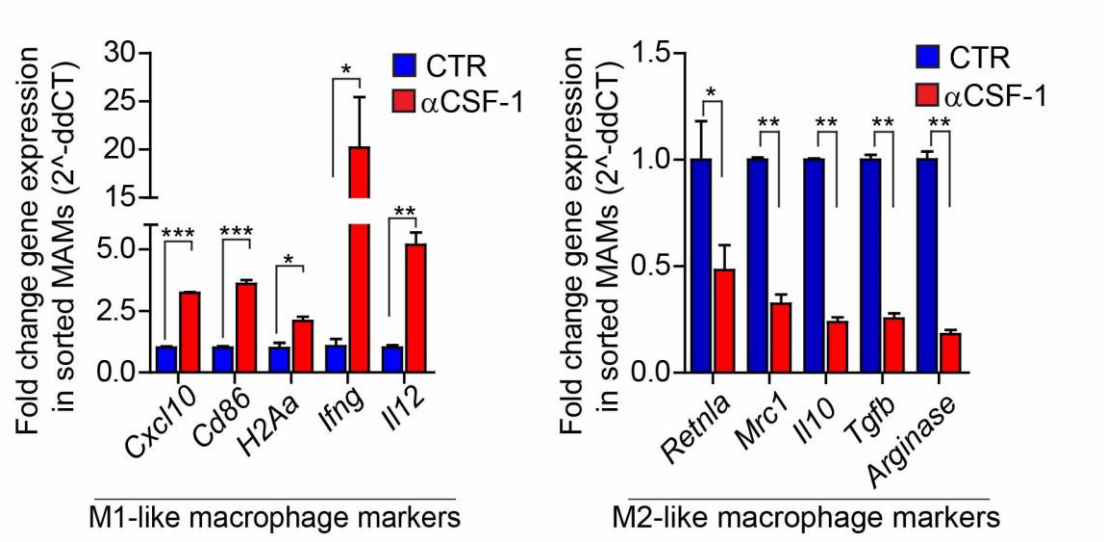

Figure 4.12 CSF-1 inhibition rewires MAMs toward an immune-stimulatory phenotype.

Liver metastasis was induced by intrasplenic implantation of KPC$^{luc/zsGreen}$ cancer cells. After 7 days metastasis bearing mice were treated either with IgG control isotype (CTR) or with neutralizing αCSF-1 antibody. Mice were sacrificed at day 20 and livers digested for flow cytometry analysis. MAMs were isolated from both treatment cohorts by flow cytometry ARIA sorter and quantitative PCR was performed on MAMs extracted RNA. Quantification of M1-like (Cxcl10, Ifng, Il12, Cd86,H2Aa) and M2-like (Tgfb, Il10, Arginase, Mrc, Relma) gene expression in MAMs. N = 4 mice / group; mean ± SEM; P<0.001; **, P < 0.01; *, P < 0.05; n.s. not significant by unpaired t-test.

Consistent with a rewired pro-inflammatory metastatic microenvironment, $CD8^+$ T cell number was increased in αCSF-1 inhibitor treated mice, and $CD8^+$ T cells showed also enhanced activation. Metastatic livers from IgG control (CTR) and αCSF-1 inhibitor treated mice were analysed by flow cytometry for $CD8^+$ T cell infiltration (Figure 4.13 a), $CD8^+$ T cells production of IFNγ (Figure 4.13 b) and GzmB (Figure 4.13 c) and for $CD8^+$ T cells expression of Ki67, a marker used to discriminate proliferating cells (Figure 4.13 d and e). It was found that MAM targeting highly potentiated $CD8^+$ T cells cytotoxic activity and proliferation, thus resulting in increased numbers of total infiltrating T cells. In particular, the enhanced proliferation rate ($Ki67^+$ cells) within $PD\text{-}1^+$ $CD8^+$ T cells, suggested a partial reinvigoration of exhausted $PD\text{-}1^+$ T cells within the metastatic niche upon αCSF-1 treatment.

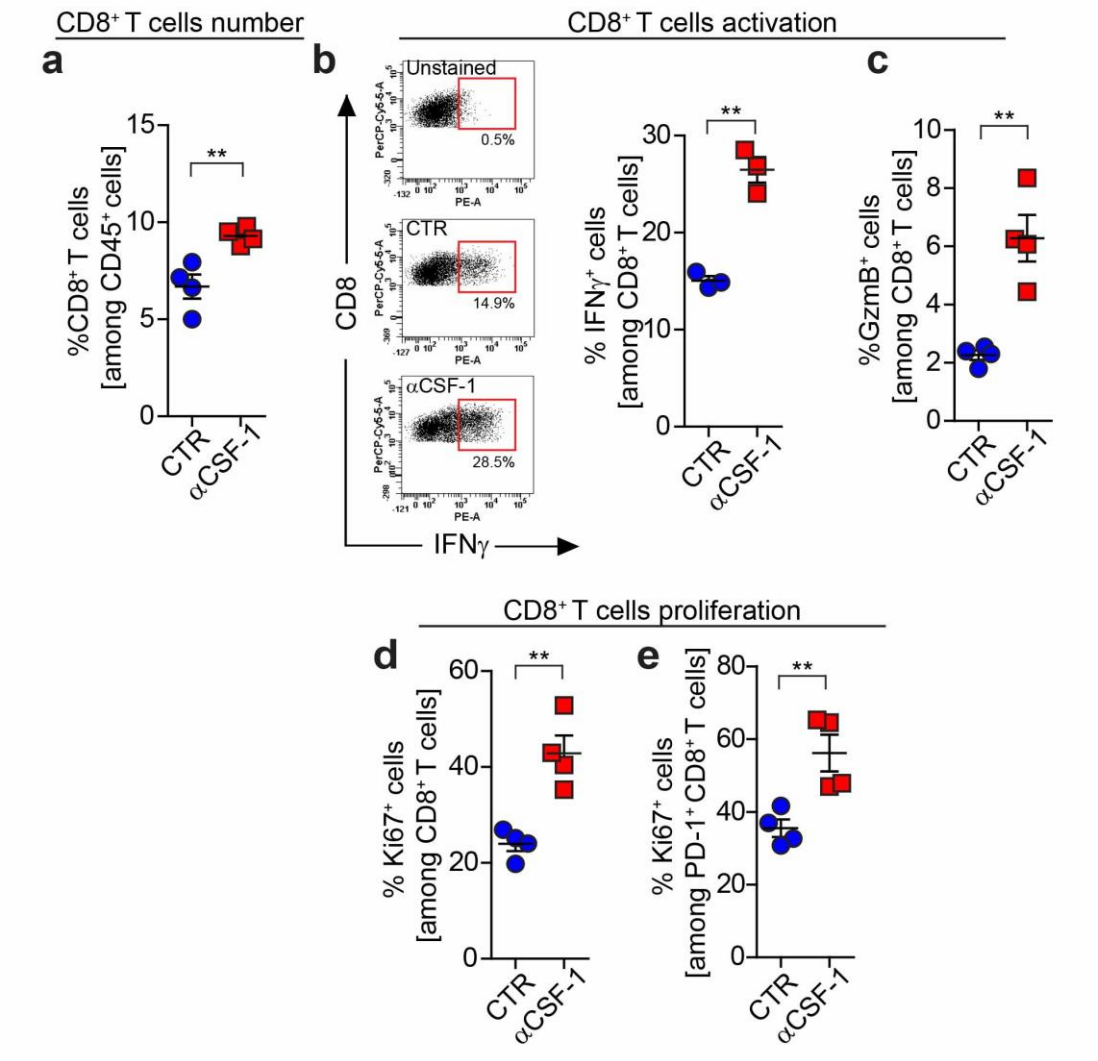

Figure 4.13 CSF-1 inhibition reinvigorates CD8$^+$ T cell cytotoxicity.

Liver metastasis was induced by intrasplenic implantation of KPC$^{luc/zsGreen}$ cancer cells. After 7 days, metastasis bearing mice were treated either with IgG control isotype (CTR) or with neutralizing αCSF-1 antibody. Mice were sacrificed at day 20 and livers digested for flow cytometry analysis. Dot plot representing quantification of **a)** metastasis infiltrating CD8$^+$ T cells, **b)** IFNγ (n = 3 mice / group) and **c)** Granzyme B (GzmB) expression levels in metastasis infiltrating CD8$^+$ T cells. **d-e)** Dot plot representing quantification of proliferating cells (Ki67$^+$) among d) total CD8$^+$ T cells and e) PD-1$^+$ CD8$^+$ T cells. N = 4 mice / group. Individual data point, horizontal lines represent mean ± SEM; P<0.001; **, P < 0.01; *, P < 0.05; n.s. not significant by unpaired t-test.

4.4 Reduction of metastatic progression induced by CSF-1 / CSF-1R axis blockade depends on $CD8^+$ T cells

Finally, it was investigated whether the reduction of pancreatic cancer metastasis progression observed upon CSF-1 / CSF1-R axis blockade was dependent on enhanced $CD8^+$ T cells mediated anti-tumour activity. Thereby, a neutralizing antibody against CD8 was used to deplete the $CD8^+$ T cell population and the effect of the depletion on liver metastatic tumour burden was analysed. Mice were treated with either IgG control (CTR) or αCD8 inhibitory antibodies two days before intrasplenic implantation of $KPC^{luc/zsGreen}$ cancer cells, on the day of surgical implantation of tumour cells, and every four days until the end of the experiment. To validate the effects of CSF-1 inhibition in the absence of $CD8^+$ T cells, mice were treated either with αCSF-1 inhibitor antibody alone or with a combination of αCSF-1 and αCD8 inhibitory antibodies, starting two days after intrasplenic injection of cancer cells and for a total of ten days (Figure 4.14 a).

At the end point (day 14), *ex-vivo* BLI of metastatic livers revealed that $CD8^+$ T cell depletion did not had any effect in terms of metastatic reduction in comparison to CTR mice and that the decrease in metastatic burden observed in mice upon CSF-1 inhibition was inhibited if blockade of CSF-1 was accompanied by $CD8^+$ T cell depletion (Figure 4.14 b).

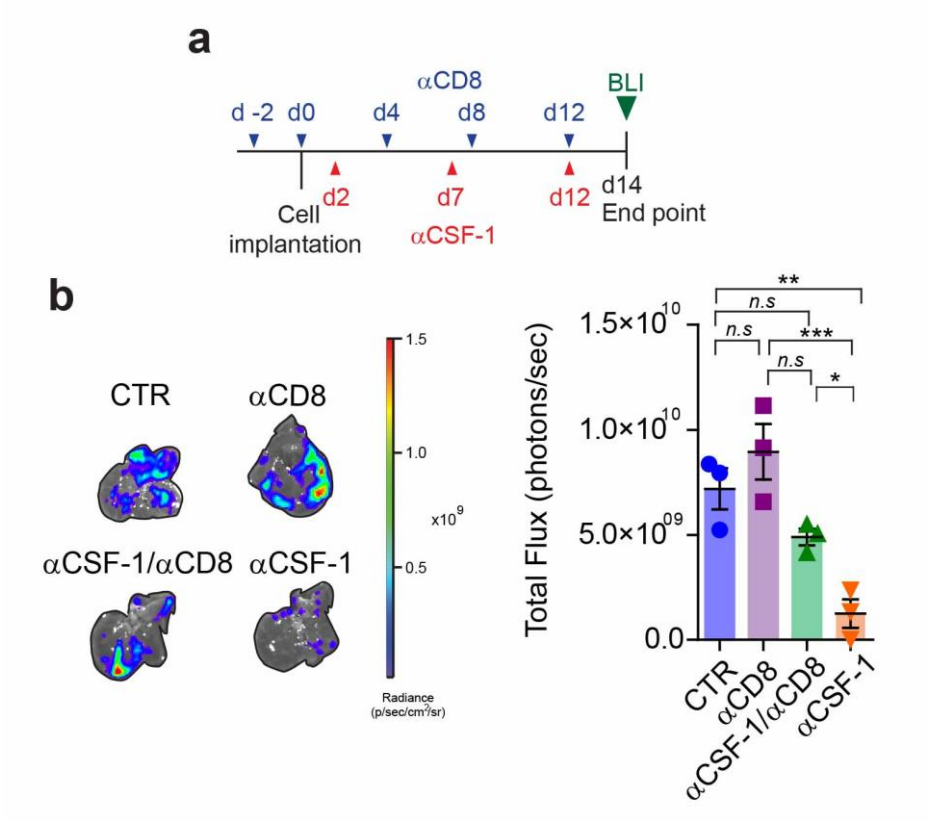

Figure 4.14 Reduction of metastasis mediated by CSF-1 blockade is CD8$^+$ T cells dependent.

Liver metastasis was induced by intrasplenic implantation of KPC$^{luc/zsGreen}$ cancer cells in IgG control or αCD8 inhibitor treated mice. Cohorts were subsequently treated with αCSF-1 or control isotype antibodies starting at day 2 for a total of 10 days. Mice were sacrificed at day 14. **a)** Schematic representation of the experiment. **b)** Metastatic livers were analysed by ex-vivo bioluminescence imaging (BLI). Representative metastatic livers showing radiance for each treatment group are shown. Metastatic tumour radiance as total flux was quantified for all treatment cohorts. N = 3 mice / group; horizontal lines represent mean ± SEM. P<0.001; **, P < 0.01; *, P < 0.05; n.s. not significant by Bonferroni multiple comparison.

At the end point, blood and livers were harvested from IgG control (CTR) and CD8 depleted mice. $CD8^+$ T cell depletion was confirmed by flow cytometry both in the liver (Figure 4.15 a) and in peripheral blood (Figure 4.15 b).

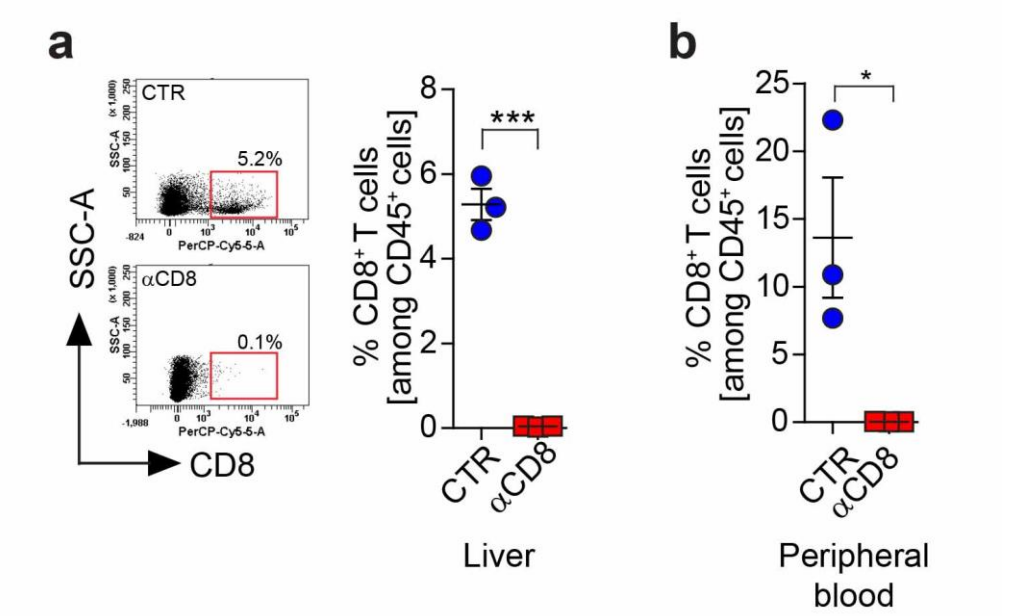

Figure 4.15 Confirmation of $CD8^+$ T cell depletion upon αCD8 inhibitory antibody treatment.

Liver metastasis was induced by intrasplenic implantation of $KPC^{luc/zsGreen}$ cancer cells in IgG control (CTR) or αCD8 inhibitory antibody treated mice. Mice were sacrificed at day 14. Representative flow cytometry dot plots and quantification showing effective $CD8^+$ T cell depletion within the **a)** liver and **b)** peripheral blood of tumour bearing mice upon αCD8 mAb administration. N = 3 mice / group; horizontal lines represent mean ± SEM. P<0.001; **, P < 0.01; *, P < 0.05; n.s. not significant by unpaired t-test.

Taken together, these findings show that reprogramming MAMs towards an immune-stimulatory phenotype using CSF-1 / CSF-1R- targeted therapies restores cytotoxic $CD8^+$ T cell mediated anti-tumour immunity and inhibits pancreatic cancer metastasis.

4.5 Discussion

Pancreatic cancer is characterized by an abundant infiltration of inflammatory cells, and macrophages are one of the major cell population types [237]. In this thesis, it has been previously shown (Chapter 3) that macrophages, in particular those associated with an M2-like phenotype, contribute to the establishment of an immunosuppressive microenvironment that dampens effective anti-tumour T cell response at metastatic site. So far, inhibition of myeloid cells trafficking or signalling transduction has been demonstrated to be an effective therapeutic route to reverse immunosuppression in pancreatic cancer [188], [189], [251], [296]. With the intent to validate MAM targeting impact on anti-tumour immunity different strategies to impair macrophages survival, differentiation and chemotaxis/recruitment were used.

PI3K signalling is one of the most common deregulated pathways that drives cancer initiation and progression [12]. However, PI3K pathway is not only acting on cancer cells, but it also contributes to TME regulation. PI3Kγ is one the isoforms of Class I PI3K enzymes and is activated in granulocytes and monocytes in response to tumour release cytokines and chemokines including IL-8, CXCL12, IL-1β, IL-6, TNFα and CSF-1 [297]. Upon activation, PI3Kγ mediates myeloid cell adhesion to the vasculature and subsequent extravasation into the tumour site, thereby playing a crucial role in stimulating angiogenesis and tumour progression [291]. Recent studies further identified PI3Kγ to be necessary for pancreatic cancer progression [292] and macrophage polarization towards an immunosuppressive phenotype [191], [192]. In our studies, we used PI3K$\gamma^{-/-}$ mice as model system to validate the effect of reduced macrophage infiltration into the metastatic site; indeed, it

has been shown that macrophages derived from PI3Kγ deficient mice have a reduced capacity to migrate toward a wide range of inflammatory chemo-attractant stimuli [298], [299]. In respect to pancreatic cancer metastasis, here it was observed that lack of PI3Kγ reduces MAM number at the metastatic site, increases $CD8^+$ T cells infiltration and cancer cell apoptosis, thereby affecting metastasis formation into the liver. Thus, these findings support the notion that depletion of PI3Kγ stimulates tumour immunity and they also suggest that the use of PI3Kγ inhibitors might be of interest to target pancreatic cancer at the metastatic site.

An alternative therapeutic approach to block the tumorigenic activity of macrophages is focused on inhibiting CSF-1 and its cognate receptor CSF-1R. CSF-1R is prominently expressed by cells of the monocyte lineage and, therefore, has become a target to interfere with TAM functions [180]. CSF-1 is the major growth and differentiation factor for cells of the monocytic-macrophage lineage, and is abundantly expressed by several tumour types, including pancreatic cancer [300]. Thus, blockade of the CSF-1 / CSF-1R axis represents an attractive strategy to target the tumour promoting functions of macrophages and it has been tested in a variety of pre-clinical tumour models, with different outcomes [51], [295]. CSF-1R inhibition reduces TAM numbers in tumour models of colon, ovarian, breast, and pancreatic cancer [182]; while in glioblastoma mouse model, inhibition of CSF-1R did not deplete TAMs, but instead promoted the re-education of macrophages from a tumour promoting M2-like phenotype to an anti-tumorigenic M1-like effector type [184]. In the study presented in this thesis, it was found that CSF-1 is highly expressed by disseminated pancreatic cancer

cells and that, within the hepatic metastatic site, CSF-1R is expressed by MAMs, and not by cancer cells. Pharmacological blockade of the CSF-1 / CSF-1R axis by using either CSF-1R small molecule inhibitor (BLZ945) or αCSF-1 inhibitory antibody reduced MAMs number, and reprogrammed remaining MAMs towards an immune-stimulatory phenotype, as suggested by high expression of the T cell attracting chemokine *Cxcl10,* T cell activating cytokines *Ifng* and *Il12* and by increased antigen presenting abilities (*H2Aa* and *Cd86* expression). In contrast, immune suppressive factors (*Tgfb, Il10, Arginase*), as well as expression of scavenger receptor (*Mrc*, CD206) were strongly down-regulated in MAMs in response to CSF-1 / CSF-1R inhibition. Reprogramming of MAMs was sufficient to elicit anti-tumour immunity, since it was observed increased infiltration of $CD8^+$ T cells with reinvigorated activity, as suggested by high level of $CD8^+$ T cell secretion of IFN_γ and GzmB cytotoxic factors, as well as increased $CD8^+$ T cell proliferation. Hence, CSF-1 / CSF-1R targeting increased effectively a $CD8^+$ T cell cytotoxic response against the metastatic pancreatic cancer, thereby leading to a reduction of the metastatic burden in a T-effector cell dependent manner. All together, these results indicate that the presence of an immunosuppressive microenvironment at the metastatic site is one of the main regulators of pancreatic tumour escape from $CD8^+$ T cell mediated elimination. Immunosuppressive macrophages are one of the principal immune cell infiltrates within the TME, thereby their targeting represents a very powerful strategy to re-establish a pro-inflammatory, cytotoxic T cell rich, anti-tumour response at the metastatic site in pancreatic cancer.

Chapter 5:

Results

5 Chapter 5: Macrophage-targeted therapies stimulate anti-tumour immunity and sensitize metastatic pancreatic cancer to PD-1 checkpoint blockade.

Inhibitory pathways that regulate $CD8^+$ T cell activity act physiologically to prevent chronic stimulation of T cells and insurgence of autoimmune diseases. The inhibitory receptor PD-1 is expressed on the surface of $CD8^+$ T cells, upon antigen recognition, during the effector phase of the anti-tumour immune response. PD-1 engagement by its ligand, PD-L1, results in inhibition of $CD8^+$ T cell proliferation and function, a process named T cell exhaustion [138], [140]. PD-1 mediated T cell exhaustion is one of the main mechanism by which tumours escape immune surveillance, thus therapeutic blockade of PD-1 has become one of the most important advances in the history of cancer treatment [301]. Despite the enormous clinical benefits derived from PD-1 inhibition for several cancer types [140], pancreatic cancer still remains refractory to a single agent therapy [280]. Immunosuppressive macrophages highly infiltrate metastatic pancreatic cancer (Chapter 3) and their targeting positively impact anti-tumour immunity (Chapter 4). In here, it was reasoned that re-activation of the $CD8^+$ T cell cytotoxic response obtained by targeting MAMs might induce expression of PD-L1 on cancer cells leading to increased tumour resistance against $CD8^+$ T cell mediated immune attacks. Blockade of PD-1 / PD-L1 axis can have a therapeutic potential only if T cells are involved in a pre-existing anti-tumour response and PD-1 and PD-L1 expression are induced. Thereby, it was examined i) whether PD-L1 is expressed on disseminated pancreatic cancer cells and/or

stroma cells at the metastatic site and ii) whether the combination of MAM targeted therapy together with PD-1 inhibition could offer a powerful approach to boost anti-tumour immunity and fight pancreatic cancer metastasis.

5.1 PD-L1 expression is up-regulated in cancer cells in response to CSF-1 / CSF-1R inhibition.

In the previous chapter (Chapter 3) it has been reported increased PD-1 expression on $CD8^+$ T cells during metastatic progression and it has been found that it correlated with the acquisition of a T cell dysfunctional phenotype. Here, PD-L1 expression within the TME in pancreatic cancer metastasis was characterized. The presence of PD-L1 has been mainly associated with a mechanism of acquired resistance induced in response to T cell release of IFNγ. To validate whether PD-L1 expression in metastatic pancreatic cancer cells is induced in response to active anti-tumour immune response, the presence of PD-L1 in KPC mice-derived cancer cells was tested *in vitro.* It was found that cultured KPC cancer cells did not express PD-L1, but PD-L1 expression was strongly induced by IFNγ stimulation (Figure 5.1).

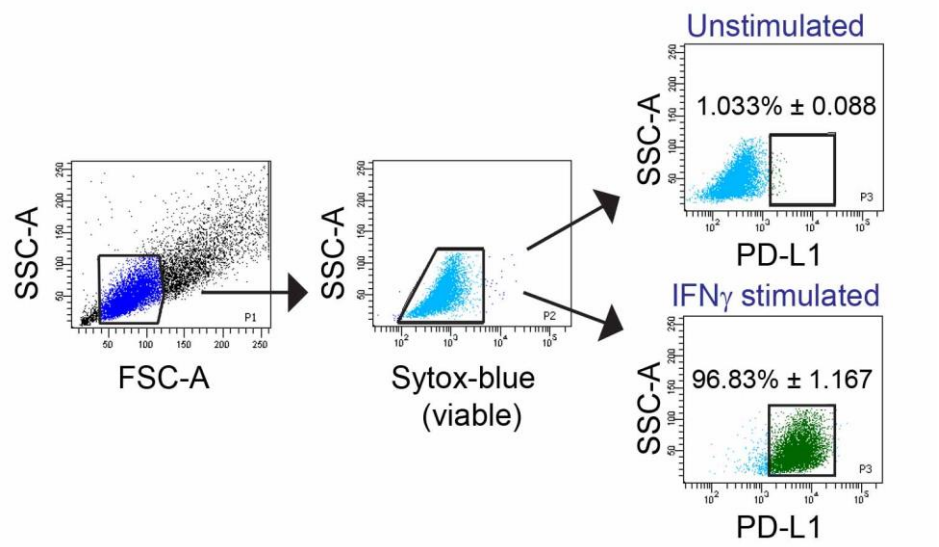

Figure 5.1 IFNγ induces the expression of PD-L1 in in vitro cultured pancreatic cancer cells.

Representative flow cytometry dot plots showing in vitro PD-L1 expression in KPC cancer cells in absence (unstimulated) or in presence of IFNγ stimulation (IFNγ stimulated). Murine recombinant IFNγ was used at a concentration of 50 ng / ml to stimulated cultured KPC cancer cells for 48 hours. Unstimulated cells were cultured for 48 hours in DMEM media supplemented with 2 % FBS. Percentage of PD-L1 positive cells is expressed as mean ± SD. Data are representative of 3 independent experiments.

Next, the expression of PD-L1 *in vivo* at the liver metastatic site was assessed. Experimental liver metastasis was induced by implanting $KPC^{luc/zsGreen}$ cancer cells into mice spleen and PD-L1 expression in resected metastatic livers was analysed after 14 days. Flow cytometry analysis of the digested livers allowed us to identify the $CD45^{neg}zsGreen^{neg}$ immune cells depleted stroma population, $F4/80^{+}$ MAMs and $zsGreen^{+}$ cancer cells. It was found that within the three cell populations, PD-L1 was highly expressed by

MAMs (Figure 5.2 a), and that MAMs were the main source of PD-L1 (Figure 5.2 b) within the metastatic tumour.

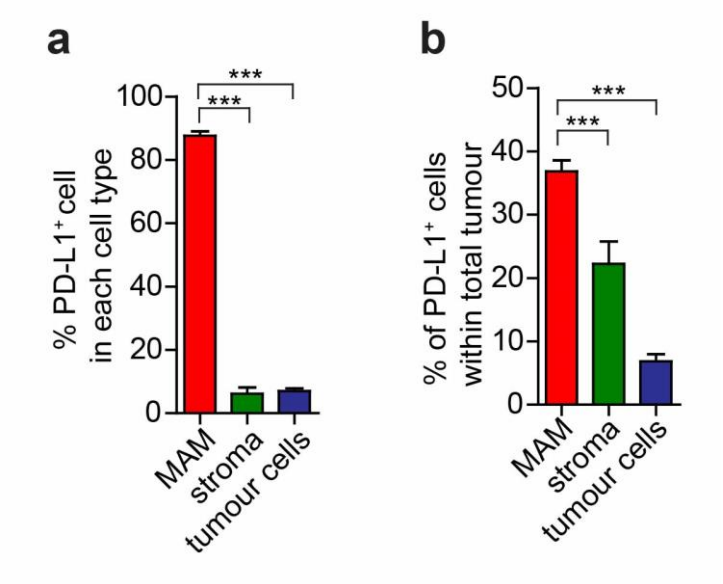

Figure 5.2 MAMs are the main source of PD-L1 in pancreatic cancer metastatic livers.

Liver metastasis was induced by intrasplenic injection of $KPC^{luc/zsGreen}$ cancer cells. After 14 days metastatic livers were resected from euthanized mice and analysed. Quantification by flow cytometry of **a)** PD-L1 expression levels in $F4/80^+$ MAMs, immune cell depleted stroma ($CD45^{neg}zsGreen^{neg}$) and tumour cells ($zsGreen^+$) at day 14; **b)** percentage of PD-L1 expressing cell types within the metastatic tumour. N = 4 mice; mean ± SEM. P<0.001; **, P < 0.01; *, P < 0.05; n.s. not significant by Bonferroni multiple comparison.

In Chapter 4, increase in IFNγ secretion by $CD8^+$ T cells was described as a consequence of MAM inhibition. To analyse whether MAM-targeted therapies affect PD-L1 expression within the metastatic niche, metastatic liver tissues from mice injected with KPC mice derived cancer cells were analysed following treatment with control vehicle (CTR), BLZ945, or αCSF-1 inhibitory antibody starting after 6 days of cancer cells injection. At the end point, day 20, flow cytometry analysis of the digested livers from all treatment cohorts of

mice, allowed identification of the $CD45^{neg}zsGreen^{neg}$ immune depleted stroma cells, $F4/80^{+}$ MAMs and $zsGreen^{+}$ cancer cells. PD-L1 expression was assessed in these three TME cell components. It was found that inhibition of CSF-1 / CSF-1R significantly increased PD-L1 expression in tumour cells (Figure 5.3 a and b), while PD-L1 expression on MAMs and immune depleted stroma cells remained unchanged (Figure 5.3 a).

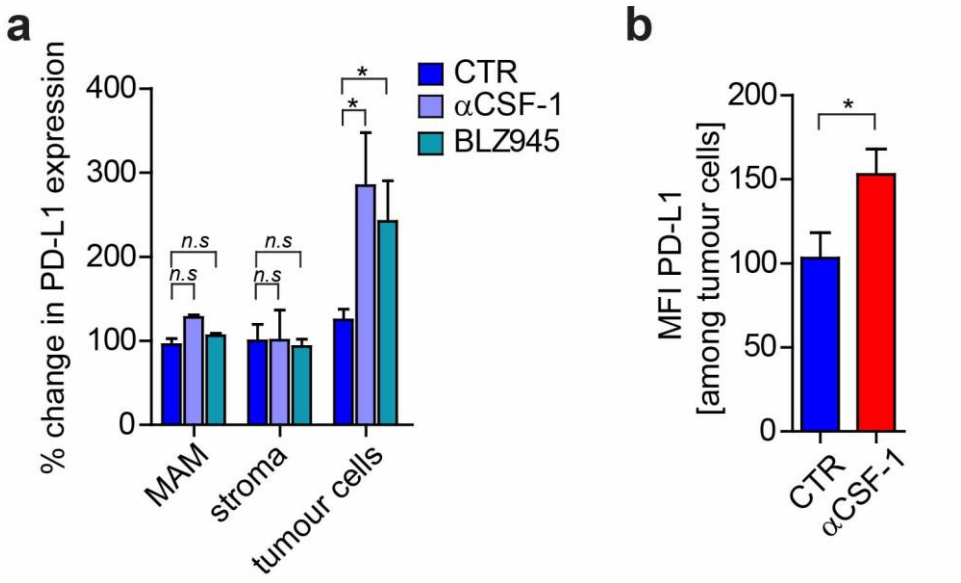

Figure 5.3 MAM targeted therapies induce PD-L1 expression on metastatic cancer cells.

Liver metastasis was induced by intrasplenic injection of $KPC^{luc/zsGreen}$ cancer cells. Metastatic tumours were treated with αCSF-1, isotype IgG control (CTR) or BLZ945 starting 6 days after cancer cells injection. At the end point (day 20) livers were resected and single cell suspension was analysed by flow cytometry. **a)** Percentage change in PD-L1 expression levels in $F4/80^{+}$ MAMs, immune cell depleted stroma ($CD45^{neg}zsGreen^{neg}$) and tumour cells ($zsGreen^{+}$) in the different treatment cohorts and compared to CTR mice. **b)** Quantification of PD-L1 expression on metastatic cancer cells ($zsGreen^{+}$) as Mean Fluorescence Intensity (MFI) in IgG antibody (CTR) and αCSF-1 antibody treated metastasis bearing mice. N = 4 mice / group; mean ± SEM. P<0.001; **, P < 0.01; *, P < 0.05; n.s. not significant by Bonferroni multiple comparison and unpaired t-test.

The increase in PD-L1 expression upon treatment with neutralizing αCSF-1 antibody was also confirmed in total metastatic tissues by IHC analysis. Interestingly, the majority of PD-L1 positive signal was found in cells forming ductal-like structures, suggesting high expression of PD-L1 on metastatic cancer cells (Figure 5.4).

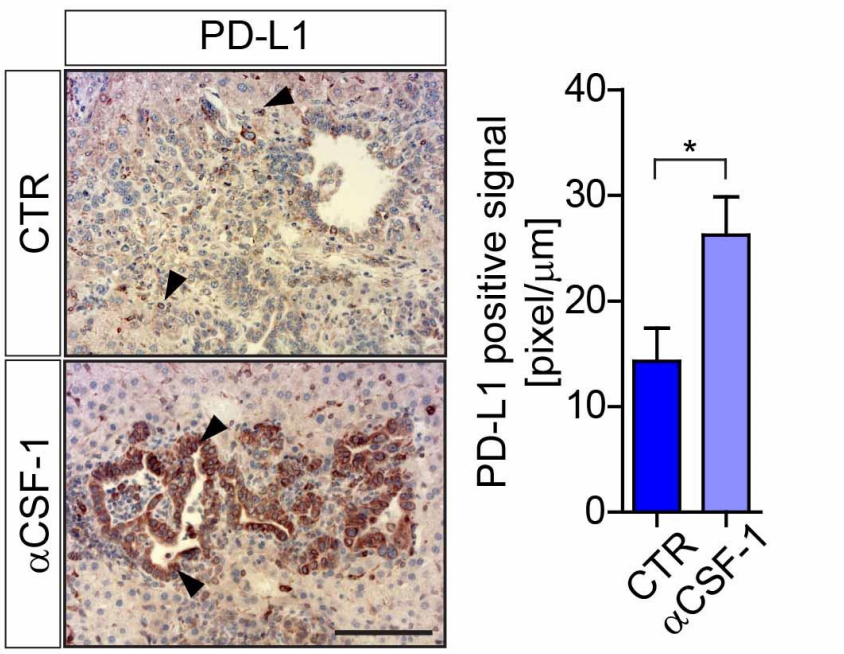

Figure 5.4 Inhibitory αCSF-1 therapy induces PD-L1 expression in metastatic livers of pancreatic cancer.

Liver metastasis was induced by intrasplenic injection of $KPC^{luc/zsGreen}$ cancer cells. Metastatic tumours were treated with αCSF-1 or isotype IgG control (CTR) starting 6 days after cancer cells injection. Immunohistochemistry (IHC) representative images and relative quantification of $PD\text{-}L1^{+}$ cells in metastatic tissues obtained from resected livers at the end point (day 20). N = 4 mice / group, n = 5 field of view / mouse; mean ± SEM. Scale bar = 100 µm; P<0.001; **, P < 0.01; *, P < 0.05; n.s. not significant by unpaired t-test. Black arrows point to $PD\text{-}L1^{+}$ cells.

It was also decided to examine whether MAM targeted therapies differently affected PD-1 expression in $CD8^+$ T cells. Flow cytometry analysis revealed that CSF-1 / CSF-1R inhibition increased PD-1 expression on cytotoxic T cells within the metastatic site, most likely as an effect of enhanced anti-tumour immune effector response induced by immunosuppressive MAMs inhibition (Figure 5.5).

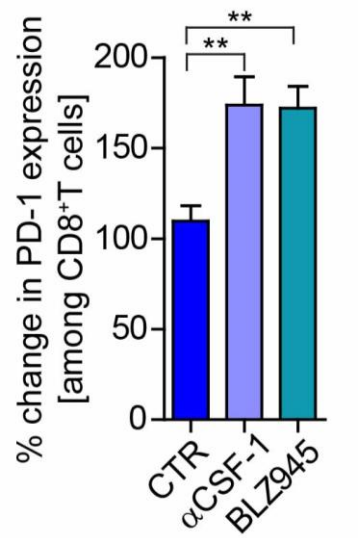

Figure 5.5 MAM targeted therapies enhance PD-1 expression in $CD8^+$ T cells.

Liver metastasis was induced by intrasplenic injection of $KPC^{luc/zsGreen}$ cancer cells. Metastatic tumours were treated with αCSF-1, isotype IgG control (CTR) or BLZ945 6 days after cancer cells injection. At the end point (day 20), livers were resected and single cell suspension was analysed by flow cytometry. Percentage change in PD-1 expression in $CD8^+$ T cells from metastatic tumours of the different mouse treatment cohorts, in comparison to CTR mice, is reported in the graph. N = 4 mice / group; mean ± SEM. P<0.001; **, P < 0.01; *, P < 0.05; n.s. not significant by Bonferroni multiple comparison.

Taken together, these results suggest that in established metastatic lesions, MAMs are the main source of PD-L1 expression, and that cancer cells respond to CSF-1 / CSF-1R blockade-mediated restoration of immune surveillance by up-regulating PD-L1.

5.2 PD-1 blockade potentiates the anti-tumoral effect of CSF-1 neutralization

It was then reasoned that the observed increase

in PD-L1 expression on metastatic pancreatic cancer cells in response to CSF-1 / CSF-1R therapy, might dampen, at least in part, the efficacy of anti-MAM therapy, and that blocking PD-1 / PD-L1 signalling could improve the anti-tumorigenic activity of CSF-1 inhibition. To address this question, liver metastasis in immunocompetent WT mice was induced by intrasplenic implantation of $KPC^{luc/zsGreen}$ cancer cells. Starting at day 7, after seeding of cancer cells to the liver, mice were treated with either αPD-1, αCSF-1 inhibitory antibodies alone or with a combination of both (Figure 5.6 a).

To assess the response of metastatic tumours to treatment, tumours volume was quantified by *in vivo* MR imaging technique, one day prior to antibody treatment (day 6) and one day before the endpoint (day 19). Strikingly, MR imaging revealed that metastatic tumour progression was significantly inhibited by both mono-therapies. However, the anti-tumorigenic effect of αCSF-1 treatment was further potentiated when administrated in combination with αPD-1 inhibitor (Figure 5.6 b and c).

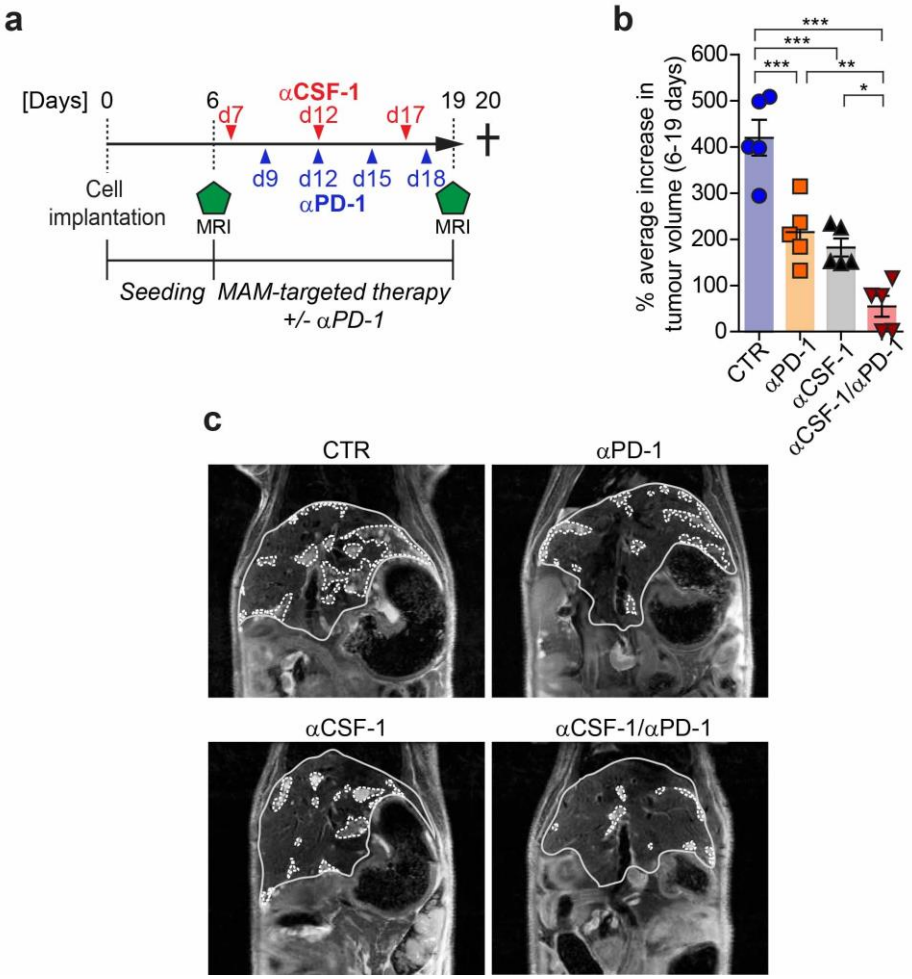

Figure 5.6 PD-1 inhibition synergises with MAM targeting to inhibit metastasis progression.

Liver metastasis was induced by intrasplenic implantation of $KPC^{luc/zsGreen}$ cancer cells. Initial tumour volume was quantified on day 6 by in vivo Magnetic Resonance (MR) imaging. Cohorts were treated with control IgG, αCSF-1, αPD-1 inhibitory antibodies alone or in combination. Treatment regimen for αCSF-1 and αPD-1 started at day 7 and day 9, respectively. At day 19 changes in tumour volume was quantified by in vivo MR imaging using T_2-weighted sequence. Mice were sacrificed on day 20. **a)** Schematic representation of the experiment. **b)** Percentage change of metastatic volume in mice before (day 6) versus after (day 19) treatment. **c)** Representative MR images of metastatic livers. N = 5 mice / group; individual data points, horizontal lines represent mean ± SEM. P<0.001; **, P < 0.01; *, P < 0.05; n.s. not significant by Bonferroni multiple comparison.

Next, the anti-tumour effects of αPD-1 and αCSF-1 blocking therapies were analysed either alone or in combination. At the endpoint, resected livers were analysed for T cell infiltration by IHC tissues staining ($CD3^+$ T cells, Figure 5.7 a) and by flow cytometry analysis ($CD8^+$ T cells, Figure 5.7 b). Very few T cells were detected in metastatic pancreatic tumours of the isotype control treated mice cohort (CTR). In contrast, mice treated with either αPD-1 or αCSF-1, single inhibitor agents, revealed a significantly higher presence of intra-metastatic T cells number, which was further potentiated in the combination treatment. It is worth mentioning that anti-CD3 antibody was used to detect T cells infiltration by IHC because a valid anti-CD8 antibody for IHC was not available at the time in which the experiment was performed. This is the reason why IHC and flow cytometry analysis were combined to investigate T cells infiltration at the metastatic site.

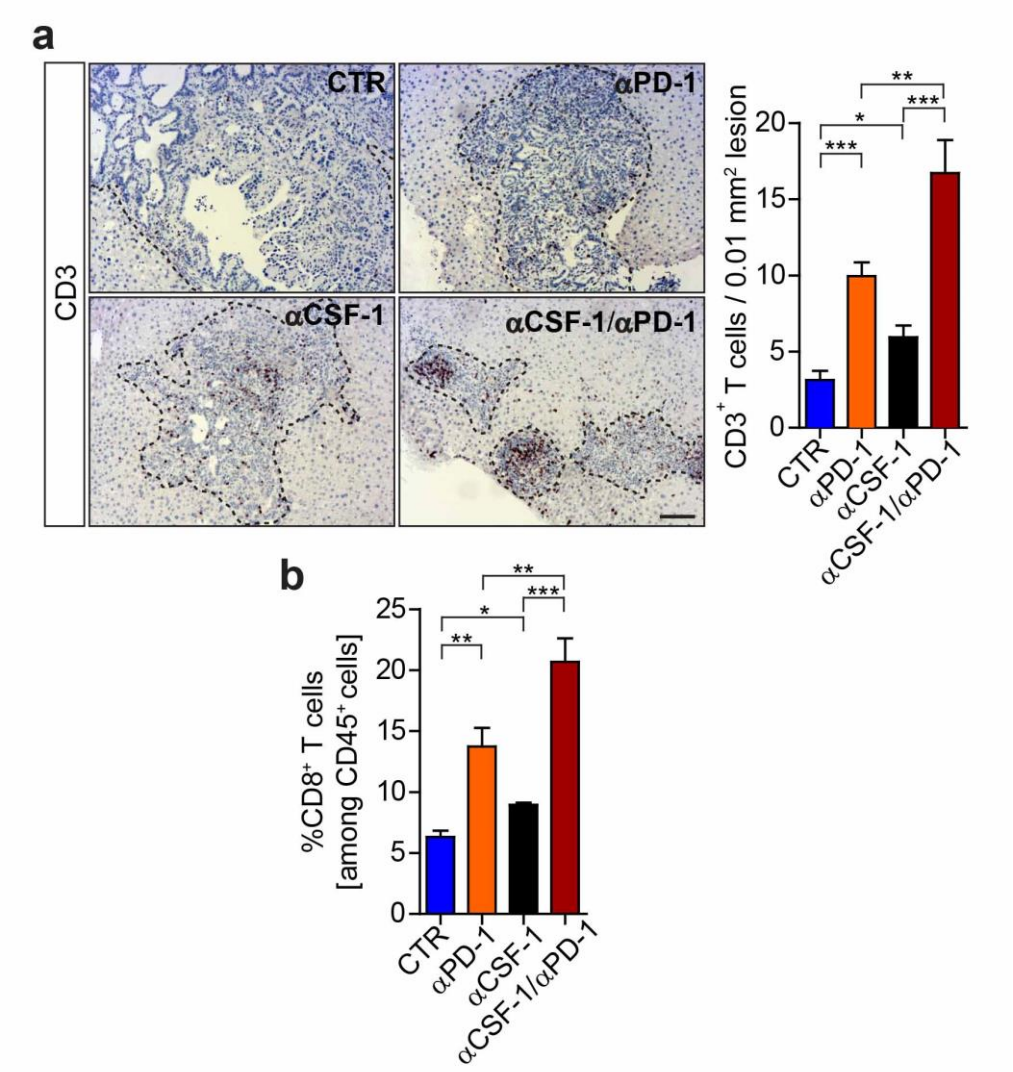

Figure 5.7 PD-1 and CSF-1 inhibition, alone or in combination, enhance T cell number in metastatic livers.

Liver metastasis was induced by intrasplenic implantation of $KPC^{luc/zsGreen}$ cancer cells. Cohorts were treated with control IgG (CTR), αCSF-1, αPD-1 antibodies alone or in combination. Mice were sacrificed on day 20 and livers harvested. **a)** Representative images and quantification of $CD3^+$ T cells in each treatment cohort by immunohistochemistry analysis. **b)** Quantification of $CD8^+$ T cells in tumour bearing livers in each treatment cohort by flow cytometry. N = 5 mice / group, n = 5 field of view / mouse; mean ± SEM. Scale bar = 100 μm; P<0.001; **, P < 0.01; *, P < 0.05; n.s. not significant by Bonferroni multiple comparison.

Quantitative gene expression analysis by PCR for T cell activation markers (*Gzmb, Tnfa, Ifng, Prf1*) on RNA extracted from $PD1^+$ $CD8^+$ T cells isolated by flow cytometry showed a reinvigoration of $CD8^+$ T cell activity in response to αCSF-1 and αPD-1 single therapies. Particularly, cytotoxicity was strongly increased in $CD8^+$ T cells when combinatorial αCSF-1/αPD-1 treatment was administered (Figure 5.8)

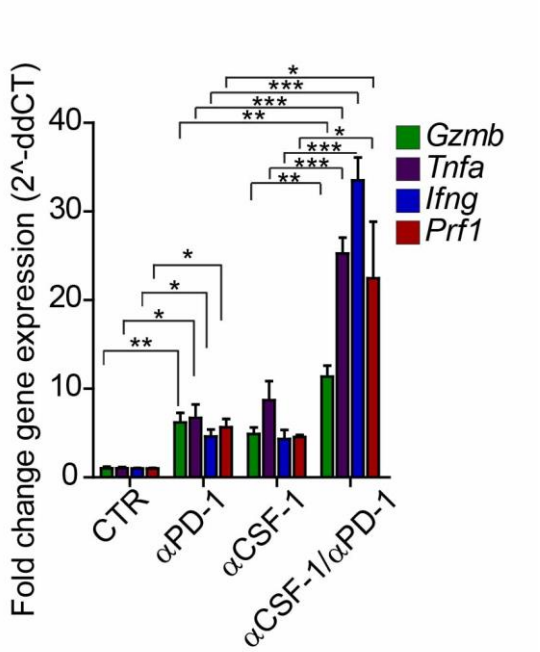

Figure 5.8 PD-1 and CSF-1 inhibition alone or in combination enhance CD8+ T cell function in metastatic livers.

Liver metastasis was induced by intrasplenic implantation of KPCluc/zsGreen cancer cells. Cohorts were treated with control IgG (CTR), αCSF-1, αPD-1 antibodies alone or in combination. Mice were sacrificed on day 20 and single cells suspension was obtained from harvested liver. CD8+ PD1+ T cells were isolated from total metastatic liver cells by flow cytometry ARIA sorter. Quantification of Granzyme B (Gzmb), Perforin (Prf1), Tnfa, Ifng expression by quantitative PCR in metastasis CD8+ PD1+ T cells from all treatment cohorts. N = 5 mice / group; mean ± SEM. P<0.001; **, P < 0.01; *, P < 0.05; n.s. not significant by Bonferroni multiple comparison.

At the end point, metastatic livers were also analysed by IF staining to determine the effects of the treatments on cancer cell death. Indeed, together with increased $CD8^+$ T cell activity, cancer cell apoptosis in mice treated with αPD-1 and αCSF-1 inhibitory antibodies alone or in combination was also higher in comparison to mice treated with control IgG antibody (CTR). Apoptotic cancer cells were quantified by percentage of $zsGreen^+$ metastatic cancer cells positive for cleaved caspase 3 (CC3) apoptotic marker (Figure 5.9).

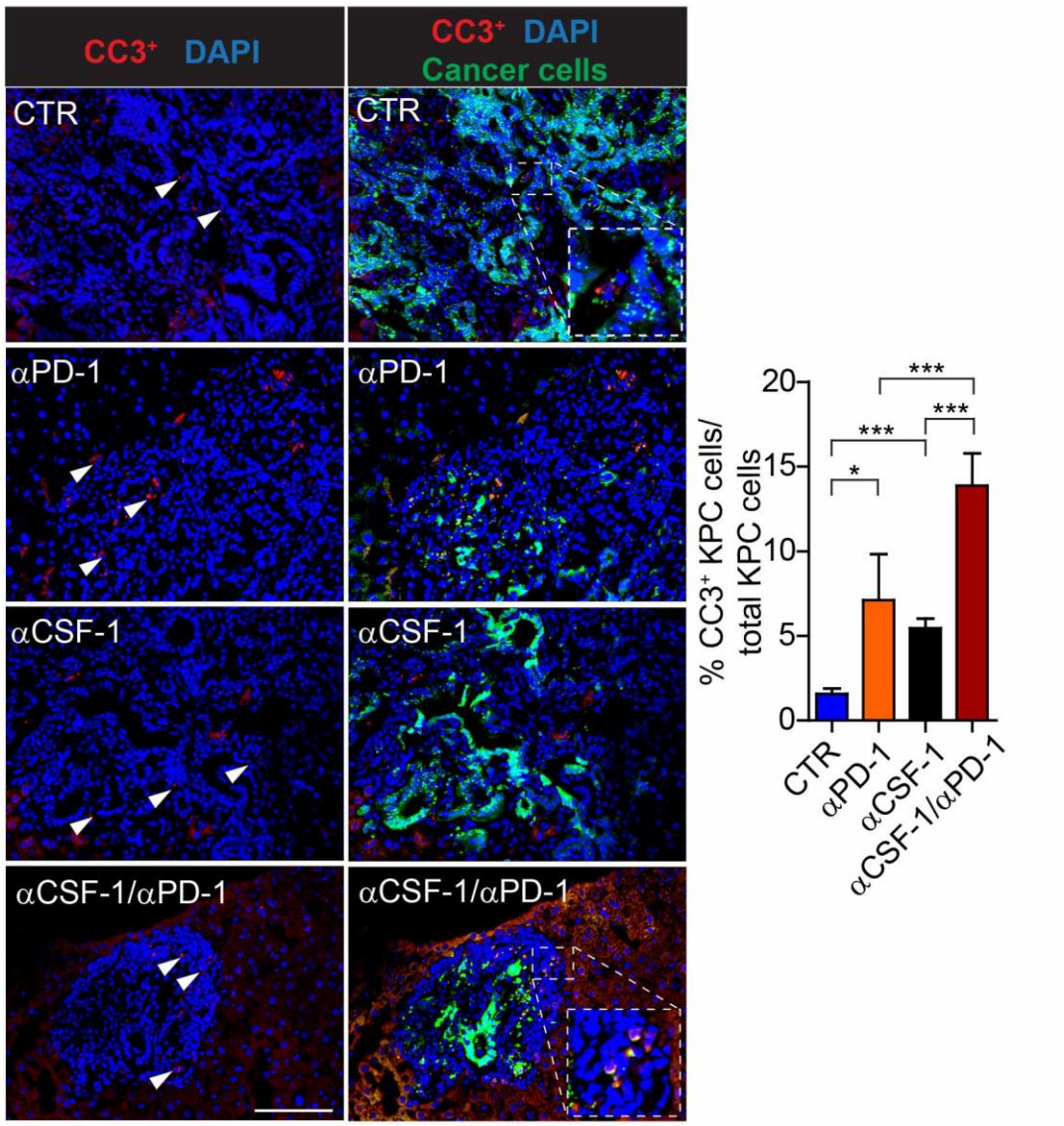

Figure 5.9 PD-1 and CSF-1 inhibition alone or in combination enhance metastatic pancreatic cells apoptosis.

Liver metastasis was induced by intrasplenic implantation of KPC$^{luc/zsGreen}$ cancer cells. Cohorts were treated with control IgG (CTR), αCSF-1, αPD-1 antibodies alone or in combination. Mice were sacrificed on day 20 and livers harvested. Representative immunofluorescence staining and quantification of cleaved caspase 3 (CC3) positive signal in metastatic cancer cells (zsGreen^{+}) in mouse livers of each treatment cohort. Nuclei were counterstained with DAPI. N = 5 mice / group; n = 5 field of view / mouse; mean ± SEM. Scale bar = 100 μm; P<0.001; **, P < 0.01; *, P < 0.05; n.s; not significant by Bonferroni multiple comparison. White arrows point to CC3^{+} cells (in red).

Taken together, these results suggest that in our experimental metastasis model single agent αPD-1 treatment improved $CD8^+$ T cell cytotoxic activity and reduced pancreatic cancer metastatic progression, if it was administrated at an early metastatic dissemination stage (day 6), when metastatic tumours are highly infiltrated by cytotoxic $CD8^+$ T cells and anti-tumorigenic M1-like macrophages (Chapter 3).

5.3 CSF-1 inhibition reduces desmoplasia and sensitizes metastatic pancreatic cancer to αPD-1 treatment.

Resistance of pancreatic cancer to PD-1 blockade as single agent therapy is well established [166], [189]. Thus, in here it was speculated that the observed positive therapeutic effect of αPD-1 blocking treatment was due to a poor establishment of immunosuppressive tumour microenvironment allowing unobstructed T cell infiltration at the time αPD-1 treatment was started (day 7). Indeed, stroma components, other than MAMs, in the tumour microenvironment can oppose T cell functions. In a previous report, our group has shown that activation of hepatic stellate cells critically promotes pancreatic cancer metastatic progression by inducing liver fibrosis [117]; other studies also suggest that myofibroblasts, as well as collagen deposition can impair T cell infiltration in the primary tumour [217], [218].

Thus, the localisation of $CD8^+$ T cells within metastatic tumours was assessed. Advanced metastatic liver tissues deriving from pancreatic cancer patients showed only few $CD8^+$ T cells within the tumour lesion, while the majority of $CD8^+$ T cells localized mainly at the periphery of metastatic lesions, where high number of αSMA^+ myofibroblasts accumulated (Figure 5.10).

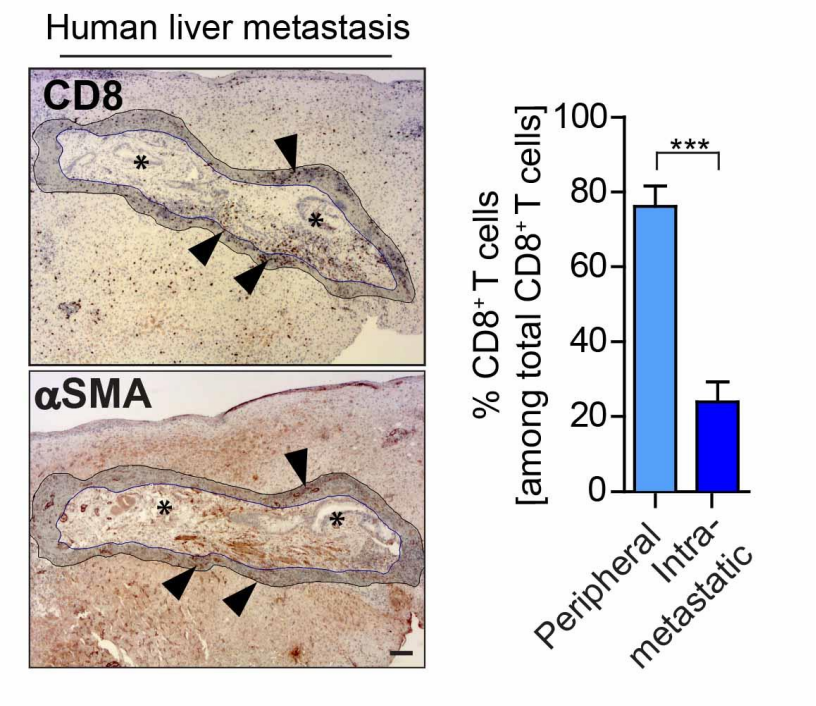

Figure 5.10 CD8$^+$ T cells localize at the periphery of metastatic lesions.

Representative immunohistochemistry (IHC) staining of CD8$^+$ T cells and myofibroblasts (αSMA$^+$) in human pancreatic cancer metastatic livers and quantification of peripheral (P) and intra-metastatic (IM) CD8$^+$ T cells. Asterisks show metastatic pancreatic ducts. N = 10 patients, n = 4 field of view / patient; mean ± SEM. Scale bar = 100 µm; P<0.001; **, P < 0.01; *, P < 0.05; n.s. not significant by unpaired t-test. Arrows point to CD8$^+$ T cells (upper panel) and to αSMA$^+$ cells (lower panel). Asterisks indicate metastatic lesions.

Analysis of murine experimental metastatic liver tissues confirmed an accumulation of fibrotic stroma in metastatic lesions after 14 days (Day 14) of intrasplenic KPC$^{luc/zsGreen}$ cancer cells injection, but not after 6 days (Day6). Strikingly, pattern of fibrotic stroma formation was completely opposite to CD8^{+} T cell accumulation, since at Day 6 metastatic livers were fully infiltrated by T cells, while in large lesions, at day 14, T cell infiltration was lost (Figure 5.11).

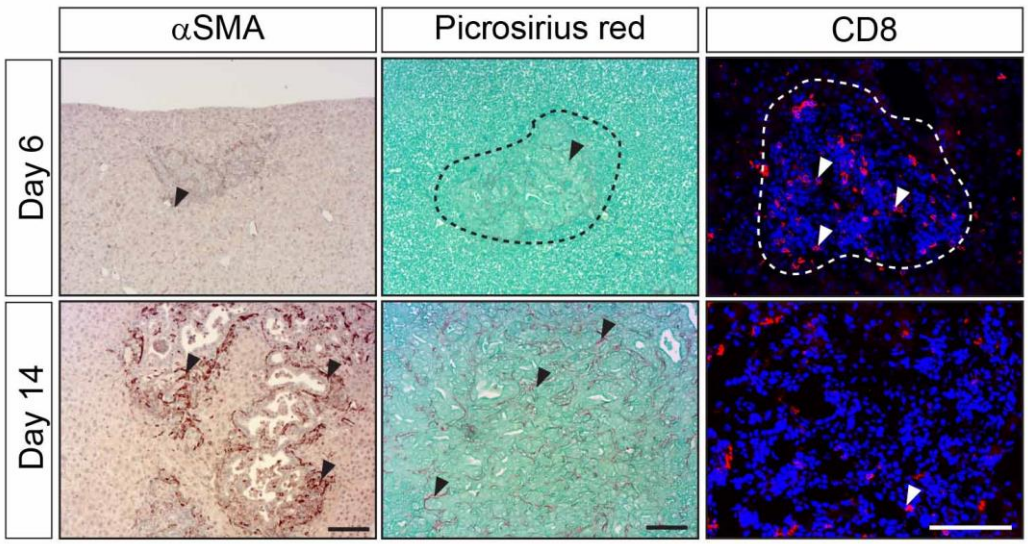

Figure 5.11 Large metastatic lesions at day 14 are highly fibrotic and poorly infiltrated by CD8^{+} T cells.

Liver metastasis was induced by intrasplenic implantation of 1x10^{6} KPC$^{luc/zsGreen}$ cancer cells. Livers were resected from sacrificed mice 6 and 14 days after tumour implantation. Tissue sections were analysed by Immunohistochemistry (IHC) and immunofluorescence (IF) staining for αSMA^{+} (myofibroblasts) and CD8^{+} T cells, respectively. Collagen deposition was assessed in metastatic tissue sections by Picrosirius red staining. N = 4 mice / group, n = 5 field of views / mouse; Scale bar = 100 μm. In each micrograph arrows point to positively stained cells. In picrosirius red stained micrographs arrows point to fibrotic area (in red).

Based on these observations, it was reasoned to repeat the treatment of metastasis bearing mice with αCSF-1 and αPD-1 inhibitory antibodies alone or in combination, this time starting the therapy at day 14, in the presence of high fibrotic stroma and poor $CD8^+$ T cell infiltration. To assure that the observed response to αPD-1 treatment was not affected by a specific cell line, the experiment was performed using two different pancreatic cancer cell lines: the $KPC^{luc/zsGreen}$ and Panc02 $^{luc/zsGreen}$ cancer cells (Figure 5.12 a). Treatments were carried out for 10 days and at the end point (day 24), livers were harvested from euthanized mice and tumour was measured by *ex-vivo* BLI (Figure 5.12 b). Reduction in tumour burden followed by use of αPD-1 inhibitor as single treatment was not observed, independently of the cell lines used to induce metastatic tumour formation. Interestingly, treatment with αCSF-1 inhibitor as mono-therapy induced only a modest reduction of tumour in comparison to CTR mice. Only combination of αPD1 and αCSF-1 neutralizing antibodies together significantly impaired metastatic progression.

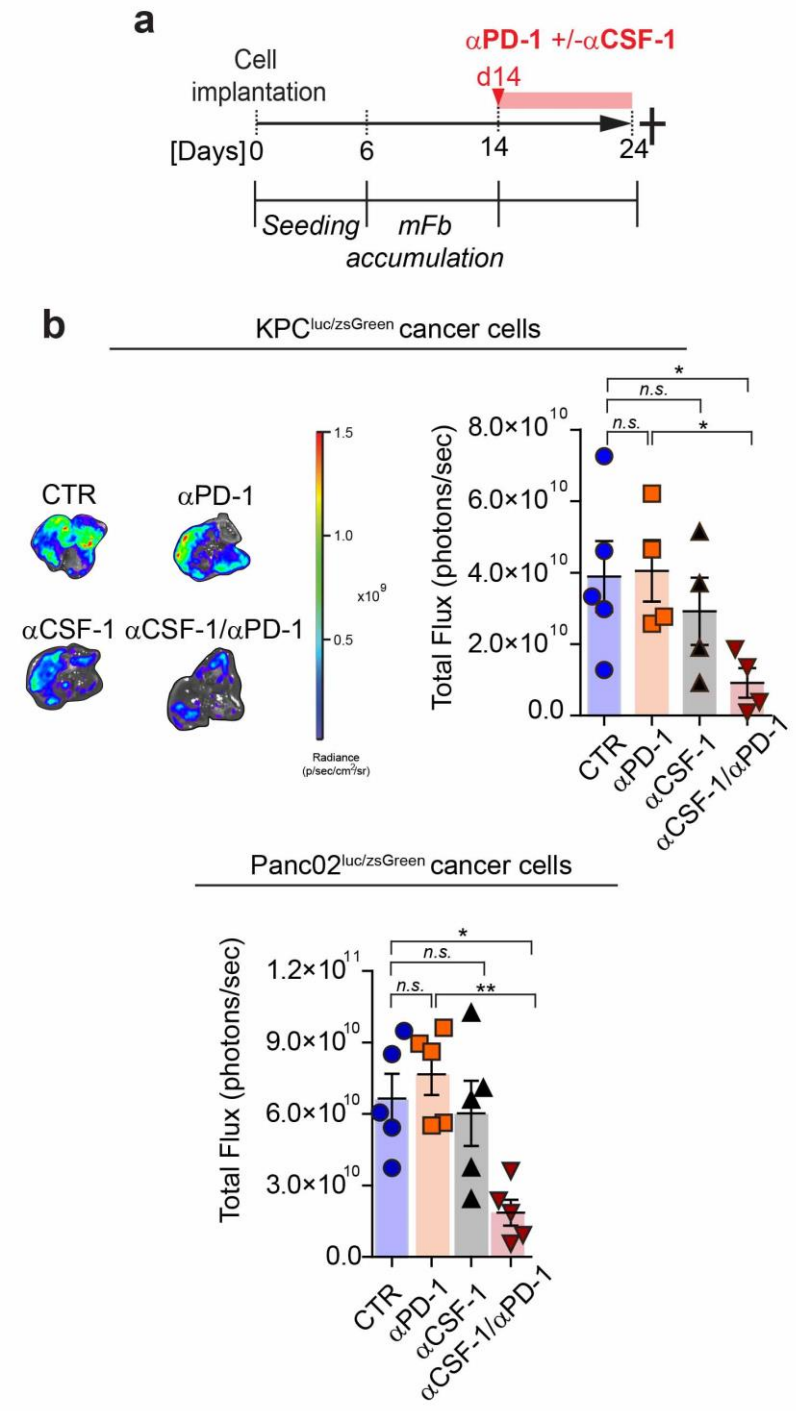
a
αPD-1 +/-αCSF-1
d14
Cell implantation
[Days] 0
6
14
24
Seeding
mFb accumulation
b
KPC luc/zsGreen cancer cells
CTR
αPD-1
αCSF-1
αCSF-1/αPD-1
1.5
1.0
0.5
x10^9
Radiance (p/sec/cm²/sr)
Total Flux (photons/sec)
8.0×10^10
6.0×10^10
4.0×10^10
2.0×10^10
0.0
n.s.
n.s.
*
*
CTR
αPD-1
αCSF-1
αCSF-1/αPD-1
Panc02 luc/zsGreen cancer cells
Total Flux (photons/sec)
1.2×10^11
9.0×10^10
6.0×10^10
3.0×10^10
0.0
n.s.
n.s.
*
**
CTR
αPD-1
αCSF-1
αCSF-1/αPD-1

Figure 5.12 PD-1 blockade impairs metastatic growth of pancreatic cancer only if administrated in combination with MAM target therapy.

Liver metastasis was induced by intrasplenic implantation of KPCluc/zsGreen or Panc02 luc/zsGreen cancer cells. Cohorts were treated with control IgG (CTR), αCSF-1, αPD-1 inhibitory antibodies alone or in combination. Treatment with αCSF-1 and αPD-1 inhibitors started at day 14 and day 17, respectively. Tumour burden was quantified and analysed at the end point (day 24) a) Schematic representation of the experiment. b) Representative ex-vivo bioluminescence images (BLI) showing metastatic tumour burden in the liver as radiance (only for KPCluc/zsGreen derived metastatic lesions). Graph: Quantification of radiance (total flux). N = 4 mice / group, n = 5 mice CTR group for KPCluc/zsGreen, n = *5 mice / group for Panc02 $^{luc/zsGreen}$ cancer cells implanted mice. Individual data points, horizontal lines represent mean ± SEM. P<0.001; **, P < 0.01; *, P < 0.05; n.s. not significant by Bonferroni multiple comparison.*

Next, KPC$^{luc/zsGreen}$ and Panc02 $^{luc/zsGreen}$ cancer cells derived metastatic lesions of the different treatment cohorts were interrogated for collagen deposition (Picrosirius red staining) (Figure 5.13 a and b) and myofibroblasts (αSMA^{+} cells) accumulation (Figure 5.14 a and b). It was observed that in IgG control (CTR) and in αPD-1 treated mice, metastatic lesions were characterized by dense fibrotic stroma, while αCSF-1 therapy either alone or in combination with αPD-1 was able to strongly reduce collagen deposition and hepatic stellate cell activation. Importantly, the observed phenotype was not cell line specific, as similar results were obtained for KPC$^{luc/zsGreen}$ and Panc02 $^{luc/zsGreen}$ induced metastasis.

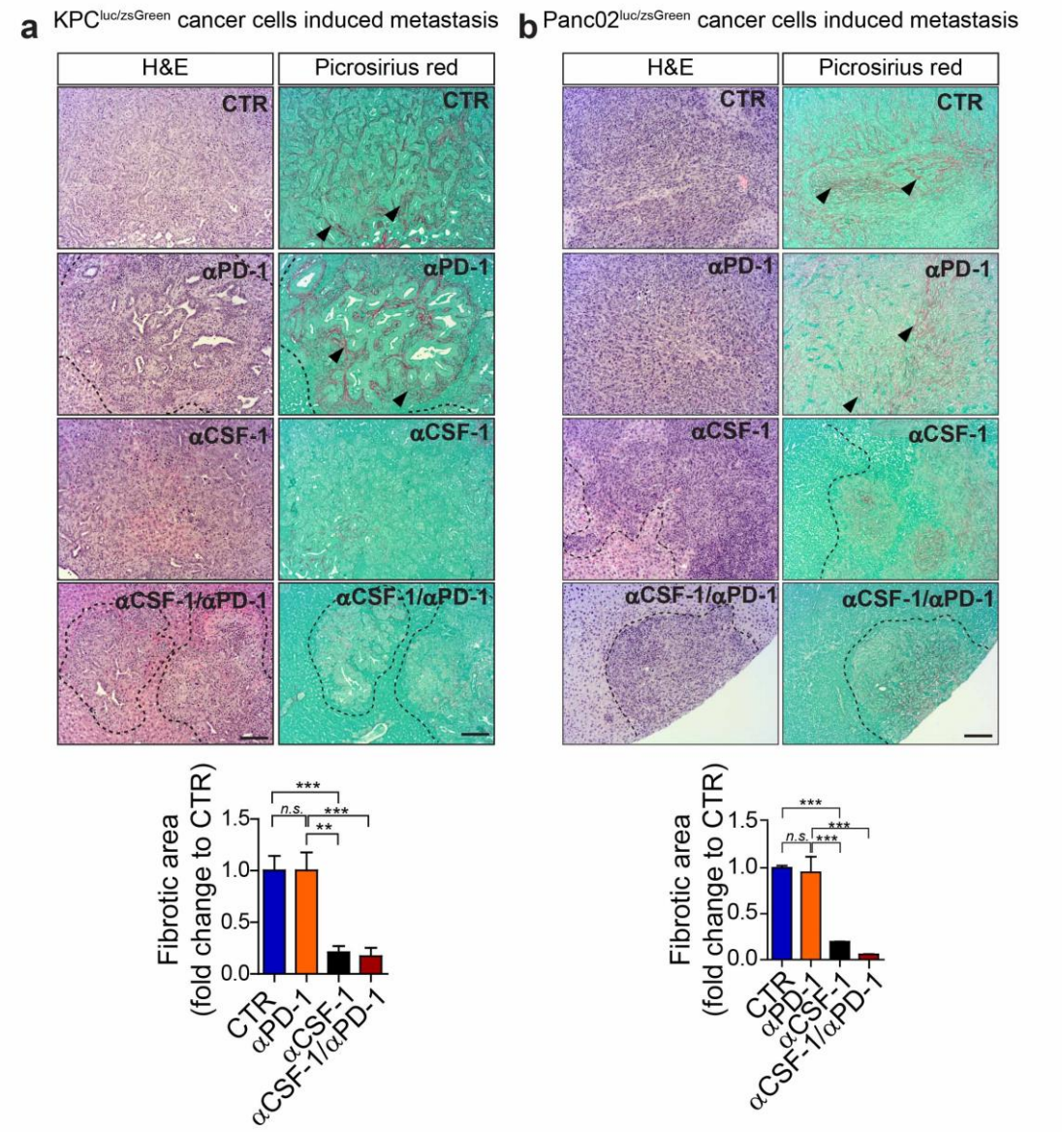

Figure 5.13 CSF-1 blockade reduces desmoplasia in pancreatic cancer metastatic lesions.

Liver metastasis was induced by intrasplenic implantation of KPC$^{luc/zsGreen}$ or Panc02 $^{luc/zsGreen}$ cancer cells. Cohorts were treated with control IgG (CTR), αCSF-1, αPD-1 antibodies alone or in combination. Livers were harvested at the end point (day 24) and analysed. Representative images and relative quantification of Hematoxylin and Eosin (H&E, left panels) and picrosirius red (right panels) staining of sequential liver sections of metastatic livers induced by **a)** KPC$^{luc/zsGreen}$ and **b)** Panc02 $^{luc/zsGreen}$ cancer cells implantation and treated with IgG control (CTR) or inhibitory antibodies. N = 4 mice / group, n = 5 mice CTR group for KPC$^{luc/zsGreen}$;. n = 5 mice / group for Panc02 $^{luc/zsGreen}$ cancer cells implanted mice. N = 5 fields of view / mouse; mean ± SEM.

Scale bar = 100 μm. P<0.001; **, P < 0.01; *, P < 0.05; n.s. not significant by Bonferroni multiple comparison. In picrosirius red staining micrographs arrows point to fibrotic area (in red).

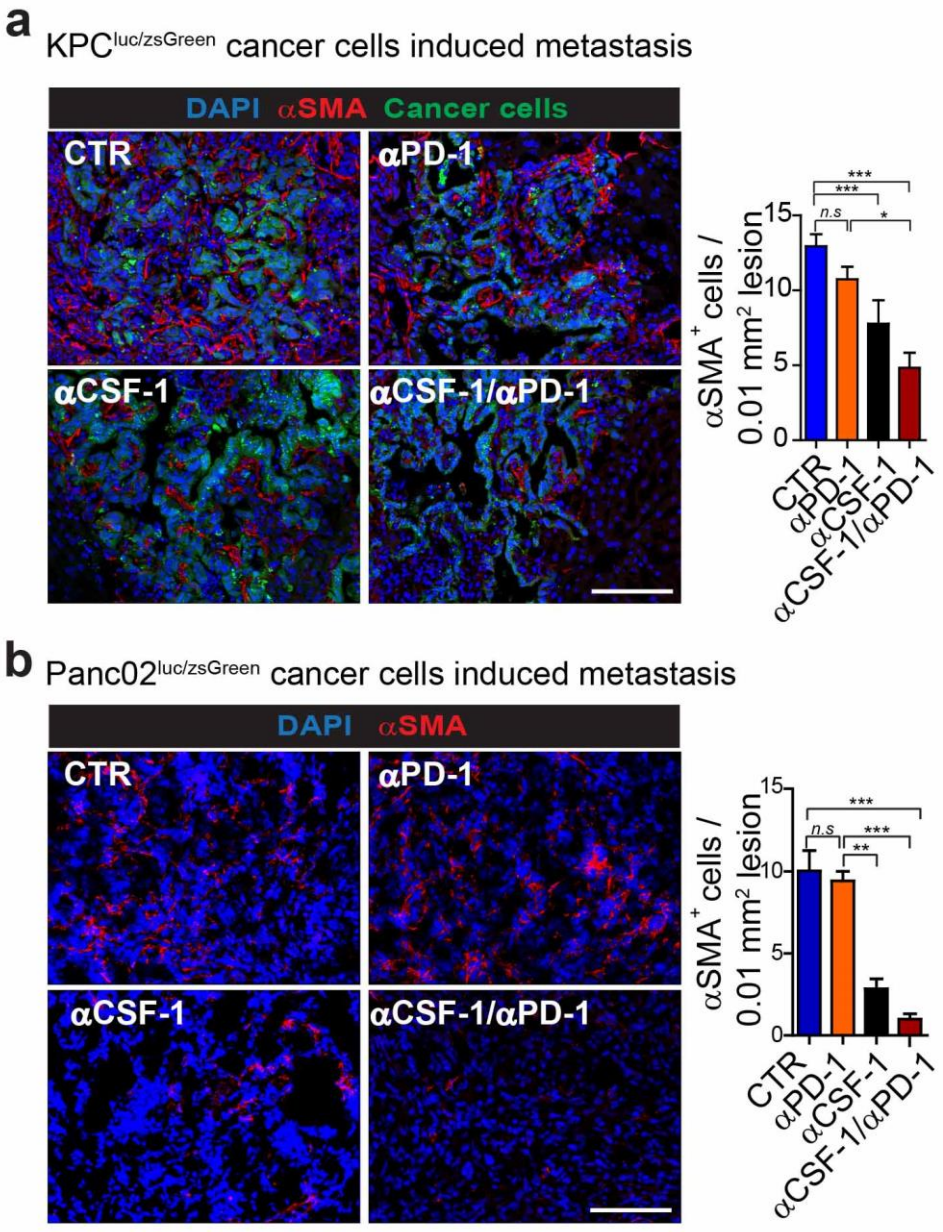

Figure 5.14 Neutralizing αCSF-1 treatment impairs hepatic stellate activation in pancreatic cancer metastatic lesions.

Liver metastasis was induced by intrasplenic implantation of KPC$^{luc/zsGreen}$ or Panc02 $^{luc/zsGreen}$ cancer cells. Cohorts were treated with control IgG, αCSF-1, αPD-1 inhibitory antibodies alone or in combination. Liver were harvested at the end point (day 24) and

analysed. Representative immunofluorescence (IF) images and relative quantification of αSMA^{+} myofibroblasts in liver sections of metastatic livers induced by **a)** KPC$^{luc/zsGreen}$ and **b)** Panc02 $^{luc/zsGreen}$ cancer cells implantation and treated with IgG control or inhibitory antibodies. Nuclei were counterstained with DAPI. In KPC $^{luc/zsGreen}$ cancer cells induced metastatic liver section, zsGreen^{+} signal from cancer cells is also detected. N = 4 mice / group, n = 5 mice CTR group for KPC$^{luc/zsGreen}$; n=5 mice / group for Panc02 $^{luc/zsGreen}$ cancer cells implanted mice. N = 5 fields of view / mouse. Mean ± SEM. Scale bar = 100 μm. P<0.001; **, P < 0.01; *, P < 0.05; n.s. not significant by Bonferroni multiple comparison.

Interestingly, analysis of fibrosis deposition (Picrosirius red staining) in mice treated at the early time point (day 7) with αPD-1 and αCSF-1 inhibitory antibodies alone or in combination (Figure 5.6), revealed that desmoplasia in metastatic lesions treated with αPD-1 was lower in comparison to control mice but also compared to late time point αPD-1 inhibitor treated metastatic lesions (Figure 5.13), thus giving a possible explanation for the inefficiency of αPD-1 therapy if administered at day 14. On contrary, αCSF-1 treatment administrated as single agent or combination with αPD-1 led to a marked fibrotic stromal reduction independent of the start of the treatment (early or late time point) (Figure 5.13 and Figure 5.15).

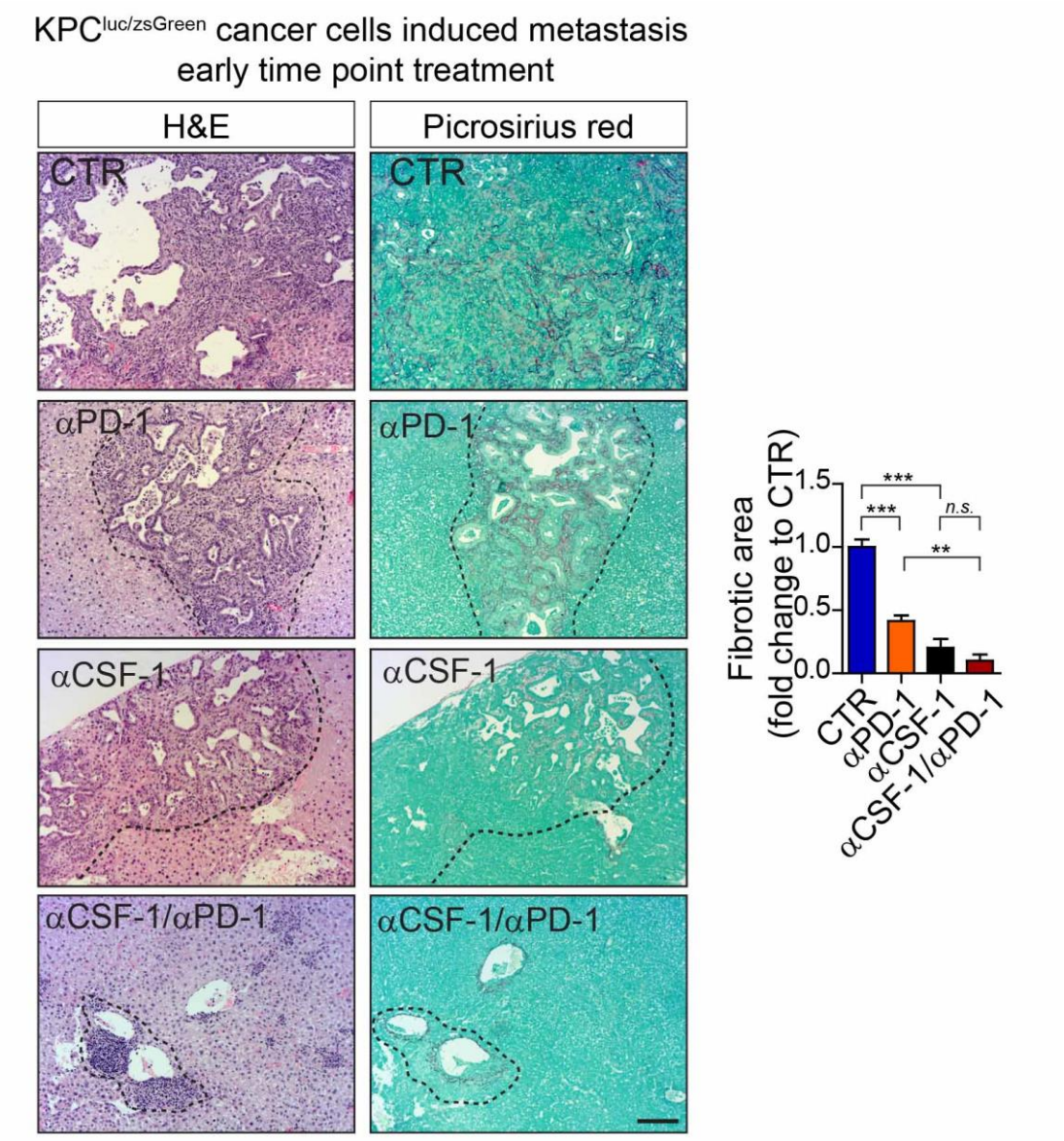

Figure 5.15 αCSF-1 inhibitor treatment reduces desmoplasia in pancreatic cancer metastatic lesions independently on treatment starting time.

Liver metastasis was induced by intrasplenic implantation of KPC$^{luc/zsGreen}$ cancer cells. Cohorts were treated with control IgG (CTR), αCSF-1, αPD-1 antibodies alone or in combination starting at day 7. Mice were sacrificed on day 20 and livers harvested. Representative images and relative quantification of Hematoxylin and Eosin (H&E) and picrosirius red stainings of sequential metastatic liver tissue sections. N = 5 mice / group, n = 5 fields of view / mouse; mean ± SEM. Scale bar = 100 μm; P<0.001; **, P < 0.01; *, P < 0.05; n.s. not significant by Bonferroni multiple comparison.

Finally, to validate whether fibrosis was affecting $CD8^+$ T cell accumulation and intra-metastatic infiltration, resected $KPC^{luc/zsGreen}$ (Figure 5.16 a) or Panc02 $^{luc/zsGreen}$ (Figure 5.16 b) cancer cell induced metastatic liver tissues were analysed by IF. Together with high fibrosis deposition, murine livers from CTR and αPD-1 inhibitors treated mice displayed few infiltrating $CD8^+$ T cells. On contrary, lesions of αCSF-1 antibody treated mice were rich in intra-metastatic $CD8^+$ T cells, a characteristic that was even more potentiated by combinatorial αPD-1 treatment.

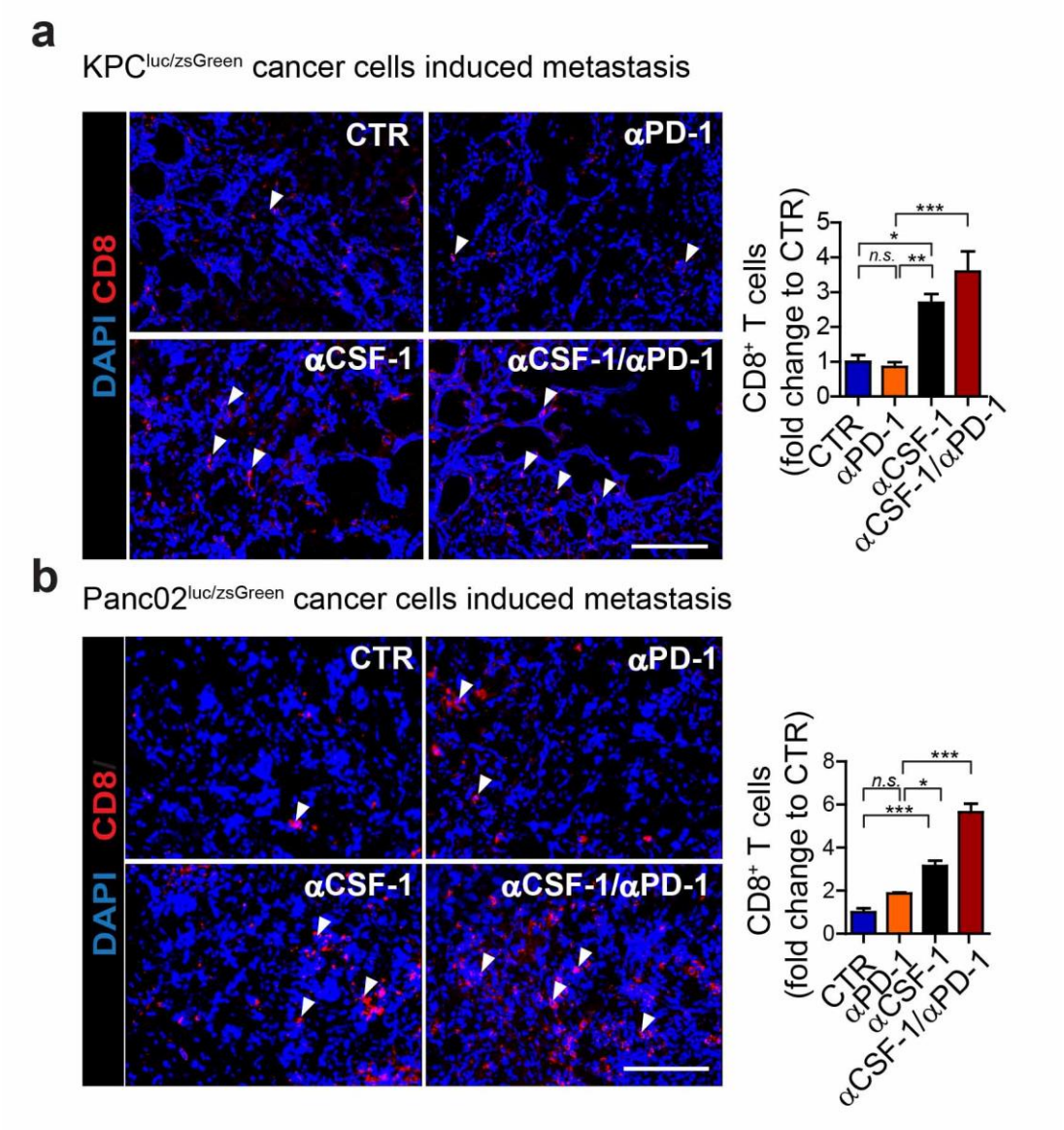

Figure 5.16 Reduction in desmoplasia induced by CSF-1 blockade is accompanied by high infiltration of CD8$^+$ T cells.

Liver metastasis was induced by intrasplenic implantation of KPC$^{luc/zsGreen}$ or Panc02 $^{luc/zsGreen}$ cancer cells. Cohorts were treated with control IgG (CTR), αCSF-1, αPD-1 antibodies alone or in combination. Livers were harvested at the end point (day 24) and analysed. Representative immunofluorescence (IF) staining images and relative quantification of CD8$^+$ T cells in liver metastatic tumours induced by **a)** KPC$^{luc/zsGreen}$ and **b)** Panc02 $^{luc/zsGreen}$ cancer cells implantation. Nuclei were counterstained with DAPI. N = 4 mice / group, n = 5 mice CTR group for KPC$^{luc/zsGreen}$; n = 5 mice / group for Panc02 $^{luc/zsGreen}$ cancer cells implanted mice. N = 5 fields of view / mouse. Mean ± SEM. Scale bar = 100 μm. P<0.001; **, P < 0.01; *, P < 0.05; n.s. not significant by Bonferroni multiple comparison. White arrows point CD8$^+$ T cells (in red).

To further confirm that the fibrosis reduction induced by αCSF-1 inhibitor treatment was improving CD8$^+$ T cell infiltration into the metastatic lesion, thereby allowing CD8$^+$ T cells to physically interact with disseminating cancer cells, the localization of CD8$^+$ T cells in metastatic was investigated in mice of the treated cohorts. Indeed, it was found that CSF-1 inhibition highly induced CD8$^+$ T cell entry into the metastatic lesion (Figure 5.17).

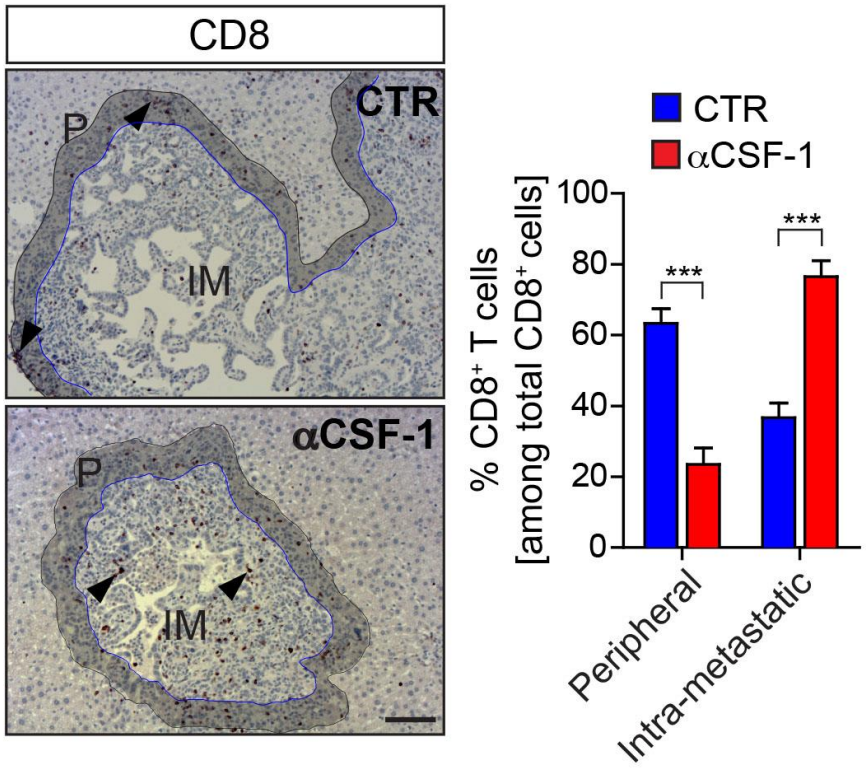

Figure 5.17 CSF-1 blockade enhances CD8$^+$ T cell entry into metastatic lesions.

Liver metastasis was induced by intrasplenic implantation of KPC$^{luc/zsGreen}$ cancer cells. Cohorts were treated with control IgG (CTR) or αCSF-1 inhibitory antibody starting 14 days after cancer cells implantation. Livers were harvested at the end point (day 24) and analysed. Representative immunohistochemistry (IHC) images and relative quantification of peripheral (P) and intra-metastatic (IM) CD8$^+$ T cells in metastatic liver tissues. N = 4 mice / group, n = 5 mice CTR group; n = 5 fields of view / mouse. Mean ± SEM. Scale bar = 100 μm. P<0.001; **, P < 0.01; *, P < 0.05; n.s. not significant by unpaired t-test. Black arrows point CD8$^+$ T cells.

To recapitulate the finding obtained so far, mice bearing KPC$^{luc/zsGreen}$ or Panc02 $^{luc/zsGreen}$ cancer cell derived metastatic lesions were treated with IgG control (CTR), αPD-1, αCSF-1 inhibitory antibodies alone or in combination starting at either early (day 7) or at later (day 14) time point, when T cell infiltration is lost and metastatic livers are highly fibrotic (Figure 5.18 a). To assess the therapeutic benefits of the different treatment regimens, the total area of metastatic lesions (identified by H&E staining) was measured in each treatment cohort, and the changes in metastatic area were compared to the control group. Similar as it was observed before, in response to early intervention (day 7) metastasis progression was inhibited by both αPD-1 and αCSF-1 delivered as mono-therapies (αPD-1 = 49 ±3 %; αCSF-1 = 50 ± 3 %), but the anti-tumorigenic effect of αCSF-1 was highly potentiated when combined with αPD-1 (αCSF-1 / αPD-1= 80 ± 3 %) (Figure 5.18 b). In contrast, in response to a later intervention on advanced metastatic lesions (day 14), neither αPD-1 nor αCSF-1 alone were able to reduce metastatic tumour burden (KPC: αPD-1 = 3 ± 3 %; αCSF-1 = 22 ± 2 %; Panc02: αPD-1 = 5 ± 3 %; αCSF-1 = 21 ± 4 %) (Figure 5.18 c). In the presence of large metastatic lesions, only combinatorial treatment of αCSF-1 / αPD-1 was able to severely decrease metastatic tumour burden by 61 ± 4 % (KPC) and 55 ± 3 % (Panc02), respectively (Figure 5.18 c). However, it is worth noting that combinatorial treatment at early intervention showed a better response (20 ± 8 % higher) in comparison with the same treatment administered at later time point (Figure 5.18 b and c).

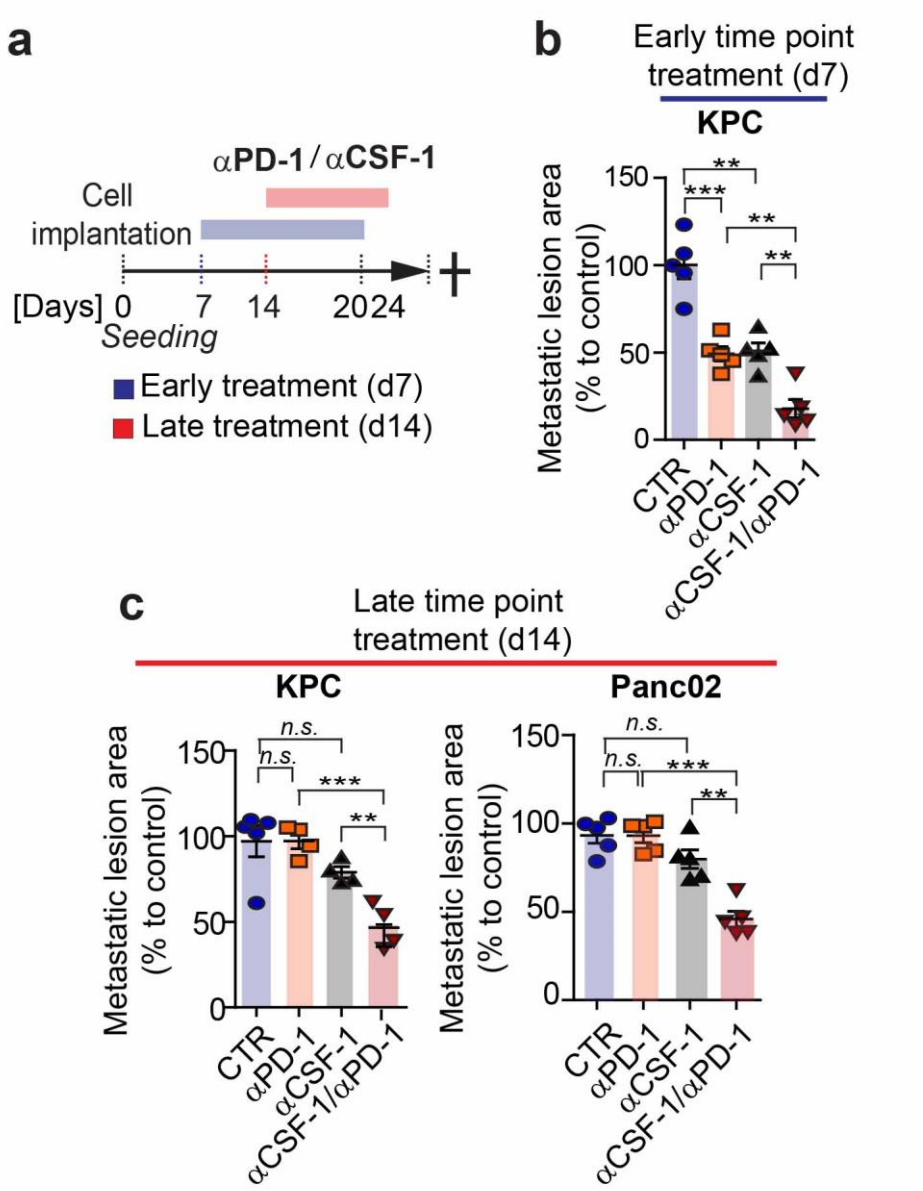

Figure 5.18 CSF-1 and PD-1 co-inhibition reduces liver metastatic progression into the liver.

Liver metastasis was induced by intrasplenic implantation of KPC$^{luc/zsGreen}$ or Panc02 $^{luc/zsGreen}$ cancer cells. Cohorts were treated with control IgG (CTR), αCSF-1, αPD-1 antibodies alone or in combination. Early time point treatment started at day 7, prior to T cell exclusion, while late time point treatment started at day 14. Metastatic lesions were quantified at the end point. **a)** Schematic representations of the experiment. Percentage average change in metastatic lesion area compared to control in response to treatment started at **b)** early and **c)** late time points and quantified by haematoxylin and eosin (H&E)

staining. N = 4-5 mice / group; individual data points, horizontal lines represent mean ± SEM . P<0.001; **, P < 0.01; *, P < 0.05; n.s. not significant by Bonferroni multiple comparison.

To address whether a difference in the treatment regimen or impaired drug delivery might have caused the inferior response of αCSF-1 / αPD-1 inhibitor therapy at late intervention in comparison to early intervention, the anti-tumoral activity of MAMs isolated from tumours exposed to combinatorial αCSF-1 and αPD-1 treatments started at early (day 7) versus late (day 14) intervention (Figure 5.19 a) was compared. $KPC^{luc/zsGreen}$ cancer cells were implanted into mice to generate liver metastasis and mice were simultaneously treated with αCSF-1 and αPD-1 inhibitors starting at early time point (day 7) or a late time point (day 14). αCSF1 / αPD-1 treatment was carried out for 10 days and at the end point (day 16 for early treatment and day 24 for late treatment), MAMs were isolated from treated metastatic livers and adoptively transferred (AT) into experimental metastasis bearing mice (Figure 5.19 b). Metastatic burden in mice receiving AT of MAMs was quantified by BLI after 5 days. In comparison to CTR mice, which were intravenously injected with PBS, mice receiving AT of MAMs from early or late αCSF-1 / αPD-1 treated tumours had reduced metastasis. However no difference in tumour size was found between mice receiving AT from day 7 (d7) or day 14 (d14) treated animals (Figure 5.19 c).

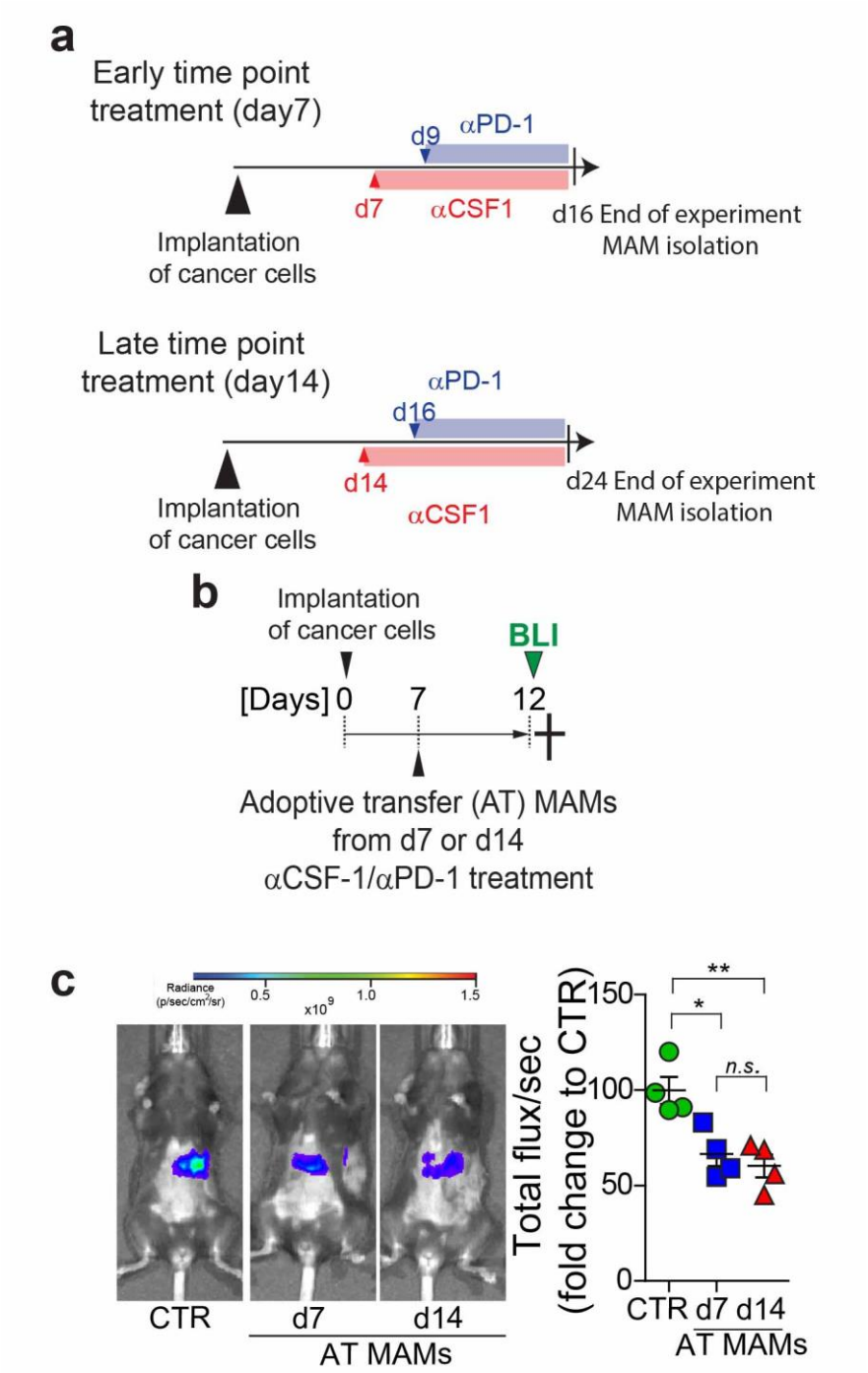

Figure 5.19 MAMs isolated from tumours exposed to αCSF-1/αPD-1 inhibitors co-treatment have anti-metastatic activity.

a) Liver metastasis was induced by intrasplenic implantation of KPC$^{zsGreen/luc}$ cancer cells and αCSF-1 and αPD-1 combination treatment was started after 7 or 14 days. F4/80^{+} MAMs were isolated at day 16 or day 24 from resected metastatic livers from each of the two treated cohorts (d7 and d14 αCSF-1 / αPD-1 treated mice) and adoptively transferred (AT) into experimental metastasis bearing mice at day 7. The

experiment was terminated after 5 days, at day 12. **a and b)** Schematic representation of the experiments. **c)** Representative in vivo bioluminescence (BLI) images of tumour burden as radiance in hepatic metastasis bearing mice, which received AT of MAMs or not (CTR mice). Quantification of the metastatic burden is expressed as fold change of total flux/sec, relative to CTR mice. N = 4 mice / group; individual data points, horizontal lines represent mean ± SEM . P<0.001; **, P < 0.01; *, P < 0.05; n.s. not significant by Bonferroni multiple comparison.

Taken together these results show that $CD8^+$ T cell entry into metastatic pancreatic cancer lesions is crucial for efficacy of αPD-1 therapy. At the metastatic site, together with immunosuppressive MAMs, fibrotic stroma represents an additional barrier that T cells need to overcome to penetrate into the tumour and exert their cytotoxic activity. Immune checkpoint blockade can only be beneficial if combined with therapeutic strategies that target the immunosuppressive barrier of TME.

5.4 Discussion

Immune checkpoint blockade has become an attractive therapeutic strategy to treat multiple cancers, but resistance is common [301]. Binding of PD-L1 to its receptor, PD-1, suppresses T cell migration, proliferation, secretion of cytotoxic mediators, and restricts tumour cell killing [146]. Increasing evidence suggest that PD-L1 expression on cancer cells, which is induced by pro-inflammatory cytokines (i.e. IFNγ), is a mechanism of adapted immune resistance in response to an active immune surveillance [121].

Beside its expression on tumour cells, PD-L1 is also expressed on tumour infiltrating immune cells, especially cells from the myeloid/macrophage lineage [302]. In agreement with a recent report on primary pancreatic tumour [167], this study also identify MAMs as the main source of PD-L1 expression in advanced metastatic lesions, while disseminated tumour cells surprisingly express only low levels of PD-L1. The relative roles and functions of PD-L1 expression on tumour and stroma cells in limiting anti-tumour immunity is not yet fully understood, however this study provides a further characterization of PD-L1 expression within the pancreatic cancer metastatic niche. Here it has been shown that reprogramming of MAMs towards an immune-stimulatory phenotype did not alter their PD-L1 expression, but instead led to up-regulation of PD-L1 expression on tumour cells and to enhanced expression of PD-1 on $CD8^+$ T cells. Recombinant IFNγ strongly induced *in vitro* expression of PD-L1 on KPC-derived pancreatic cancer cells, thereby suggesting that in response to a reduced immunosuppressive TME generated by CSF-1 / CSF-1R inhibition and associated increase of IFNγ levels (expressed by $CD8^+$ T cells and inflammatory MAMs), disseminated

pancreatic cancer cells shield themselves from activated cytotoxic T cells by up-regulating PD-L1.

Anti-tumour activity of PD-1 / PD-L1 pathway blockade has been observed in a variety of cancers such as Hodgkin's lymphoma [303], desmoplastic melanoma [304], head and neck [305], non-small lung [306] and urothelial cancers [21],[22]. In pancreatic cancer, PD-1 blockade (as well as CTLA-4 blockade) has been shown to be inefficient to reduce tumour burden both in murine models and patients [189], [280], [309]. The importance of targeting the immunosuppressive TME in pancreatic cancer to obtain clinical benefit from immunotherapy is becoming increasingly more evident [150]. Indeed, we (Chapter 3 and 4) and others [256] have demonstrated the crucial role of macrophages in dominating the immunosuppressive TME both at the primary and secondary metastatic site of pancreatic cancer. This immunosuppressive microenvironment is responsible for impairment of cytotoxic T cell function; thereby its targeting represents a powerful strategy to reinvigorate the effector immune response. PD-1 / PD-L1 blockade can offer therapeutic benefits only if both PD-1 and PD-L1 are expressed within the TME, and this is a consequence of both $CD8^+$ T cells tumour infiltration and activation of the cytotoxic phase of T cell response [310]. Thus, a combination of stroma targeting agents that allow first a boost of anti-tumour immunity may be necessary for checkpoint-blockade therapy to work. In accordance with this, here it was found that αPD-1 inhibitor treatment was beneficial in enhancing $CD8^+$ T cell response and in consequence, in reducing metastatic burden only if the treatment was started at day 6, when high numbers of $CD8^+$ T cells and M1-like inflammatory macrophages were present in the metastatic

tumour. Moreover, the immunosuppressive TME also altered trafficking of T cells within metastatic tumours causing T cell dysfunction and dampening the efficacy of PD-1 immune checkpoint blockade.

Fibrotic stroma is an hallmark of pancreatic cancer and T cell infiltration can be profoundly affected by this [218]. Interestingly, here it was observed that in large metastatic human pancreatic cancers, $CD8^+$ T cells were located in proximity of αSMA^+ myofibroblasts rich regions, mainly found at the periphery of tumour lesions.

Inhibitory αPD-1 treatment was found to be inefficient in suppressing metastatic cancer if it was administered at later stage of metastatic development, at the point in which immunosuppressive microenvironment and extensive fibrotic deposit were already formed at the metastatic site (day 14). αPD-1 neutralizing treatment was able to induce a therapeutic benefit, independently on the time of treatment administration if it was combined with immunosuppressive MAM-targeted therapy. Interestingly, MAM-targeting strategies not only reprogrammed the TME towards an immune-stimulatory phenotype, but also strongly enhanced T cell intra-metastatic infiltration by reducing the dense fibrotic structure that surrounds and protects metastatic tumour lesions. The molecular mechanism by which T cells are excluded remains elusive and needs further investigation. However, in pancreatic cancer, fibrosis components, including CAFs, collagen deposition and ECM are now recognized as regulators of immune surveillance and immunotherapy efficacy for primary pancreatic tumours [215], [218]. In this regards, the secretion of CXCL12 by CAFs has been proposed as mechanism by which pancreatic tumour evade $CD8^+$ T cell killing [201], [311].

A similar mechanism has been also observed in breast cancer; CXCL12 secreted by a subset of immunosuppressive CAFs has been shown to play an immunosuppressive function by recruitment of T_{reg} cells, which survival and proliferation was further sustained by CAF expression of several receptors, including PD-L2 [210]. CAF-associated PD-L2 and Fas ligand have been shown to drive T cells dysfunction and death of tumour infiltrating T cells [312].

Taken together, these findings suggest that PD-1 blockade as anti-cancer therapy is limited by the presence of an immunosuppressive microenvironment and dense fibrotic stroma, which provides a barrier for intra-metastatic T cells infiltration and cytotoxic functions. This barrier can be overcome by using MAM-targeted therapy, thereby rendering fibrotic metastatic pancreatic cancer tumours responsive to immune checkpoint blockade therapy.

Chapter 6:

Results

6 Chapter 6: Granulin drives resistance to PD-1 blockade in metastatic pancreatic cancer

Granulin is a secreted glycoprotein that has been associated with fibrosis formation in diverse pathological conditions and cancer [95], [117]. Our lab previously identified macrophage-derived granulin as a pro-metastatic key effector protein responsible for HSCs activation and fibrosis during pancreatic cancer metastatic outgrowth into the liver [117]. Here, it was validated whether the observed reduction of HSCs activation and fibrosis in response to CSF-1 inhibition (Chapter 5) was due to reduced granulin expression. Therefore the impact of CSF-1 on granulin expression in macrophages was assessed.

6.1 CSF-1 inhibition reduces granulin expression in macrophages, both *in vitro* and *in vivo*.

To test whether granulin expression in macrophages was dependent on CSF-1, bone marrow from naïve mice was isolated and monocytes were *in vitro* differentiated into macrophages. Primary BMMs were then exposed to recombinant CSF-1 (Rec. CSF-1) for 24 hours. RNA was extracted from the BMMs and subsequent quantitative PCR revealed that *granulin* expression in BMMs was strongly induced by CSF-1 (Figure 6.1).

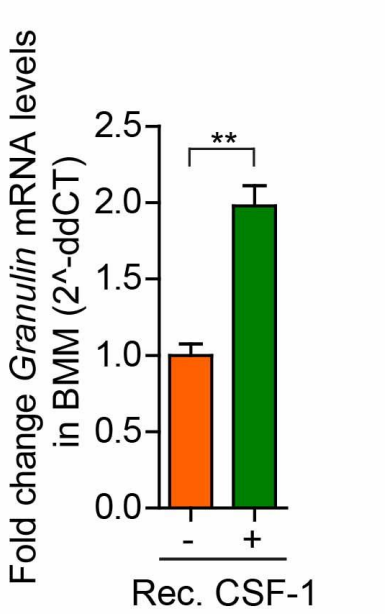

Figure 6.1 CSF-1 stimulates granulin expression in BMMs.

Quantification of granulin mRNA by quantitative PCR (qPCR) in primary unstimulated macrophages and macrophages exposed to 10 ng / ml recombinant CSF-1 (Rec. CSF-1) for 24 hours. Data are mean ± SD of 3 independent experiments. P<0.001; **, P < 0.01; *, P < 0.05; n.s. not significant, by unpaired t-test.

Previously in this thesis it has been reported that cancer cells express high levels of CSF-1 (Chapter 4). Here it was validated whether pancreatic cancer cell derived CSF-1 induced expression of granulin in macrophages. It was found that *in vitro* cultured primary BMMs exposed to KPC or Panc02 cancer cells conditioned media (CM) significantly down-regulated *granulin* expression in the presence of αCSF-1 neutralizing antibody (Figure 6.2).

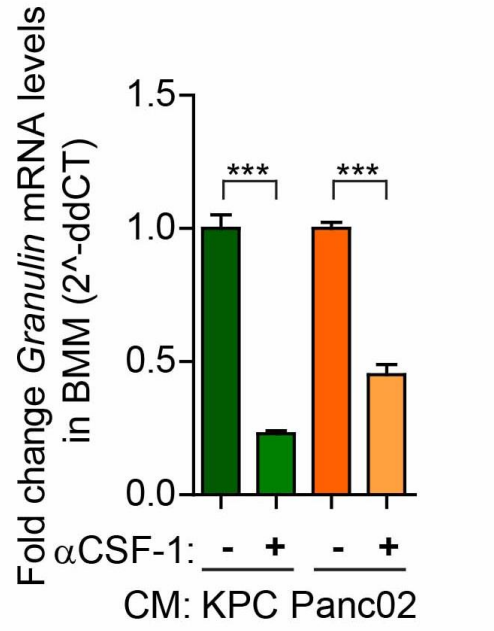

Figure 6.2 ***Pancreatic cancer cells induce granulin expression in a CSF-1 dependent manner.***

Quantification of granulin mRNA levels by quantitative PCR (qPCR) in primary macrophages exposed to KPC and Panc02 conditioned media (CM) in the presence of 2.5 µg / ml IgG control or αCSF-1 neutralizing antibodies for 24 hours. Data are mean ± SD of 3 independent experiments. P<0.001; **, P < 0.01; *, P < 0.05; n.s. not significant, by unpaired t-test.

.

To further elucidate whether a specific subtype of macrophages contributed to granulin expression, granulin production was quantified by ELISA in *in vitro* derived BMMs stimulated with different cytokines generally recognized as M1-like (IFNγ and LPS) or M2-like (CSF-1, IL-4, IL-10 and IL-13) macrophage polarizing agents. Alternatively (M2-like) activated macrophages, especially those exposed to CSF-1 (or M-CSF-1) and IL-4 correlated with higher granulin expression levels (Figure 6.3).

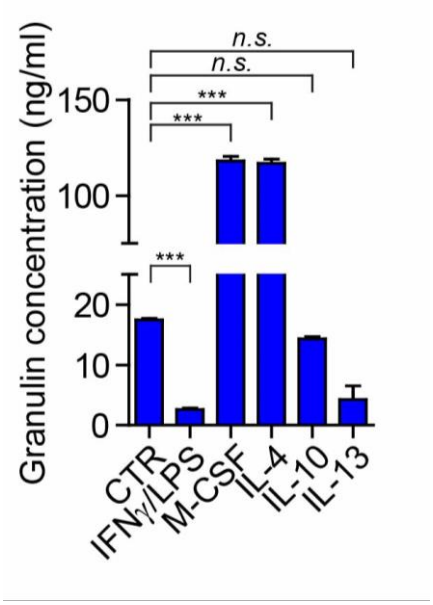

Figure 6.3 M2-like macrophages express high level of granulin.

ELISA quantification of granulin protein level in bone marrow macrophages (BMMs) stimulated with IFNγ/LPS (M1-like) or CSF-1, IL-4, IL10, IL-13 (M2-like) macrophage polarizing agents for 24 hours. Data are mean ± SD of 3 independent experiments. P<0.001; **, P < 0.01; *, P < 0.05; n.s. not significant, by unpaired t-test

Next, experimental metastasis bearing mice were treated with αCSF-1 inhibitor or IgG control (CTR) antibodies to validate granulin expression *in vivo*. Quantitative PCR on MAMs isolated from metastatic livers of mice treated cohorts revealed a decrease in *granulin* expression in MAMs derived from αCSF-1 treated mice (Figure 6.4 a). Similarly, IHC staining on tissues derived from KPC$^{luc/zsGreen}$ or Panc02$^{luc/zsGreen}$ cancer cells induced metastatic livers treated with αCSF-1 inhibitor or IgG control (CTR) antibodies, confirmed reduced granulin expression at protein level in αCSF-1 treated mice cohort (Figure 6.4 b).

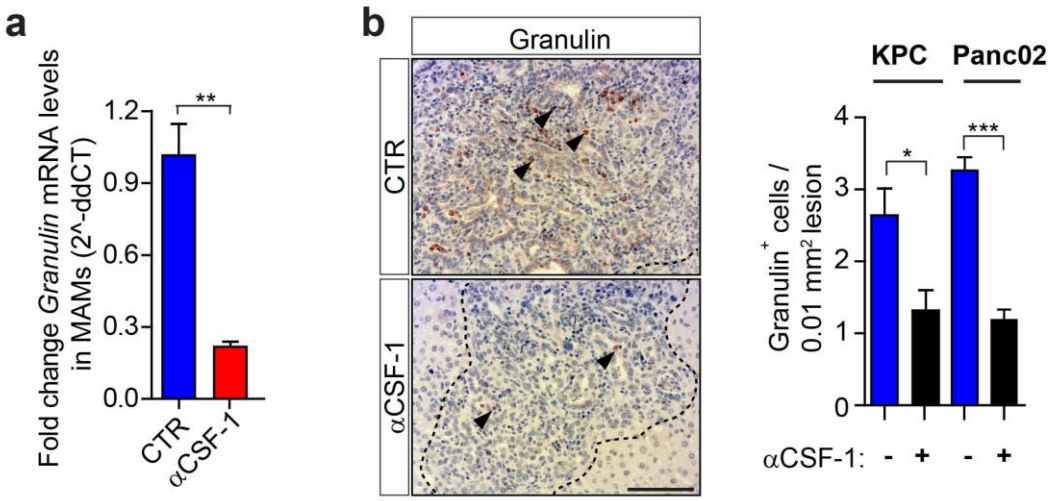

Figure 6.4 CSF-1 induces granulin expression in liver metastasis.

Mice were implanted with KPC$^{luc/zsGreen}$ or Panc02$^{luc/zsGreen}$ cancer cells and treated with IgG control (CTR) or neutralizing αCSF-1 antibodies after 14 days. Livers were harvested from euthanized mice at the end point (day 24). **a)** Quantitative PCR analysis of granulin expression in MAMs isolated by flow cytometer ARIA sorter from metastatic lesions induced by KPC$^{luc/zsGreen}$ cancer cells (n = 4 mice / group; mean ± SEM). **b)** Representative immunohistochemistry images and quantification of Granulin in metastatic livers induced by KPC$^{luc/zsGreen}$ or Panc02$^{luc/zsGreen}$ cancer cells (n = 6 mice / group; mean ± SEM). P<0.001; **, P < 0.01; *, P < 0.05; n.s. not significant, by unpaired t-test. Black arrows point to cells positive for Granulin expression.

Taken together, these results demonstrate that CSF-1, abundantly expressed by pancreatic cancer cells, induces granulin expression in macrophages both *in vitro* and *in vivo*.

6.2 Genetic depletion of granulin restores $CD8^+$ T cell infiltration in metastatic tumours, but T cell dysfunction remains.

Since granulin expression is triggered by CSF-1 and CSF-1 inhibition decreases fibrosis and increases $CD8^+$ T cell infiltration in metastatic lesions of pancreatic cancer (Chapter 5), the effect of granulin depletion on effector T cell infiltration was interrogated. To address this question, a bone marrow transplantation experiment was first performed. Bone marrow (BM) derived from WT and $Grn^{-/-}$ mice was transplanted into WT naïve mice. In this way, granulin was depleted exclusively in bone marrow cells, including macrophages. Afterwards, intrasplenic injection of KPC-derived cells into chimeric mice WT or deficient for granulin ($Grn^{-/-}$) in the BM compartment (WT + WT BM and WT + $Grn^{-/-}$ BM mice) was performed (Figure 6.5 a). First, the reduced activation of HSCs in WT + $Grn^{-/-}$ BM mice in comparison to control WT + WT BM mice was confirmed by quantifying IF staining of αSMA^+ cells (Figure 6.5 b and d) [117]. Together with a reduction of αSMA^+ myofibroblasts, intra-metastatic (IM) $CD8^+$ T cell accumulation was markedly improved in mice with granulin deficient bone marrow. On contrary, $CD8^+$ T cells appeared to confined at the periphery (P) of metastatic lesions rich in αSMA^+ fibroblasts in WT + WT BM mice (Figure 6.5 b and c).

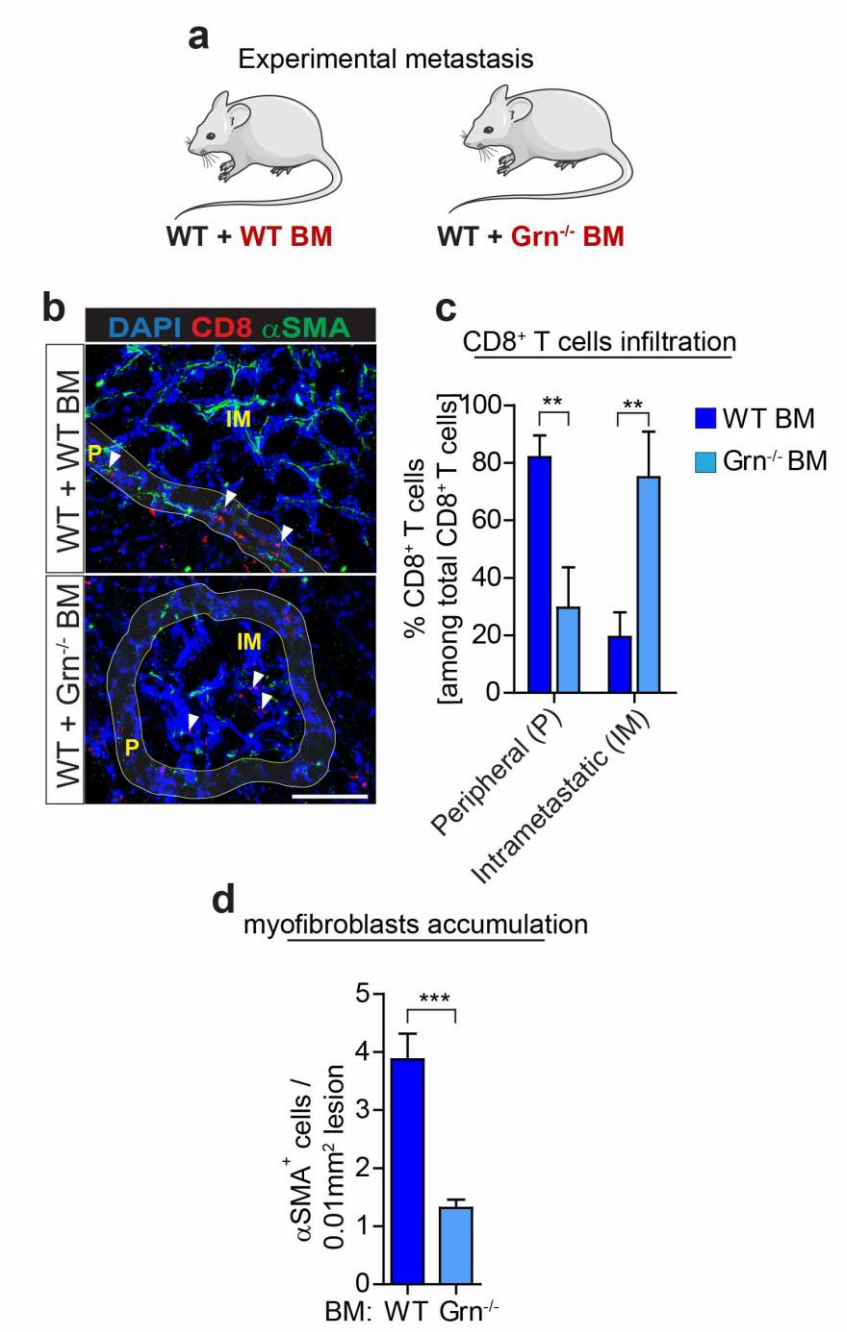

Figure 6.5 Genetic depletion of granulin increases CD8+ T cell entry at the metastatic site.

Bone marrow (BM) from WT or granulin deficient mice ($Grn^{-/-}$) was transplanted into WT mice to generate chimeric WT mice with WT BM or WT mice with $Grn^{-/-}$ BM. Transplantation of bone marrow allowed to have selective depletion of granulin in bone marrow derived cells. Liver metastasis was induced by intrasplenic implantation of $5x10^5$ KPC cells into chimeric WT + WT BM and WT + $Grn^{-/-}$ BM mice. Entire livers were resected 14 days later and analysed. **a)** Schematic representing the WT

+ WT BM and WT + $Grn^{-/-}$ BM chimeric mice. **b)** Representative immunofluorescence staining of $CD8^+$ T cells and αSMA^+ myofibroblasts in metastatic livers. Intra-metastatic (IM) and peripheral areas (P) are indicated. **c)** Quantification of peripheral (P) and intra-metastatic (IM) $CD8^+$ T cells in metastatic livers. **d)** Quantification of αSMA^+ cells in metastatic livers. αSMA^+ cells are in green, $CD8^+$ T cells are in red and nuclei were counter stained with DAPI. WT BM n = 5; $Grn^{-/-}$ BM n = 6, n= 5 fields of view / mouse; mean ± SEM. Scale bar = 100 μm; P<0.001; **, P < 0.01; *, P < 0.05; n.s. not significant by unpaired t-test. White arrows point to P (upper panel) and IM (lower panel) $CD8^+$ T cells.

So far, reduction in $CD8^+$ T cells infiltration within the metastatic site in response to the formation of a dense fibrotic stroma was observed. It was also found that granulin depletion could restore T cells entry at the metastatic site. To further investigate whether granulin deficiency could also drive changes in T cell functional status, the total number of $CD8^+$ T cells and their activity mice were analysed in WT and granulin deficient.

Interestingly, flow cytometry analysis of digested liver metastatic lesions, derived from WT and $Grn^{-/-}$ experimental metastasis bearing mice, revealed no difference in either total $CD8^+$ T cell number or (Figure 6.6 a) $CD8^+$ T cells activation status (measured as $IFN\gamma$ expression) (Figure 6.6 b), suggesting that the main effect of granulin depletion is related to regulation of T cell trafficking.

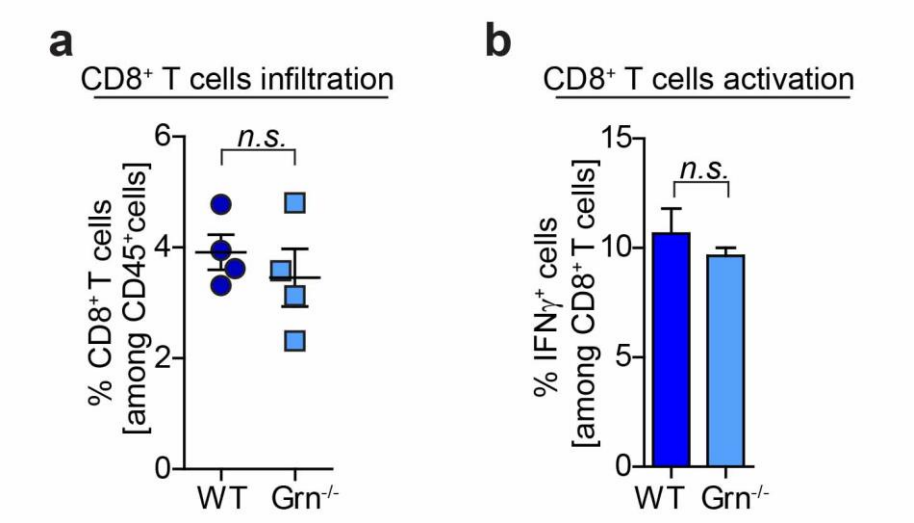

Figure 6.6 CD8$^+$ T cell number and activation remains the same in WT and Grn$^{-/-}$ mice.

Flow cytometric quantification of **a)** CD8$^+$ T cell total number and **b)** CD8$^+$ T cell activation (IFNγ$^+$ CD8$^+$ T cells) in WT and Grn$^{-/-}$ mice hepatic metastatic tumours resected 14 days after intrasplenic injection of KPC cells. N = 4 mice / group; mean ± SEM. For quantification of CD8$^+$ T cell number: individual data point, horizontal lines represent mean ± SEM. P<0.001; **, P < 0.01; *, P < 0.05; n.s. not significant by unpaired t-test.

Noteworthy is the observation that granulin depletion did not affect overall hematopoietic (CD45$^+$), T (CD3$^+$), neutrophil (Ly6G$^+$), macrophage (F4/80$^+$) and B (B220$^+$) cells number in metastatic tumours (Figure 6.7 a-e). The analysis was performed by flow cytometry and IHC staining of metastatic tissue sections derived from WT and Grn$^{-/-}$ mice.

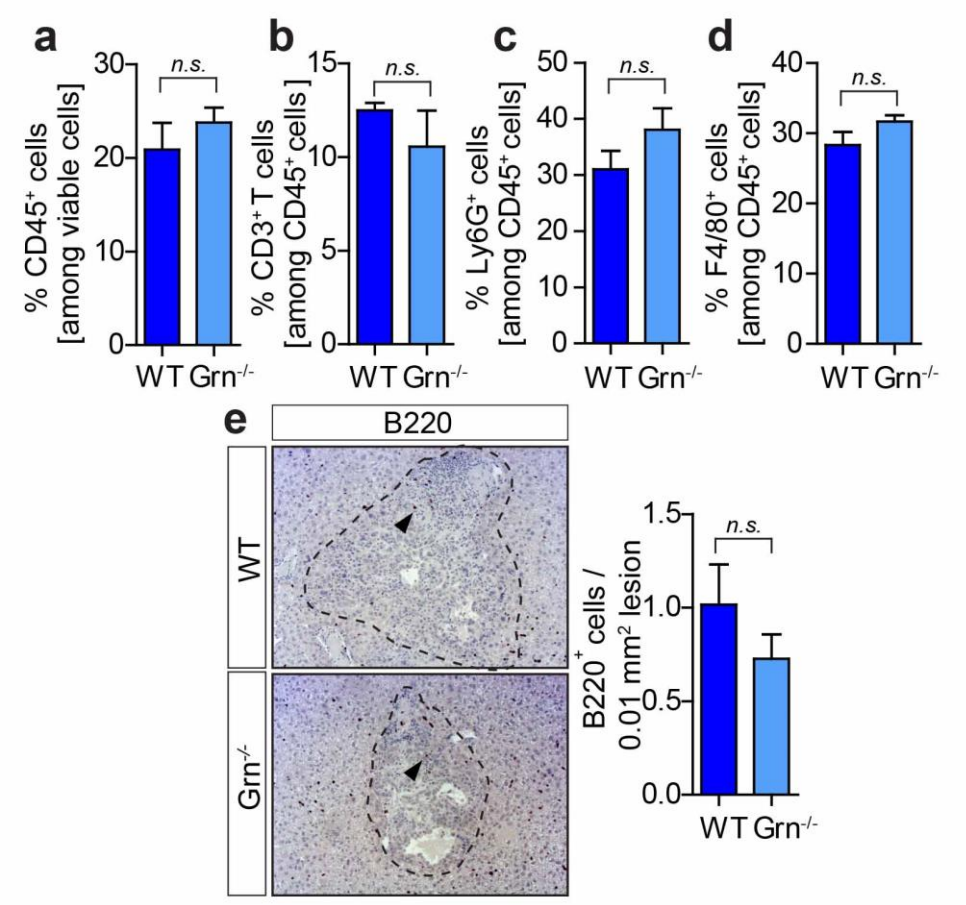

Figure 6.7 Granulin depletion does not affect numbers of immune cells infiltration at the metastatic site.

Liver metastasis was induced by intrasplenic implantation of KPCzsGreen/luc in WT or Grn-/- mice. Quantification of a) CD45+, b) CD3+, c) Ly6G+, d) F4-80+, e) B220+ immune cell populations by flow cytometric or immunohistochemical analysis. N = 4 WT and n = 4 Grn-/- mice; for e, n = 5 fields of view / mouse were analysed. Mean ± SEM). Scale bar = 100 µm; P<0.001; **, P < 0.01; *, P < 0.05; n.s. not significant by unpaired t-test. In e, black arrows point to $B220^+$ B cells.

Since a previous report of our lab reported that granulin depletion decreases metastatic tumour burden [117] and in this study it was observed that smaller metastatic lesions have higher infiltration of cytotoxic T cells (Chapter 3), one could think that the effect of granulin depletion on $CD8^+$ T cell infiltration was a consequence of the reduction in the size of the metastatic lesions. To understand whether granulin depletion had a direct impact on $CD8^+$ T cell infiltration, an adoptive transfer (AT) of tumour infiltrating $CD8^+$ T cells (derived from tdTomatoRed metastasis bearing WT mice; tdTR) was performed into metastasis bearing WT and $Grn^{-/-}$ mice (Figure 6.8 a). The metastatic infiltration of adoptively transferred $CD8^+$ T cell was compared in lesions of equal sizes found in WT and $Grn^{-/-}$ mice. Depletion of granulin caused a significant increase of intra-metastatic (IM) infiltration of tdTR $CD8^+$ T cells compared to WT tumours. In $Grn^{-/-}$ mice the number of peripheral (P) $CD8^+$ T cells decreased, while in WT mice T cells appeared mainly trapped at the tumour border (Figure 6.8 b).

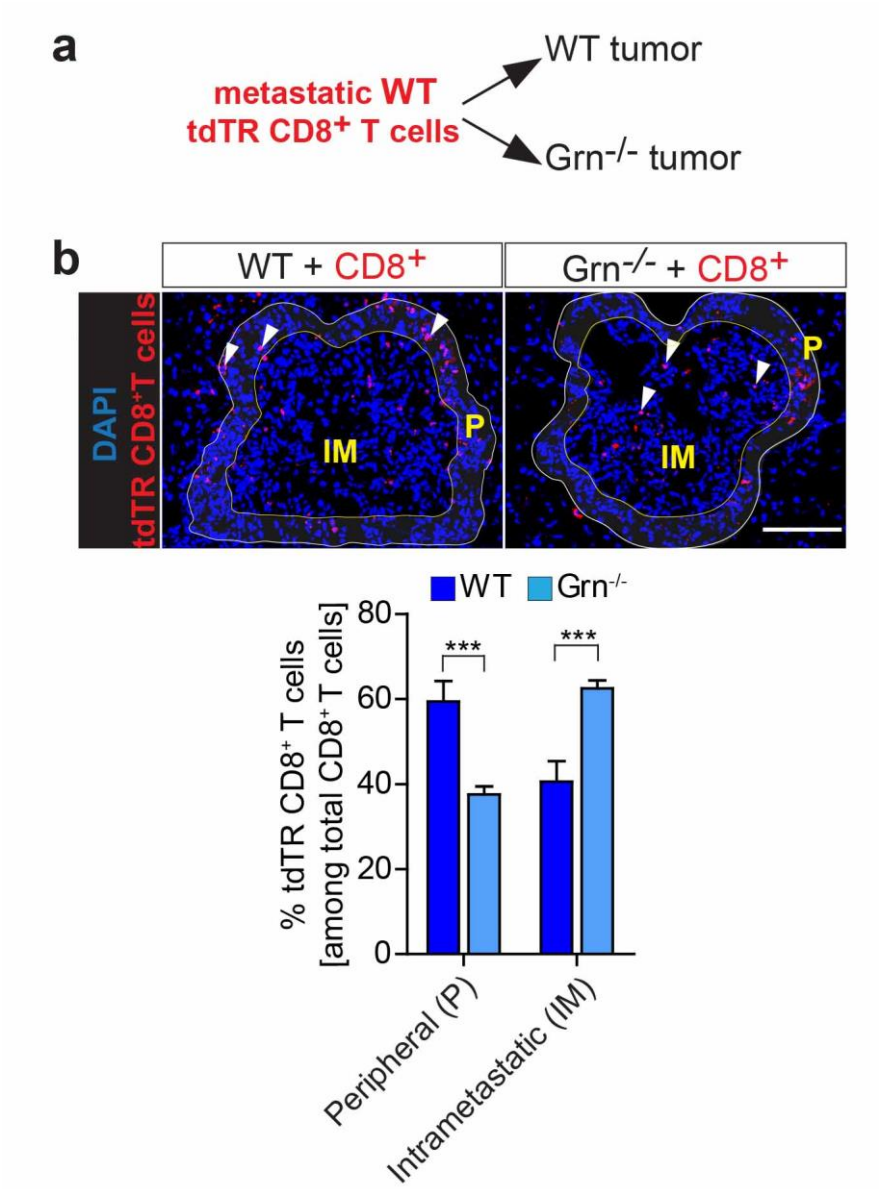

Figure 6.8 Adoptively transferred CD8^{+} T cells infiltrate into the tumour in Grn$^{-/-}$ mice, while they stay at the periphery in WT mice.

Liver metastasis was induced by intrasplenic implantation of KPCluc/zsGreen into dtTomatoRed WT mice (tdTR). At day 13, CD8+ T cells were isolated from tdTR mice and adoptively transferred into 14 days metastatic bearing WT and Grn-/- mice. 24 hours later, livers were resected and analysed for tdTR CD8+ T cell infiltration a) Schematic of the experiment. b) Representative images of tdTR CD8+ T cell in liver tissues derived from WT and Grn-/- mice and relative quantification of data. Percentage of tdTR CD8+ T cell (in red) found in peripheral (P) and intra-metastatic (IM) regions upon adoptive transfer. Nuclei were

counter stained with DAPI. N =3 mice / group; n = 6 fields of view / mouse; mean ± SEM. Scale bar = 100 μm; P<0.001; **, P < 0.01; *, P < 0.05; n.s. not significant by unpaired t-test. White arrows point to P (left panel) and IM (right panel) $CD8^+$ T cells.

It was then reasoned whether granulin could affect effector T cell functions in a direct mechanism other than influencing $CD8^+$ T cell infiltration indirectly through the activation of HSCs. For this reason, CD3/CD28 dynabeads (BD) activated splenic $CD8^+$ T cells were interrogated for IFNγ expression and proliferation upon stimulation with either recombinant granulin alone (rec. Grn) or in co-culture with BMMs derived from WT and $Grn^{-/-}$ mice. It was found that granulin did not have a direct effect on T cell function since recombinant granulin was unable to suppress $CD8^+$ T cell proliferation (Figure 6.9 a) and activation (Figure 6.9 b), while macrophages retained their $CD8^+$ T cell suppressive capacity in the absence of granulin.

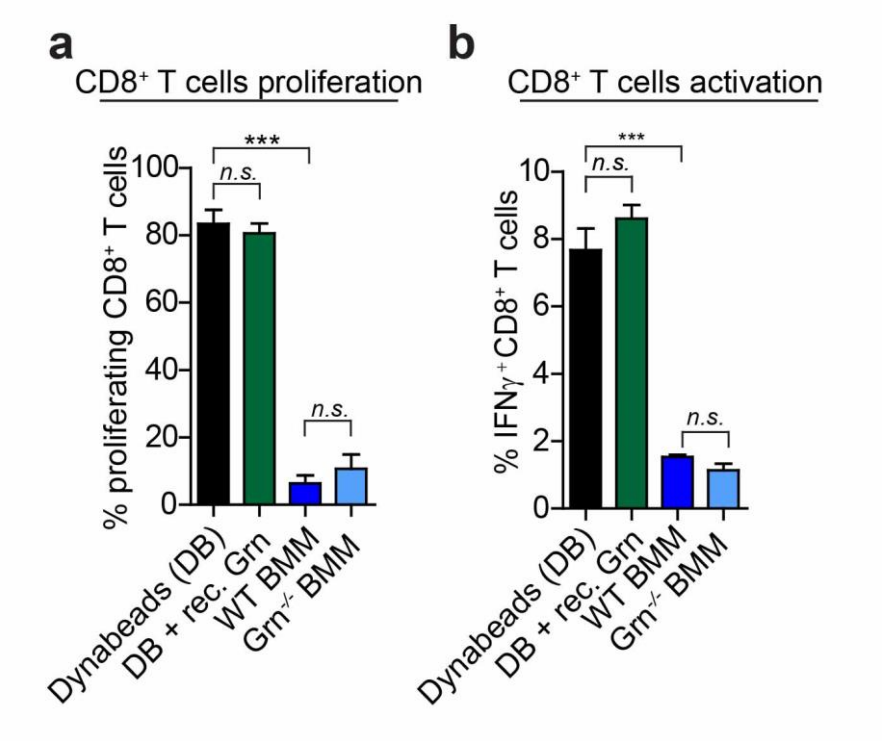

Figure 6.9 Granulin does not directly affect ex-vivo CD8+ T cells activation and proliferation.

Bone marrow isolated macrophages (BMMs) derived from WT and $Grn^{-/-}$ mice and 1 µg / ml recombinant granulin (rec. Grn) were tested for the capacity of suppress splenic $CD8^+$ T cell **a)** proliferation (CFSE dilution) and **b)** activation (IFNγ expression levels). Data are mean ± SEM of 3 independent experiments. P<0.001; **, P < 0.01; *, P < 0.05; n.s. not significant, by Bonferroni multiple comparison.

Taken together, these results suggest that depletion of granulin does not change overall $CD8^+$ T cells number nor their cytotoxic activity, but it significantly improves $CD8^+$ T cell entry into metastatic tumours as a consequence of reduced fibrosis surrounding the liver metastatic site.

6.3 Depletion of granulin restores the response of metastatic pancreatic cancer to αPD-1 inhibitor therapy.

In Chapter 5, it was demonstrated that the presence of fibrosis at the metastatic site profoundly affects $CD8^+$ T cells infiltration and induce resistance of metastatic pancreatic cancer to αPD-1 treatment. In this part of the study, it was investigated whether the observed increase in $CD8^+$ T cell entry into granulin deficient metastatic tumours might also improve their response to αPD-1 therapy. To address this question, liver metastasis in WT and granulin deficient mice were induced by intrasplenic implantation of $KPC^{luc/zsGreen}$ cancer cells. Starting at day 14, when WT metastatic lesions were large, poorly infiltrated by $CD8^+$ T cells and rich in myofibroblasts and collagen deposition (Chapter 5, Figure 5.11), mice were treated with either αPD-1 or IgG control antibody. To assess the response of metastatic tumours to treatments, metastatic tumour burden was quantified by *in vivo* BLI technique at day 14, prior treatment, and at endpoint (day 24) (Figure 6.10 a and b). Metastatic burden was quantified in radiance (total flux/sec) as percentage average increase of metastatic tumour after treatment in comparison to prior treatment. In agreement with previously made observations (Chapter 5), single agent αPD-1 therapy did not reduce tumour burden in WT mice. Reduction in HSCs activation in granulin deficient mice caused decreased metastatic tumour burden [117], however PD-1 blockade in $Grn^{-/-}$ caused a dramatic decrease in metastatic progression, with even partial regression (Figure 6.10 c).

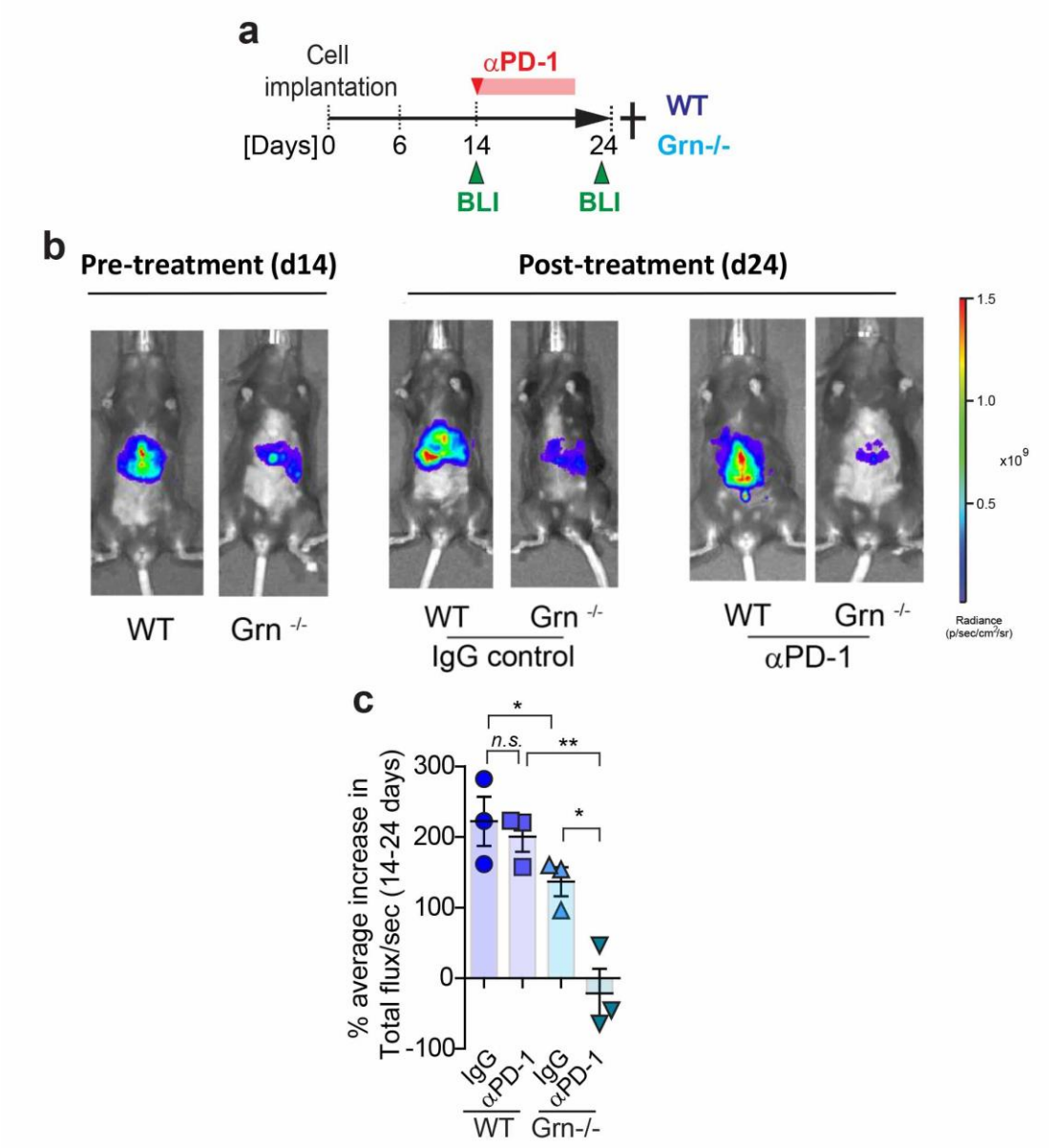

Figure 6.10 Depletion of granulin restores response of metastatic pancreatic cancer to αPD-1 therapy.

Liver metastasis was induced by intrasplenic implantation of KPCluc/zsGreen cancer cells. After 14 days, WT and Grn-/- mice were treated with αPD-1 or IgG isotype control antibodies. Metastatic burden was measured by in vivo bioluminescence imaging (BLI) before (day 14, d14) and after (day 24, d24) treatment. a) Schematic of the experiment. b) Representative bioluminescence images of metastatic bearing mice before (day 14) and after (day 24) treatment with αPD-1 inhibitor or IgG antibodies. c) Percentage of average change in metastatic tumour burden (total flux/sec) in response to

treatments and assessed by BLI. N = 3 mice / group; individual data points, horizontal lines represent mean ± SEM. P<0.001; **, P < 0.01; *, P < 0.05; n.s. not significant by Bonferroni multiple comparison.

IF analysis of metastatic livers derived from WT and $Grn^{-/-}$ mice of the different treatment cohorts revealed, as expected, that lack of granulin resulted in a significant reduction of αSMA^{+} myofibroblast accumulation, independently on αPD-1 treatment (Figure 6.11 a and c). In WT tumours, few $CD8^{+}$ T cells within metastatic lesions of control IgG treated tumours were found, and $CD8^{+}$ T cell numbers remained unaffected by αPD-1 administration. In contrast, depletion of granulin caused a significant increase in metastasis infiltrating $CD8^{+}$ T cell numbers in response to αPD-1 treatment (Figure 6.11 a and b).

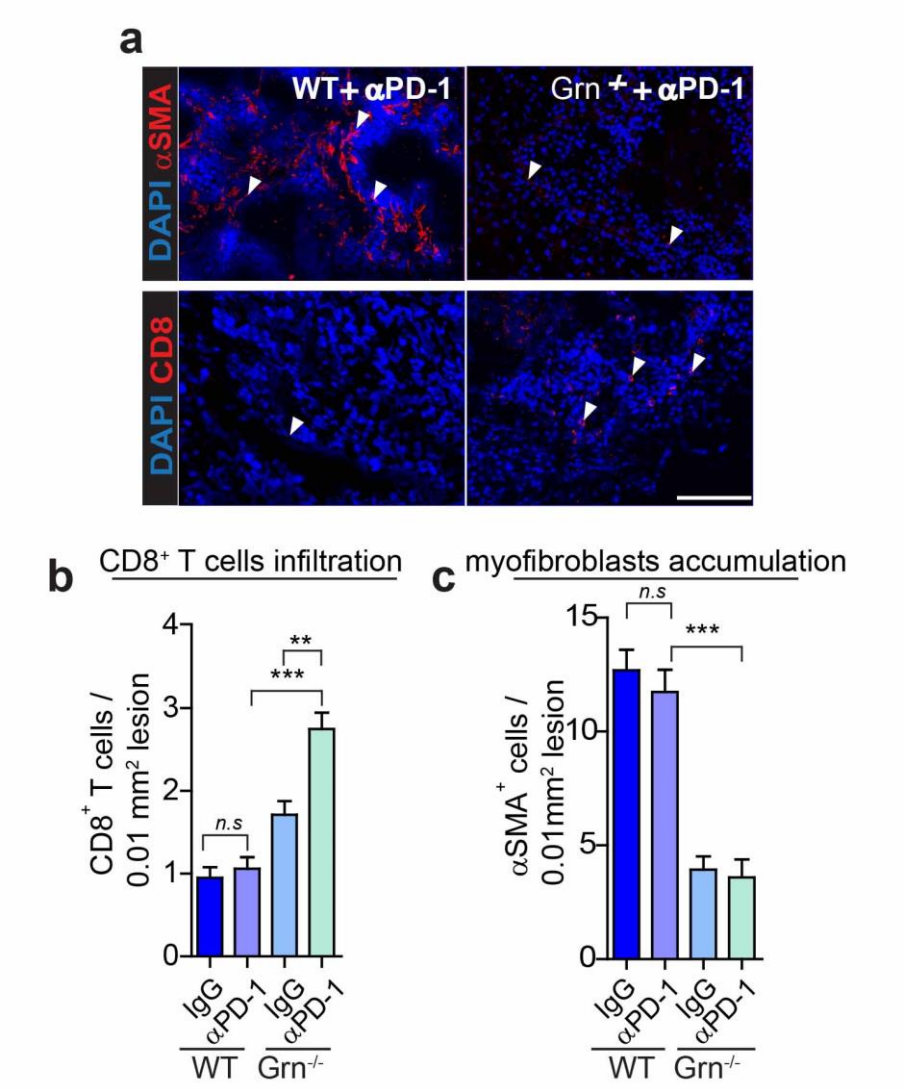

Figure 6.11 αPD-1 treatment in granulin-depleted mice induces high infiltration of CD8+ T cells.

Liver metastasis was induced by intrasplenic implantation of $KPC^{luc/zsGreen}$ cancer cells. After 14 days, WT and $Grn^{-/-}$ mice were treated with αPD-1 or IgG isotype control antibodies. At the end point (day 24), livers were resected and analysed. **a)** Representative immunofluorescence images of myofibroblasts ($αSMA^+$) and $CD8^+$ T cells staining in sequential liver tissue sections from WT and $Grn^{-/-}$ mice treated with αPD-1. $αSMA^+$ or $CD8^+$ cells are stained in red. Nuclei were counter stained with DAPI. Quantification of **b)** $CD8^+$ T cells infiltration and **c)** myofibroblasts ($αSMA^+$) accumulation in all mouse treatment cohorts. N = 3 mice / group, n = 6 fields of view / mouse. Mean ± SEM. Scale bar = 100 μm. P<0.001; **, P < 0.01; *, P < 0.05; n.s. not

significant by Bonferroni multiple comparison. White arrows point to αSMA$^+$ cells (upper panels) and CD8$^+$ T cells (lower panels).

The activation state of CD8$^+$ T cells was next assessed by flow cytometry. GzmB and IFNγ expression levels were measured in CD8$^+$ T cells isolated from metastatic tumours. While αPD-1 treatment did not alter GzmB nor IFNγ expression in CD8$^+$ T cells isolated from WT tumours, depletion of granulin led to a significant up-regulation of GzmB (Figure 6.12 a) and IFNγ expression (Figure 6.12 b) in CD8$^+$ T cells in response to αPD-1 administration.

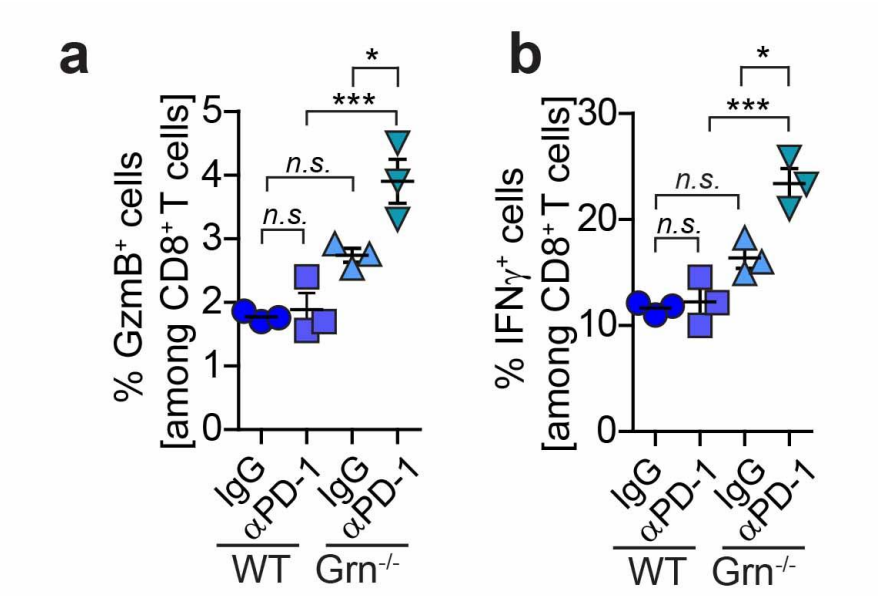

Figure 6.12 CD8$^+$ T cell cytotoxic activity is restored upon αPD-1 treatment in Grn$^{-/-}$ mice.

Liver metastasis was induced by intrasplenic implantation of KPC$^{luc/zsGreen}$ cancer cells in WT and Grn$^{-/-}$ mice. After 14 days mice were treated with αPD-1 or IgG isotype control antibodies. At the end point (day 24), livers were resected and analysed. Flow cytometry quantification of **a)** Granzyme B$^+$ (GzmB) and **b)** IFNγ$^+$ cells among metastasis infiltrating CD8$^+$ T cells. N = 3 mice / group, individual data

points, horizontal line represent mean ± SEM. P<0.001; **, P < 0.01; *, P < 0.05; n.s. not significant by Bonferroni multiple comparison.

Macrophages are a very plastic cell population and depending of the cytokine milieu within the tumour microenvironment they can acquire pro- or anti-tumorigenic roles [51]. Thus, it was investigated whether the observed increase in IFNγ expression by $CD8^+$ T cells in αPD-1 treated $Grn^{-/-}$ mice could promote an immune stimulatory M1-like MAM phenotype, allowing them to further fuel an anti-tumour immune attack. Indeed, in granulin deficient tumours treated with αPD-1, an increased presence of immune stimulatory MAMs with high expression of the pro-inflammatory markers iNOS, MHC-II, and COX-2 was found. In contrary, these tumours displayed lower numbers of M2-like $Ym\text{-}1^+$ and $CD206^+$ MAM markers compared to untreated $Grn^{-/-}$ tumours (Figure 6.13 a). Interestingly, the total macrophage numbers remained the same in treated and untreated $Grn^{-/-}$ metastatic tumours (Figure 6.13 b).

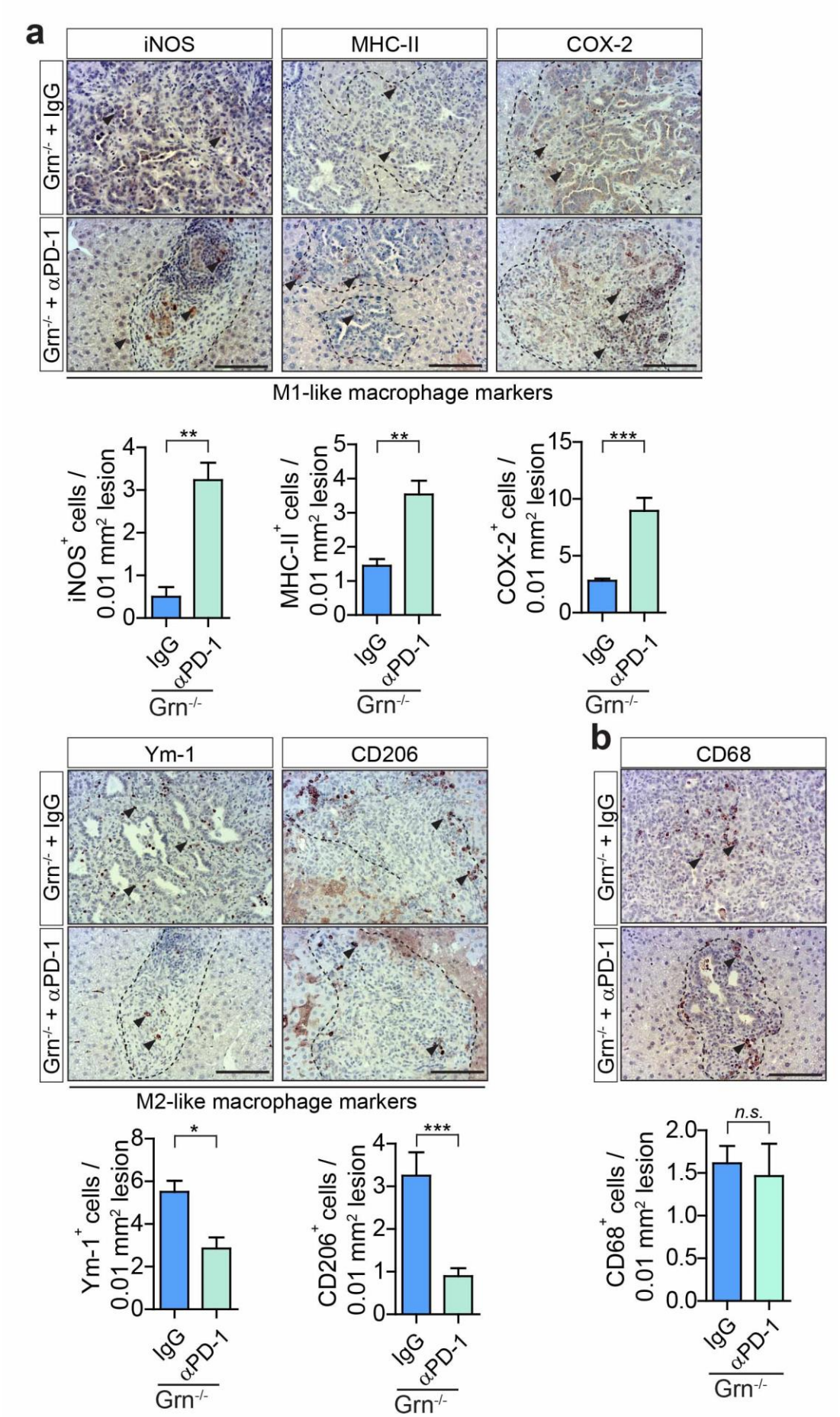
a
iNOS
MHC-II
COX-2
Grn-/- + IgG
Grn-/- + αPD-1
M1-like macrophage markers
iNOS+ cells / 0.01 mm2 lesion
MHC-II+ cells / 0.01 mm2 lesion
COX-2+ cells / 0.01 mm2 lesion
**
**
***
IgG
αPD-1
Grn-/-
b
Ym-1
CD206
CD68
M2-like macrophage markers
Ym-1+ cells / 0.01 mm2 lesion
CD206+ cells / 0.01 mm2 lesion
CD68+ cells / 0.01 mm2 lesion
*
***
n.s.

Figure 6.13 Neutralizing αPD-1 therapy in absence of granulin rewires macrophage toward a pro-inflammatory phenotype.

Liver metastasis was induced by intrasplenic implantation of $KPC^{luc/zsGreen}$ cancer cells in $Grn^{-/-}$ mice. After 14 days of cancer cells injection, mice were treated with αPD-1 or IgG isotype control antibodies. At the end point (day 24), resected livers were analysed. Representative immunohistochemistry (IHC) images and quantification of cells positive for **a)** M1-like MAM markers (iNOS, MHC-II, COX-2), M2-like MAM markers (Ym-1, CD206) and **b)** pan MAM marker (CD68) in hepatic metastatic tumours. N = 3 mice / group; n = 6 fields of view / mouse. Mean ± SEM. Scale bar = 100 μm; P<0.001; **, P < 0.01; *, P < 0.05; n.s. not significant by unpaired t-test. In each IHC micrograph arrows point to positively stained cells.

So far it has been observed that both CSF-1 inhibition and granulin depletion were able to restore cytotoxic T cell infiltration in metastatic tumours and to sensitize metastatic pancreatic cancer to PD-1 blockade. Thereby, it was examined whether CSF-1 inhibition in $Grn^{-/-}$ mice could provide any additional benefit to αPD-1 therapy. With this aim, experimental metastasis was induced into WT and $Grn^{-/-}$ mice and mice were treated with αPD-1 inhibitory antibody alone or in combination with αCSF-1 antibody, starting 14 days after pancreatic cancer cells implantation (Figure 6.14 a). The response of metastatic tumours to treatments was quantified by *in vivo* BLI techniques at day 14, prior treatments, and at the endpoint (day 24). Metastatic burden was quantified in radiance (total flux/sec) as percentage average increase in metastatic tumour after treatment in comparison to before treatment. As previously reported, αCSF-1 inhibition in combination with neutralizing αPD-1 dampened metastatic outgrowth in WT mice (Chapter 5 Figure 5.18), while although not significant, it rather had a counteracting effect in granulin deficient mice (Figure 6.14 b).

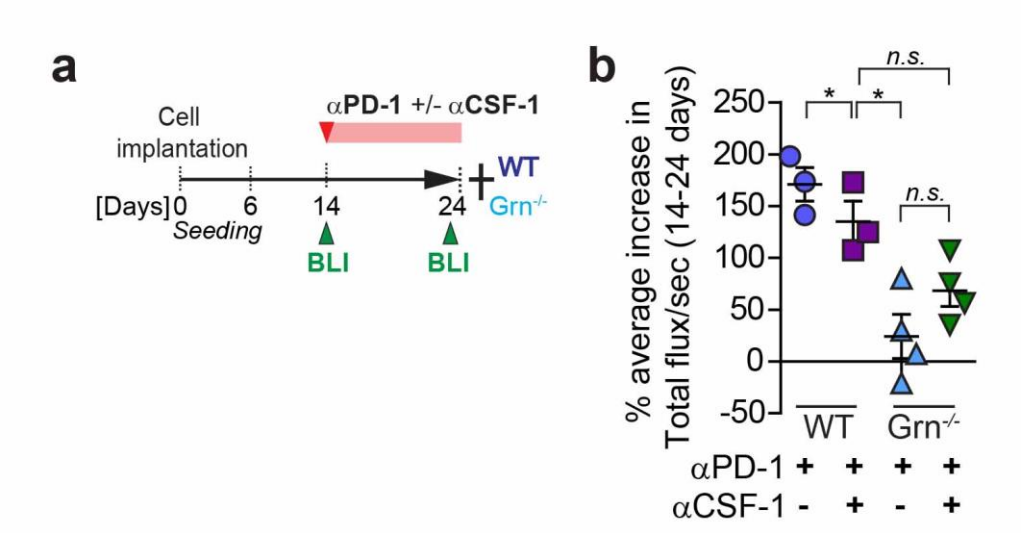

Figure 6.14 In granulin deficient mice, αCSF-1 treatment reduces the anti-tumorigenic effect of PD-1 blockade.

Liver metastasis was induced by intrasplenic implantation of $KPC^{luc/zsGreen}$ cancer cells in WT and $Grn^{-/-}$ mice. Initial tumor burden was quantified on day 14 by in vivo bioluminescence imaging (BLI). On the same day, treatment regimen with αPD-1 alone or in combination with αCSF-1 inhibitory antibody was started. At day 24, change in tumor burden was quantified by in vivo BLI imaging and livers were resected and analyzed. **a)** Schematic representation of the experiment. **b)** Percentage of average change in metastatic tumor burden in response to treatment assessed by BLI. N = 3 WT and n= 4 $Grn^{-/-}$ mice / group. Individual data points, horizontal lines represent mean ± SEM. P<0.001; **, P < 0.01; *, P < 0.05; n.s. not significant by Bonferroni multiple comparison.

The results obtained in the above experiment, which confirm the observations described in Chapter 5, brought our attention to the fact that αPD-1 treatment was more effective in impairing metastatic growth when it was administered in granulin deficient mice (Figure 6.10 c and Figure 6.14 b) rather than when it was used in combination with αCSF-1 in WT mice (Figure 5.12 and Figure 5.18 and Figure 6.14 b). Thus, it was reasoned that CSF-1 / CSF-1R axis blockade could have other effects on the tumour

microenvironment, thereby influencing differently the tumour response to checkpoint blockade. In accordance with this hypothesis, a recent study revealed that blockade of CSF-1R expressed on CAFs can induce the accumulation of immunosuppressive $Ly6G^+$ cells (recognized as neutrophil population [190]), thereby counteracting the therapeutic benefit of CSF-1R and/or αPD-1 inhibition [190]. To address whether a similar compensatory infiltration of $Ly6G^+$ neutrophils in response to CSF-1 blockade could occur in the model used in this study, $Ly6G^+$ cell numbers were quantified in metastatic tumours derived from WT mice treated with either IgG control or αCSF-1 antibodies. It was found that metastatic livers treated with αCSF-1 had increased infiltration of $Ly6G^+$ neutophils compared to tumours treated with the IgG control. Interestingly, in tumours derived from granulin deficient mice $Ly6G^+$ cell numbers were similar to the one found in WT control group but significantly less compared to αCSF-1 treated tumour. Thus, the observed marked increase of $Ly6G^+$ neutrophils in response to αCSF-1 treatment might explain the reduced effects of αPD-1 / αCSF-1 therapy in comparison to single PD-1 inhibition in $Grn^{-/-}$ mice (Figure 6.15).

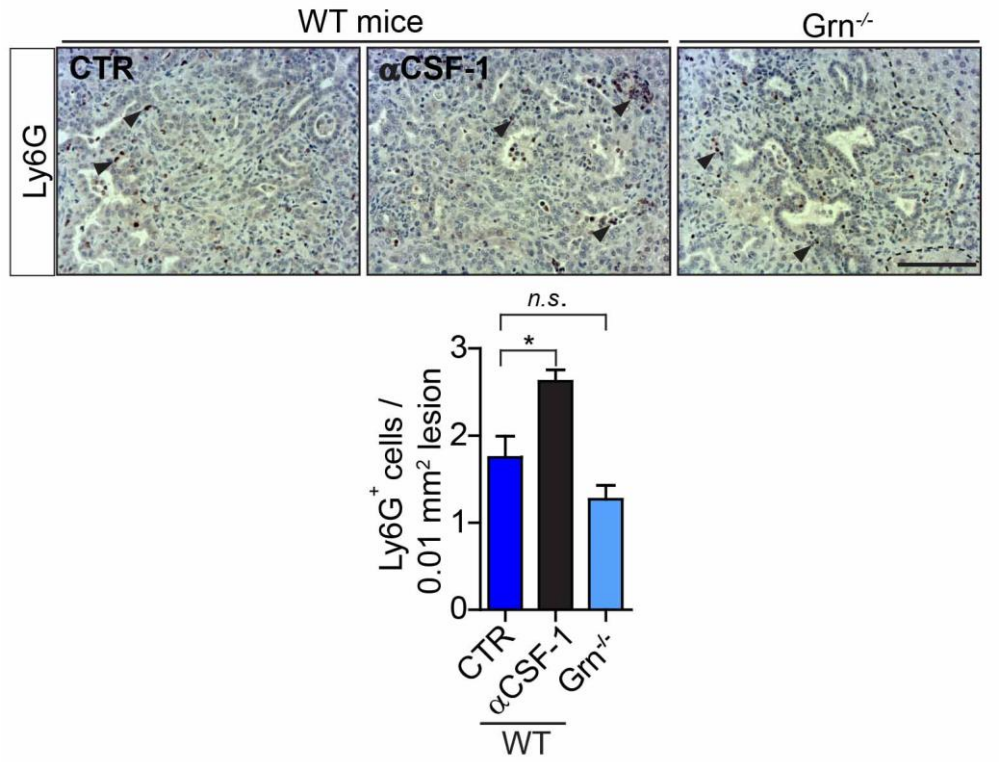

Figure 6.15 Ly6G$^+$ neutrophil infiltration is induced upon CSF-1 blockade.

Liver metastasis was induced by intrasplenic implantation of 1x10^6 KPC$^{zsGreen/luc}$ cancer cells in WT and granulin deficient mice (Grn$^{-/-}$) mice. WT mice were treated with IgG control (CTR) or αCSF-1 antibody 14 days later. All mice were sacrificed at day 24 and resected livers were analysed. Representative immunohistochemistry staining and quantification of Ly6G$^+$ cells in WT mice treated with IgG control (CTR) and αCSF-1 antibodies and in Grn$^{-/-}$ mice. N = 4 mice / group; n = 5 fields of view / mouse. Data expressed as mean ± SEM. Scale bar = 100 μm; P<0.001; **, P < 0.01; *, P < 0.05; n.s. not significant by Bonferroni multiple comparison. Black arrows point to Ly6G$^+$ cells.

Taken together, these findings demonstrated that depletion of granulin dramatically improved the response of metastatic pancreatic tumours to αPD-1 inhibitor treatment and that targeting a macrophage secreted factor,

such as granulin, might be more effective than targeting depletion of the entire macrophage population.

6.4 Reduction in liver fibrosis improves CD8$^+$ T cell infiltration and enhances αPD-1 therapy in metastatic pancreatic cancer.

To further confirm that the effect of granulin depletion on CD8$^+$ T cell infiltration was dependent on reduced fibrosis, tumour bearing mice were treated with the Vitamin D analogue Calcipotriol (Cal), an agent which has previously been shown to revert activated stellate cells to quiescent cells, resulting in reduced fibrosis in pre-clinical mouse models [228].

Metastasis bearing mice were treated with Calcipotriol and αPD-1 inhibitory antibody alone or in combination, starting 14 days after intrasplenic injection of pancreatic cancer cells, and in the presence of highly fibrotic metastatic tumour (Figure 6.16 a). At the end point (day 24), livers were harvested from euthanized mice and metastatic lesion area was analysed by H&E staining of liver tissues (Figure 6.17). Treatment with Calcipotriol alone reduced metastatic lesions area; and the anti-tumorigenic effect was further pronounced when Calcipotriol was administered in combination with neutralizing αPD-1 (Figure 6.16 b).

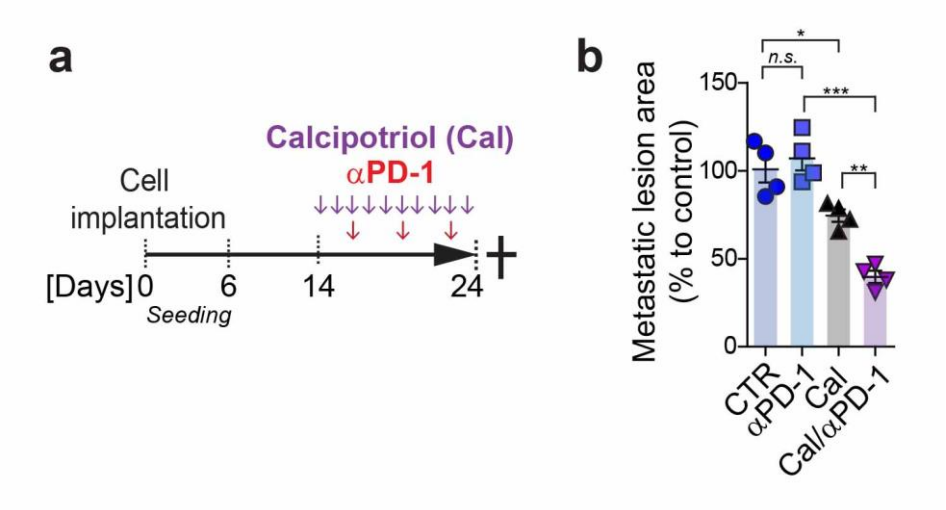

Figure 6.16 Calcipotriol attenuates metastatic fibrosis and increases αPD-1 therapeutic benefit.

Liver metastasis was induced by intrasplenic implantation of KPC$^{zsGreen/luc}$ cancer cells. Metastatic mice were treated with PD-1 inhibitor or Calcipotriol (Cal) alone or in combination, starting 14 days after cancer cells injection. Saline and IgG antibody were used as vehicle control (CTR). At the end point, day 24, metastatic livers were resected and analysed. **a)** Schematic representation of the experiment. **b)** Percentage of average change in metastatic lesion area compared to control in response to treatment assessed by haematoxylin and eosin (H&E) staining at endpoint. N = 4 mice / group; n = 6 fields of view / mouse. Individual data points, horizontal lines represent mean ± SEM. Scale bar = 100 μm; P<0.001; **, P < 0.01; *, P < 0.05; n.s. not significant by Bonferroni multiple comparison.

Picrosirius red staining of metastatic tissues from resected livers confirmed that tumours treated with Calcipotriol alone or in combination with αPD-1 had reduced fibrosis in comparison to untreated or αPD-1 single-therapy treated mice. Blockade of PD-1 as single agent did not affect fibrotic stroma deposition compared to control mice. Similarly, a further reduction of the fibrotic stroma in Calcipotriol treated mice was not observed when αPD-1 was added (Figure 6.17).

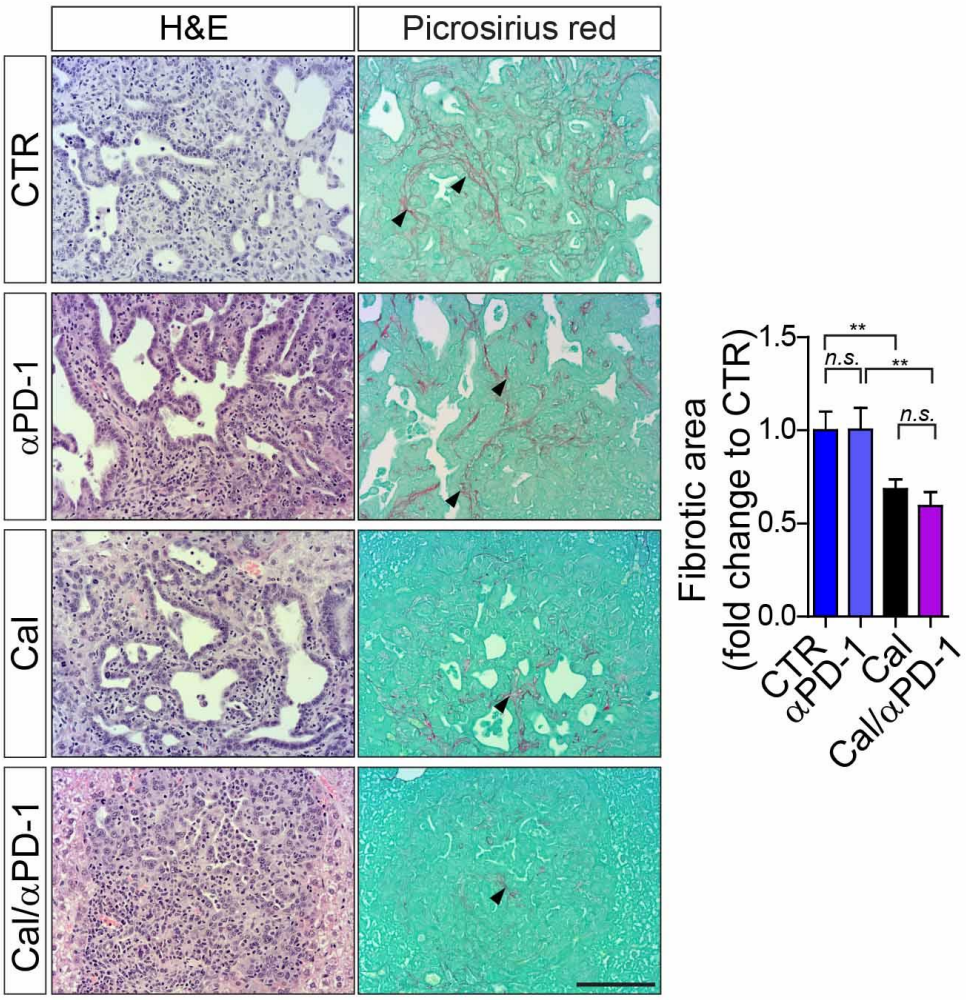

Figure 6.17 Calcipotriol reduces collagen deposition in metastatic livers of pancreatic cancer.

Liver metastasis was induced by intrasplenic implantation of $KPC^{zsGreen/luc}$ cancer cells. Metastatic mice were treated with αPD-1 or Calcipotriol (Cal) alone or in combination starting 14 days after cancer cells injection. Saline and IgG Ab were used as vehicle control (CTR). At the end point, day 24, metastatic livers were resected and analysed. Representative H&E (left panel) and picrosirius red staining (right panel) of sequential tumour sections showing area occupied by fibrotic stroma in all treatment cohorts. Change in liver fibrosis (assessed by collagen deposition) compared to CTR. N = 4 mice / group, n = 6 fields of view / mouse; data represented as mean ± SEM. Scale bar = 100 μm; P<0.001; **, P < 0.01; *, P < 0.05; n.s. not significant by Bonferroni multiple comparison. In picrosirius red staining micrographs arrows point to fibrotic area (in red).

In accordance with the above result, Calcipotriol or combinational Calcipotriol and αPD-1 treatment also impaired HSCs activation, as suggested by decreased number of $αSMA^+$ myofibroblasts found in metastatic livers. In contrast, IHC staining of metastatic liver tissues for CD8 expression revealed only a modest increase in $CD8^+$ T cell number in response to Calcipotriol treatment. However, Calcipotriol and αPD-1 co-treatment, highly enhanced $CD8^+$ T cells infiltration at the metastatic site (Figure 6.18).

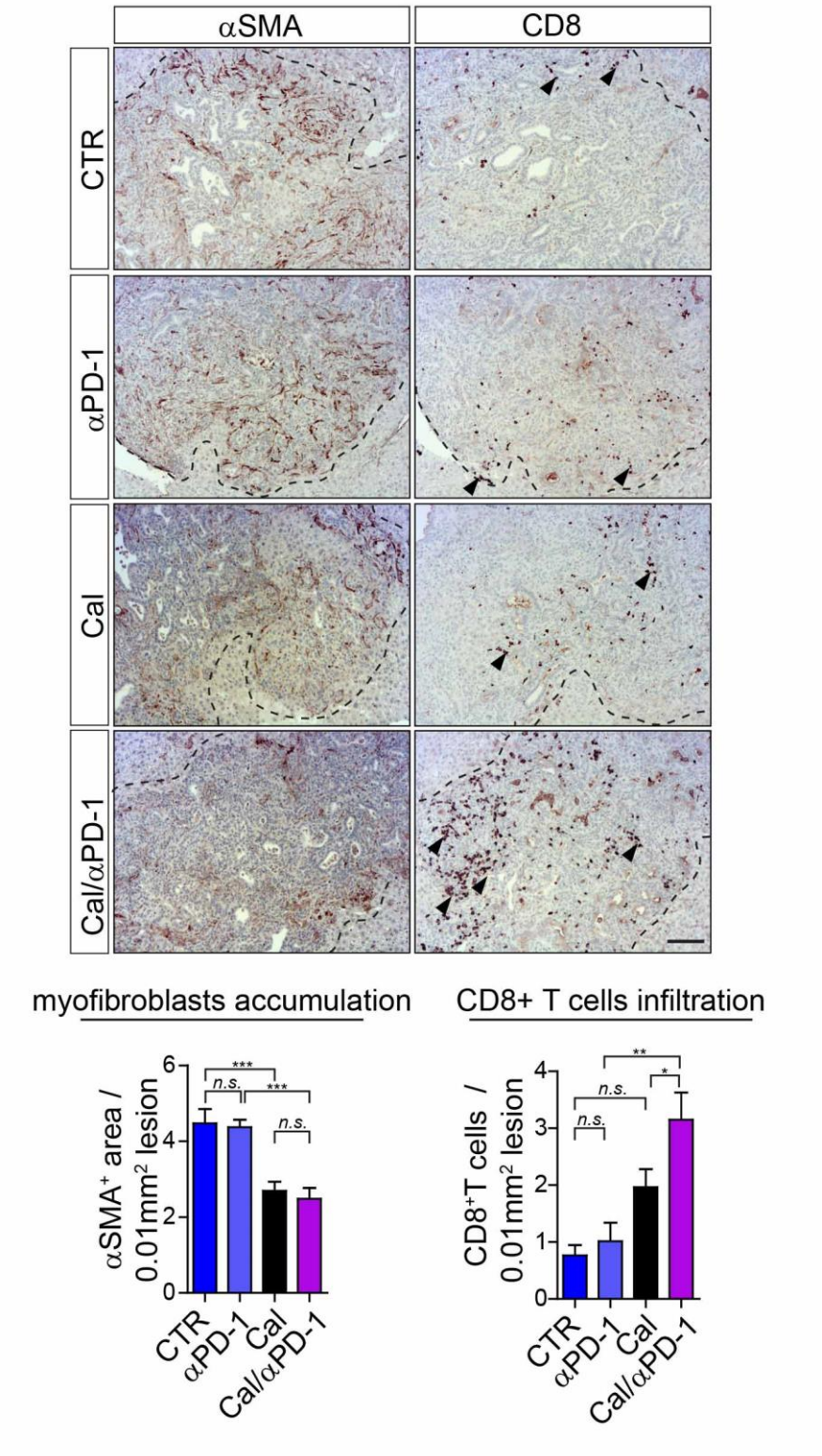

Figure 6.18 αPD-1 treatment in the presence of reduced fibrosis enhances CD8$^+$ T cell infiltration.

Liver metastasis was induced by intrasplenic implantation of $KPC^{zsGreen/luc}$ cancer cells. Metastatic mice were treated with αPD-1 or Calcipotriol (Cal) alone or in combination starting 14 days after cancer cells injection. Saline and IgG antibody were used as vehicle control (CTR). At the end point, day 24, metastatic livers were resected and analysed. Representative immunohistochemistry (IHC) images and quantification of myofibroblast (αSMA^+, left panels) and $CD8^+$ T cell (right panels) numbers. N = 4 mice / group, n = 6 fields of view / mouse; data represented as mean ± SEM. Scale bar = 100 μm; P<0.001; **, P < 0.01; *, P < 0.05; n.s. not significant by Bonferroni multiple comparison. Arrows point $CD8^+$ T cells.

Taken together, these data suggest that granulin-induced fibrosis in metastatic pancreatic cancer impedes $CD8^+$ T cell intra-metastatic infiltration and negatively affects the effectiveness of PD-1 blockade. Restoring $CD8^+$ T cell infiltration by targeting granulin and/or other pro-fibrotic factors is a prerequisite for successful αPD-1 therapy in metastatic pancreatic cancer.

6.5 Discussion

Central to the efficacy of immune checkpoint blockade is the infiltration of $CD8^+$ T cells into the tumour [121]. The presence of fibrotic stroma surrounding the tumour mass generates a barrier that impedes T cell trafficking, thereby preventing cytotoxic T cells to get in close contact with cancer cells (Chapter 5) [215].

In this chapter, it has been shown that reduced fibrosis increases intra-metastatic $CD8^+$ T cell numbers. Macrophage-derived granulin is a key protein responsible for HSCs transactivation into myofibroblasts in the metastatic liver of pancreatic cancer [117]. Our group and others have previously shown that hepatic myofibroblasts secrete high levels of ECM components promoting liver fibrosis [56], [117]. Here, it was showed that cancer cell derived CSF-1 is one of the main inducers of granulin secretion in macrophages and that M2-like macrophages are the main source of granulin. αCSF-1 treatment reprograms MAMs towards an immunostimulatory M1 phenotype (Chapter 4), and at the same time, reduces the expression of the fibrosis-promoting protein granulin, thereby decreasing the formation of metastatic desmoplasia. The contribution of macrophages, in particular those with an alternative M2-like phenotype, to fibrosis has been extensively reported [89]. In accordance with this, previous work in pancreatic cancer have shown that a change in the balance of MMPs expression by M1 polarized macrophages can lead to reduced fibrosis at the primary tumour site [94]. Recently, the role of CSF-1 / CSF-1R axis in regulating tumour fibrosis has been shown in the autochthonous KPC mouse model of pancreatic cancer, although no molecular mechanisms have been elucidated

yet [167]. Here, macrophage-secreted granulin was proposed as a key factor in driving fibrotic stroma formation in liver metastatic pancreatic cancer.

Granulin deficient mice had an altered spatial localization of $CD8^+$ T cells at the metastatic site as result of the scarce desmoplastic reaction. However, overall cytotoxic T cell numbers and functions remain unchanged. It was found that lack of granulin enhanced $CD8^+$ T cell entry into fibrotic-poor metastatic tumours, while in WT mice, T cells mainly accumulated in the peripheral fibrotic-rich regions. Restoration of T cell infiltration in metastatic lesions of granulin-depleted mice led these mice to having a superior response to αPD-1 treatment compared to WT mice. Importantly, αPD-1 treatment correlated with a markedly increase in $CD8^+$ T cell cytotoxicity and this was associated with metastatic tumour regression. Moreover, αPD-1 therapy in granulin deficient mice, other than enhancing $CD8^+$ T cells mediated anti-tumour activity, also rewired macrophages toward a pro-inflammatory M1-like phenotype, thereby facilitating the mounting of an effective immune response against cancer. αPD-1 therapy in mice lacking granulin showed increased therapeutic efficacy in comparison to the combination of αPD-1 and αCSF-1 treatments in WT mice. In addition, in granulin deficient mice, the administration of αCSF-1 in combination with αPD-1 rather dampened the therapeutic benefits of αPD-1 treatment in these mice.

Thus, the data showed in here suggest that in αCSF-1 treated tumours, the observed anti-tumorigenic immune response might still be in part dampened by a reduction of total MAM numbers, including those with an immune-stimulatory phenotype, and by a compensatory infiltration of $Ly6G^+$

neutrophils. In contrast, we did not observe a reduction of MAM numbers, neither a compensatory infiltration of $Ly6G^+$ neutrophils in granulin deficient tumours.

In conclusion, this study shows that in metastatic pancreatic cancer, macrophage secretion of granulin is induced by cancer cell-derived CSF-1, and it prevents cytotoxic $CD8^+$ T cell infiltration into metastatic lesions by promoting the formation of fibrotic stroma. Depletion of granulin restores $CD8^+$ T cell infiltration and renders metastatic pancreatic cancer responsive to αPD-1 therapy.

Conclusions

7 Chapter 7: Conclusions

Pancreatic cancer is one of the most deadly cancer types and its treatment still remains an unmet clinical need. Surgical resection is currently the only potential curative therapy but, unfortunately, more than 60 % of patients who undergo resection suffer from tumour relapse within the first 24 months after surgery [236]. The reason for this is associated with the early metastatic dissemination of cancer cells during cancer progression [237]. Moreover, at the time of diagnosis, the majority of patients with pancreatic cancer present an advanced or metastatic form of the disease already. In the metastatic setting, treatments with nab-paclitaxel plus gemcitabine or FOLFIRINOX represent the standard of care, although only in 10 % of patients the survival has increased to two years [237]. Thus, there is an urgent need to find more effective strategies to fight pancreatic cancer. New therapeutic approaches are starting to emerge based on advances made in understanding the biology and genetics of pancreatic cancer, including new findings regarding pancreatic cancer mutational landscape, tumour metabolism and tumour immunology [313].

Immune checkpoint blockade based immunotherapy is designed to amplify an endogenous anti-tumour T cell response. Nowadays, checkpoint blockade, in particular the targeting of PD-1 / PD-L1 pathway, is considered one of the most promising anti-cancer treatments and enormous therapeutic benefits have been reported for its use in different cancer types [140]. Central for immunotherapy to work is infiltration of $CD8^+$ T cells at the tumour site and initial activation of the cytotoxic $CD8^+$ T cell mediated anti-tumour response [122], [157]. $CD8^+$ T cell accumulation at the site of tumour

formation is a characteristic that depends on tumour mutational load and presence of neo-epitopes; and this has been positively correlated with overall survival across many cancer types, including ovarian, colon and breast cancer [314]. Pancreatic cancer, for long, has been considered as a poor immunogenic (or 'cold') type of cancer compared to other cancers, such as melanoma or non-small-cell lung cancer (NSCLC) [315]. In accordance to this, studies performed using KPC pancreatic cancer mouse models have also reported the presence of low mutational burden and poor T cell infiltration not only in primary tumour, but also at the secondary site [256], [280]. Pancreatic cancer also remains almost completely refractory to immune checkpoint blockade therapy as single agent [150]; the exception is represented by patients with microsatellite instability, which indeed have high mutational burden, but these patients only represent >1 % of total pancreatic cancer patients [271].

More recently a study conducted by Balachandran et al. demonstrated that human pancreatic tumours express a range of non-synonymous mutations that are predictive to function as new epitopes. The study also correlated the presence of tumour infiltrated $CD8^+$ T cells and high numbers of neo-antigens to patients with the longest survival, thus emphasizing the critical role of $CD8^+$ T cell in inhibiting pancreatic cancer progression [274]. In this regards, a genomic analysis has divided pancreatic cancer into 4 different subtypes: squamous, ADEX, progenitor and immunogenic. Among them, it has been found that the immunogenic subtype has a predominant gene expression profile correlated with presence of immune cells, including $CD8^+$ T cells. However, no improved prognosis has been linked with the immunogenic

subtype of pancreatic cancer [240]. In accordance to this, another study showed no correlation between overall $CD8^+$ T cells number and patient survival, but the presence of moderate to high mutational burden has been associated with macrophage infiltration [316]. Importantly, macrophage-related genes expression, in particular of those correlating with an M2-like macrophage phenotype, have been found to have a negative effect on patient survival, in both immunogenic and squamous subtypes of pancreatic cancer [240]. In agreement with these findings, the presence of TAMs has been associated with a worst cancer prognosis [90], [317].

The data showed in my thesis demonstrate that liver metastatic lesions of pancreatic cancer patients are infiltrated by $CD8^+$ T cells, and that the number of cytotoxic T cells inversely correlated with the number of cancer cells forming metastatic deposits. A similar phenotype was observed in spontaneous metastatic tumours derived from KPC mice and in the experimental liver metastasis mouse model. The latter metastasis model enabled to follow the metastatic progression of cancer cells in the liver and to monitor the changes in the TME associated with it. It was found that during early stage of metastasis, metastatic lesions are highly infiltrated by $CD8^+$ T cells. However, during metastatic progression $CD8^+$ T cell infiltration and cytotoxic functions are lost, thereby suggesting that in the early phases of metastatic growth, disseminating cancer cells are able to trigger an anti-tumour immune response mediated by $CD8^+$ T cells, but tumours then acquire the ability to escape immune surveillance.

A hallmark of pancreatic cancer is the presence of an extensive stroma compartment that can represent up to 80 % of the tumour mass [236]. An

extensive stroma compartment has been reported to be present not only at the primary site, but also at the metastatic site, which is mainly the liver. Our group and others have demonstrated that in both human and KPC mice, liver pancreatic cancer metastatic growth is accompanied by the accumulation of macrophages and desmoplasia [117], [257]. In this study, it was found that the tumour stroma in metastatic pancreatic cancer is also immunosuppressive, leading to T cell dysfunction. Several mechanisms can cause T cell dysfunction and one of them is the presence of an immunosuppressive microenvironment, which impairs infiltration and function of T cells within the tumour [150]. Immunosuppressive TME has been also considered a cause of tumour resistance to single agents immune checkpoint blockers [121]. Thus, to overcome the barrier posed by immunosuppressive microenvironment and / or to increase the recruitment and infiltration of cytotoxic T cells into the tumour, the development of TME targeted approaches in combination with immunotherapy is needed.

In this study it was also observed that metastatic livers of pancreatic cancer are highly infiltrated by M2-like MAMs with immunosuppressive functions. MAMs targeting by CSF-1 / CSF-1R axis blockade inhibited MAM recruitment and induced a phenotypic switch of remaining MAMs toward a pro-inflammatory, M1-like phenotype. Moreover, CSF-1 / CSF-1R targeting was sufficient to increase effectively a $CD8^+$ T cell cytotoxic response against metastatic pancreatic cancer, thereby leading to a reduction of metastatic burden in a T-effector cell dependent manner.

Blockade of the CSF-1/CSF-1R axis represents an attractive strategy to target the tumour-promoting functions of macrophages and it has been tested

in a variety of pre-clinical and clinical tumour models, with different outcomes [51]. Pancreatic tumours in the KPC mouse model recapitulate the characteristics of the four identified human pancreatic cancer subtypes [167], [240]. Interestingly, targeting macrophages by CSF-1R inhibitor has been shown not only to increase $CD8^+$ T cell infiltration but also to decrease fibrosis, thus inducing an overall change in tumour architecture due to down-regulation of squamous subtype gene programs and up-regulation of gene programs of the immunogenic subtype instead [167]. Importantly, in the experimental metastasis model used in this study it was found that targeting macrophages by CSF-1 blockade also reduced activation of HSCs (αSMA^+ myofibroblasts) and fibrosis at the metastatic site. M2-like macrophages are involved in fibrosis regulation by different routes, including secretion of MMPs or TGFβ [318]. Granulin is a protein that has been associated with tissue repair processes and has been shown to activate pro-inflammatory and matrix remodelling genes expression in fibroblasts, thus inducing tumour desmoplasia and sustaining breast cancer progression [95], [116]. Our group previously found that macrophage-secreted granulin activates resident HSCs, which sustain metastatic growth of pancreatic cancer by promoting fibrosis [117].

Here it was showed that fibrosis in metastatic pancreatic cancer inhibit $CD8^+$ T cell infiltration, thereby impeding effector T cells to enter in close contact with cancer cells and exert their cytotoxic function. Granulin was identified as potential therapeutic target to manipulate and re-educate the TME, and to enhance $CD8^+$ T cells infiltration at the metastatic site.

Both granulin depletion and MAM targeting by CSF-1 / CSF-1R axis blockade led to a reduction in fibrosis and restored pancreatic cancer sensitivity to PD-1 checkpoint blockade. However, granulin targeting had an increased therapeutic benefit in comparison to CSF-1 / CSF-1R blockade. This was associated with the fact that depletion of granulin did not affect the total number of macrophages, but its combination with αPD-1, rewired macrophages towards an M1-like phenotype. The presence of M1-like MAMs boosted anti-tumour immunity and induced a further reduction in metastatic tumour burden.

The effect of fibrosis on $CD8^+$ T cells mediated anti-tumour immunity was also confirmed by using Calcipotriol, a Vitamin D analogue, which is responsible of reverting activated HSCs into a quiescence status [228]. Fibrosis depletion induced by Calcipotriol increased $CD8^+$ T cells infiltration and sensitized pancreatic cancer to PD-1 blockade.

Taken together the research reported in this thesis demonstrates that:

- $CD8^+$ T cells highly infiltrate metastatic pancreatic cancer lesions during the early phases of metastatic progression, thus revealing that an anti-tumour immunity is triggered in response to pancreatic cancer metastatic colonization into the liver;
- Metastatic progression is accompanied by loss of $CD8^+$ T cell infiltration, accumulation of immunosuppressive M2-like MAMs and generation of a dense fibrotic stroma, which act as barrier for T cell infiltration;

- CSF-1 secreted by disseminating pancreatic cancer cells polarizes MAMs toward a M2-like phenotype and induces MAM expression of granulin;
- Blockade of CSF-1/CSF1-R axis or genetic depletion of granulin reduces fibrosis and restores $CD8^+$ T cell infiltration, thus sensitizing pancreatic cancer to PD-1 immune-checkpoint blockade;
- In comparison to macrophage targeting by CSF-1 / CSF-1R axis blockade, granulin depletion in combination with PD-1 blockade rewires macrophage polarization toward a pro-inflammatory type. Thus, this strategy could be more beneficial for treatment of metastatic pancreatic cancer since it aims to re-educate the metastatic TME rather than targeting it for depletion.

7.1 Future direction

Fibroblasts in cancer are a very heterogeneous population, thereby also their role in cancer has been associated with different functions [56]. An increasing number of reports describe an immunosuppressive role of CAFs in tumours. Different studies suggest that the immunosuppressive action of fibroblasts is mediated by CXCL12 secretion, which can either promote $CD8^+$ T cells exclusion [201] or induces recruitment of immunosuppressive T_{regs} , thereby affecting $CD8^+$ T cells functions indirectly [210], [311]. Other reports suggest that expression of inhibitory receptors such as PD-L1 and PD-L2 on CAFs induces T cell dysfunction [204], [312]. Based on the results obtained in this thesis, future work could be directed toward a better understating of the mechanisms by which tumour fibrosis impairs $CD8^+$ T cell mediated anti-

tumour immunity. Indeed, whether at the metastatic site in pancreatic cancer, activated HSCs only promote $CD8^+$ T cell exclusion by acting as a mechanical obstacle for T cells infiltration, still needs to be elucidated. In this regards, our group observed that CM from HSCs affects $CD8^+$ T cells activation and proliferation, suggesting that HSCs secreted factors can also mediate suppression of T cells activity [319]. Moreover, based on the recent identification of different CAF subtypes in primary breast and pancreatic tumours [210], [65], would it be interesting to investigate whether different populations of activated fibroblasts populate metastatic lesions of pancreatic cancer and which kind of fibroblast populations are regulated by macrophage-derived granulin. Also, the correlation between different CAFs subtypes, $CD8^+$ T cells infiltration and their functional status, mutational landscape, and prognosis of metastatic pancreatic cancer patients has not yet been explored. In this time, in which enormous technology advances have been obtained in genomics, data sequencing and immunotherapy, the characterization of the genome landscape, as well as of the TME associated with it, can open the possibility to identify new predictive biomarkers for immunotherapy use and hopefully might lead to the development of personalized therapies for each cancer patients.

References

8 References

[1] *The Biology of Cancer, Second Edition - Robert Weinberg - Google Libri*. .

[2] B. Alberts, A. Johnson, J. Lewis, M. Raff, K. Roberts, and P. Walter, *Molecular biology of the cell*. Garland Science, 2002.

[3] P. Mehlen and A. Puisieux, “Metastasis: a question of life or death,” *Nat. Rev. Cancer*, vol. 6, no. 6, pp. 449–458, Jun. 2006.

[4] J. Massagué and A. C. Obenauf, “Metastatic colonization by circulating tumour cells,” *Nature*, vol. 529, no. 7586, pp. 298–306, Jan. 2016.

[5] J. Eyles, A.-L. Puaux, X. Wang, B. Toh, C. Prakash, M. Hong, T. G. Tan, L. Zheng, L. C. Ong, Y. Jin, M. Kato, A. Prévost-Blondel, P. Chow, H. Yang, and J.-P. Abastado, “Tumor cells disseminate early, but immunosurveillance limits metastatic outgrowth, in a mouse model of melanoma.,” *J. Clin. Invest.*, vol. 120, no. 6, pp. 2030–9, Jun. 2010.

[6] B. Psaila and D. Lyden, “The metastatic niche: adapting the foreign soil,” *Nat. Rev. Cancer*, vol. 9, no. 4, pp. 285–293, Apr. 2009.

[7] B. Costa-silva, N. M. Aiello, A. J. Ocean, S. Singh, H. Zhang, B. K. Thakur, A. Becker, A. Hoshino, M. T. Mark, H. Molina, J. Xiang, T. Zhang, T. Theilen, G. García-santos, C. Williams, Y. Ararso, Y. Huang, G. Rodrigues, T. Shen, K. J. Labori, I. Marie, B. Lothe, E. H. Kure, J. Hernandez, A. Doussot, and S. H. Ebbesen, “Pancreatic cancer exosomes initiate pre-metastatic niche formation in the liver,” vol. 17, no. 6, 2015.

[8] M. S. Sosa, P. Bragado, and J. A. Aguirre-Ghiso, “Mechanisms of disseminated cancer cell dormancy: an awakening field,” *Nat. Rev. Cancer*, vol. 14, no. 9, pp. 611–622, Sep. 2014.

[9] P. Beauchesne, “Letter to the Editor: The natural history of extra-cranial metastasis from glioblastoma multiform [J Neurooncol DOI 10.1007/s11060-011-0575-8],” *J. Neurooncol.*, vol. 109, no. 3, pp. 593–594, Sep. 2012.

[10] J. Werner, S. E. Combs, C. Springfeld, W. Hartwig, T. Hackert, and M. W. Büchler, “Advanced-stage pancreatic cancer: therapy options,” *Nat. Rev. Clin. Oncol.*, vol. 10, no. 6, pp. 323–333, Jun. 2013.

[11] C. Holohan, S. Van Schaeybroeck, D. B. Longley, and P. G. Johnston, “Cancer drug resistance: an evolving paradigm,” *Nat. Rev. Cancer*, vol. 13, no. 10, pp. 714–726, Oct. 2013.

[12] D. Hanahan and R. A. Weinberg, “Hallmarks of cancer: The next generation,” *Cell*, vol. 144, no. 5, pp. 646–674, 2011.

[13] J. A. Joyce and J. W. Pollard, “Microenvironmental regulation of

metastasis," *Nat. Rev. Cancer*, vol. 9, no. ApRII, pp. 239–252, Apr. 2009.

[14] D. Hanahan and L. M. Coussens, "Accessories to the crime: functions of cells recruited to the tumor microenvironment.," *Cancer Cell*, vol. 21, no. 3, pp. 309–22, Mar. 2012.

[15] P. Carmeliet and R. K. Jain, "Molecular mechanisms and clinical applications of angiogenesis," *Nature*, vol. 473, no. 7347, pp. 298–307, May 2011.

[16] M. De Palma, D. Biziato, and T. V. Petrova, "Microenvironmental regulation of tumour angiogenesis," *Nat. Rev. Cancer*, vol. 17, no. 8, pp. 457–474, 2017.

[17] G. Bergers and S. Song, "The role of pericytes in blood-vessel formation and maintenance," *Neuro. Oncol.*, vol. 7, no. 4, pp. 452–464, Oct. 2005.

[18] K. Pietras and A. Östman, "Hallmarks of cancer: Interactions with the tumor stroma," *Exp. Cell Res.*, vol. 316, no. 8, pp. 1324–1331, May 2010.

[19] K. E. de Visser, A. Eichten, and L. M. Coussens, "Paradoxical roles of the immune system during cancer development," *Nat. Rev. Cancer*, vol. 6, no. 1, pp. 24–37, Jan. 2006.

[20] R. Kim, M. Emi, and K. Tanabe, "Cancer immunoediting from immune surveillance to immune escape.," *Immunology*, vol. 121, no. 1, pp. 1–14, May 2007.

[21] J. A. Bluestone, C. R. Mackay, J. J. O'Shea, and B. Stockinger, "The functional plasticity of T cell subsets," *Nat. Rev. Immunol.*, vol. 9, no. 11, pp. 811–816, Nov. 2009.

[22] C. Aspord, A. Pedroza-Gonzalez, M. Gallegos, S. Tindle, E. C. Burton, D. Su, F. Marches, J. Banchereau, and A. K. Palucka, "Breast cancer instructs dendritic cells to prime interleukin 13–secreting CD4 $^{+}$ T cells that facilitate tumor development," *J. Exp. Med.*, vol. 204, no. 5, pp. 1037–1047, May 2007.

[23] V. Gocheva, H.-W. Wang, B. B. Gadea, T. Shree, K. E. Hunter, A. L. Garfall, T. Berman, and J. A. Joyce, "IL-4 induces cathepsin protease activity in tumor-associated macrophages to promote cancer growth and invasion," *Genes Dev.*, vol. 24, no. 3, pp. 241–255, Feb. 2010.

[24] S. Wei, E. Zhao, I. Kryczek, and W. Zou, "Th17 cells have stem cell-like features and promote long-term immunity.," *Oncoimmunology*, vol. 1, no. 4, pp. 516–519, Jul. 2012.

[25] H. Pere, C. Tanchot, J. Bayry, M. Terme, J. Taieb, C. Badoual, O. Adotevi, N. Merillon, E. Marcheteau, V. Quillien, C. Banissi, A.

Carpentier, F. Sandoval, M. Nizard, F. Quintin-Colonna, G. Kroemer, W. H. Fridman, L. Zitvogel, S. Oudard, and E. Tartour, “Comprehensive analysis of current approaches to inhibit regulatory T cells in cancer,” *Oncoimmunology*, vol. 1, no. 3, pp. 326–333, May 2012.

[26] W. Tan, W. Zhang, A. Strasner, S. Grivennikov, J. Q. Cheng, R. M. Hoffman, and M. Karin, “Tumour-infiltrating regulatory T cells stimulate mammary cancer metastasis through RANKL–RANK signalling,” *Nature*, vol. 470, no. 7335, pp. 548–553, Feb. 2011.

[27] Z. G. Fridlender and S. M. Albelda, “Tumor-associated neutrophils: friend or foe?,” *Carcinogenesis*, vol. 33, no. 5, pp. 949–955, May 2012.

[28] Z. Granot, E. Henke, E. A. Comen, T. A. King, L. Norton, and R. Benezra, “Tumor entrained neutrophils inhibit seeding in the premetastatic lung.,” *Cancer Cell*, vol. 20, no. 3, pp. 300–14, Sep. 2011.

[29] J. Cools-Lartigue, J. Spicer, S. Najmeh, and L. Ferri, “Neutrophil extracellular traps in cancer progression,” *Cell. Mol. Life Sci.*, vol. 71, no. 21, pp. 4179–4194, Nov. 2014.

[30] D. I. Gabrilovich, S. Ostrand-Rosenberg, and V. Bronte, “Coordinated regulation of myeloid cells by tumours,” *Nat. Rev. Immunol.*, vol. 12, no. 4, pp. 253–268, Apr. 2012.

[31] L. J. J. Bayne, G. L. L. Beatty, N. Jhala, C. E. E. Clark, A. D. D. Rhim, B. Z. Z. Stanger, and R. H. Vonderheide, “Stimulating Factor Regulates Myeloid Inflammation and T Cell Immunity in Pancreatic Cancer,” *Cancer Cell*, vol. 21, no. 6, pp. 822–835, Jun. 2012.

[32] P. Andreu, M. Johansson, N. I. Affara, F. Pucci, T. Tan, S. Junankar, L. Korets, J. Lam, D. Tawfik, D. G. DeNardo, L. Naldini, K. E. de Visser, M. De Palma, and L. M. Coussens, “FcRγ Activation Regulates Inflammation-Associated Squamous Carcinogenesis,” *Cancer Cell*, vol. 17, no. 2, pp. 121–134, Feb. 2010.

[33] T. Schioppa, R. Moore, R. G. Thompson, E. C. Rosser, H. Kulbe, S. Nedospasov, C. Mauri, L. M. Coussens, and F. R. Balkwill, “B regulatory cells and the tumor-promoting actions of TNF-α during squamous carcinogenesis.,” *Proc. Natl. Acad. Sci. U. S. A.*, vol. 108, no. 26, pp. 10662–7, Jun. 2011.

[34] P. B. Olkhanud, B. Damdinsuren, M. Bodogai, R. E. Gress, R. Sen, K. Wejksza, E. Malchinkhuu, R. P. Wersto, and A. Biragyn, “Tumor-Evoked Regulatory B Cells Promote Breast Cancer Metastasis by Converting Resting CD4+ T Cells to T-Regulatory Cells,” *Cancer Res.*, vol. 71, no. 10, pp. 3505–3515, May 2011.

[35] P. J. Murray and T. A. Wynn, “Protective and pathogenic functions of macrophage subsets,” *Nat. Rev. Immunol.*, vol. 11, no. 11, pp. 723–737, Nov. 2011.

[36] C. Shi, T. Jia, S. Mendez-Ferrer, T. M. Hohl, N. V. Serbina, L. Lipuma, I. Leiner, M. O. Li, P. S. Frenette, and E. G. Pamer, “Bone Marrow Mesenchymal Stem and Progenitor Cells Induce Monocyte Emigration in Response to Circulating Toll-like Receptor Ligands,” *Immunity*, vol. 34, no. 4, pp. 590–601, Apr. 2011.

[37] E. G. Perdiguero and F. Geissmann, “The development and maintenance of resident macrophages,” *Nat. Immunol.*, vol. 17, no. 1, pp. 2–8, Jan. 2016.

[38] N. V. Serbina, T. Jia, T. M. Hohl, and E. G. Pamer, “Monocyte-Mediated Defense Against Microbial Pathogens,” *Annu. Rev. Immunol.*, vol. 26, no. 1, pp. 421–452, Apr. 2008.

[39] F. Geissmann, M. G. Manz, S. Jung, M. H. Sieweke, M. Merad, and K. Ley, “Development of Monocytes, Macrophages, and Dendritic Cells,” *Science (80-.).*, vol. 327, no. 5966, pp. 656–661, Feb. 2010.

[40] R. N. Hanna, C. Cekic, D. Sag, R. Tacke, G. D. Thomas, H. Nowyhed, E. Herrley, N. Rasquinha, S. McArdle, R. Wu, E. Peluso, D. Metzger, H. Ichinose, I. Shaked, G. Chodaczek, S. K. Biswas, and C. C. Hedrick, “Patrolling monocytes control tumor metastasis to the lung,” *Science (80-.).*, vol. 350, no. 6263, pp. 985–990, Nov. 2015.

[41] S. Gordon and P. R. Taylor, “Monocyte and macrophage heterogeneity,” *Nat. Rev. Immunol.*, vol. 5, no. 12, pp. 953–964, Dec. 2005.

[42] D. M. Mosser and J. P. Edwards, “Exploring the full spectrum of macrophage activation.,” *Nat. Rev. Immunol.*, vol. 8, no. 12, pp. 958–69, Dec. 2008.

[43] F. Ginhoux, J. L. Schultze, P. J. Murray, J. Ochando, and S. K. Biswas, “New insights into the multidimensional concept of macrophage ontogeny, activation and function,” *Nat. Immunol.*, vol. 17, no. 1, pp. 34–40, Jan. 2016.

[44] R. A. Franklin, W. Liao, A. Sarkar, M. V. Kim, M. R. Bivona, K. Liu, E. G. Pamer, and M. O. Li, “The cellular and molecular origin of tumor-associated macrophages,” *Science (80-.).*, vol. 344, no. 6186, pp. 921–925, May 2014.

[45] V. Kumar, P. Cheng, T. Condamine, S. Mony, L. R. Languino, J. C. McCaffrey, N. Hockstein, M. Guarino, G. Masters, E. Penman, F. Denstman, X. Xu, D. C. Altieri, H. Du, C. Yan, and D. I. Gabrilovich, “CD45 Phosphatase Inhibits STAT3 Transcription Factor Activity in Myeloid Cells and Promotes Tumor-Associated Macrophage Differentiation,” *Immunity*, vol. 44, no. 2, pp. 303–315, Feb. 2016.

[46] K. Movahedi and J. A. Van Ginderachter, “The Ontogeny and Microenvironmental Regulation of Tumor-Associated Macrophages,” *Antioxid. Redox Signal.*, vol. 25, no. 14, pp. 775–791, Nov. 2016.

[47] J. Cook and T. Hagemann, “Tumour-associated macrophages and cancer,” *Curr. Opin. Pharmacol.*, vol. 13, no. 4, pp. 595–601, Aug. 2013.

[48] H.-W. Lee, H.-J. Choi, S.-J. Ha, K.-T. Lee, and Y.-G. Kwon, “Recruitment of monocytes/macrophages in different tumor microenvironments,” *Biochim. Biophys. Acta - Rev. Cancer*, vol. 1835, no. 2, pp. 170–179, Apr. 2013.

[49] J. W. Pollard, “Trophic macrophages in development and disease,” *Nat. Rev. Immunol.*, vol. 9, no. 4, pp. 259–270, Apr. 2009.

[50] C. Murdoch, M. Muthana, S. B. Coffelt, and C. E. Lewis, “The role of myeloid cells in the promotion of tumour angiogenesis,” *Nat. Rev. Cancer*, vol. 8, no. 8, pp. 618–631, Aug. 2008.

[51] A. Mantovani, F. Marchesi, A. Malesci, L. Laghi, and P. Allavena, “Tumour-associated macrophages as treatment targets in oncology,” *Nat. Rev. Clin. Oncol.*, vol. 14, no. 7, pp. 399–416, Jan. 2017.

[52] B. Ruffell, N. I. Affara, and L. M. Coussens, “Differential macrophage programming in the tumor microenvironment,” *Trends Immunol.*, vol. 33, no. 3, pp. 119–126, Mar. 2012.

[53] F. Pucci, M. A. Venneri, D. Biziato, A. Nonis, D. Moi, A. Sica, C. Di Serio, L. Naldini, and M. De Palma, “A distinguishing gene signature shared by tumor-infiltrating Tie2-expressing monocytes, blood "resident" monocytes, and embryonic macrophages suggests common functions and developmental relationships,” *Blood*, vol. 114, no. 4, pp. 901–914, Jul. 2009.

[54] K. Movahedi, D. Laoui, C. Gysemans, M. Baeten, G. Stange, J. Van den Bossche, M. Mack, D. Pipeleers, P. In’t Veld, P. De Baetselier, and J. A. Van Ginderachter, “Different Tumor Microenvironments Contain Functionally Distinct Subsets of Macrophages Derived from Ly6C(high) Monocytes,” *Cancer Res.*, vol. 70, no. 14, pp. 5728–5739, Jul. 2010.

[55] L. Bingle, N. J. Brown, and C. E. Lewis, “The role of tumour-associated macrophages in tumour progression: implications for new anticancer therapies,” *J. Pathol.*, vol. 196, no. 3, pp. 254–265, Mar. 2002.

[56] D. Öhlund, E. Elyada, and D. Tuveson, “Fibroblast heterogeneity in the cancer wound,” *J. Exp. Med.*, vol. 211, no. 8, pp. 1503–1523, 2014.

[57] J. J. Tomasek, G. Gabbiani, B. Hinz, C. Chaponnier, and R. A. Brown, “Myofibroblasts and mechano-regulation of connective tissue remodelling,” *Nat. Rev. Mol. Cell Biol.*, vol. 3, no. 5, pp. 349–363, May 2002.

[58] H. Y. Chang, J.-T. Chi, S. Dudoit, C. Bondre, M. van de Rijn, D. Botstein, and P. O. Brown, “Diversity, topographic differentiation, and positional memory in human fibroblasts.,” *Proc. Natl. Acad. Sci. U. S.*

A., vol. 99, no. 20, pp. 12877–82, Oct. 2002.

[59] M. Simian, Y. Hirai, M. Navre, Z. Werb, A. Lochter, and M. J. Bissell, "The interplay of matrix metalloproteinases, morphogens and growth factors is necessary for branching of mammary epithelial cells.," *Development*, vol. 128, no. 16, pp. 3117–31, Aug. 2001.

[60] L. Rønnov-Jessen and O. W. Petersen, "Induction of alpha-smooth muscle actin by transforming growth factor-beta 1 in quiescent human breast gland fibroblasts. Implications for myofibroblast generation in breast neoplasia.," *Lab. Invest.*, vol. 68, no. 6, pp. 696–707, Jun. 1993.

[61] G. Serini, M. L. Bochaton-Piallat, P. Ropraz, A. Geinoz, L. Borsi, L. Zardi, and G. Gabbiani, "The fibronectin domain ED-A is crucial for myofibroblastic phenotype induction by transforming growth factor-beta1.," *J. Cell Biol.*, vol. 142, no. 3, pp. 873–81, Aug. 1998.

[62] G. A. Müller and H. P. Rodemann, "Characterization of human renal fibroblasts in health and disease: I. Immunophenotyping of cultured tubular epithelial cells and fibroblasts derived from kidneys with histologically proven interstitial fibrosis.," *Am. J. Kidney Dis.*, vol. 17, no. 6, pp. 680–3, Jun. 1991.

[63] R. Kalluri and M. Zeisberg, "Fibroblasts in cancer," *Nat. Rev. Cancer*, vol. 6, no. 5, pp. 392–401, May 2006.

[64] J. Bizik, E. Kankuri, A. Ristimäki, A. Taïeb, H. Vapaatalo, W. Lubitz, and A. Vaheri, "Cell–cell contacts trigger programmed necrosis and induce cyclooxygenase-2 expression," *Cell Death Differ.*, vol. 11, no. 2, pp. 183–195, Feb. 2004.

[65] D. Öhlund, A. Handly-Santana, G. Biffi, E. Elyada, A. S. Almeida, M. Ponz-Sarvise, V. Corbo, T. E. Oni, S. A. Hearn, E. J. Lee, I. I. C. Chio, C.-I. Hwang, H. Tiriac, L. A. Baker, D. D. Engle, C. Feig, A. Kultti, M. Egeblad, D. T. Fearon, J. M. Crawford, H. Clevers, Y. Park, and D. A. Tuveson, "Distinct populations of inflammatory fibroblasts and myofibroblasts in pancreatic cancer," *J. Exp. Med.*, vol. 214, no. 3, p. jem.20162024, Mar. 2017.

[66] Y. Kojima, A. Acar, E. N. Eaton, K. T. Mellody, C. Scheel, I. Ben-Porath, T. T. Onder, Z. C. Wang, A. L. Richardson, R. A. Weinberg, and A. Orimo, "Autocrine TGF- and stromal cell-derived factor-1 (SDF-1) signaling drives the evolution of tumor-promoting mammary stromal myofibroblasts," *Proc. Natl. Acad. Sci.*, vol. 107, no. 46, pp. 20009–20014, Nov. 2010.

[67] P. J. Mishra, P. J. Mishra, R. Humeniuk, D. J. Medina, G. Alexe, J. P. Mesirov, S. Ganesan, J. W. Glod, and D. Banerjee, "Carcinoma-Associated Fibroblast-Like Differentiation of Human Mesenchymal Stem Cells," *Cancer Res.*, vol. 68, no. 11, pp. 4331–4339, Jun. 2008.

[68] S. Kidd, E. Spaeth, K. Watson, J. Burks, H. Lu, A. Klopp, M. Andreeff,

and F. C. Marini, “Origins of the Tumor Microenvironment: Quantitative Assessment of Adipose-Derived and Bone Marrow–Derived Stroma,” *PLoS One*, vol. 7, no. 2, p. e30563, Feb. 2012.

[69] C. Kordes, I. Sawitza, and D. Häussinger, “Hepatic and pancreatic stellate cells in focus,” *Biol. Chem.*, vol. 390, no. 10, pp. 1003–12, Jan. 2009.

[70] M. G. Bachem*, E. Schneider*, H. Groß*, H. Weidenbach‡, R. M. Schmid‡, A. Menke‡, M. Siech§, H. Beger§, A. Grünert*, and G. Adler‡, “Identification, culture, and characterization of pancreatic stellate cells in rats and humans,” *Gastroenterology*, vol. 115, no. 2, pp. 421–432, Aug. 1998.

[71] A. Desmouliere, C. Guyot, and G. Gabbiani, “The stroma reaction myofibroblast: a key player in the control of tumor cell behavior,” *Int. J. Dev. Biol.*, vol. 48, no. 5–6, pp. 509–517, 2004.

[72] O. Wendling, J.-M. Bornert, P. Chambon, and D. Metzger, “Efficient temporally-controlled targeted mutagenesis in smooth muscle cells of the adult mouse,” *genesis*, vol. 47, no. 1, pp. 14–18, Jan. 2009.

[73] H. Sugimoto, T. M. Mundel, M. W. Kieran, and R. Kalluri, “Identification of fibroblast heterogeneity in the tumor microenvironment.,” *Cancer Biol. Ther.*, vol. 5, no. 12, pp. 1640–6, Dec. 2006.

[74] R. Kalluri, “The biology and function of fibroblasts in cancer,” *Nat. Rev. Cancer*, vol. 16, no. 9, pp. 582–598, Sep. 2016.

[75] A. J. Trimboli, C. Z. Cantemir-Stone, F. Li, J. A. Wallace, A. Merchant, N. Creasap, J. C. Thompson, E. Caserta, H. Wang, J.-L. Chong, S. Naidu, G. Wei, S. M. Sharma, J. A. Stephens, S. A. Fernandez, M. N. Gurcan, M. B. Weinstein, S. H. Barsky, L. Yee, T. J. Rosol, P. C. Stromberg, M. L. Robinson, F. Pepin, M. Hallett, M. Park, M. C. Ostrowski, and G. Leone, “Pten in stromal fibroblasts suppresses mammary epithelial tumours,” *Nature*, vol. 461, no. 7267, pp. 1084–1091, Oct. 2009.

[76] E. Flaberg, L. Markasz, G. Petranyi, G. Stuber, F. Dicső, N. Alchihabi, È. Oláh, I. Csízy, T. Józsa, O. Andrén, J.-E. Johansson, S.-O. Andersson, G. Klein, and L. Szekely, “High-throughput live-cell imaging reveals differential inhibition of tumor cell proliferation by human fibroblasts,” *Int. J. Cancer*, vol. 128, no. 12, pp. 2793–2802, Jun. 2011.

[77] M. Pickup, S. Novitskiy, and H. L. Moses, “The roles of TGFβ in the tumour microenvironment,” *Nat. Rev. Cancer*, vol. 13, no. 11, pp. 788–799, Nov. 2013.

[78] Z.-M. Shao, M. Nguyen, and S. H. Barsky, “Human breast carcinoma desmoplasia is PDGF initiated,” *Oncogene*, vol. 19, no. 38, pp. 4337–4345, Sep. 2000.

[79] B. Kwabi-Addo, M. Ozen, and M. Ittmann, “The role of fibroblast growth factors and their receptors in prostate cancer,” *Endocr. Relat. Cancer*, vol. 11, no. 4, pp. 709–724, Dec. 2004.

[80] E. Giannoni, F. Bianchini, L. Masieri, S. Serni, E. Torre, L. Calorini, and P. Chiarugi, “Reciprocal Activation of Prostate Cancer Cells and Cancer-Associated Fibroblasts Stimulates Epithelial-Mesenchymal Transition and Cancer Stemness,” *Cancer Res.*, vol. 70, no. 17, pp. 6945–6956, Sep. 2010.

[81] E. S. Jeon, H. J. Moon, M. J. Lee, H. Y. Song, Y. M. Kim, M. Cho, D.-S. Suh, M.-S. Yoon, C. L. Chang, J. S. Jung, and J. H. Kim, “Cancer-Derived Lysophosphatidic Acid Stimulates Differentiation of Human Mesenchymal Stem Cells to Myofibroblast-Like Cells,” *Stem Cells*, vol. 26, no. 3, pp. 789–797, Mar. 2008.

[82] C. Kahlert and R. Kalluri, “Exosomes in tumor microenvironment influence cancer progression and metastasis,” *J. Mol. Med.*, vol. 91, no. 4, pp. 431–437, Apr. 2013.

[83] A. Toullec, D. Gerald, G. Despouy, B. Bourachot, M. Cardon, S. Lefort, M. Richardson, G. Rigaill, M.-C. Parrini, C. Lucchesi, D. Bellanger, M.-H. Stern, T. Dubois, X. Sastre-Garau, O. Delattre, A. Vincent-Salomon, and F. Mechta-Grigoriou, “Oxidative stress promotes myofibroblast differentiation and tumour spreading,” *EMBO Mol. Med.*, vol. 2, no. 6, pp. 211–230, Jun. 2010.

[84] K. R. Levental, H. Yu, L. Kass, J. N. Lakins, M. Egeblad, J. T. Erler, S. F. T. Fong, K. Csiszar, A. Giaccia, W. Weninger, M. Yamauchi, D. L. Gasser, and V. M. Weaver, “Matrix Crosslinking Forces Tumor Progression by Enhancing Integrin Signaling,” *Cell*, vol. 139, no. 5, pp. 891–906, Nov. 2009.

[85] B. C. C. Özdemir, T. Pentcheva-Hoang, J. L. L. Carstens, X. Zheng, C.-C. C. Wu, T. R. R. Simpson, H. Laklai, H. Sugimoto, C. Kahlert, S. V. V. Novitskiy, A. DeJesus-Acosta, P. Sharma, P. Heidari, U. Mahmood, L. Chin, H. L. L. Moses, V. M. M. Weaver, A. Maitra, J. P. P. Allison, V. S. S. LeBleu, R. Kalluri, A. De Jesus-Acosta, P. Sharma, P. Heidari, U. Mahmood, L. Chin, H. L. L. Moses, V. M. M. Weaver, A. Maitra, J. P. P. Allison, V. S. S. LeBleu, and R. Kalluri, “Depletion of carcinoma-associated fibroblasts and fibrosis induces immunosuppression and accelerates pancreas cancer with reduced survival,” *Cancer Cell*, vol. 25, no. 6, pp. 719–734, Jun. 2014.

[86] T. Silzle, G. J. Randolph, M. Kreutz, and L. A. Kunz-Schughart, “The fibroblast: Sentinel cell and local immune modulator in tumor tissue,” *Int. J. Cancer*, vol. 108, no. 2, pp. 173–180, Jan. 2004.

[87] K. P. Olive, M. A. Jacobetz, C. J. Davidson, A. Gopinathan, D. McIntyre, D. Honess, B. Madhu, M. A. Goldgraben, M. E. Caldwell, D. Allard, K. K. Frese, G. DeNicola, C. Feig, C. Combs, S. P. Winter, H.

Ireland-Zecchini, S. Reichelt, W. J. Howat, A. Chang, M. Dhara, L. Wang, F. Ruckert, R. Grutzmann, C. Pilarsky, K. Izeradjene, S. R. Hingorani, P. Huang, S. E. Davies, W. Plunkett, M. Egorin, R. H. Hruban, N. Whitebread, K. McGovern, J. Adams, C. Iacobuzio-Donahue, J. Griffiths, and D. A. Tuveson, "Inhibition of Hedgehog Signaling Enhances Delivery of Chemotherapy in a Mouse Model of Pancreatic Cancer," *Science (80-.).*, vol. 324, no. 5933, pp. 1457–1461, Jun. 2009.

[88] A. D. D. Rhim, P. E. E. Oberstein, D. H. H. Thomas, E. T. T. Mirek, C. F. F. Palermo, S. A. A. Sastra, E. N. N. Dekleva, T. Saunders, C. P. P. Becerra, I. W. W. Tattersall, C. B. B. Westphalen, J. Kitajewski, M. G. G. Fernandez-Barrena, M. E. E. Fernandez-Zapico, C. Iacobuzio-Donahue, K. P. P. Olive, and B. Z. Z. Stanger, "Stromal elements act to restrain, rather than support, pancreatic ductal adenocarcinoma," *Cancer Cell*, vol. 25, no. 6, pp. 735–747, Jun. 2014.

[89] T. Wynn and L. Barron, "Macrophages: Master Regulators of Inflammation and Fibrosis," *Semin. Liver Dis.*, vol. 30, no. 03, pp. 245–257, Aug. 2010.

[90] B.-Z. Qian and J. W. Pollard, "Macrophage Diversity Enhances Tumor Progression and Metastasis," *Cell*, vol. 141, no. 1, pp. 39–51, Apr. 2010.

[91] M. A. Gibbons, A. C. MacKinnon, P. Ramachandran, K. Dhaliwal, R. Duffin, A. T. Phythian-Adams, N. van Rooijen, C. Haslett, S. E. Howie, A. J. Simpson, N. Hirani, J. Gauldie, J. P. Iredale, T. Sethi, and S. J. Forbes, "Ly6C ^{hi} Monocytes Direct Alternatively Activated Profibrotic Macrophage Regulation of Lung Fibrosis," *Am. J. Respir. Crit. Care Med.*, vol. 184, no. 5, pp. 569–581, Sep. 2011.

[92] L. A. Murray, Q. Chen, M. S. Kramer, D. P. Hesson, R. L. Argentieri, X. Peng, M. Gulati, R. J. Homer, T. Russell, N. van Rooijen, J. A. Elias, C. M. Hogaboam, and E. L. Herzog, "TGF-beta driven lung fibrosis is macrophage dependent and blocked by Serum amyloid P," *Int. J. Biochem. Cell Biol.*, vol. 43, no. 1, pp. 154–162, Jan. 2011.

[93] J.-P. Pradere, J. Kluwe, S. De Minicis, J.-J. Jiao, G.-Y. Gwak, D. H. Dapito, M.-K. Jang, N. D. Guenther, I. Mederacke, R. Friedman, A.-C. Dragomir, C. Aloman, and R. F. Schwabe, "Hepatic macrophages but not dendritic cells contribute to liver fibrosis by promoting the survival of activated hepatic stellate cells in mice," *Hepatology*, vol. 58, no. 4, pp. 1461–1473, Oct. 2013.

[94] K. B. Long, W. L. Gladney, G. M. Tooker, K. Graham, J. A. Fraietta, and G. L. Beatty, "efficacy in pancreatic carcinoma," vol. 6, no. 4, pp. 400–413, 2017.

[95] A. Bateman and H. P. J. Bennett, "The granulin gene family: From cancer to dementia," *BioEssays*, vol. 31, no. 11, pp. 1245–1254, 2009.

[96] D. Tolkatchev, S. Malik, A. Vinogradova, P. Wang, Z. Chen, P. Xu, H. P. J. Bennett, A. Bateman, and F. Ni, “Structure dissection of human progranulin identifies well-folded granulin/epithelin modules with unique functional activities,” *Protein Sci.*, vol. 17, no. 4, pp. 711–724, Apr. 2008.

[97] D. Xu, N. Suenaga, M. J. Edelmann, R. Fridman, R. J. Muschel, and B. M. Kessler, “Novel MMP-9 substrates in cancer cells revealed by a label-free quantitative proteomics approach.,” *Mol. Cell. Proteomics*, vol. 7, no. 11, pp. 2215–28, Nov. 2008.

[98] H.-S. Suh, N. Choi, L. Tarassishin, and S. C. Lee, “Regulation of Progranulin Expression in Human Microglia and Proteolysis of Progranulin by Matrix Metalloproteinase-12 (MMP-12),” *PLoS One*, vol. 7, no. 4, p. e35115, Apr. 2012.

[99] K. Kessenbrock, L. Fröhlich, M. Sixt, T. Lämmermann, H. Pfister, A. Bateman, A. Belaaouaj, J. Ring, M. Ollert, R. Fässler, and D. E. Jenne, “Proteinase 3 and neutrophil elastase enhance inflammation in mice by inactivating antiinflammatory progranulin,” *J. Clin. Invest.*, vol. 118, no. 7, pp. 2438–47, Jun. 2008.

[100] G. S. Butler, R. A. Dean, E. M. Tam, and C. M. Overall, “Pharmacoproteomics of a metalloproteinase hydroxamate inhibitor in breast cancer cells: dynamics of membrane type 1 matrix metalloproteinase-mediated membrane protein shedding.,” *Mol. Cell. Biol.*, vol. 28, no. 15, pp. 4896–914, Aug. 2008.

[101] F. Arechavaleta-Velasco, C. E. Perez-Juarez, G. L. Gerton, and L. Diaz-Cueto, “Progranulin and its biological effects in cancer,” *Med. Oncol.*, vol. 34, no. 12, pp. 1–11, 2017.

[102] T. Neill, S. Buraschi, A. Goyal, C. Sharpe, E. Natkanski, L. Schaefer, A. Morrione, and R. V Iozzo, “EphA2 is a functional receptor for the growth factor progranulin.,” *J. Cell Biol.*, vol. 215, no. 5, pp. 687–703, Dec. 2016.

[103] R. Daniel, Z. He, K. P. Carmichael, J. Halper, and A. Bateman, “Cellular Localization of Gene Expression for Progranulin,” *J. Histochem. Cytochem.*, vol. 48, no. 7, pp. 999–1009, Jul. 2000.

[104] Z. He, C. H. P. Ong, J. Halper, and A. Bateman, “Progranulin is a mediator of the wound response,” *Nat. Med.*, vol. 9, no. 2, pp. 225–229, Feb. 2003.

[105] W. Tang, Y. Lu, Q.-Y. Tian, Y. Zhang, F.-J. Guo, G.-Y. Liu, N. M. Syed, Y. Lai, E. A. Lin, L. Kong, J. Su, F. Yin, A.-H. Ding, A. Zanin-Zhorov, M. L. Dustin, J. Tao, J. Craft, Z. Yin, J. Q. Feng, S. B. Abramson, X.-P. Yu, and C. -j. Liu, “The Growth Factor Progranulin Binds to TNF Receptors and Is Therapeutic Against Inflammatory Arthritis in Mice,” *Science (80-.).*, vol. 332, no. 6028, pp. 478–484, Apr. 2011.

[106] H. Toh, M. Cao, E. Daniels, and A. Bateman, “Expression of the Growth Factor Progranulin in Endothelial Cells Influences Growth and Development of Blood Vessels: A Novel Mouse Model,” *PLoS One*, vol. 8, no. 5, p. e64989, May 2013.

[107] A. W. Kao, A. McKay, P. P. Singh, A. Brunet, and E. J. Huang, “Progranulin, lysosomal regulation and neurodegenerative disease,” *Nat. Rev. Neurosci.*, vol. 18, no. 6, pp. 325–333, Apr. 2017.

[108] T. L. Petkau and B. R. Leavitt, “Progranulin in neurodegenerative disease,” *Trends Neurosci.*, vol. 37, no. 7, pp. 388–398, Jul. 2014.

[109] P. F. Y. Cheung, C. W. Yip, N. C. L. Wong, D. Y. T. Fong, L. W. C. Ng, A. M. Y. Wan, C. K. Wong, T. T. Cheung, I. O. L. Ng, R. T. P. Poon, S. T. Fan, and S. T. Cheung, “Granulin-Epithelin Precursor Renders Hepatocellular Carcinoma Cells Resistant to Natural Killer Cytotoxicity,” *Cancer Immunol. Res.*, vol. 2, no. 12, pp. 1209–1219, Dec. 2014.

[110] J. J. Han, M. Yu, N. Houston, S. M. Steinberg, and E. C. Kohn, “Progranulin is a potential prognostic biomarker in advanced epithelial ovarian cancers.,” *Gynecol. Oncol.*, vol. 120, no. 1, pp. 5–10, Jan. 2011.

[111] R. Cuevas-Antonio, C. Cancino, F. Arechavaleta-Velasco, A. Andrade, L. Barron, I. Estrada, R. L. Fernandez, V. Olguin, S. Ruiz, F. Imani, M. Zeferino-Toquero, A. Ulloa-Aguirre, G. L. Gerton, and L. Diaz-Cueto, “Expression of Progranulin (Acrogranin/PCDGF/Granulin-Epithelin Precursor) in Benign and Malignant Ovarian Tumors and Activation of MAPK Signaling in Ovarian Cancer Cell Line,” *Cancer Invest.*, vol. 28, no. 5, pp. 452–458, May 2010.

[112] A. M. Carlson, M. J. Maurer, K. M. Goergen, K. R. Kalli, C. L. Erskine, M. D. Behrens, K. L. Knutson, and M. S. Block, “Utility of Progranulin and Serum Leukocyte Protease Inhibitor as Diagnostic and Prognostic Biomarkers in Ovarian Cancer,” *Cancer Epidemiol. Biomarkers Prev.*, vol. 22, no. 10, pp. 1730–1735, Oct. 2013.

[113] D. H. Koo, C.-Y. Park, E. S. Lee, J. Ro, and S. W. Oh, “Progranulin as a Prognostic Biomarker for Breast Cancer Recurrence in Patients Who Had Hormone Receptor-Positive Tumors: A Cohort Study,” *PLoS One*, vol. 7, no. 6, p. e39880, Jun. 2012.

[114] V. Soukup, M. Kalousov&#65533;, O. Capoun, R. Sobotka, Z. Breyl, M. Pe&#65533;l, T. Zima, and T. Hanu&#65533;, “Panel of Urinary Diagnostic Markers for Non-Invasive Detection of Primary and Recurrent Urothelial Urinary Bladder Carcinoma,” *Urol. Int.*, vol. 95, no. 1, pp. 56–64, Feb. 2015.

[115] C.-X. Pan, M. S. Kinch, P. A. Kiener, S. Langermann, G. Serrero, L. Sun, J. Corvera, C. J. Sweeney, L. Li, S. Zhang, L. A. Baldridge, T. D. Jones, M. O. Koch, T. M. Ulbright, J. N. Eble, and L. Cheng, “PC cell-derived growth factor expression in prostatic intraepithelial neoplasia

and prostatic adenocarcinoma.," *Clin. Cancer Res.*, vol. 10, no. 4, pp. 1333–7, Feb. 2004.

[116] M. Elkabets, A. M. Gifford, C. Scheel, B. Nilsson, F. Reinhardt, M. A. Bray, A. E. Carpenter, K. Jirström, K. Magnusson, B. L. Ebert, F. Pontén, R. A. Weinberg, and S. S. McAllister, "Human tumors instigate granulin-expressing hematopoietic cells that promote malignancy by activating stromal fibroblasts in mice," *J. Clin. Invest.*, vol. 121, no. 2, pp. 784–799, 2011.

[117] S. R. Nielsen, V. Quaranta, A. Linford, P. Emeagi, C. Rainer, A. Santos, L. Ireland, T. Sakai, K. Sakai, Y. Kim, D. Engle, F. Campbell, D. Palmer, J. H. Ko, D. A. Tuveson, E. Hirsch, A. Mielgo, and M. C. Schmid, "Macrophage-secreted granulin supports pancreatic cancer metastasis by inducing liver fibrosis," vol. 18, no. 5, 2016.

[118] N. Erez, "Fibroblasts form a hospitable metastatic niche in the liver," *Nat. Cell Biol.*, vol. 18, no. 5, pp. 465–466, May 2016.

[119] G. P. Dunn, A. T. Bruce, H. Ikeda, L. J. Old, and R. D. Schreiber, "Cancer immunoediting: from immuno- surveillance to tumor escape The cancer immunosurveillance hypothesis."

[120] P. Sharma, J. P. Allison, and Sharma, "the Future of Immune Checkpoint 4," *Science (80-.).*, vol. 348, no. 6230, pp. 56–61, Apr. 2015.

[121] P. Sharma, S. Hu-Lieskovan, J. A. Wargo, and A. Ribas, "Primary, Adaptive, and Acquired Resistance to Cancer Immunotherapy," *Cell*, vol. 168, no. 4, pp. 707–723, 2017.

[122] D. S. Chen and I. Mellman, "Oncology meets immunology: The cancer-immunity cycle," *Immunity*, vol. 39, no. 1, pp. 1–10, 2013.

[123] S. E. Townsend and J. P. Allison, "Tumor rejection after direct costimulation of CD8+ T cells by B7-transfected melanoma cells.," *Science*, vol. 259, no. 5093, pp. 368–70, Jan. 1993.

[124] R. J. Greenwald, G. J. Freeman, and A. H. Sharpe, "The B7 family revisited.," *Annu. Rev. Immunol.*, vol. 23, no. 1, pp. 515–48, Apr. 2005.

[125] S. H. Baumeister, G. J. Freeman, G. Dranoff, and A. H. Sharpe, "Coinhibitory Pathways in Immunotherapy for Cancer," *Annu. Rev. Immunol.*, vol. 34, no. 1, pp. 539–573, May 2016.

[126] D. R. Leach, M. F. Krummel, and J. P. Allison, "Enhancement of antitumor immunity by CTLA-4 blockade.," *Science*, vol. 271, no. 5256, pp. 1734–6, Mar. 1996.

[127] R. Waitz, M. Fassò, and J. P. Allison, "CTLA-4 blockade synergizes with cryoablation to mediate tumor rejection.," *Oncoimmunology*, vol. 1, no. 4, pp. 544–546, Jul. 2012.

[128] A. van Elsas, A. A. Hurwitz, and J. P. Allison, “Combination immunotherapy of B16 melanoma using anti-cytotoxic T lymphocyte-associated antigen 4 (CTLA-4) and granulocyte/macrophage colony-stimulating factor (GM-CSF)-producing vaccines induces rejection of subcutaneous and metastatic tumors accompanied by autoimmune depigmentation.,” *J. Exp. Med.*, vol. 190, no. 3, pp. 355–66, Aug. 1999.

[129] A. A. Hurwitz, T. F. Yu, D. R. Leach, J. P. Allison, F. G. Haluska, A. Kruse, S. MacRae, M. Nelson, C. Canning, I. Lowy, A. Korman, D. Lautz, S. Russell, M. T. Jaklitsch, N. Ramaiya, T. C. Chen, D. Neuberg, J. P. Allison, M. C. Mihm, and G. Dranoff, “CTLA-4 blockade synergizes with tumor-derived granulocyte-macrophage colony-stimulating factor for treatment of an experimental mammary carcinoma.,” *Proc. Natl. Acad. Sci. U. S. A.*, vol. 95, no. 17, pp. 10067–71, Aug. 1998.

[130] C. Robert, L. Thomas, I. Bondarenko, S. O’Day, J. Weber, C. Garbe, C. Lebbe, J.-F. Baurain, A. Testori, J.-J. Grob, N. Davidson, J. Richards, M. Maio, A. Hauschild, W. H. Miller, P. Gascon, M. Lotem, K. Harmankaya, R. Ibrahim, S. Francis, T.-T. Chen, R. Humphrey, A. Hoos, and J. D. Wolchok, “Ipilimumab plus Dacarbazine for Previously Untreated Metastatic Melanoma,” *N. Engl. J. Med.*, vol. 364, no. 26, pp. 2517–2526, Jun. 2011.

[131] F. S. Hodi, S. J. O’Day, D. F. McDermott, R. W. Weber, J. A. Sosman, J. B. Haanen, R. Gonzalez, C. Robert, D. Schadendorf, J. C. Hassel, W. Akerley, A. J. M. van den Eertwegh, J. Lutzky, P. Lorigan, J. M. Vaubel, G. P. Linette, D. Hogg, C. H. Ottensmeier, C. Lebbé, C. Peschel, I. Quirt, J. I. Clark, J. D. Wolchok, J. S. Weber, J. Tian, M. J. Yellin, G. M. Nichol, A. Hoos, and W. J. Urba, “Improved Survival with Ipilimumab in Patients with Metastatic Melanoma,” *N. Engl. J. Med.*, vol. 363, no. 8, pp. 711–723, Aug. 2010.

[132] J. C. Yang, M. Hughes, U. Kammula, R. Royal, R. M. Sherry, S. L. Topalian, K. B. Suri, C. Levy, T. Allen, S. Mavroukakis, I. Lowy, D. E. White, and S. A. Rosenberg, “Ipilimumab (Anti-CTLA4 Antibody) Causes Regression of Metastatic Renal Cell Cancer Associated With Enteritis and Hypophysitis,” *J. Immunother.*, vol. 30, no. 8, pp. 825–830, Nov. 2007.

[133] E. D. Kwon, C. G. Drake, H. I. Scher, K. Fizazi, A. Bossi, A. J. M. van den Eertwegh, M. Krainer, N. Houede, R. Santos, H. Mahammedi, S. Ng, M. Maio, F. A. Franke, S. Sundar, N. Agarwal, A. M. Bergman, T. E. Ciuleanu, E. Korbenfeld, L. Sengeløv, S. Hansen, C. Logothetis, T. M. Beer, M. B. McHenry, P. Gagnier, D. Liu, W. R. Gerritsen, and CA184-043 Investigators, “Ipilimumab versus placebo after radiotherapy in patients with metastatic castration-resistant prostate cancer that had progressed after docetaxel chemotherapy (CA184-043): a multicentre, randomised, double-blind, phase 3 trial,” *Lancet Oncol.*, vol. 15, no. 7, pp. 700–712, Jun. 2014.

[134] B. C. Carthon, J. D. Wolchok, J. Yuan, A. Kamat, D. S. Ng Tang, J. Sun, G. Ku, P. Troncoso, C. J. Logothetis, J. P. Allison, and P. Sharma, “Preoperative CTLA-4 Blockade: Tolerability and Immune Monitoring in the Setting of a Presurgical Clinical Trial,” *Clin. Cancer Res.*, vol. 16, no. 10, pp. 2861–2871, May 2010.

[135] G. J. Freeman, A. J. Long, Y. Iwai, K. Bourque, T. Chernova, H. Nishimura, L. J. Fitz, N. Malenkovich, T. Okazaki, M. C. Byrne, H. F. Horton, L. Fouser, L. Carter, V. Ling, M. R. Bowman, B. M. Carreno, M. Collins, C. R. Wood, and T. Honjo, “Engagement of the PD-1 immunoinhibitory receptor by a novel B7 family member leads to negative regulation of lymphocyte activation.,” *J. Exp. Med.*, vol. 192, no. 7, pp. 1027–34, Oct. 2000.

[136] A. Garcia-Diaz, D. S. Shin, B. Homet, R. Damoiseaux, R. S. Lo, and A. Ribas, “Interferon Receptor Signaling Pathways Regulating PD-L1 and PD-L2 Expression,” *CellReports*, vol. 19, pp. 1189–1201, 2017.

[137] S. M. Kaech and W. Cui, “Transcriptional control of effector and memory CD8+ T cell differentiation,” *Nat. Publ. Gr.*, vol. 12, no. 11, pp. 749–761, Nov. 2012.

[138] E. J. Wherry, “T cell exhaustion,” *Nat. Publ. Gr.*, vol. 131, no. 6, pp. 492–499, Jun. 2011.

[139] C. Robert, J. Schachter, G. V. Long, A. Arance, J. J. Grob, L. Mortier, A. Daud, M. S. Carlino, C. McNeil, M. Lotem, J. Larkin, P. Lorigan, B. Neyns, C. U. Blank, O. Hamid, C. Mateus, R. Shapira-Frommer, M. Kosh, H. Zhou, N. Ibrahim, S. Ebbinghaus, A. Ribas, and KEYNOTE-006 investigators, “Pembrolizumab versus Ipilimumab in Advanced Melanoma,” *N. Engl. J. Med.*, vol. 372, no. 26, pp. 2521–2532, Jun. 2015.

[140] A. Ribas and J. D. Wolchok, “Cancer immunotherapy using checkpoint blockade,” *Science (80-.).*, vol. 359, no. 6382, pp. 1350–1355, 2018.

[141] M. A. Curran, W. Montalvo, H. Yagita, and J. P. Allison, “PD-1 and CTLA-4 combination blockade expands infiltrating T cells and reduces regulatory T and myeloid cells within B16 melanoma tumors,” *Proc. Natl. Acad. Sci.*, vol. 107, no. 9, pp. 4275–4280, Mar. 2010.

[142] J. D. Wolchok, H. Kluger, M. K. Callahan, M. A. Postow, N. A. Rizvi, A. M. Lesokhin, N. H. Segal, C. E. Ariyan, R.-A. Gordon, K. Reed, M. M. Burke, A. Caldwell, S. A. Kronenberg, B. U. Agunwamba, X. Zhang, I. Lowy, H. D. Inzunza, W. Feely, C. E. Horak, Q. Hong, A. J. Korman, J. M. Wigginton, A. Gupta, and M. Sznol, “Nivolumab plus Ipilimumab in Advanced Melanoma,” *N. Engl. J. Med.*, vol. 369, no. 2, pp. 122–133, Jul. 2013.

[143] R. S. Herbst, J.-C. Soria, M. Kowanetz, G. D. Fine, O. Hamid, M. S. Gordon, J. A. Sosman, D. F. McDermott, J. D. Powderly, S. N.

Gettinger, H. E. K. Kohrt, L. Horn, D. P. Lawrence, S. Rost, M. Leabman, Y. Xiao, A. Mokatrin, H. Koeppen, P. S. Hegde, I. Mellman, D. S. Chen, and F. S. Hodi, “Predictive correlates of response to the anti-PD-L1 antibody MPDL3280A in cancer patients,” *Nature*, vol. 515, no. 7528, pp. 563–567, Nov. 2014.

[144] T. Powles, J. P. Eder, G. D. Fine, F. S. Braiteh, Y. Loriot, C. Cruz, J. Bellmunt, H. A. Burris, D. P. Petrylak, S. Teng, X. Shen, Z. Boyd, P. S. Hegde, D. S. Chen, and N. J. Vogelzang, “MPDL3280A (anti-PD-L1) treatment leads to clinical activity in metastatic bladder cancer,” *Nature*, vol. 515, no. 7528, pp. 558–562, Nov. 2014.

[145] J. Madore, R. E. Vilain, A. M. Menzies, H. Kakavand, J. S. Wilmott, J. Hyman, J. H. Yearley, R. F. Kefford, J. F. Thompson, G. V. Long, P. Hersey, and R. A. Scolyer, “PD-L1 expression in melanoma shows marked heterogeneity within and between patients: implications for anti-PD-1/PD-L1 clinical trials,” *Pigment Cell Melanoma Res.*, vol. 28, no. 3, pp. 245–253, May 2015.

[146] D. M. Pardoll, “The blockade of immune checkpoints in cancer immunotherapy,” *Nat. Rev. Cancer*, vol. 12, no. 4, pp. 252–264, Apr. 2012.

[147] J. M. Taube, R. A. Anders, G. D. Young, H. Xu, R. Sharma, T. L. McMiller, S. Chen, A. P. Klein, D. M. Pardoll, S. L. Topalian, and L. Chen, “Colocalization of Inflammatory Response with B7-H1 Expression in Human Melanocytic Lesions Supports an Adaptive Resistance Mechanism of Immune Escape,” *Sci. Transl. Med.*, vol. 4, no. 127, p. 127ra37-127ra37, Mar. 2012.

[148] T. N. Schumacher and R. D. Schreiber, “Neoantigens in cancer immunotherapy,” *Science (80-.).*, vol. 348, no. 6230, pp. 69–74, Apr. 2015.

[149] N. A. Rizvi, M. D. Hellmann, A. Snyder, P. Kvistborg, V. Makarov, J. J. Havel, W. Lee, J. Yuan, P. Wong, T. S. Ho, M. L. Miller, N. Rekhtman, A. L. Moreira, F. Ibrahim, C. Bruggeman, B. Gasmi, R. Zappasodi, Y. Maeda, C. Sander, E. B. Garon, T. Merghoub, J. D. Wolchok, T. N. Schumacher, and T. A. Chan, “Mutational landscape determines sensitivity to PD-1 blockade in non-small cell lung cancer,” *Science (80-.).*, vol. 348, no. 6230, pp. 124–128, Apr. 2015.

[150] K. G. Anderson, I. M. Stromnes, and P. D. Greenberg, “Perspective Obstacles Posed by the Tumor Microenvironment to T cell Activity : A Case for Synergistic Therapies,” *Cancer Cell*, vol. 31, no. 3, pp. 311–325, 2017.

[151] S. A. Forbes, N. Bindal, S. Bamford, C. Cole, C. Y. Kok, D. Beare, M. Jia, R. Shepherd, K. Leung, A. Menzies, J. W. Teague, P. J. Campbell, M. R. Stratton, and P. A. Futreal, “COSMIC: mining complete cancer genomes in the Catalogue of Somatic Mutations in Cancer,” *Nucleic*

Acids Res., vol. 39, no. Database, pp. D945–D950, Jan. 2011.

[152] Y. Pylayeva-Gupta, K. E. Lee, C. H. Hajdu, G. Miller, and D. Bar-Sagi, “Oncogenic Kras-induced GM-CSF production promotes the development of pancreatic neoplasia.,” *Cancer Cell*, vol. 21, no. 6, pp. 836–47, Jun. 2012.

[153] M. A. Collins, F. Bednar, Y. Zhang, J.-C. Brisset, S. Galbán, C. J. Galbán, S. Rakshit, K. S. Flannagan, N. V. Adsay, and M. Pasca di Magliano, “Oncogenic Kras is required for both the initiation and maintenance of pancreatic cancer in mice.,” *J. Clin. Invest.*, vol. 122, no. 2, pp. 639–53, Feb. 2012.

[154] J. Galon, A. Costes, F. Sanchez-Cabo, A. Kirilovsky, B. Mlecnik, C. Lagorce-Pagès, M. Tosolini, M. Camus, A. Berger, P. Wind, F. Zinzindohoué, P. Bruneval, P.-H. Cugnenc, Z. Trajanoski, W.-H. Fridman, and F. Pagès, “Type, Density, and Location of Immune Cells Within Human Colorectal Tumors Predict Clinical Outcome,” *Science (80-.).*, vol. 313, no. 5795, pp. 1960–1964, Sep. 2006.

[155] L. Zhang, J. R. Conejo-Garcia, D. Katsaros, P. A. Gimotty, M. Massobrio, G. Regnani, A. Makrigiannakis, H. Gray, K. Schlienger, M. N. Liebman, S. C. Rubin, and G. Coukos, “Intratumoral T Cells, Recurrence, and Survival in Epithelial Ovarian Cancer,” *N. Engl. J. Med.*, vol. 348, no. 3, pp. 203–213, Jan. 2003.

[156] E. Sato, S. H. Olson, J. Ahn, B. Bundy, H. Nishikawa, F. Qian, A. A. Jungbluth, D. Frosina, S. Gnjatic, C. Ambrosone, J. Kepner, T. Odunsi, G. Ritter, S. Lele, Y.-T. Chen, H. Ohtani, L. J. Old, and K. Odunsi, “Intraepithelial CD8+ tumor-infiltrating lymphocytes and a high CD8+/regulatory T cell ratio are associated with favorable prognosis in ovarian cancer,” *Proc. Natl. Acad. Sci.*, vol. 102, no. 51, pp. 18538–18543, Dec. 2005.

[157] J. A. Joyce and D. T. Fearon, “T cell exclusion, immune privilege, and the tumor microenvironment.,” *Science*, vol. 348, no. 6230, pp. 74–80, Apr. 2015.

[158] G. T. Motz, S. P. Santoro, L.-P. Wang, T. Garrabrant, R. R. Lastra, I. S. Hagemann, P. Lal, M. D. Feldman, F. Benencia, and G. Coukos, “Tumor endothelium FasL establishes a selective immune barrier promoting tolerance in tumors,” *Nat. Med.*, vol. 20, no. 6, pp. 607–615, Jun. 2014.

[159] A. J. Gunderson, M. M. Kaneda, T. Tsujikawa, A. V. Nguyen, N. I. Affara, B. Ruffell, S. Gorjestani, S. M. Liudahl, M. Truitt, P. Olson, G. Kim, D. Hanahan, M. A. Tempero, B. Sheppard, B. Irving, B. Y. Chang, J. A. Varner, and L. M. Coussens, “Bruton Tyrosine Kinase – Dependent Immune Cell Cross-talk Drives Pancreas Cancer,” *Cancer Discov.*, vol. 6, no. March, pp. 270–285, Mar. 2016.

[160] D. Wesch, C. Peters, and G. M. Siegers, “Human gamma delta T regulatory cells in cancer: fact or fiction?,” *Front. Immunol.*, vol. 5, p. 598, 2014.

[161] D. Daley, C. P. Zambirinis, L. Seifert, N. Akkad, N. Mohan, G. Werba, R. Barilla, A. Torres-Hernandez, M. Hundeyin, V. R. K. Mani, A. Avanzi, D. Tippens, R. Narayanan, J.-E. Jang, E. Newman, V. G. Pillarisetty, M. L. Dustin, D. Bar-Sagi, C. Hajdu, and G. Miller, “γδ T Cells Support Pancreatic Oncogenesis by Restraining αβ T Cell Activation,” *Cell*, vol. 166, no. 6, p. 1485–1499.e15, Sep. 2016.

[162] M. Z. Noman, G. Desantis, B. Janji, M. Hasmim, S. Karray, P. Dessen, V. Bronte, and S. Chouaib, “PD-L1 is a novel direct target of HIF-1α, and its blockade under hypoxia enhanced MDSC-mediated T cell activation,” *J. Exp. Med.*, vol. 211, no. 5, pp. 781–790, May 2014.

[163] P. Loke and J. P. Allison, “PD-L1 and PD-L2 are differentially regulated by Th1 and Th2 cells,” *Proc. Natl. Acad. Sci.*, vol. 100, no. 9, pp. 5336–5341, Apr. 2003.

[164] D.-M. Kuang, Q. Zhao, C. Peng, J. Xu, J.-P. Zhang, C. Wu, and L. Zheng, “Activated monocytes in peritumoral stroma of hepatocellular carcinoma foster immune privilege and disease progression through PD-L1.,” *J. Exp. Med.*, vol. 206, no. 6, pp. 1327–37, Jun. 2009.

[165] O. Bloch, C. A. Crane, R. Kaur, M. Safaee, M. J. Rutkowski, and A. T. Parsa, “Gliomas Promote Immunosuppression through Induction of B7-H1 Expression in Tumor-Associated Macrophages,” *Clin. Cancer Res.*, vol. 19, no. 12, pp. 3165–3175, Jun. 2013.

[166] R. Winograd, K. T. Byrne, R. A. Evans, P. M. Odorizzi, A. R. L. Meyer, D. L. Bajor, C. Clendenin, B. Z. Stanger, E. E. Furth, E. J. Wherry, and R. H. Vonderheide, “Induction of T-cell Immunity Overcomes Complete Resistance to PD-1 and CTLA-4 Blockade and Improves Survival in Pancreatic Carcinoma,” *Cancer Immunol. Res.*, vol. 3, no. 4, pp. 399–411, Apr. 2015.

[167] J. B. Candido, J. P. Morton, P. Bailey, A. D. Campbell, S. A. Karim, T. Jamieson, L. Lapienyte, A. Gopinathan, W. Clark, E. J. McGhee, J. Wang, M. Escorcio-Correia, R. Zollinger, R. Roshani, L. Drew, L. Rishi, R. Arkell, T. R. J. Evans, C. Nixon, D. I. Jodrell, R. W. Wilkinson, A. V. Biankin, S. T. Barry, F. R. Balkwill, and O. J. Sansom, “CSF1R+Macrophages Sustain Pancreatic Tumor Growth through T Cell Suppression and Maintenance of Key Gene Programs that Define the Squamous Subtype,” *Cell Rep.*, vol. 23, no. 5, pp. 1448–1460, 2018.

[168] J. A. Trapani, “The dual adverse effects of TGF-β secretion on tumor progression,” *Cancer Cell*, vol. 8, no. 5, pp. 349–350, Nov. 2005.

[169] D. A. Thomas and J. Massagué, “TGF-β directly targets cytotoxic T cell

functions during tumor evasion of immune surveillance," *Cancer Cell*, vol. 8, no. 5, pp. 369–380, Nov. 2005.

[170] W. Chen, W. Jin, N. Hardegen, K. Lei, L. Li, N. Marinos, G. McGrady, and S. M. Wahl, "Conversion of Peripheral CD4 $^{+}$ CD25 $^{-}$ Naive T Cells to CD4 $^{+}$ CD25 $^{+}$ Regulatory T Cells by TGF-β Induction of Transcription Factor *Foxp3*," *J. Exp. Med.*, vol. 198, no. 12, pp. 1875–1886, Dec. 2003.

[171] M. G. Roncarolo, R. Bacchetta, C. Bordignon, S. Narula, and M. K. Levings, "Type 1 T regulatory cells.," *Immunol. Rev.*, vol. 182, pp. 68–79, Aug. 2001.

[172] Y.-J. Kim, S.-J. Park, and H. E. Broxmeyer, "Phagocytosis, a Potential Mechanism for Myeloid-Derived Suppressor Cell Regulation of CD8+ T Cell Function Mediated through Programmed Cell Death-1 and Programmed Cell Death-1 Ligand Interaction," *J. Immunol.*, vol. 187, no. 5, pp. 2291–2301, Sep. 2011.

[173] B. Ruffell, D. Chang-strachan, V. Chan, A. Rosenbusch, C. M. T. Ho, N. Pryer, D. Daniel, E. S. Hwang, H. S. Rugo, and L. M. Coussens, "Article Responses to Chemotherapy by Suppressing IL-12 Expression in Intratumoral Dendritic Cells," *Cancer Cell*, vol. 26, no. 5, pp. 623–637, 2014.

[174] P. J. J. Murray, J. E. E. Allen, S. K. K. Biswas, E. A. A. Fisher, D. W. W. Gilroy, S. Goerdt, S. Gordon, J. A. A. Hamilton, L. B. B. Ivashkiv, T. Lawrence, M. Locati, A. Mantovani, F. O. O. Martinez, J.-L. L. Mege, D. M. M. Mosser, G. Natoli, J. P. P. Saeij, J. L. L. Schultze, K. A. A. Shirey, A. Sica, J. Suttles, I. Udalova, J. A. van Ginderachter, S. N. N. Vogel, T. A. A. Wynn, J. A. vanGinderachter, S. N. N. Vogel, and T. A. A. Wynn, "Macrophage Activation and Polarization: Nomenclature and Experimental Guidelines," *Immunity*, vol. 41, no. 1, pp. 14–20, Jul. 2014.

[175] S. K. Biswas, "Metabolic Reprogramming of Immune Cells in Cancer Progression," *Immunity*, vol. 43, no. 3, pp. 435–449, Sep. 2015.

[176] J. C. Lenzo, A. L. Turner, A. D. Cook, R. Vlahos, G. P. Anderson, E. C. Reynolds, and J. A. Hamilton, "Control of macrophage lineage populations by CSF-1 receptor and GM-CSF in homeostasis and inflammation," *Immunol. Cell Biol.*, vol. 90, no. 4, pp. 429–440, Apr. 2012.

[177] Y. W. Koh, C. Park, D. H. Yoon, C. Suh, and J. Huh, "CSF-1R Expression in Tumor-Associated Macrophages Is Associated With Worse Prognosis in Classical Hodgkin Lymphoma," *Am. J. Clin. Pathol.*, vol. 141, no. 4, pp. 573–583, Apr. 2014.

[178] X.-D. Zhu, J.-B. Zhang, P.-Y. Zhuang, H.-G. Zhu, W. Zhang, Y.-Q. Xiong, W.-Z. Wu, L. Wang, Z.-Y. Tang, and H.-C. Sun, "High

Expression of Macrophage Colony-Stimulating Factor in Peritumoral Liver Tissue Is Associated With Poor Survival After Curative Resection of Hepatocellular Carcinoma," *J. Clin. Oncol.*, vol. 26, no. 16, pp. 2707–2716, Jun. 2008.

[179] S. Goswami, E. Sahai, J. B. Wyckoff, M. Cammer, D. Cox, F. J. Pixley, E. R. Stanley, J. E. Segall, and J. S. Condeelis, "Macrophages Promote the Invasion of Breast Carcinoma Cells via a Colony-Stimulating Factor-1/Epidermal Growth Factor Paracrine Loop," *Cancer Res.*, vol. 65, no. 12, pp. 5278–5283, Jun. 2005.

[180] E. Y. Lin, A. V Nguyen, R. G. Russell, and J. W. Pollard, "Colony-stimulating factor 1 promotes progression of mammary tumors to malignancy.," *J. Exp. Med.*, vol. 193, no. 6, pp. 727–40, Mar. 2001.

[181] D. A. Hume and K. P. A. MacDonald, "Therapeutic applications of macrophage colony-stimulating factor-1 (CSF-1) and antagonists of CSF-1 receptor (CSF-1R) signaling," *Blood*, vol. 119, no. 8, pp. 1810–1820, Feb. 2012.

[182] K. Wartha, V. Runza, C. H. H. Ries, M. A. A. Cannarile, S. Hoves, F. Rey-giraud, L. P. P. Pradel, F. Feuerhake, I. Klaman, T. Jones, U. Jucknischke, S. Scheiblich, K. Kaluza, I. H. H. Gorr, A. Walz, K. Abiraj, P. A. A. Cassier, A. Sica, C. Gomez-Roca, K. E. De Visser, A. Italiano, C. Le Tourneau, J. Delord, H. Levitsky, J.-Y. Blay, D. Ru, J. Benz, K. Wartha, V. Runza, F. Rey-giraud, L. P. P. Pradel, F. Feuerhake, I. Klaman, T. Jones, U. Jucknischke, S. Scheiblich, K. Kaluza, I. H. H. Gorr, A. Walz, K. Abiraj, P. A. A. Cassier, A. Sica, C. Gomez-Roca, K. E. de Visser, A. Italiano, C. Le Tourneau, J. Delord, H. Levitsky, J.-Y. Blay, and D. Rüttinger, "Article Targeting Tumor-Associated Macrophages with Anti-CSF-1R Antibody Reveals a Strategy for Cancer Therapy," *Cancer Cell*, vol. 25, no. 6, pp. 846–859, Jun. 2014.

[183] J. H. Stafford, T. Hirai, L. Deng, S. B. Chernikova, K. Urata, B. L. West, and J. M. Brown, "Colony stimulating factor 1 receptor inhibition delays recurrence of glioblastoma after radiation by altering myeloid cell recruitment and polarization," *Neuro. Oncol.*, vol. 18, no. 6, pp. 797–806, Jun. 2016.

[184] S. M. Pyonteck, L. Akkari, A. J. Schuhmacher, R. L. Bowman, L. Sevenich, D. F. Quail, O. C. Olson, M. L. Quick, J. T. Huse, V. Teijeiro, M. Setty, C. S. Leslie, Y. Oei, A. Pedraza, J. Zhang, C. W. Brennan, J. C. Sutton, E. C. Holland, D. Daniel, and J. A. Joyce, "Articles CSF-1R inhibition alters macrophage polarization and blocks glioma progression," *Nat. Med.*, vol. 19, no. 10, pp. 1264–1272, Oct. 2013.

[185] D. L. Moughon, H. He, S. Schokrpur, Z. K. Jiang, M. Yaqoob, J. David, C. Lin, M. L. Iruela-Arispe, O. Dorigo, and L. Wu, "Macrophage Blockade Using CSF1R Inhibitors Reverses the Vascular Leakage Underlying Malignant Ascites in Late-Stage Epithelial Ovarian Cancer.," *Cancer Res.*, vol. 75, no. 22, pp. 4742–52, Nov. 2015.

[186] N. Weizman, Y. Krelin, A. Shabtay-Orbach, M. Amit, Y. Binenbaum, R. J. Wong, and Z. Gil, “Macrophages mediate gemcitabine resistance of pancreatic adenocarcinoma by upregulating cytidine deaminase,” *Oncogene*, vol. 33, no. 29, pp. 3812–3819, Jul. 2014.

[187] D. G. DeNardo, D. J. Brennan, E. Rexhepaj, B. Ruffell, S. L. Shiao, S. F. Madden, W. M. Gallagher, N. Wadhwani, S. D. Keil, S. A. Junaid, H. S. Rugo, E. S. Hwang, K. Jirström, B. L. West, L. M. Coussens, and E. Shelley, “Leukocyte Complexity Predicts Breast Cancer Survival and Functionally Regulates Response to Chemotherapy,” *Cancer Discov.*, vol. 1, no. 1, pp. 54–67, Jun. 2011.

[188] J. B. Mitchem, D. J. Brennan, B. L. Knolhoff, B. A. Belt, Y. Zhu, D. E. Sanford, L. Belaygorod, D. Carpenter, L. Collins, D. Piwnica-worms, S. Hewitt, G. M. Udupi, W. M. Gallagher, C. Wegner, B. L. West, A. Wang-gillam, P. Goedegebuure, D. C. Linehan, and D. G. Denardo, “Targeting Tumor-In fi ltrating Macrophages Decreases Tumor-Initiating Cells , Relieves Immunosuppression , and Improves Chemotherapeutic Responses,” vol. 73, no. 9, pp. 1128–1141, 2013.

[189] Y. Zhu, B. L. Knolhoff, M. A. Meyer, T. M. Nywening, B. L. West, J. Luo, A. Wang-Gillam, S. P. Goedegebuure, D. C. Linehan, and D. G. De Nardo, “CSF1/CSF1R blockade reprograms tumor-infiltrating macrophages and improves response to T-cell checkpoint immunotherapy in pancreatic cancer models,” *Cancer Res.*, vol. 74, no. 18, pp. 5057–5069, 2014.

[190] V. Kumar, L. Donthireddy, D. Marvel, T. Condamine, F. Wang, S. Lavilla-Alonso, A. Hashimoto, P. Vonteddu, R. Behera, M. A. Goins, C. Mulligan, B. Nam, N. Hockstein, F. Denstman, S. Shakamuri, D. W. Speicher, A. T. Weeraratna, T. Chao, R. H. Vonderheide, L. R. Languino, P. Ordentlich, Q. Liu, X. Xu, A. Lo, E. Puré, C. Zhang, A. Loboda, M. A. Sepulveda, L. A. Snyder, and D. I. Gabrilovich, “Cancer-Associated Fibroblasts Neutralize the Anti-tumor Effect of CSF1 Receptor Blockade by Inducing PMN-MDSC Infiltration of Tumors,” *Cancer Cell*, vol. 32, no. 5, p. 654–668.e5, 2017.

[191] O. De Henau, M. Rausch, D. Winkler, L. F. Campesato, C. Liu, D. Hirschhorn-cymerman, S. Budhu, A. Ghosh, M. Pink, J. Tchaicha, M. Douglas, T. Tibbitts, S. Sharma, J. Proctor, N. Kosmider, K. White, H. Stern, J. Soglia, J. Adams, V. J. Palombella, K. Mcgovern, J. L. Kutok, J. D. Wolchok, and T. Merghoub, “therapy by targeting PI3K γ in myeloid cells,” *Nat. Publ. Gr.*, vol. 539, no. 7629, pp. 443–447, 2016.

[192] M. M. Kaneda, K. S. Messer, N. Ralainirina, H. Li, C. J. Leem, S. Gorjestani, C. C. Figueiredo, P. Foubert, M. C. Schmid, M. Pink, G. Woo, V. Abraham, D. G. Winkler, M. Rausch, V. J. Palombella, J. Kutok, K. Mcgovern, K. A. Frazer, X. Wu, J. A. Varner, M. Karin, R. Sasik, and E. W. Ezra, “suppression,” *Nat. Publ. Gr.*, vol. 539, no. 7629, pp. 437–442, 2016.

[193] E. Pujade-Lauraine, J. P. Guastalla, N. Colombo, P. Devillier, E. François, P. Fumoleau, A. Monnier, M. Nooy, L. Mignot, R. Bugat, C. Marques, M. Mousseau, G. Netter, F. Maloisel, S. Larbaoui, and M. Brandely, "Intraperitoneal recombinant interferon gamma in ovarian cancer patients with residual disease at second-look laparotomy.," *J. Clin. Oncol.*, vol. 14, no. 2, pp. 343–350, Feb. 1996.

[194] G. L. Beatty, E. G. Chiorean, M. P. Fishman, B. Saboury, U. R. Teitelbaum, W. Sun, R. D. Huhn, W. Song, D. Li, L. L. Sharp, D. A. Torigian, P. J. O'Dwyer, and R. H. Vonderheide, "CD40 Agonists Alter Tumor Stroma and Show Efficacy Against Pancreatic Carcinoma in Mice and Humans," *Science (80-.).*, vol. 331, no. 6024, pp. 1612–1616, Mar. 2011.

[195] G. L. Beatty, D. A. Torigian, E. G. Chiorean, B. Saboury, A. Brothers, A. Alavi, A. B. Troxel, W. Sun, U. R. Teitelbaum, R. H. Vonderheide, and P. J. O'Dwyer, "A Phase I Study of an Agonist CD40 Monoclonal Antibody (CP-870,893) in Combination with Gemcitabine in Patients with Advanced Pancreatic Ductal Adenocarcinoma," *Clin. Cancer Res.*, vol. 19, no. 22, pp. 6286–6295, Nov. 2013.

[196] S. Hoves, C.-H. Ooi, C. Wolter, H. Sade, S. Bissinger, M. Schmittnaegel, O. Ast, A. M. Giusti, K. Wartha, V. Runza, W. Xu, Y. Kienast, M. A. Cannarile, H. Levitsky, S. Romagnoli, M. De Palma, D. Rüttinger, and C. H. Ries, "Rapid activation of tumor-associated macrophages boosts preexisting tumor immunity," *J. Exp. Med.*, vol. 215, no. 3, p. jem.20171440, Mar. 2018.

[197] J. Harper and R. C. A. Sainson, "Regulation of the anti-tumour immune response by cancer-associated fibroblasts," *Semin. Cancer Biol.*, vol. 25, pp. 69–77, Apr. 2014.

[198] L. Raffaghello and F. Dazzi, "Classification and biology of tumour associated stromal cells," *Immunol. Lett.*, vol. 168, no. 2, pp. 175–182, Dec. 2015.

[199] T. A. Wynn and T. R. Ramalingam, "Mechanisms of fibrosis: therapeutic translation for fibrotic disease," *Nat. Med.*, vol. 18, no. 7, pp. 1028–1040, Jul. 2012.

[200] Y. Ino, R. Yamazaki-Itoh, S. Oguro, K. Shimada, T. Kosuge, J. Zavada, Y. Kanai, and N. Hiraoka, "Arginase II Expressed in Cancer-Associated Fibroblasts Indicates Tissue Hypoxia and Predicts Poor Outcome in Patients with Pancreatic Cancer," *PLoS One*, vol. 8, no. 2, p. e55146, Feb. 2013.

[201] C. Feig, J. O. Jones, M. Kraman, R. J. B. Wells, A. Deonarine, D. S. Chan, C. M. Connell, E. W. Roberts, Q. Zhao, O. L. Caballero, S. A. Teichmann, T. Janowitz, D. I. Jodrell, D. A. Tuveson, and D. T. Fearon, "Targeting CXCL12 from FAP-expressing carcinoma-associated fibroblasts synergizes with anti-PD-L1 immunotherapy in pancreatic

cancer.," *Proc. Natl. Acad. Sci. U. S. A.*, vol. 110, no. 50, pp. 20212–7, Dec. 2013.

[202] Y. Wen, C.-T. Wang, T.-T. Ma, Z.-Y. Li, L.-N. Zhou, B. Mu, F. Leng, H.-S. Shi, Y.-O. Li, and Y.-Q. Wei, "Immunotherapy targeting fibroblast activation protein inhibits tumor growth and increases survival in a murine colon cancer model," *Cancer Sci.*, vol. 101, no. 11, pp. 2325–2332, Nov. 2010.

[203] M. Kraman, P. J. Bambrough, J. N. Arnold, E. W. Roberts, L. Magiera, J. O. Jones, A. Gopinathan, D. A. Tuveson, and D. T. Fearon, "Suppression of Antitumor Immunity by Stromal Cells Expressing Fibroblast Activation Protein-," *Science (80-.).*, vol. 330, no. 6005, pp. 827–830, Nov. 2010.

[204] I. V. Pinchuk, J. I. Saada, E. J. Beswick, G. Boya, S. M. Qiu, R. C. Mifflin, G. S. Raju, V. E. Reyes, and D. W. Powell, "PD-1 Ligand Expression by Human Colonic Myofibroblasts/Fibroblasts Regulates CD4+ T-Cell Activity," *Gastroenterology*, vol. 135, no. 4, p. 1228–1237.e2, Oct. 2008.

[205] M. R. Nazareth, L. Broderick, M. R. Simpson-Abelson, R. J. Kelleher, S. J. Yokota, and R. B. Bankert, "Characterization of human lung tumor-associated fibroblasts and their ability to modulate the activation of tumor-associated T cells.," *J. Immunol.*, vol. 178, no. 9, pp. 5552–62, May 2007.

[206] P. L. Simonian, C. L. Roark, F. Wehrmann, A. K. Lanham, F. Diaz del Valle, W. K. Born, R. L. O'Brien, and A. P. Fontenot, "Th17-polarized immune response in a murine model of hypersensitivity pneumonitis and lung fibrosis.," *J. Immunol.*, vol. 182, no. 1, pp. 657–65, Jan. 2009.

[207] T. A. Mace, Z. Ameen, A. Collins, S. Wojcik, M. Mair, G. S. Young, J. R. Fuchs, T. D. Eubank, W. L. Frankel, T. Bekaii-Saab, M. Bloomston, and G. B. Lesinski, "Pancreatic Cancer-Associated Stellate Cells Promote Differentiation of Myeloid-Derived Suppressor Cells in a STAT3-Dependent Manner," *Cancer Res.*, vol. 73, no. 10, pp. 3007–3018, May 2013.

[208] J. H. Kim, S.-H. OH, E.-J. Kim, S. J. Park, S. P. Hong, J. H. Cheon, T. Il Kim, and W. H. Kim, "The role of myofibroblasts in upregulation of S100A8 and S100A9 and the differentiation of myeloid cells in the colorectal cancer microenvironment," *Biochem. Biophys. Res. Commun.*, vol. 423, no. 1, pp. 60–66, Jun. 2012.

[209] D. Liao, Y. Luo, D. Markowitz, R. Xiang, and R. A. Reisfeld, "Cancer Associated Fibroblasts Promote Tumor Growth and Metastasis by Modulating the Tumor Immune Microenvironment in a 4T1 Murine Breast Cancer Model," *PLoS One*, vol. 4, no. 11, p. e7965, Nov. 2009.

[210] A. Costa, Y. Kieffer, A. Scholer-Dahirel, F. Pelon, B. Bourachot, M.

Cardon, P. Sirven, I. Magagna, L. Fuhrmann, C. Bernard, C. Bonneau, M. Kondratova, I. Kuperstein, A. Zinovyev, A. M. Givel, M. C. Parrini, V. Soumelis, A. Vincent-Salomon, and F. Mechta-Grigoriou, “Fibroblast Heterogeneity and Immunosuppressive Environment in Human Breast Cancer,” *Cancer Cell*, vol. 33, no. 3, p. 463–479.e10, 2018.

[211] P. Chomarat, J. Banchereau, J. Davoust, and A. Karolina Palucka, “IL-6 switches the differentiation of monocytes from dendritic cells to macrophages,” *Nat. Immunol.*, vol. 1, no. 6, pp. 510–514, Dec. 2000.

[212] E. Mathew, A. L. Brannon, A. Del Vecchio, P. E. Garcia, M. K. Penny, K. T. Kane, A. Vinta, R. J. Buckanovich, and M. P. di Magliano, “Mesenchymal Stem Cells Promote Pancreatic Tumor Growth by Inducing Alternative Polarization of Macrophages,” *Neoplasia*, vol. 18, no. 3, pp. 142–151, Mar. 2016.

[213] S. Torres, R. A. Bartolomé, M. Mendes, R. Barderas, M. J. Fernandez-Aceñero, A. Peláez-García, C. Peña, M. Lopez-Lucendo, R. Villar-Vázquez, A. G. de Herreros, F. Bonilla, and J. I. Casal, “Proteome profiling of cancer-associated fibroblasts identifies novel proinflammatory signatures and prognostic markers for colorectal cancer.,” *Clin. Cancer Res.*, vol. 19, no. 21, pp. 6006–19, Nov. 2013.

[214] Y.-P. Sher, J.-Y. Shih, P.-C. Yang, S. R. Roffler, Y.-W. Chu, C.-W. Wu, C.-L. Yu, and K. Peck, “Prognosis of non-small cell lung cancer patients by detecting circulating cancer cells in the peripheral blood with multiple marker genes.,” *Clin. Cancer Res.*, vol. 11, no. 1, pp. 173–9, Jan. 2005.

[215] H. Jiang, S. Hegde, and D. G. DeNardo, “Tumor-associated fibrosis as a regulator of tumor immunity and response to immunotherapy,” *Cancer Immunol. Immunother.*, vol. 66, no. 8, pp. 1037–1048, 2017.

[216] N. Hartmann, N. A. Giese, T. Giese, I. Poschke, R. Offringa, J. Werner, and E. Ryschich, “Prevailing role of contact guidance in intrastromal T-cell trapping in human pancreatic cancer.,” *Clin. Cancer Res.*, vol. 20, no. 13, pp. 3422–33, Jul. 2014.

[217] H. Salmon, K. Franciszkiewicz, D. Damotte, M.-C. Dieu-Nosjean, P. Validire, A. Trautmann, F. Mami-Chouaib, and E. Donnadieu, “Matrix architecture defines the preferential localization and migration of T cells into the stroma of human lung tumors.,” *J. Clin. Invest.*, vol. 122, no. 3, pp. 899–910, Mar. 2012.

[218] H. Jiang, S. Hegde, B. L. Knolhoff, Y. Zhu, J. M. Herndon, M. A. Meyer, T. M. Nywening, W. G. Hawkins, I. M. Shapiro, D. T. Weaver, J. A. Pachter, A. Wang-gillam, and D. G. Denardo, “Targeting focal adhesion kinase renders pancreatic cancers responsive to checkpoint immunotherapy,” *Nat. Med.*, vol. 22, no. July, pp. 1–13, Aug. 2016.

[219] E. Van Goethem, R. Poincloux, F. Gauffre, I. Maridonneau-Parini, and

V. Le Cabec, “Matrix architecture dictates three-dimensional migration modes of human macrophages: differential involvement of proteases and podosome-like structures.,” *J. Immunol.*, vol. 184, no. 2, pp. 1049–61, Jan. 2010.

[220] F. Y. McWhorter, C. T. Davis, and W. F. Liu, “Physical and mechanical regulation of macrophage phenotype and function,” *Cell. Mol. Life Sci.*, vol. 72, no. 7, pp. 1303–1316, Apr. 2015.

[221] T. Cramer, Y. Yamanishi, B. E. Clausen, I. Förster, R. Pawlinski, N. Mackman, V. H. Haase, R. Jaenisch, M. Corr, V. Nizet, G. S. Firestein, H. P. Gerber, N. Ferrara, and R. S. Johnson, “HIF-1alpha is essential for myeloid cell-mediated inflammation.,” *Cell*, vol. 112, no. 5, pp. 645–57, Mar. 2003.

[222] M. Z. Noman, G. Desantis, B. Janji, M. Hasmim, S. Karray, P. Dessen, V. Bronte, and S. Chouaib, “PD-L1 is a novel direct target of HIF-1α, and its blockade under hypoxia enhanced MDSC-mediated T cell activation.,” *J. Exp. Med.*, vol. 211, no. 5, pp. 781–90, May 2014.

[223] O. Zion, O. Genin, N. Kawada, K. Yoshizato, S. Roffe, A. Nagler, J. L. Iovanna, O. Halevy, and M. Pines, “Inhibition of Transforming Growth Factor β Signaling by Halofuginone as a Modality for Pancreas Fibrosis Prevention,” *Pancreas*, vol. 38, no. 4, pp. 427–435, May 2009.

[224] B. W. Miller, J. P. Morton, M. Pinese, G. Saturno, N. B. Jamieson, E. McGhee, P. Timpson, J. Leach, L. McGarry, E. Shanks, P. Bailey, D. Chang, K. Oien, S. Karim, A. Au, C. Steele, C. R. Carter, C. McKay, K. Anderson, T. R. J. Evans, R. Marais, C. Springer, A. Biankin, J. T. Erler, and O. J. Sansom, “Targeting the LOX/hypoxia axis reverses many of the features that make pancreatic cancer deadly: inhibition of LOX abrogates metastasis and enhances drug efficacy,” *EMBO Mol. Med.*, vol. 7, no. 8, pp. 1063–1076, Aug. 2015.

[225] D. M. Gilkes, P. Chaturvedi, S. Bajpai, C. C. Wong, H. Wei, S. Pitcairn, M. E. Hubbi, D. Wirtz, and G. L. Semenza, “Collagen prolyl hydroxylases are essential for breast cancer metastasis.,” *Cancer Res.*, vol. 73, no. 11, pp. 3285–96, Jun. 2013.

[226] A. Chronopoulos, B. Robinson, M. Sarper, E. Cortes, V. Auernheimer, D. Lachowski, S. Attwood, R. García, S. Ghassemi, B. Fabry, and A. del Río Hernández, “ATRA mechanically reprograms pancreatic stellate cells to suppress matrix remodelling and inhibit cancer cell invasion,” *Nat. Commun.*, vol. 7, p. 12630, Sep. 2016.

[227] P. P. Provenzano, C. Cuevas, A. E. Chang, V. K. Goel, D. D. Von Hoff, and S. R. Hingorani, “Enzymatic Targeting of the Stroma Ablates Physical Barriers to Treatment of Pancreatic Ductal Adenocarcinoma,” *Cancer Cell*, vol. 21, no. 3, pp. 418–429, 2012.

[228] M. H. Sherman, R. T. Yu, D. D. Engle, N. Ding, A. R. Atkins, H. Tiriac,

E. A. Collisson, F. Connor, T. Van Dyke, S. Kozlov, P. Martin, T. W. Tseng, D. W. Dawson, T. R. Donahue, A. Masamune, T. Shimosegawa, M. V. Apte, J. S. Wilson, B. Ng, S. L. Lau, J. E. Gunton, G. M. Wahl, T. Hunter, J. A. Drebin, P. J. O'Dwyer, C. Liddle, D. A. Tuveson, M. Downes, and R. M. Evans, "Vitamin D receptor-mediated stromal reprogramming suppresses pancreatitis and enhances pancreatic cancer therapy," *Cell*, vol. 159, no. 1, pp. 80–93, 2014.

[229] Y. Takeda, K. Tsujino, T. Kijima, and A. Kumanogoh, "Efficacy and safety of pirfenidone for idiopathic pulmonary fibrosis," *Patient Prefer. Adherence*, vol. 8, p. 361, Mar. 2014.

[230] M. Chen, R. Xiang, Y. Wen, G. Xu, C. Wang, S. Luo, T. Yin, X. Wei, B. Shao, N. Liu, F. Guo, M. Li, S. Zhang, M. Li, K. Ren, Y. Wang, and Y. Wei, "A whole-cell tumor vaccine modified to express fibroblast activation protein induces antitumor immunity against both tumor cells and cancer-associated fibroblasts," *Sci. Rep.*, vol. 5, no. 1, p. 14421, Nov. 2015.

[231] L.-C. S. Wang, A. Lo, J. Scholler, J. Sun, R. S. Majumdar, V. Kapoor, M. Antzis, C. E. Cotner, L. A. Johnson, A. C. Durham, C. C. Solomides, C. H. June, E. Puré, and S. M. Albelda, "Targeting fibroblast activation protein in tumor stroma with chimeric antigen receptor T cells can inhibit tumor growth and augment host immunity without severe toxicity.," *Cancer Immunol. Res.*, vol. 2, no. 2, pp. 154–66, Feb. 2014.

[232] F. J. Sulzmaier, C. Jean, and D. D. Schlaepfer, "FAK in cancer: mechanistic findings and clinical applications," *Nat. Rev. Cancer*, vol. 14, no. 9, pp. 598–610, Sep. 2014.

[233] A. Serrels, T. Lund, B. Serrels, A. Byron, R. C. McPherson, A. von Kriegsheim, L. Gómez-Cuadrado, M. Canel, M. Muir, J. E. Ring, E. Maniati, A. H. Sims, J. A. Pachter, V. G. Brunton, N. Gilbert, S. M. Anderton, R. J. B. Nibbs, and M. C. Frame, "Nuclear FAK controls chemokine transcription, Tregs, and evasion of anti-tumor immunity.," *Cell*, vol. 163, no. 1, pp. 160–73, Sep. 2015.

[234] T. A. Mace, R. Shakya, J. R. Pitarresi, B. Swanson, C. W. McQuinn, S. Loftus, E. Nordquist, Z. Cruz-Monserrate, L. Yu, G. Young, X. Zhong, T. A. Zimmers, M. C. Ostrowski, T. Ludwig, M. Bloomston, T. Bekaii-Saab, and G. B. Lesinski, "IL-6 and PD-L1 antibody blockade combination therapy reduces tumour progression in murine models of pancreatic cancer.," *Gut*, vol. 67, no. 2, p. gutjnl-2016-311585, Feb. 2016.

[235] J. Ferlay, I. Soerjomataram, R. Dikshit, S. Eser, C. Mathers, M. Rebelo, D. M. Parkin, D. Forman, and F. Bray, "Cancer incidence and mortality worldwide: Sources, methods and major patterns in GLOBOCAN 2012," *Int. J. Cancer*, vol. 136, no. 5, pp. E359–E386, Mar. 2015.

[236] J. Kleeff, M. Korc, M. Apte, C. La Vecchia, and C. D. Johnson,

"Pancreatic cancer," *Nat. Publ. Gr.*, vol. 2, no. April, pp. 1–23, 2016.

[237] D. P. Ryan, T. S. Hong, and N. Bardeesy, "Pancreatic Adenocarcinoma," pp. 1039–1049, 2014.

[238] R. H. Hruban, M. Goggins, J. Parsons, and S. E. Kern, "Progression Model for Pancreatic Cancer Progression Model for Pancreatic Cancer 1," vol. 6, no. August, pp. 2969–2972, 2000.

[239] N. Waddell, M. Pajic, A.-M. Patch, D. K. Chang, K. S. Kassahn, P. Bailey, A. L. Johns, D. Miller, K. Nones, K. Quek, M. C. J. Quinn, A. J. Robertson, M. Z. H. Fadlullah, T. J. C. Bruxner, A. N. Christ, I. Harliwong, S. Idrisoglu, S. Manning, C. Nourse, E. Nourbakhsh, S. Wani, P. J. Wilson, E. Markham, N. Cloonan, M. J. Anderson, J. L. Fink, O. Holmes, S. H. Kazakoff, C. Leonard, F. Newell, B. Poudel, S. Song, D. Taylor, N. Waddell, S. Wood, Q. Xu, J. Wu, M. Pinese, M. J. Cowley, H. C. Lee, M. D. Jones, A. M. Nagrial, J. Humphris, L. A. Chantrill, V. Chin, A. M. Steinmann, A. Mawson, E. S. Humphrey, E. K. Colvin, A. Chou, C. J. Scarlett, A. V Pinho, M. Giry-Laterriere, I. Rooman, J. S. Samra, J. G. Kench, J. A. Pettitt, N. D. Merrett, C. Toon, K. Epari, N. Q. Nguyen, A. Barbour, N. Zeps, N. B. Jamieson, J. S. Graham, S. P. Niclou, R. Bjerkvig, R. Grützmann, D. Aust, R. H. Hruban, A. Maitra, C. A. Iacobuzio-Donahue, C. L. Wolfgang, R. A. Morgan, R. T. Lawlor, V. Corbo, C. Bassi, M. Falconi, G. Zamboni, G. Tortora, M. A. Tempero, A. P. C. G. Australian Pancreatic Cancer Genome Initiative, A. J. Gill, J. R. Eshleman, C. Pilarsky, A. Scarpa, E. A. Musgrove, J. V Pearson, A. V Biankin, and S. M. Grimmond, "Whole genomes redefine the mutational landscape of pancreatic cancer.," *Nature*, vol. 518, no. 7540, pp. 495–501, Feb. 2015.

[240] P. Bailey, D. K. Chang, K. Nones, A. L. Johns, A. M. Patch, M. C. Gingras, D. K. Miller, A. N. Christ, T. J. C. Bruxner, M. C. Quinn, C. Nourse, L. C. Murtaugh, I. Harliwong, S. Idrisoglu, S. Manning, E. Nourbakhsh, S. Wani, L. Fink, O. Holmes, V. Chin, M. J. Anderson, S. Kazakoff, C. Leonard, F. Newell, N. Waddell, S. Wood, Q. Xu, P. J. Wilson, N. Cloonan, K. S. Kassahn, D. Taylor, K. Quek, A. Robertson, L. Pantano, L. Mincarelli, L. N. Sanchez, L. Evers, J. Wu, M. Pinese, M. J. Cowley, M. D. Jones, E. K. Colvin, A. M. Nagrial, E. S. Humphrey, L. A. Chantrill, A. Mawson, J. Humphris, A. Chou, M. Pajic, C. J. Scarlett, A. V. Pinho, M. Giry-Laterriere, I. Rooman, J. S. Samra, J. G. Kench, J. A. Lovell, N. D. Merrett, C. W. Toon, K. Epari, N. Q. Nguyen, A. Barbour, N. Zeps, K. Moran-Jones, N. B. Jamieson, J. S. Graham, F. Duthie, K. Oien, J. Hair, R. Grützmann, A. Maitra, C. A. Iacobuzio-Donahue, C. L. Wolfgang, R. A. Morgan, R. T. Lawlor, V. Corbo, C. Bassi, B. Rusev, P. Capelli, R. Salvia, G. Tortora, D. Mukhopadhyay, G. M. Petersen, D. M. Munzy, W. E. Fisher, S. A. Karim, J. R. Eshleman, R. H. Hruban, C. Pilarsky, J. P. Morton, O. J. Sansom, A. Scarpa, E. A. Musgrove, U. M. H. Bailey, O. Hofmann, R. L. Sutherland, D. A. Wheeler, A. J. Gill, R. A. Gibbs, J. V. Pearson, N. Waddell, A. V. Biankin, and S. M. Grimmond, "Genomic analyses identify molecular subtypes of pancreatic cancer," *Nature*, vol. 531, no.

7592, pp. 47–52, 2016.

[241] S. Weissmueller, E. Manchado, M. Saborowski, J. P. Morris, E. Wagenblast, C. A. Davis, S.-H. Moon, N. T. Pfister, D. F. Tschaharganeh, T. Kitzing, D. Aust, E. K. Markert, J. Wu, S. M. Grimmond, C. Pilarsky, C. Prives, A. V. Biankin, and S. W. Lowe, “Mutant p53 Drives Pancreatic Cancer Metastasis through Cell-Autonomous PDGF Receptor β Signaling,” *Cell*, vol. 157, no. 2, pp. 382–394, Apr. 2014.

[242] M. A. Hale, H. Kagami, L. Shi, A. M. Holland, H.-P. Elsässer, R. E. Hammer, and R. J. MacDonald, “The homeodomain protein PDX1 is required at mid-pancreatic development for the formation of the exocrine pancreas,” *Dev. Biol.*, vol. 286, no. 1, pp. 225–237, Oct. 2005.

[243] C. Feig, A. Gopinathan, A. Neesse, D. S. Chan, N. Cook, and D. A. Tuveson, “The Pancreas Cancer Microenvironment,” *Clin. Cancer Res.*, vol. 18, no. 16, pp. 4266–4276, Aug. 2012.

[244] L. M. Wang, M. A. Silva, Z. D’Costa, R. Bockelmann, Z. Soonawalla, S. Liu, E. O’Neill, S. Mukherjee, W. G. McKenna, R. Muschel, and E. Fokas, “The prognostic role of desmoplastic stroma in pancreatic ductal adenocarcinoma.,” *Oncotarget*, vol. 7, no. 4, pp. 4183–94, Jan. 2016.

[245] M. V. Apte, J. S. Wilson, A. Lugea, and S. J. Pandol, “A Starring Role for Stellate Cells in the Pancreatic Cancer Microenvironment,” *Gastroenterology*, vol. 144, no. 6, pp. 1210–1219, May 2013.

[246] S. Hamada, A. Masamune, T. Takikawa, N. Suzuki, K. Kikuta, M. Hirota, H. Hamada, M. Kobune, K. Satoh, and T. Shimosegawa, “Pancreatic stellate cells enhance stem cell-like phenotypes in pancreatic cancer cells,” *Biochem. Biophys. Res. Commun.*, vol. 421, no. 2, pp. 349–354, May 2012.

[247] Z. Xu, A. Vonlaufen, P. A. Phillips, E. Fiala-Beer, X. Zhang, L. Yang, A. V Biankin, D. Goldstein, R. C. Pirola, J. S. Wilson, and M. V Apte, “Role of pancreatic stellate cells in pancreatic cancer metastasis.,” *Am. J. Pathol.*, vol. 177, no. 5, pp. 2585–96, Nov. 2010.

[248] M. B. Patel, S. P. Pothula, Z. Xu, A. K. Lee, D. Goldstein, R. C. Pirola, M. V. Apte, and J. S. Wilson, “The role of the hepatocyte growth factor/c-MET pathway in pancreatic stellate cell–endothelial cell interactions: antiangiogenic implications in pancreatic cancer,” *Carcinogenesis*, vol. 35, no. 8, pp. 1891–1900, Aug. 2014.

[249] A. Ene–Obong, A. J. Clear, J. Watt, J. Wang, R. Fatah, J. C. Riches, J. F. Marshall, J. Chin–Aleong, C. Chelala, J. G. Gribben, A. G. Ramsay, and H. M. Kocher, “Activated Pancreatic Stellate Cells Sequester CD8+ T Cells to Reduce Their Infiltration of the Juxtatumoral Compartment of Pancreatic Ductal Adenocarcinoma,”

Gastroenterology, vol. 145, no. 5, pp. 1121–1132, Nov. 2013.

[250] D. Tang, Z. Yuan, X. Xue, Z. Lu, Y. Zhang, H. Wang, M. Chen, Y. An, J. Wei, Y. Zhu, Y. Miao, and K. Jiang, “High expression of Galectin-1 in pancreatic stellate cells plays a role in the development and maintenance of an immunosuppressive microenvironment in pancreatic cancer,” *Int. J. Cancer*, vol. 130, no. 10, pp. 2337–2348, May 2012.

[251] R. H. Vonderheide and L. J. Bayne, “Inflammatory networks and immune surveillance of pancreatic carcinoma,” *Curr. Opin. Immunol.*, vol. 25, no. 2, pp. 200–205, Apr. 2013.

[252] M. Lesina, M. U. Kurkowski, K. Ludes, S. Rose-John, M. Treiber, G. Klöppel, A. Yoshimura, W. Reindl, B. Sipos, S. Akira, R. M. Schmid, and H. Algül, “Stat3/Socs3 Activation by IL-6 Transsignaling Promotes Progression of Pancreatic Intraepithelial Neoplasia and Development of Pancreatic Cancer,” *Cancer Cell*, vol. 19, no. 4, pp. 456–469, Apr. 2011.

[253] S. R. Hingorani, L. Wang, A. S. Multani, C. Combs, T. B. Deramaudt, R. H. Hruban, A. K. Rustgi, S. Chang, and D. A. Tuveson, “Trp53R172H and KrasG12D cooperate to promote chromosomal instability and widely metastatic pancreatic ductal adenocarcinoma in mice,” *Cancer Cell*, vol. 7, no. 5, pp. 469–483, 2005.

[254] S. R. Hingorani, E. F. P. Iii, A. Maitra, V. Rajapakse, C. King, M. A. Jacobetz, S. Ross, T. P. Conrads, T. D. Veenstra, B. A. Hitt, Y. Kawaguchi, D. Johann, L. A. Liotta, H. C. Crawford, M. E. Putt, T. Jacks, C. V. E. Wright, R. H. Hruban, A. M. Lowy, and D. A. Tuveson, “Preinvasive and invasive ductal pancreatic cancer and its early detection in the mouse,” vol. 4, no. December, pp. 437–450, 2003.

[255] E. L. Jackson, N. Willis, K. Mercer, R. T. Bronson, D. Crowley, R. Montoya, T. Jacks, and D. A. Tuveson, “Analysis of lung tumor initiation and progression using conditional expression of oncogenic K-ras,” *Genes Dev.*, vol. 15, no. 24, pp. 3243–3248, Dec. 2001.

[256] C. E. Clark, S. R. Hingorani, R. Mick, C. Combs, D. A. Tuveson, and R. H. Vonderheide, “Dynamics of the immune reaction to pancreatic cancer from inception to invasion,” *Cancer Res.*, vol. 67, no. 19, pp. 9518–9527, Oct. 2007.

[257] N. M. Aiello, D. L. Bajor, R. J. Norgard, A. Sahmoud, N. Bhagwat, M. N. Pham, T. C. Cornish, C. A. Iacobuzio-donahue, R. H. Vonderheide, and B. Z. Stanger, “changes in the local microenvironment,” *Nat. Commun.*, vol. 7, pp. 1–9, 2016.

[258] M. A. Jacobetz, D. S. Chan, A. Neesse, T. E. Bapiro, N. Cook, K. K. Frese, C. Feig, T. Nakagawa, M. E. Caldwell, H. I. Zecchini, M. P. Lolkema, P. Jiang, A. Kultti, C. B. Thompson, D. C. Maneval, D. I. Jodrell, G. I. Frost, H. M. Shepard, J. N. Skepper, and D. A. Tuveson,

"Hyaluronan impairs vascular function and drug delivery in a mouse model of pancreatic cancer," *Gut*, vol. 62, no. 1, pp. 112–120, Jan. 2013.

[259] D. Bausch, S. Thomas, M. Mino-Kenudson, C. C. Fernandez-del, T. W. Bauer, M. Williams, A. L. Warshaw, S. P. Thayer, and K. A. Kelly, "Plectin-1 as a Novel Biomarker for Pancreatic Cancer," *Clin. Cancer Res.*, vol. 17, no. 2, pp. 302–309, Jan. 2011.

[260] A. Neesse, A. Hahnenkamp, H. Griesmann, M. Buchholz, S. A. Hahn, A. Maghnouj, V. Fendrich, J. Ring, B. Sipos, D. A. Tuveson, C. Bremer, T. M. Gress, and P. Michl, "Claudin-4-targeted optical imaging detects pancreatic cancer and its precursor lesions," *Gut*, vol. 62, no. 7, pp. 1034–1043, Jul. 2013.

[261] V. M. Faca, K. S. Song, H. Wang, Q. Zhang, A. L. Krasnoselsky, L. F. Newcomb, R. R. Plentz, S. Gurumurthy, M. S. Redston, S. J. Pitteri, S. R. Pereira-Faca, R. C. Ireton, H. Katayama, V. Glukhova, D. Phanstiel, D. E. Brenner, M. A. Anderson, D. Misek, N. Scholler, N. D. Urban, M. J. Barnett, C. Edelstein, G. E. Goodman, M. D. Thornquist, M. W. McIntosh, R. A. DePinho, N. Bardeesy, and S. M. Hanash, "A Mouse to Human Search for Plasma Proteome Changes Associated with Pancreatic Tumor Development," *PLoS Med.*, vol. 5, no. 6, p. e123, Jun. 2008.

[262] S. A. Melo, L. B. Luecke, C. Kahlert, A. F. Fernandez, S. T. Gammon, J. Kaye, V. S. LeBleu, E. A. Mittendorf, J. Weitz, N. Rahbari, C. Reissfelder, C. Pilarsky, M. F. Fraga, D. Piwnica-Worms, and R. Kalluri, "Glypican-1 identifies cancer exosomes and detects early pancreatic cancer," *Nature*, vol. 523, no. 7559, pp. 177–182, Jul. 2015.

[263] M. Porta, X. Fabregat, N. Malats, L. Guarner, A. Carrato, A. de Miguel, L. Ruiz, M. Jariod, S. Costafreda, S. Coll, J. Alguacil, J. M. Corominas, R. Solà, A. Salas, and F. X. Real, "Exocrine pancreatic cancer: symptoms at presentation and their relation to tumour site and stage.," *Clin. Transl. Oncol.*, vol. 7, no. 5, pp. 189–97, Jun. 2005.

[264] I. T. Konstantinidis, A. L. Warshaw, J. N. Allen, L. S. Blaszkowsky, C. F. Castillo, V. Deshpande, T. S. Hong, E. L. Kwak, G. Y. Lauwers, D. P. Ryan, J. A. Wargo, K. D. Lillemoe, and C. R. Ferrone, "Pancreatic Ductal Adenocarcinoma," *Ann. Surg.*, vol. 257, no. 4, pp. 731–736, Apr. 2013.

[265] T. Conroy, F. Desseigne, M. Ychou, O. Bouché, R. Guimbaud, Y. Bécouarn, A. Adenis, J.-L. Raoul, S. Gourgou-Bourgade, C. de la Fouchardière, J. Bennouna, J.-B. Bachet, F. Khemissa-Akouz, D. Péré-Vergé, C. Delbaldo, E. Assenat, B. Chauffert, P. Michel, C. Montoto-Grillot, and M. Ducreux, "FOLFIRINOX versus Gemcitabine for Metastatic Pancreatic Cancer," *N. Engl. J. Med.*, vol. 364, no. 19, pp. 1817–1825, May 2011.

[266] D. D. Von Hoff, T. Ervin, F. P. Arena, E. G. Chiorean, J. Infante, M. Moore, T. Seay, S. A. Tjulandin, W. W. Ma, M. N. Saleh, M. Harris, M. Reni, S. Dowden, D. Laheru, N. Bahary, R. K. Ramanathan, J. Tabernero, M. Hidalgo, D. Goldstein, E. Van Cutsem, X. Wei, J. Iglesias, and M. F. Renschler, "Increased Survival in Pancreatic Cancer with nab-Paclitaxel plus Gemcitabine," *N. Engl. J. Med.*, vol. 369, no. 18, pp. 1691–1703, Oct. 2013.

[267] S. Mukherjee, C. N. Hurt, J. Bridgewater, S. Falk, S. Cummins, H. Wasan, T. Crosby, C. Jephcott, R. Roy, G. Radhakrishna, A. McDonald, R. Ray, G. Joseph, J. Staffurth, R. A. Abrams, G. Griffiths, and T. Maughan, "Gemcitabine-based or capecitabine-based chemoradiotherapy for locally advanced pancreatic cancer (SCALOP): a multicentre, randomised, phase 2 trial," *Lancet Oncol.*, vol. 14, no. 4, pp. 317–326, Apr. 2013.

[268] B. Chauffert, F. Mornex, F. Bonnetain, P. Rougier, C. Mariette, O. Bouche, J. F. Bosset, T. Aparicio, L. Mineur, A. Azzedine, P. Hammel, J. Butel, N. Stremsdoerfer, P. Maingon, and L. Bedenne, "Phase III trial comparing intensive induction chemoradiotherapy (60 Gy, infusional 5-FU and intermittent cisplatin) followed by maintenance gemcitabine with gemcitabine alone for locally advanced unresectable pancreatic cancer. Definitive results of the 2000-01 FFCD/SFRO study," *Ann. Oncol.*, vol. 19, no. 9, pp. 1592–1599, May 2008.

[269] D. V. T. Catenacci, M. R. Junttila, T. Karrison, N. Bahary, M. N. Horiba, S. R. Nattam, R. Marsh, J. Wallace, M. Kozloff, L. Rajdev, D. Cohen, J. Wade, B. Sleckman, H.-J. Lenz, P. Stiff, P. Kumar, P. Xu, L. Henderson, N. Takebe, R. Salgia, X. Wang, W. M. Stadler, F. J. de Sauvage, and H. L. Kindler, "Randomized Phase Ib/II Study of Gemcitabine Plus Placebo or Vismodegib, a Hedgehog Pathway Inhibitor, in Patients With Metastatic Pancreatic Cancer," *J. Clin. Oncol.*, vol. 33, no. 36, pp. 4284–4292, Dec. 2015.

[270] G. Di Caro, N. Cortese, G. F. Castino, F. Grizzi, F. Gavazzi, C. Ridolfi, G. Capretti, R. Mineri, J. Todoric, A. Zerbi, P. Allavena, A. Mantovani, and F. Marchesi, "Dual prognostic significance of tumour-associated macrophages in human pancreatic adenocarcinoma treated or untreated with chemotherapy," *Gut*, vol. 65, no. 10, pp. 1710–1720, Oct. 2016.

[271] D. T. Le, J. N. Durham, K. N. Smith, H. Wang, B. R. Bartlett, L. K. Aulakh, S. Lu, H. Kemberling, C. Wilt, B. S. Luber, F. Wong, N. S. Azad, A. A. Rucki, D. Laheru, R. Donehower, A. Zaheer, G. A. Fisher, T. S. Crocenzi, J. J. Lee, T. F. Greten, A. G. Duffy, K. K. Ciombor, A. D. Eyring, B. H. Lam, A. Joe, S. P. Kang, M. Holdhoff, L. Danilova, L. Cope, C. Meyer, S. Zhou, R. M. Goldberg, D. K. Armstrong, K. M. Bever, A. N. Fader, J. Taube, F. Housseau, D. Spetzler, N. Xiao, D. M. Pardoll, N. Papadopoulos, K. W. Kinzler, J. R. Eshleman, B. Vogelstein, R. A. Anders, and L. A. Diaz, "Mismatch repair deficiency predicts response of solid tumors to PD-1 blockade," *Science (80-.).*,

vol. 357, no. 6349, pp. 409–413, Jul. 2017.

[272] “nCounter® Technology | NanoString Technologies.” [Online]. Available: https://www.nanostring.com/scientific-content/technology-overview/ncounter-technology. [Accessed: 15-Sep-2018].

[273] A. Ribas and D. Ph, “edi t or i a l s Tumor Immunotherapy Directed at PD-1,” pp. 2517–2519, 2012.

[274] V. P. Balachandran, M. Luksza, J. N. Zhao, V. Makarov, J. A. Moral, R. Remark, B. Herbst, G. Askan, U. Bhanot, Y. Senbabaoglu, D. K. Wells, C. I. O. Cary, O. Grbovic-Huezo, M. Attiyeh, B. Medina, J. Zhang, J. Loo, J. Saglimbeni, M. Abu-Akeel, R. Zappasodi, N. Riaz, M. Smoragiewicz, Z. L. Kelley, O. Basturk, M. Gönen, A. J. Levine, P. J. Allen, D. T. Fearon, M. Merad, S. Gnjatic, C. A. Iacobuzio-Donahue, J. D. Wolchok, R. P. DeMatteo, T. A. Chan, B. D. Greenbaum, T. Merghoub, and S. D. Leach, “Identification of unique neoantigen qualities in long-term survivors of pancreatic cancer,” *Nature*, vol. 551, no. 7681, pp. S12–S16, 2017.

[275] E. J. Wherry and M. Kurachi, “Molecular and cellular insights into T cell exhaustion,” *Nat. Publ. Gr.*, vol. 15, no. 8, pp. 486–499, 2015.

[276] M. Mohme, S. Riethdorf, and K. Pantel, “Circulating and disseminated tumour cells — mechanisms of immune surveillance and escape,” *Nat. Publ. Gr.*, pp. 1–13, 2016.

[277] R. Noy and J. W. Pollard, “Tumor-Associated Macrophages: From Mechanisms to Therapy,” *Immunity*, vol. 41, no. 1, pp. 49–61, 2014.

[278] A. L. Doedens, C. Stockmann, M. P. Rubinstein, D. Liao, N. Zhang, D. G. DeNardo, L. M. Coussens, M. Karin, A. W. Goldrath, and R. S. Johnson, “Macrophage Expression of Hypoxia-Inducible Factor-1 Suppresses T-Cell Function and Promotes Tumor Progression,” *Cancer Res.*, vol. 70, no. 19, pp. 7465–7475, Oct. 2010.

[279] C. Sperti, C. Pasquali, A. Piccoli, and S. Pedrazzoli, “Survival after resection for ductal adenocarcinoma of the pancreas,” *Br.J.Surg.*, vol. 83, pp. 625–631, 1996.

[280] R. H. Vonderheide, “The Immune Revolution: A Case for Priming, Not Checkpoint,” *Cancer Cell*, vol. 33, no. 4, pp. 563–569, 2018.

[281] S. Guo, M. Contratto, G. Miller, L. Leichman, and J. Wu, “Immunotherapy in pancreatic cancer: Unleash its potential through novel combinations.,” *World J. Clin. Oncol.*, vol. 8, no. 3, pp. 230–240, Jun. 2017.

[282] C. Bauer, B. Kühnemuth, P. Duewell, S. Ormanns, T. Gress, and M. Schnurr, “immunotherapy of pancreatic cancer,” *Cancer Lett.*, 2016.

[283] S. M. Wörmann, K. N. Diakopoulos, M. Lesina, and H. Algül, “The

immune network in pancreatic cancer development and progression," *Oncogene*, vol. 33, no. 23, pp. 2956–2967, Jun. 2014.

[284] Y. Ino, R. Yamazaki-Itoh, K. Shimada, M. Iwasaki, T. Kosuge, Y. Kanai, and N. Hiraoka, "Immune cell infiltration as an indicator of the immune microenvironment of pancreatic cancer," *Br. J. Cancer*, vol. 108, no. 4, pp. 914–923, Mar. 2013.

[285] D. Balli, A. J. Rech, B. Z. Stanger, and R. H. Vonderheide, "Immune Cytolytic Activity Stratifies Molecular Subsets of Human Pancreatic Cancer," *Clin. Cancer Res.*, vol. 23, no. 12, pp. 3129–3138, Jun. 2017.

[286] G.-Y. Liou, H. Döppler, B. Necela, B. Edenfield, L. Zhang, D. W. Dawson, and P. Storz, "Mutant KRAS–Induced Expression of ICAM-1 in Pancreatic Acinar Cells Causes Attraction of Macrophages to Expedite the Formation of Precancerous Lesions," *Cancer Discov.*, vol. 5, no. 1, pp. 52–63, Jan. 2015.

[287] N. M. Luheshi, J. Coates-Ulrichsen, J. Harper, S. Mullins, M. G. Sulikowski, P. Martin, L. Brown, A. Lewis, G. Davies, M. Morrow, and R. W. Wilkinson, "Transformation of the tumour microenvironment by a CD40 agonist antibody correlates with improved responses to PD-L1 blockade in a mouse orthotopic pancreatic tumour model.," *Oncotarget*, vol. 7, no. 14, pp. 18508–20, Apr. 2016.

[288] C. W. Steele, S. A. Karim, J. D. G. Leach, P. Bailey, R. Upstill-Goddard, L. Rishi, M. Foth, S. Bryson, K. McDaid, Z. Wilson, C. Eberlein, J. B. Candido, M. Clarke, C. Nixon, J. Connelly, N. Jamieson, C. R. Carter, F. Balkwill, D. K. Chang, T. R. J. Evans, D. Strathdee, A. V Biankin, R. J. B. Nibbs, S. T. Barry, O. J. Sansom, and J. P. Morton, "CXCR2 Inhibition Profoundly Suppresses Metastases and Augments Immunotherapy in Pancreatic Ductal Adenocarcinoma.," *Cancer Cell*, vol. 29, no. 6, pp. 832–845, Jun. 2016.

[289] A. Sica and A. Mantovani, "Macrophage plasticity and polarization: in vivo veritas," *J. Clin. Invest.*, vol. 122, no. 3, pp. 787–795, Mar. 2012.

[290] M. De Palma and C. E. Lewis, "Review Macrophage Regulation of Tumor Responses to Anticancer Therapies," *Cancer Cell*, vol. 23, no. 3, pp. 277–286, 2013.

[291] M. C. Schmid, C. J. Avraamides, H. C. Dippold, I. Franco, P. Foubert, L. G. Ellies, L. M. Acevedo, J. R. E. Manglicmot, X. Song, W. Wrasidlo, S. L. Blair, M. H. Ginsberg, D. A. Cheresh, E. Hirsch, S. J. Field, and J. A. Varner, "Receptor tyrosine kinases and TLR/IL1Rs unexpectedly activate myeloid cell PI3kγ, a single convergent point promoting tumor inflammation and progression.," *Cancer Cell*, vol. 19, no. 6, pp. 715–27, Jun. 2011.

[292] M. M. Kaneda, P. Cappello, A. V Nguyen, N. Ralainirina, C. R. Hardamon, P. Foubert, M. C. Schmid, P. Sun, E. Mose, M. Bouvet, A.

M. Lowy, M. A. Valasek, R. Sasik, F. Novelli, E. Hirsch, and J. A. Varner, “Macrophage PI3K g Drives Pancreatic Ductal Adenocarcinoma Progression,” no. August, pp. 870–886, 2016.

[293] M. M. Kaneda, K. S. Messer, N. Ralainirina, H. Li, C. J. Leem, S. Gorjestani, G. Woo, A. V. Nguyen, C. C. Figueiredo, P. Foubert, M. C. Schmid, M. Pink, D. G. Winkler, M. Rausch, V. J. Palombella, J. Kutok, K. McGovern, K. A. Frazer, X. Wu, M. Karin, R. Sasik, E. E. W. Cohen, and J. A. Varner, “PI3Kγ is a molecular switch that controls immune suppression,” *Nature*, vol. 539, no. 7629, pp. 437–442, Nov. 2016.

[294] D. C. Lacey, A. Achuthan, A. J. Fleetwood, H. Dinh, J. Roiniotis, G. M. Scholz, M. W. Chang, S. K. Beckman, A. D. Cook, and J. A. Hamilton, “Defining GM-CSF- and Macrophage-CSF-Dependent Macrophage Responses by In Vitro Models,” *J. Immunol.*, vol. 188, no. 11, pp. 5752–5765, Jun. 2012.

[295] M. A. Cannarile, M. Weisser, W. Jacob, A.-M. Jegg, C. H. Ries, and D. Rüttinger, “Colony-stimulating factor 1 receptor (CSF1R) inhibitors in cancer therapy,” *J. Immunother. Cancer*, vol. 5, no. 1, p. 53, Dec. 2017.

[296] H. Griesmann, C. Drexel, N. Milosevic, B. Sipos, J. Rosendahl, T. M. Gress, and P. Michl, “Pharmacological macrophage inhibition decreases metastasis formation in a genetic model of pancreatic cancer,” *Gut*, p. gutjnl-2015-310049, 2016.

[297] E. Hirsch, E. Ciraolo, I. Franco, A. Ghigo, and M. Martini, “PI3K in cancer–stroma interactions: bad in seed and ugly in soil,” *Oncogene*, vol. 33, no. 24, pp. 3083–3090, Jun. 2014.

[298] E. Hirsch, V. L. Katanaev, C. Garlanda, O. Azzolino, L. Pirola, L. Silengo, S. Sozzani, A. Mantovani, F. Altruda, and M. P. Wymann, “Central role for G protein-coupled phosphoinositide 3-kinase gamma in inflammation,” *Science (80-.).*, vol. 287, no. 5455, pp. 1049–1053, 2000.

[299] H. Ji, V. Ardissone, F. Rintelen, J. Shaw, T. Ru, T. Martin, D. Gretener, C. Ferrandi, C. Chabert, C. Gillieron, B. Franc, D. Perrin, D. Leroy, P. Vitte, E. Hirsch, M. P. Wymann, R. Cirillo, M. K. Schwarz, C. Rommel, M. Camps, T. Rückle, H. Ji, V. Ardissone, F. Rintelen, J. Shaw, C. Ferrandi, C. Chabert, C. Gillieron, B. Françon, T. Martin, D. Gretener, D. Perrin, D. Leroy, P. Vitte, E. Hirsch, M. P. Wymann, R. Cirillo, M. K. Schwarz, and C. Rommel, “Blockade of PI3K g suppresses joint inflammation and damage in mouse models of rheumatoid arthritis,” *Nat. Med.*, vol. 11, no. 9, pp. 936–943, Sep. 2005.

[300] J. A. Hamilton, A. D. Cook, and P. P. Tak, “Anti-colony-stimulating factor therapies for inflammatory and autoimmune diseases,” *Nat. Publ. Gr.*, vol. 16, no. 1, pp. 53–70, Jan. 2017.

[301] A. K. Palucka and L. M. Coussens, “Review The Basis of

Oncoimmunology," *Cell*, vol. 164, no. 6, pp. 1233–1247, Mar. 2016.

[302] B. Ruffell and L. M. Coussens, "Perspective Macrophages and Therapeutic Resistance in Cancer," *Cancer Cell*, vol. 27, no. 4, pp. 462–472, 2015.

[303] S. M. Ansell, A. M. Lesokhin, I. Borrello, A. Halwani, E. C. Scott, M. Gutierrez, S. J. Schuster, M. M. Millenson, D. Cattry, G. J. Freeman, S. J. Rodig, B. Chapuy, A. H. Ligon, L. Zhu, J. F. Grosso, S. Y. Kim, J. M. Timmerman, M. A. Shipp, and P. Armand, "PD-1 Blockade with Nivolumab in Relapsed or Refractory Hodgkin's Lymphoma," *N. Engl. J. Med.*, vol. 372, no. 4, pp. 311–319, Jan. 2015.

[304] Z. Eroglu, J. M. Zaretsky, S. Hu-Lieskovan, D. W. Kim, A. Algazi, D. B. Johnson, E. Liniker, B. Ben Kong, R. Munhoz, S. Rapisuwon, P. F. Gherardini, B. Chmielowski, X. Wang, I. P. Shintaku, C. Wei, J. A. Sosman, R. W. Joseph, M. A. Postow, M. S. Carlino, W.-J. Hwu, R. A. Scolyer, J. Messina, A. J. Cochran, G. V. Long, and A. Ribas, "High response rate to PD-1 blockade in desmoplastic melanomas," *Nature*, vol. 553, no. 7688, pp. 347–350, Jan. 2018.

[305] R. L. Ferris, G. Blumenschein, J. Fayette, J. Guigay, A. D. Colevas, L. Licitra, K. Harrington, S. Kasper, E. E. Vokes, C. Even, F. Worden, N. F. Saba, L. C. Iglesias Docampo, R. Haddad, T. Rordorf, N. Kiyota, M. Tahara, M. Monga, M. Lynch, W. J. Geese, J. Kopit, J. W. Shaw, and M. L. Gillison, "Nivolumab for Recurrent Squamous-Cell Carcinoma of the Head and Neck," *N. Engl. J. Med.*, vol. 375, no. 19, pp. 1856–1867, Nov. 2016.

[306] E. B. Garon, N. A. Rizvi, R. Hui, N. Leighl, A. S. Balmanoukian, J. P. Eder, A. Patnaik, C. Aggarwal, M. Gubens, L. Horn, E. Carcereny, M.-J. Ahn, E. Felip, J.-S. Lee, M. D. Hellmann, O. Hamid, J. W. Goldman, J.-C. Soria, M. Dolled-Filhart, R. Z. Rutledge, J. Zhang, J. K. Lunceford, R. Rangwala, G. M. Lubiniecki, C. Roach, K. Emancipator, and L. Gandhi, "Pembrolizumab for the Treatment of Non–Small-Cell Lung Cancer," *N. Engl. J. Med.*, vol. 372, no. 21, pp. 2018–2028, May 2015.

[307] J. Bellmunt, R. de Wit, D. J. Vaughn, Y. Fradet, J.-L. Lee, L. Fong, N. J. Vogelzang, M. A. Climent, D. P. Petrylak, T. K. Choueiri, A. Necchi, W. Gerritsen, H. Gurney, D. I. Quinn, S. Culine, C. N. Sternberg, Y. Mai, C. H. Poehlein, R. F. Perini, and D. F. Bajorin, "Pembrolizumab as Second-Line Therapy for Advanced Urothelial Carcinoma," *N. Engl. J. Med.*, vol. 376, no. 11, pp. 1015–1026, Mar. 2017.

[308] J. E. Rosenberg, J. Hoffman-Censits, T. Powles, M. S. van der Heijden, A. V Balar, A. Necchi, N. Dawson, P. H. O'Donnell, A. Balmanoukian, Y. Loriot, S. Srinivas, M. M. Retz, P. Grivas, R. W. Joseph, M. D. Galsky, M. T. Fleming, D. P. Petrylak, J. L. Perez-Gracia, H. A. Burris, D. Castellano, C. Canil, J. Bellmunt, D. Bajorin, D. Nickles, R. Bourgon, G. M. Frampton, N. Cui, S. Mariathasan, O.

Abidoye, G. D. Fine, and R. Dreicer, “Atezolizumab in patients with locally advanced and metastatic urothelial carcinoma who have progressed following treatment with platinum-based chemotherapy: a single-arm, multicentre, phase 2 trial,” *Lancet*, vol. 387, no. 10031, pp. 1909–1920, May 2016.

[309] D. T. Le, E. Lutz, J. N. Uram, E. A. Sugar, B. Onners, S. Solt, L. Zheng, L. A. Diaz, R. C. Donehower, E. M. Jaffee, and D. A. Laheru, “Evaluation of Ipilimumab in Combination With Allogeneic Pancreatic Tumor Cells Transfected With a GM-CSF Gene in Previously Treated Pancreatic Cancer,” *J. Immunother.*, vol. 36, no. 7, pp. 382–389, Sep. 2013.

[310] S. L. Topalian, C. G. Drake, and D. M. Pardoll, “Targeting the PD-1/B7-H1(PD-L1) pathway to activate anti-tumor immunity,” *Curr. Opin. Immunol.*, vol. 24, no. 2, pp. 207–212, Apr. 2012.

[311] C. J. Hasson, G. E. Caldwell, and R. E. A. Van Emmerik, “NIH Public Access,” *Motor Control*, vol. 27, no. 4, pp. 590–609, 2009.

[312] M. A. Lakins, E. Ghorani, H. Munir, C. P. Martins, and J. D. Shields, “Cancer-associated fibroblasts induce antigen-specific deletion of CD8+T Cells to protect tumour cells,” *Nat. Commun.*, vol. 9, no. 1, pp. 1–9, 2018.

[313] I. Garrido-laguna and M. Hidalgo, “treatments to promising novel therapies,” *Nat. Publ. Gr.*, vol. 12, no. 6, pp. 319–334, 2015.

[314] J. R. Brahmer, “Safety and activity of anti-PD-L1 antibody in patients with advanced cancer,” *N. Engl. J. Med.*, vol. 366, pp. 2455–2465, 2012.

[315] M. S. Lawrence, P. Stojanov, P. Polak, G. V. Kryukov, K. Cibulskis, A. Sivachenko, S. L. Carter, C. Stewart, C. H. Mermel, S. A. Roberts, A. Kiezun, P. S. Hammerman, A. McKenna, Y. Drier, L. Zou, A. H. Ramos, T. J. Pugh, N. Stransky, E. Helman, J. Kim, C. Sougnez, L. Ambrogio, E. Nickerson, E. Shefler, M. L. Cortés, D. Auclair, G. Saksena, D. Voet, M. Noble, D. DiCara, P. Lin, L. Lichtenstein, D. I. Heiman, T. Fennell, M. Imielinski, B. Hernandez, E. Hodis, S. Baca, A. M. Dulak, J. Lohr, D.-A. Landau, C. J. Wu, J. Melendez-Zajgla, A. Hidalgo-Miranda, A. Koren, S. A. McCarroll, J. Mora, R. S. Lee, B. Crompton, R. Onofrio, M. Parkin, W. Winckler, K. Ardlie, S. B. Gabriel, C. W. M. Roberts, J. A. Biegel, K. Stegmaier, A. J. Bass, L. A. Garraway, M. Meyerson, T. R. Golub, D. A. Gordenin, S. Sunyaev, E. S. Lander, and G. Getz, “Mutational heterogeneity in cancer and the search for new cancer-associated genes,” *Nature*, vol. 499, no. 7457, pp. 214–218, Jul. 2013.

[316] E. S. Knudsen, P. Vail, U. Balaji, H. Ngo, I. W. Botros, V. Makarov, N. Riaz, V. Balachandran, S. Leach, D. M. Thompson, T. A. Chan, and A. K. Witkiewicz, “Biology of Human Tumors Stratification of Pancreatic

Ductal Adenocarcinoma: Combinatorial Genetic, Stromal, and Immunologic Markers," 2017.

[317] S. K. Biswas, P. Allavena, and A. Mantovani, "Tumor-associated macrophages: functional diversity, clinical significance, and open questions," *Semin. Immunopathol.*, vol. 35, no. 5, pp. 585–600, Sep. 2013.

[318] T. A. Wynn and K. M. Vannella, "Macrophages in Tissue Repair, Regeneration, and Fibrosis," *Immunity*, vol. 44, no. 3, pp. 450–462, 2016.

[319] V. Quaranta, C. Rainer, S. R. Nielsen, M. L. Raymant, M. S. Ahmed, D. D. Engle, A. Taylor, T. Murray, F. Campbell, D. H. Palmer, D. A. Tuveson, A. Mielgo, and M. C. Schmid, "Macrophage-Derived Granulin Drives Resistance to Immune Checkpoint Inhibition in Metastatic Pancreatic Cancer.," *Cancer Res.*, vol. 78, no. 15, pp. 4253–4269, Aug. 2018.